Encoding of Communication Signals in Heterogeneous Populations of Electroreceptors

Dissertation
der Mathematisch-Naturwissenschaftlichen Fakultät
der Eberhard Karls Universität Tübingen
zur Erlangung des Grades eines
Doktors der Naturwissenschaften
(Dr. rer. nat.)

vorgelegt von
Diplom-Biologin Henriette Walz
aus Berlin

Tübingen
2013

Tag der mündlichen Prüfung: 20.1.2014
Dekan: Prof. Dr. Wolfgang Rosenstiel
1. Berichterstatter: Prof. Dr. Jan Benda
2. Berichterstatter: Prof. Dr. Hanspeter A. Mallot

Der Fisch ist mein Lieblingstier,
er ist sehr interessant.
– *Funny van Dannen*

Contents

List of Figures

List of Tables

Zusammenfassung

Sinnesreize wie Töne, Bilder oder Gerüche gelangen ins Nervensystem, indem sie von Rezeptorzellen kodiert werden. Nur die Informationen, die in Rezeptorzellen aufgenommen werden, können weiter verarbeitet werden, eine Empfindung erzeugen und das Verhalten beeinflussen. Wie im gesamten Nervensystem, werden auch hier Sinnesreize nicht in Einzelneuronen, sondern in Neuronenpopulationen kodiert. Einzelneurone in derartigen Populationen unterscheiden sich oft untereinander in ihren Antworteigenschaften, ein Phänomen, das man Heterogenität nennt. Diese Dissertation befasst sich damit, wie Sinnesreize in heterogenen Rezeptorpopulationen kodiert werden. Dies habe ich am Beispiel der Kodierung von Kommunikationssignalen in Populationen von Elektrorezeptoren des schwach-elektrischen Fisches *Apteronotus leptorhynchus* untersucht. Bevor ich im Folgenden die Ergebnisse genauer darstelle, möchte ich hier einen Überblick über die Herangehensweise geben: Zunächst habe ich die Antworten einzelner Rezeptorzellen auf Kommunikationssignale mittels elektrophysiologischer Untersuchungen beschrieben. Der Fokus lag hierbei auf der Kodierung dieser Signale bei verschiedenen, natürlich vorkommenden Kontexten. Auf den so erlangten Ergebnissen aufbauend, habe ich ein Computermodel entwickelt, das auf die Anworten auf statische Stimuli angepasst wurde und Rezeptorantworten auf dynamische Stimuli mit hoher Genauigkeit nachbildete. Das Modell ermöglichte die Simulation einer Population von Neuronen, deren Heterogenität der der natürlichen Population entspricht. Somit habe ich schließlich den Einfluss von Heterogenität auf die Kodierung eines natürlich vorkommenden, verhaltensrelevanten Signals in Rezeptorpopulationen untersucht. Um heterogene Populationen zu untersuchen, sind Messungen vieler verschiedener Zellen notwendig, die nur mittels Modellsimulationen möglich sind.

Schwach-elektrische Fische erzeugen ein elektrisches Feld (electric organ discharge, EOD), das sie fortwährend wahrnehmen. Sie benutzen Modulationen desselben, um Gegenstände zu detektieren oder mit anderen Fischen zu kommunizieren. Sie sind ein etabliertes Modellsystem, um Sinneswahrnehmung zu untersuchen. Das EOD lässt sich in Experimenten leicht beobachten und simulieren. Eine Verhaltensantwort dieser Fische – die Jamming Avoidance Response – stellt eines der wenigen Beispiele dar, bei denen von der Sinneswahrnehmung bis hin zur Erzeugung des Verhaltens jede Stufe

der Informationsverarbeitung beschrieben ist. *A. leptorhynchus* erzeugt ein quasisinusoidales EOD, dessen Frequenz im Zeitablauf extrem stabil ist. Allerdings modulieren die Fische die EOD-Frequenz, um zu kommunizieren. Meine Arbeit befasst sich ausschließlich mit Chirps. Chirps sind ein gut beschriebenes Kommunikationssignal, bei dem ein Fisch seine EOD-Frequenz vorübergehend erhöht.

Chirps treten vor dem Hintergrund einer sogenannten Schwebung auf, die sich bildet, wenn sich die EODs zweier Fische überlagern. Schwebungen sind sinusoidale Amplitudenmodulationen (AM) des EODs. Die Frequenz einer Schwebung ergibt sich aus dem Frequenzunterschied der beiden Einzelsignale, in diesem Fall der EOD-Frequenzen zweier Fische, die miteinander kommunizieren. Bei *A. leptorhynchus* treten Schwebungsfrequenzen zwischen wenigen und einigen Hundert Hertz auf. Da die EOD-Frequenz von Geschlecht, Größe und sozialem Status eines Tieres abhängt, bildet die Schwebungsfrequenz einer Begegnung ab, ob beide Fische sich in diesen Eigenschaften ähneln (bei niedrigen Schwebungsfrequenzen) oder nicht (bei hohen Schwebungsfrequenzen). AMs der EOD werden in erster Linie von P-typ Elektrorezeptoren (P-units) kodiert. Ich habe mich auf einen Typ Chirp, den kleinen Chirp, konzentriert. P-unit-Antworten auf kleine Chirps wurden bisher nur bei niedrigen Schwebungsfrequenzen untersucht. Die Fische produzieren das Signal allerdings bei vielen, unterschiedlichen Schwebungen. Die Frage des ersten Projektes lautete daher: *Beeinflusst die zugrunde liegende Schwebung die Kodierung eines Chirps in P-typ Elektrorezeptoren?*

Ein Chirp unterbricht die gleichmäßige Amplitudenmodulation einer Schwebung und verändert sie in einer Weise, die von der Schwebungsfrequenz und -phase abhängt. Die Ergebnisse meiner elektrophysiologischen Ableitungen zeigen, dass die Antworten von P-units ebenfalls von der zugrundeliegenden Schwebung beeinflusst sind: Die Neurone antworteten je nach Schwebungsfrequenz entweder durch Synchronisation oder durch Desynchronisation auf einen kleinen Chirp. Bei langsamen Schwebungen spielte zudem die Phase der Schwebung eine entscheidende Rolle für die P-unit Antwort. Die P-unit-Antworten unterteilen den Bereich natürlich vorkommender Schwebungsfrequenzen in vier Abschnitte. Diese Unterteilung entspricht keinem heute bekannten Verhalten. Bisher wird angenommen, dass kleine Chirps unabhängig von der Schwebung dieselbe Verhaltensrelevanz haben. Meine Ergebnisse stellen diese Annahme jedoch in Frage. Sie deuten an, dass die Wahrnehmung eines Chirps vom Hintergrund, dem Kontext, abhängt und Chirps somit je nach Schwebungsfrequenz unterschiedliche Verhaltensantworten auslösen könnten.

Die Frequenzselektivität der P-units, das heißt, wie diese auf Schwebungen unterschiedlicher Frequenz reagieren, bestimmt ihre Antwort auf Chirps. Ein einfaches Modell konnte vorhersagen, ob ein Chirp die Aktivität synchronisieren oder desynchronisieren würde und zwar, indem es ausschließlich die Frequenzselektivität zusammen mit der Frequenz der Amplitudenmodulation in Betracht nahm, die sich aus Chirp- und Schwebungsfrequenz ergibt. Die Aussagekraft der Frequenzselektivität in Bezug auf die P-unit-Antworten führte zu der Frage, auf der das nächste Projekt aufbaute: *Welche Mechanismen bilden die Grundlage der Frequenzselektivität von P-units?* Zur Behandlung dieser Frage habe ich ein Leaky Integrate-and-Fire-Modell entwickelt, um die Antwor-

ten von P-units nachzubilden. Ich habe das Modell zu konstantem EOD und zu Stufenreizen kalibriert. Das Modell konnte dann die Antworten der entsprechenden Zelle detailliert reproduzieren.

Das Modell weist gegenüber Sinus- und Rauschstimuli außerdem dieselbe Frequenzselektivität auf wie die Zelle. Die Frequenzselektivität ergibt sich damit direkt aus den Antworten auf konstante Stufenreize. Frühere P-unit Modelle hatte jeweils nur eine Eigenschaft der P-units korrekt nachgebildet – die phasengekoppelte Antwort auf konstantes EOD oder die Frequenzselektivität zu Amplitudenmodulationen. Entscheidend für die gute Abbildung beider P-unit-Antworten in meinem Modell ist ein dendritisches Filter, dessen Parametrisierung ich aus den experimentellen Daten ableiten konnte. Das Modell lässt sich sowohl über Reize als auch über Zellen sehr gut generalisieren. So konnte das Modell zu allen P-units, von denen ich elektrophysiologisch abgeleitet hatten, kalibriert werden. Diese P-units unterschieden sich zum Teil stark in ihren Eigenschaften wie mittlerer Aktionspotentialrate und Variabilität ihrer Antworten.

Dass das Modell Antworten verschiedener P-units nachbilden konnte, hat es mir ermöglicht, heterogene Populationen zu simulieren, die natürlichen Populationen ähneln. Die Grundlage für diese Simulationen war eine genaue Charakterisierung der Parametervariabilität. Diese war entstanden, wenn das Modell auf verschiedene Zellen, oder aber mehrfach zu einer Zelle justiert worden war. Für alle Parameter konnte ich Verteilungen beschreiben, aus denen ich neue, repräsentative Parameterkombinationen ziehen konnte. So konnte ich eine größere Population bauen, die in der Heterogenität ihrer Antworteigenschaften den natürlichen P-unit-Populationen entspricht. Außerdem reproduziert die Population die Antworten auf Chirpstimuli sowohl auf Einzelzell- als auch auf Populationsebene. Ich konnte die Population daher nutzen, um die folgende Frage zu untersuchen: *Wie wirkt sich realitätsnahe Heterogenität auf die Populationskodierung eines natürlichen, verhaltensrelevanten Signals aus?*

Eine genauere Untersuchung der Chirpantworten hat gezeigt, dass Einzelzellen mit bestimmten Eigenschaften stärker auf bestimmte Chirpstimuli antworten. Allerdings haben sich jeweils unterschiedliche Eigenschaften als günstig heraus gestellt, um unterschiedliche Chirps zu kodieren. Heterogenität könnte so sicherstellen, dass innerhalb einer Population starke Antworten zu allen verschiedenen, natürlich vorkommenden Reizen vorhanden sind. Eine heterogene Population hätte dann einen Vorteil gegenüber einer homogenen Population, die bei einem gegebenen Reiz möglicherweise nur auf schwache Antworten zurückgreifen kann. Der Vorteil der Heterogenität wurde nur deshalb deutlich, weil ich die natürlich vorkommene Variabilität der Signale benutzt habe.

Zusammenfassend lassen die Ergebnisse folgende Rückschlüsse auf die Informationskodierung in Elektrorezeptoren zu:

- Chirps werden je nach Kontext unterschiedlich in Rezeptorneuronen kodiert. Da diese Kodierung den Rahmen für jede weitere Verarbeitung setzt, deutet dies auf eine differentielle Empfindung und Bedeutung dieses Kommunikationssig-

nals für das Verhalten hin. Die Ergebnisse demonstrieren, wie durch genaue Untersuchung der Physiologie Rückschlüsse auf das Verhalten möglich sind.

- Die Synchronität der Elektrorezeptoren ändert sich sehr schnell in Reaktion auf einen Stimulus. Sie bildet linear die Frequenzen ab, die in einem Stimulus vorhanden sind. Der Mechanismus der Synchronitätsantwort ist sehr grundsätzlich und könnte auch von Zellen in anderen Sinnessystemen angewandt werden.

- Ein einfaches Neuronenmodell kann die Antworten von P-units auf komplexe und neuartige Stimuli genau vorhersagen. Das unterstreicht einerseits die Linearität der P-unit-Antworten, andererseits das Mächtigkeit einfacher Neuronenmodelle.

- Die Heterogenität der P-unit Population lässt sich durch Parametervariabilität nachbilden. Verschiedene Einzelneurone erweisen sich als optimal für die Kodierung einzelner Stimuli. Dies deutet an, dass eine heterogene Population robuster darin ist, viele verschiedene Stimuli zu kodieren.

- Die Kernergebnisse meiner Arbeit ergaben sich erst, als ich die Variabilität natürlicher Signale benutzte. Dies unterstreicht, wie essentiell eine genaue und vollständige Betrachtung der natürlichen Sinnesreize für die Beschreibung eines Sinnessystems ist.

Summary

Sensory stimuli such as sound or light enter the nervous system through receptor cells. Only the information that is encoded in receptor cells can be further processed, perceived and eventually influence behaviour. As in other parts of the nervous system, information is not taken up by a single receptor but by many receptor neurons that form a population. Individual neurons in a population often differ slightly in the way they encode a stimulus. The population is then said to exhibit heterogeneity. This thesis deals with the encoding of sensory signals in heterogeneous populations of electroreceptor neurons. The investigation is based on the example of the encoding of communication signals in electroreceptor populations in the weakly-electric fish *Apteronotus leptorhynchus*. Before I describe the findings in detail, I want give an overview of the methodological approach that was applied: I first characterised the responses of the receptor neurons to communication signals in a broad range of natural contexts via electrophysiological recordings. Using these results, I developed a computational model that was capable of reproducing the responses with a high degree of accuracy. The model could reproduce the activity of neurons of different properties and therefore allowed for a simulation of a heterogeneous population of model neurons. This enabled me to investigate the encoding of a natural, behaviourally-relevant signal in a model population whose heterogeneity resembles that of a natural population. The investigation of heterogeneous populations necessitates recordings of many cells, which are only feasible in model simulations.

Weakly-electric fish generate an electric organ discharge (EOD) and use perturbations and modulations of it to navigate and communicate. They have become an established model system for the study of sensory encoding. The EOD can easily be observed as well as simulated during experiments. One of the behavioural patterns of these fish, the jamming avoidance response, represents one of the few examples of a behavioural response in which every stage of neuronal processing, from sensation to behaviour, is described. *A. leptorhynchus* generates a quasisinusoidal EOD with a frequency that is very stable over time under baseline conditions. Frequency modulations are used by the fish to communicate. I focused on chirps, which are well-studied communication signals that consist of transient (on the order of milliseconds) increases in EOD fre-

quency.

Chirps occur on top of beats, sinusoidal amplitude modulations (AM) formed by the superposition of the EODs of two communicating fish. AMs are sensed by P-type electroreceptors that are distributed over the whole body of the fish. The frequency of the beat is determined by the difference between the EOD frequencies of the two fish. In *A. leptorhynchus* beat frequencies range from a couple up to a couple of hundred hertz. Since the EOD frequency of each fish depends on its gender, size and social status, the beat frequency reflects how similar the fish are in these aspects. This thesis only deals with the encoding of one type of chirp, the small chirp. The encoding of small chirps in P-units has been studied only when superposed on a slow beat. However, chirps occur on a range of different beat frequencies and the AMs they generate are influenced by the underlying beat. My first question therefore was: *Does the background beat influence the encoding of small chirps in P-units?*

My electrophysiological recordings show that the P-unit responses indeed strongly depend on the underlying beat: P-units responded either by synchronisation or desynchronisation to a small chirp depending on the beat frequency. The responses partition the range of beat frequencies into four distinct regimes that do not correspond to known behavioural categories. Chirps are assumed to have the same behavioural relevance regardless of the underlying beat. My findings challenge this assumption suggesting that the chirp might be perceived differently in different social encounters.

The P-unit response variations to chirps can be explained by their frequency tuning. By taking into account only the P-units' response to different frequencies and the combined frequency of chirp and beat, a simple model could predict whether P-units would be synchronised or desynchronised in response to a chirp. The importance of the frequency tuning led to the question of the next project: *Which mechanisms underlie the P-unit frequency tuning?* To approach this question, I developed a leaky integrate-and-fire model to reproduce P-unit responses. The model was designed and calibrated to baseline conditions and step stimuli and reproduces the P-units' responses to these stimuli very well.

Furthermore, the model exhibits the same frequency tuning to both sinusoidal and random stimuli as the target P-unit. The frequency tuning is thus an emergent property from the responses to constant EOD and step stimuli. Previous P-unit models had typically reproduced either baseline activity or frequency tuning. Crucial for the good fit of my model to both these responses is a dendritic filter that I could derive from the electrophysiological data. It allows for a correct reproduction of phase-locked responses to the EOD and responses to AMs. The model exhibits a high degree of generalisability, not across stimulation paradigms, but also cells. It could be fit to all P-units we had recorded from, although they differed substantially in various physiological properties such as rate and variability of the baseline discharge.

The latter feature of the model allowed me to simulate a model population with natural-like heterogeneity. A detailed characterization of the parameter variability underlying the fits to different P-units formed the basis for the simulation. By defining parameter distributions and drawing new representative values from them, I was able

to build a large population of model neurons. It resembles the heterogeneity of P-units in terms of baseline response characteristics. It also reproduces chirp responses on the single cell level as well as in terms of population response. It thus allowed for the investigation of the question: *How does natural-like heterogeneity influence the encoding of a well-described, behaviourally relevant signal in a neuron model population?*

Chirp responses of single model neurons within the population differ systematically with baseline characteristics. Model neurons of certain baseline characteristic encode a chirp better than others. However, this relationship depends on the parameters of the chirp and beat. For different beat-chirp combinations, P-units with different characteristics are best suited. My findings suggest that a heterogeneous population has an advantage in encoding natural signals, because it has access to good responses to all possible stimuli. For some stimuli homogeneous populations might only possess weak responses, although they are well suited for others. The benefit of heterogeneity was thus only revealed because I took into account a range of naturally occurring signals.

Overall, these finding allow the following implications on information coding in electroreceptor cells:

- Electroreceptors encode small chirps differently depending on the context. Since this encoding sets the frame for any subsequent processing, it suggests a differential perception and behavioural relevance of this communication signal. This demonstrates how a detailed investigation of the physiology can allow for predictions of the behaviour of an animal.

- The synchrony response of electroreceptors is fast and linear. It reflects the frequencies of a stimulus and changes quickly upon changes therein. Since the mechanism that underlies the response does not require unique properties of the cells, it could also be applied by cells in other sensory modalities for the encoding of fast, transient signals.

- A simple model of spike generation can reproduce the responses of electroreceptors to complex, novel stimuli. This emphasises the linearity of the responses, but also the power of simple neuron models.

- The heterogeneity of the electroreceptor population can be reproduced by varying the parameter values in the model. Different neurons encode different stimuli optimally. suggesting that a heterogeneous population has an advantage over a homogeneous popuation, because it can encode all different naturally occurring stimuli. This indicates that the whole natural stimulus ensemble might put a selective pressure on the development of a neuron population.

- Important aspects of my findings only became evident when taking into account the variability of natural stimuli. This highlights the importance of a detailed observation of the natural sensory environment when characterising a sensory system.

Contributions

Parts of this thesis were carried out in collaboration and have been published in peer-reviewed journals. I here want to indicate the contributions by collaborators and the parts that have already been published.

Chapter 2 builds on a review published in the *Journal of Physiology Paris* (Walz H, Hupé GJ, Benda J, Lewis JE (2012) *J Physiol Paris* 107: 13–25). The parts taken into this thesis – about electrocommunication signals, the physiological results on their encoding and the influence of parameters on chirp production in chirp chambers – were primarily written by me, while the other parts were primarily written by Ginette Hupé. They concerned behaviour under more natural conditions and were left out of this thesis. Jan Benda and John Lewis edited the text. The full publication is added in the appendix.

The single cell recordings shown in **Chapter 3** were done by Jan Grewe and myself in about equal contribution. This chapter has been submitted in a slightly different version to the *Journal of Neurophysiology* under the title "Static frequency tuning properties account for changes in neural synchrony evoked by transient communication signals". The text had in the publication process been edited by Jan Benda and Jan Grewe. The manuscript is currently under review.

The data from single cell recordings used in **Chapter 4** were obtained by Franziska Kümpfbeck and myself. 6 of the 23 cells were recorded by F.K. The model was developed in extensive discussions with Len Maler and André Longtin.

Publications

During the course of this thesis research findings were presented in various form. They are listed in the following.

Publications in peer-reviewed journals

Walz H, Hupé GJ, Benda J, Lewis JE (2013) The neuroethology of electrocommunication: How signal background influences sensory encoding and behaviour in *Apteronotus leptorhynchus*. *J Physiol Paris* 107: 13–25.

Alda F, Picq S, De León LF, González R, Walz H, Bermingham E, Krahe R (2013) First record of *Gymnotus henni* (Albert, Crampton and Maldonado, 2003) in Panama: phylogenetic position and electric signal characterization. *Check List* 9(3): 655–659.

Published Conference Abstracts

Walz H, Grewe J, Benda J (2012) Heterogeneity improves the encoding of natural stimuli in a neuronal population. *Front. Comput. Neurosci. Conference Abstract: Bernstein Conference 2012*

Kümpfbeck F, Grewe J, Walz H and Benda J (2012). Comparative study on the encoding of communication signals in two species of weakly electric fish. *Front. Comput. Neurosci. Conference Abstract: Bernstein Conference 2012*

Grewe J, Sharafi N, Walz H, Lindner B and Benda J (2012). Amplitude Dependency of Synchrony Codes. *Front. Comput. Neurosci. Conference Abstract: Bernstein Conference 2012*

Walz H, Grewe J and Benda J (2012). The impact of heterogeneity on the encoding of natural stimuli in a neuronal population. *Front. Behav. Neurosci. Conference Abstract: Tenth International Congress of Neuroethology*

Walz H, Longtin A, Benda J (2011) Responses to complex novel stimuli can be predicted by a simple neuron model of spike generation. *Front. Comput. Neurosci. Conference Abstract: BC11 : Computational Neuroscience & Neurotechnology Bernstein Conference & Neurex Annual Meeting 2011*

Grewe J, Walz H and Benda J (2011). Coding of electrical signals in different subsystems of the electrosensory system of the weakly electric fish. *Front. Comput. Neurosci. Conference Abstract: BC11 : Computational Neuroscience & Neurotechnology Bernstein Conference & Neurex Annual Meeting 2011*

Walz H, Grewe J, Benda J (2010) Communication signals in a wave-type electric fish are encoded by synchronization and desynchronization depending on the social context. *Front. Comput. Neurosci. Conference Abstract: Bernstein Conference on Computational Neuroscience 2010*

Conference Poster Contributions

Walz H, Grewe J, Benda J (2012) Heterogeneity improves encoding of natural stimuli in a neuronal population. *Bernstein Conference*, Munich, September 2012

Walz H, Grewe J, Benda, J (2012) The impact of heterogeneity on the encoding of natural stimuli in a neuronal population. *International Conference for Neuroethology*, Maryland, August 2012

Walz H, Ender A, Krahe R, Benda J (2012) Electrocommunication and dominance of

wave-type weakly-electric fish in their natural habitat. *Satellite meeting to the ICN "Electric fishes: neural systems, behavior and evolution"*, Maryland, August 2012

Walz H, Grewe J, Benda J (2012) Encoding strategies of communication signals in a weakly-electric fish depend on behavioral context. *HERTIE Winter School*, Obergurgl, January 2012

Walz H, Longtin A, Benda J (2011) Responses to complex novel stimuli can be predicted by a simple neuron model of spike generation. *Computational Neuroscience & Neurotechnology Bernstein Conference & Neurex Annual Meeting 2011*, October 2011.

Walz H, Grewe J, Benda J (2011) Behavioral contexts influence the encoding of communication signals in a weakly-electric fish. *Tagung der Deutschen Zoologischen Gesellschaft*, Saarbrücken, September 2011.

Walz H, Grewe J, Benda J (2011) A synchrony population-code for communication signals in weakly-electric fish depends on social context. *Tagung der Neurowissenschaftlichen Gesellschaft*, Göttingen, März 2011.

Walz H, Benda J (2010) Spike-frequency adaptation plays a different role in decoding communication signals depending on the social context in a weakly-electric fish. *MPI Workshop Spike Frequency Adaptation*, Dresden 2010

Walz H, Grewe J, Benda J (2010) Communication signals in a wave-type electric fish are encoded by synchronization and desynchronization depending on the social context. *Bernstein Conference on Computational Neuroscience*, Freiburg, October 2010.

Walz H, Grewe J, Benda J (2010) Encoding of communication signals at different contexts in a wave-type electric fish. *International Conference on Neuroethology*, Salamanca, Spain, August 2010.

INVITED TALKS

Walz H, Grewe J, Benda J, "The neuroethology of communication signals in the wave-type weakly-electric fish *Apteronotus leptorhynchus*", *Brain and Behaviour Seminar*, Bielefeld, April 2012.

Walz H, Grewe J, Benda J, "The neuroethology of communication signals in the wave-type weakly-electric fish *Apteronotus leptorhynchus*", *Zooglogisches Kolloquium der Universität Bonn*, Bonn, January 2012.

Walz H, Grewe J, Benda J, "Encoding of a communication signal in a weakly electric fish depends on behavioral context", *Satellite meeting "Neuroethology" to the DZG*, Saarbrücken, September 2011.

Walz H, Grewe J, Benda J, "The encoding of small chirps at different contexts", *St. Hilaire meeting on electric fish*, Montreal, Canada, May 2011.

Part I. INTRODUCTION

Preface

Only through their senses do animals have access to information about the external world. In sensory receptors an environmental stimulus is transduced via mechanical or chemical processes into electrical cell activity, extensively processed in subsequent neural networks and transformed into an internal representation. Any behaviour is based on this neuronal representation. The nervous system constitutes a close link between sensation and behaviour. This implies that all neural processing of sensory information takes place with respect to the behavioural relevance. Similarly, any behavioural response to a stimulus is limited by the ability of the nervous system to represent this stimulus. An integrated description of how neural responses and behaviour change during the interaction of an animal with its environment is therefore beneficial for both physiologists and ethologists.

In this thesis I studies the encoding of communication signals in sensory neurons of the weakly-electric fish *Apteronotus leptorhynchus* with a focus on the range of naturally occurring signals. The signal occurs on a background that represents the encounter with a second fish. The background continuously varies the electrocommunication signal as well as the corresponding behaviour. Recent studies had shown that the signal is perceived at all backgrounds. This finding set the starting point for studying the representation of various combinations of background and signal in receptor cells. Information is encoded in a population of these neurons rather than in single cells. I studied the signal encoding in single neurons by electrophysiological recordings and then reproduced population responses by computational modelling.

In this first part of the thesis I will introduce general aspects of neuronal information processing as well as the model system that was used to tackle the questions that were asked in the other parts. It is divided into two parts: The first chapter, “Sensory Coding”, deals with general questions on neural information encoding and how this is influenced by the sensory world. The second chapter is called “Electrosensory System” and introduces the electrosensory system and its communication signals, leading to the specific research questions that were investigated in the thesis.

Chapter 1

Sensory Coding

Characterising the rules that underlie the translation from an environmental variable to neuronal activity is a central goal of neuroscience. Many aspects of this translation are the subject of extensive investigation. In the temporal dimension this concerns the features of single neuron activity that carry information. On the spatial scale the distribution of information over groups of neurons is explored, as is the question of how information is propagated between neurons. Together, the facets of neuronal activity that represent information constitute the neural code. Some of the questions regarding the neural code shall be introduced in this chapter setting the framework for the questions addressed in this thesis. For detailed reviews on information coding see for example Panzeri et al., 2010; Rolls and Treves, 2011.

Opening the introduction will a description on how information can be stored in neural activity. I will start with the different ways single neurons can embed information, proceed with the same for neuron populations and eventually come to the propagation of information between neurons. Along the way noise and heterogeneity in neurons shall be introduced. The last part then deals with the influences that the choice of stimulation paradigm can have on the study of sensory encoding.

1.1 Information Coding in Single Neurons

Single neurons are the building blocks of the nervous system (Cajal, 1899). Since activation of a vast majority of them evokes action potentials and mainly action potentials get transmitted between neurons, patterns of action potentials are regarded as the main carrier of information in the nervous system. A neuron that is stimulated with an appropriate stimulus changes its neural activity in a stimulus-dependant way, thereby encoding the stimulus characteristics. There are, however, several ways in which it could do so and thus many ways in which information could be embedded in the pattern of generated action potentials. I will in the following refer to action potentials as spikes, a

term used equivalently. Temporal series of action potentials are also referred to as spike trains.

The most basic measure of a neuron's activity is the number of spikes the neuron fires in a certain amount of time. A relation between the stimulation and the number of spikes has been the first description of an encoding scheme (Adrian, 1928). Such a code in which the information about a stimulus is encoded in the number of spikes regardless of their temporal pattern is referred to as a "rate code" and many examples of rate coding have been described since then. The intensity of a light flash, for example, correlates directly with the number of action potentials in a retinal ganglion cell (Barlow et al., 1971), the direction of a moving bar corresponds to the response of visual cortical neurons (Hubel and Wiesel, 1959) or the direction of a limb movement with the activity in thalamic neurons (Werner and Mountcastle, 1963).

A stronger stimulus can also decrease the latency of a response (Gollisch and Meister, 2008; Tovée et al., 1993), that is, the time between the onset of stimulus presentation and the neuronal response becomes shorter. This allows information to be encoded in the temporal pattern in which spikes are fired regardless of or in addition to the number of spikes. Besides the latency of the first spike the pattern of inter-spike intervals can also carry information, or the phase of spikes in relation to an underlying oscillation (Singer and Gray, 1995). All such encoding strategies are referred to as "temporal coding".

In response to a static stimulus the distinction between temporal and rate coding is evident. The rate response is simply given by the number of spikes and any aspect of their patterning is a temporal information. In such cases, most information is carried in the rate response (Rolls and Treves, 2011; Tovée et al., 1993). In response to time-varying stimuli, however, the rate also changes over time and one has to define a time window that constitutes the basic unit of the code, in which, for example, spikes are counted, or latency is measured. This time window resembles the time scale in which encoding is assumed to take place within the nervous system and has therefore been called the "encoding time window" (Theunissen and Miller, 1995). The length of the encoding time window is unknown, but the behavioural response sets a lower limit to it, because the encoding has to occur before the response. It also has to be shorter than the stimulus, at least shorter than those aspects of the stimulus that are perceived by the animal. A rigorous definition of a temporal code therefore necessitates that information is contained in frequencies that are higher than those in the stimulus (Theunissen and Miller, 1995).

Neural responses are noisy

What complicates the study of information embedding in spike trains is the high degree of noise inherent to neuronal responses. This means that responses vary in both the rate and the exact timing even if the same stimulus is presented repeatedly (Mainen and Sejnowski, 1995; Tolhurst et al., 1983; Tomko and Crapper, 1974, see Faisal et al., 2008 for a review). Neuronal variability has been attributed to multiple sources. In many

modalities, the stimulus itself is probabilistic. Photons arrive at photoreceptors with a stochastic rate and at low intensities, this accounts for the variability in the activity of sensory neurons (Barlow et al., 1971). Thermodynamic processes influence perception of molecules in smell (Bialek and Setayeshgar, 2005). But the membrane potential of neurons fluctuates even to identical input when all other conditions are fixed, in part because of the stochastic nature of ion channels and synapses (van Rossum et al., 2003). An additional aspect is the background activity of neurons that influences the response to a stimulus. Many neurons are spontaneously active and this activity fluctuates. Whether the neuron is active at stimulus onset or not also influences how strongly it responds to the stimulus (Arieli et al., 1996).

Noise can be beneficial for stimulus encoding

While noise is usually seen as detrimental for signal transmission, it can be advantageous in certain situations. One such condition is referred to with the term "stochastic resonance". It occurs when a threshold-device is activated by a weak stimulus. In such a case, the device transmits a maximum of information about the stimulus with an intermediate degree of noise (Benzi et al., 1981). While the stimulus by itself is not strong enough to bring the system above threshold, noise increases the probability that it does. Still, the probability of reaching the threshold is dependant on the stimulus. When the noise is too high, it becomes the main input to the device. The output of the device then tells less about the stimulus. Since action potentials are triggered only above a threshold, neurons are threshold devices and exhibit stochastic resonance (Douglass et al., 1993; Longtin et al., 1991).

1.2 Population Coding

Although single neurons are anatomically and computationally independant units, the representation and processing of information in vertebrate nervous systems is distributed over groups or networks of cells (for a review, see Pouget et al., 2000). Population coding occurs in all areas of the nervous system. Sensory neurons are selective for certain values of the environmental feature they encode, such as the orientation of a visual stimulus, the frequency of a tone et cetera. The relation between average response and feature value is called the tuning curve of the cell. Tuning curves are usually broad and overlap with those of other cells. This means that a given sensory stimulus (Fitzpatrick et al., 1997; Kilgard and Merzenich, 1999; Wilson and McNaughton, 1993) or an intended motor action (Georgopoulos et al., 1986) influences the activity in a group of neurons rather than in a single cell. The degree to which information is distributed, varies between neuron population of different hierarchical stages and modalities. If only few cells or a single cell are active in response to a given stimulus, the coding is called local, while it is called distributed if many cells are active. Sparse coding has been established as the description of codes that lie in between local and distributed

(Olshausen and Field, 2004). However, since the evidence for local codes in neuronal systems is small, more selective codes are usually referred to as being sparse.

As we have seen for the case of single cells, it is not evident which features of the activity of a neuron population carries information. Again, one can distinguish rate and temporal coding. Information could lie exclusively in the mean firing frequency of the population during a certain time window (Fig. 1.1 A), or in the pattern of spikes among the population. In a latency code, the relative spike latency between different cells would carry information (Gollisch and Meister, 2008). Another temporal aspect of population activity is the synchrony among single cells. When a group of neurons that project to the same target neuron spikes in synchrony, they enhance their impact on that target neuron. It has been shown that the synchrony among cells carries information on a very fine temporal scale in different modalities, from olfaction (Laurent, 1996) to vision (Dan et al., 1998), and that it shapes selectivity in upstream neurons (the locust visual system; Jones and Gabbiani, 2010). In the electrosensory system it has been shown that communication signals change the synchrony of the receptor population (Benda et al., 2005, 2006) and that this is read out by cells in the successive stages of the electrosensory pathway (Marsat and Maler, 2010, 2012; Marsat et al., 2009).

When a stimulus changes the rate of several neurons in a population, this translates into a population rate following the stimulus. The rate averaged over a population of neurons has been shown to carry information in various sensory systems as for example in the olfactory system (Blumhagen et al., 2011; Miura et al., 2012) and in the visual system (Franco et al., 2007), but also in higher cognitive areas (frontal cortex, Pennartz et al., 2011). An advantage of rate coding in populations is that it is fast. The rate in single neurons has to be averaged over a time window, that is at least as long as the minimum interspike interval. In contrast, the population rate can follow the stimulus instantaneous, as it does not have to be averaged over time but can be averaged over cells (Knight, 1972a).

Besides the benefit of a fast rate response, what are other advantages of encoding a stimulus distributed over a population of cells? If the population consists of identical cells that respond with the same selectivity to a stimulus, this resembles a form of redundancy. This already can bear some advantages, for example, because it makes the system more robust against response failures or even the death of neurons. It can also be used for cancelling out noise inherent in the responses by averaging over many cells (Pouget et al., 2000). This is, however, limited by the fact that the variability of cell responses in different cells of one population is often correlated (Zohary et al., 1994). Averaging over responses exhibiting noise correlation significantly impairs information coding (Kohn and Smith, 2005).

In a population of neurons subject to neuronal noise, stochastic resonance occurs even if the stimulus is strong enough to trigger action potentials itself (supra-threshold stochastic resonance described by Stocks, 2000; see Fig. 1.1 B for a demonstration). If the neurons were identical, they would all spike at exactly the same time, thus transmitting the same, redundant, information. A moderate level of noise adds variability to the activity in different neurons. Since the activity is still modulated by the stimulus,

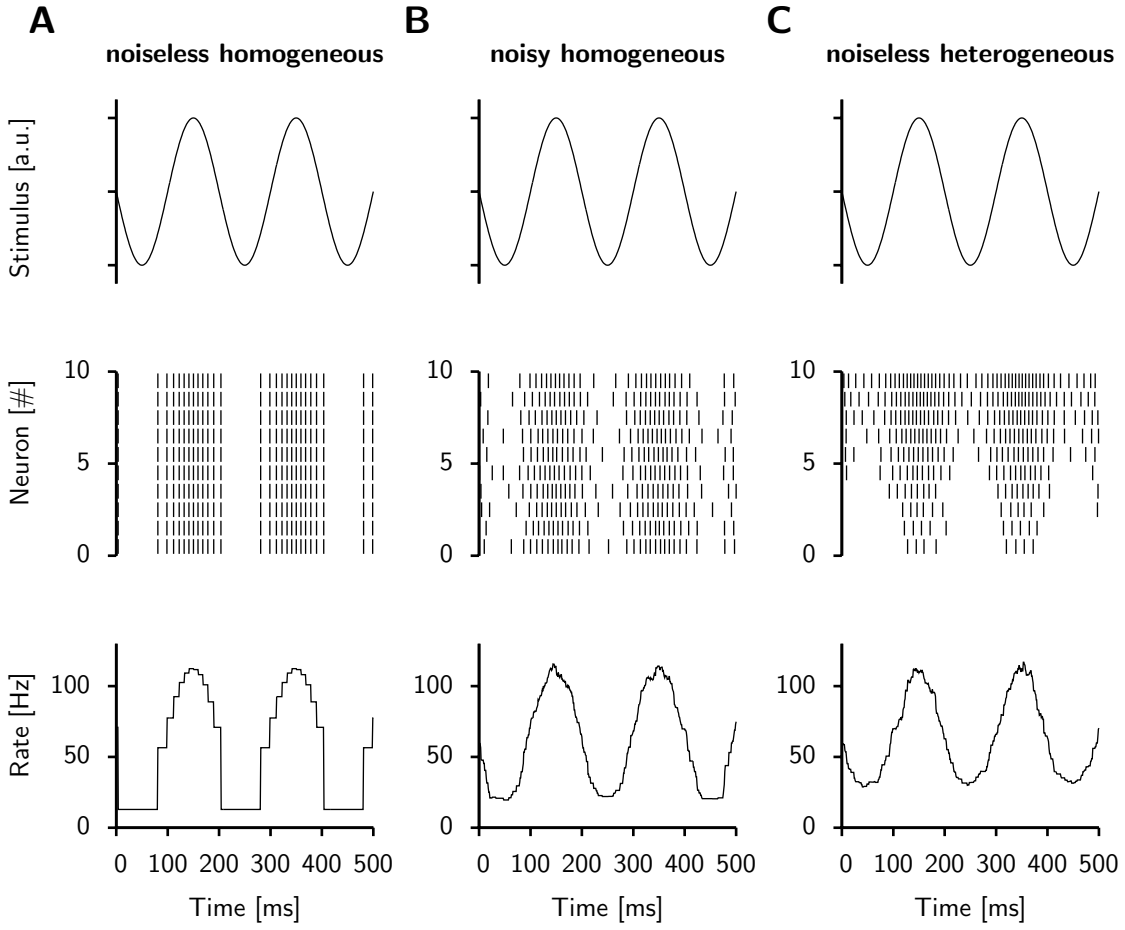

Figure 1.1: Heterogeneity and noise in neuron populations. The response of different populations of leaky integrate-and-fire (LIF) model neurons is simulated in response to a sinusoidal stimulus. The stimulus is shown in the top panels (a.u.=arbitrary units), the middle panels show the spiking responses of individual neurons and the third panel shows the average rate response as derived from the inverse of the interspike intervals from the middle panel. **A** An identical neuron model is simulated repeatedly to replicate a homogeneous population without noise. The rate shows discontinuities and thus considerably differs from the sinusoidal stimulus. **B** The same neuron model is now extended to include a Gaussian white noise current that mimics neuronal noise. The realisation of the white noise is unique in each single model neuron. This model is then stimulated with the same sinusoidal stimulus. The noise smooths out the discontinuities and the rate response now represents the stimulus more closely. **C** The model is simulated with a different mean current every time to simulate a heterogeneous population. Each neuron model is stimulated by the sinusoidal stimulus only, thus resembling a noise-free heterogeneous population. The heterogeneity again smooths out the discontinuities and the stimulus is represented well in the rate response. The dynamics of the membrane potential of a LIF neuron follow the dynamics $\tau_V \frac{dV}{dt} = -V + I$, with t being time, V the membrane potential, τ_V the membrane time constant and I the driving input current. It thus integrates the input with a leak term "-V" to account for the flow of ions over the membrane when the equilibrium state is not reached. When the threshold $V_{\text{threshold}}$ is reached, a spike is noted and V is reset to 0. I in our case was given by the sum of a sine wave stimulus of frequency f, a constant offset current I_{Bias} and a Gaussian white noise current ξ of strength $\sqrt{2D}$ as $I = \sin(2\pi f t) + I_{\text{Bias}} + \sqrt{2D}\xi$. The parameters for all simulations were: $\tau_V = 10\,\text{ms}$, $I_{\text{Bias}} = 13$, $V_{\text{threshold}} = 10$, $D = 0.003$ and $f = 5\,\text{Hz}$. In C, the mean bias current was varied from 8 to 18, such that the mean current remained the same. For the same reason the bias current in B was 12.997.

this increases the information capacity of the population response. If the noise becomes too strong, the response is driven predominantly by the noise and transmits less information about the stimulus.

Populations exhibit heterogeneity

Cells of the same type and from the same population often vary in their stimulus sensitivity (Ringach et al., 2002) as well as in their baseline activity properties (Gussin et al., 2007; Hospedales et al., 2008) giving rise to heterogeneous populations. Similar to supra-threshold stochastic resonance (described in previous paragraph), heterogeneity can increase the information content in a population simply by giving rise to different responses to the same stimulus (see Fig. 1.1 C, Stocks, 2000).

When heterogeneity leads to different responses as described in the last paragraph, this has been referred to as decorrelating responses (Shamir and Sompolinsky, 2006). Neural responses are correlated by common input that can either stem from a stimulus or from shared noise. Peripheral neurons are often correlated mainly by a common stimulus, while downstream neurons also often share the noise, as it originates from background activity in the network. Heterogeneity has been shown to improve information coding in both situations, in the presence of noise correlations, for example in cells of the visual system (Chelaru and Dragoi, 2008) or when correlations mainly originate from shared input as in the olfactory system (Padmanabhan and Urban, 2010).

1.3 Information Propagation

An organisational principle of the nervous system is its modularity, that is the distribution of information over different specialised groups of neurons, nuclei or brain regions. This requires that information is propagated from one group of cells to the next. A prerequisite to a neural code thus is that it can be read out by other neurons (Perkel and Bullock, 1968). The ultimate proof that a certain code is being used by the nervous system includes the description of the read-out in subsequent processing stages. Up to now, information propagation has mainly been studied in computational models (for a review, see Kumar et al., 2010). Interestingly, networks that are well-suited for propagating asynchronous information (van Rossum et al., 2002) differ from those that propagate synchronous information (Diesmann et al., 1999), in which the former refers to signal encoding in firing rate modulations and the latter to temporal coding.

One common feature about the hierarchical organisation of neuronal regions is that the encoding becomes sparser the further downstream in the processing stream the region is located (Barlow, 1972). That the code becomes sparser, implies that neurons further downstream encode fewer features of the stimulus and are thus more selective than those at the periphery (Barlow, 1972). For this, information is often separated into different streams of processing (Nassi and Callaway, 2009). Heterogeneity of cells can lead to a sparse code, in that cells of different characteristics respond to different features

in the response of peripheral neurons (Chechik et al., 2006; Vonderschen and Chacron, 2011; Yang et al., 2012).

1.4 Sensory Environment

A detailed description about the stimulus, that is, the information to be encoded and the time available for the encoding process is necessary when describing the neural code. As mentioned above, the response variability of visual interneurons at their detection threshold could be attributed to the variability in the stimulus (Barlow and Kaplan, 1971). The detailed characterisation of the stimulus thus aided the investigation of encoding. Similarly, the careful observation of behaviour can constrain proposed mechanisms of encoding. In the human visual system, the description of behavioural time scales have led to the prediction that most encoding is done feed-forward, as extensive feedback would require more processing time (Thorpe et al., 1996). Similarly, in olfaction, Uchida and Mainen (2003) showed that robust responses can be very fast, questioning the earlier propositions, that the information increases when processing time is increased. The study of sensory neurons is advantageous in this respect, as stimuli can be described as well as controlled much better than in neurons coding for complexer cognitive tasks, and the perception of stimuli can be assessed in behavioural experiments.

Sensory coding might be optimised to natural stimuli

Many processing mechanisms in sensory encoding have been described using artificial stimuli, such as gratings in the visual or white noise in the auditory system. However, these stimuli differ in first and higher order statistics from the natural stimuli an animal is exposed to and might be optimised to. Developement and evolution shape the functioning of many physiological systems and there is evidence that they also shape the encoding mechanisms of nervous systems. For example, the development of frequency selectivity in the auditory cortex has been shown to be delayed in animals stimulated with white noise only (Chang and Merzenich, 2003). Also, several encoding mechanisms can be related to the selective pressure that the energetic consumption of the nervous system has exerted on its evolution (Laughlin, 2001; Niven and Laughlin, 2008). These finding conformed earlier theoretical predictions that had proposed that coding should be optimised to encode natural stimuli in an energy-efficient way (Barlow, 1972).

Various aspects of sensory coding have been shown to be affected by the statistics of a stimulus. In the visual cortex, precision of spiking correlated directly with the time scale of the stimulus (Butts et al., 2007), and the stimulus statistics influenced spike-time jitter *in vitro* (Mainen and Sejnowski, 1995). Natural stimuli also elicited sparser responses in the visual cortex (Vinje and Gallant, 2000) and in auditory neurons of invertebrates (Machens et al., 2001).

These results imply that stimuli of natural statistics allow for a more realistic description of neural coding. Nevertheless, a description of the natural stimuli is not always straightforward. For example, an animal's active exploration of its surrounding has to be considered. In the visual system this means that head and eye movements have to be taken into account. In active senses such as touch and electrosensation, the movement of the animal actively influences the stimulation. Even if it is known in detail which stimuli an animal passively receives, this does not tell us, whether these are really the ones that are processed and perceived inside the nervous system. This can only be shown by a behavioural response of the animal.

Communication signals are behaviourally relevant [1]

During social encounters, many animals use communication signals to transmit a variety of information, such as individual identity and motivational state, that is used to dynamically modulate behavioural strategies. Across taxa, signals involving mechanical (including acoustic and vibrational stimuli; Hill, 2009; Kelley and Bass, 2010), visual (Osorio and Vorobyev, 2008), chemical (Johansson and Jones, 2007; Stacey et al., 2003) and electric modalities as well as a mixture of them (Bro-Jørgensen, 2010) have been characterised. Responding to these signals appropriately can be crucial for reproductive success, as well as the survival of an individual (Kelley and Bass, 2010). The study of communication offers an optimal framework for studying the encoding of sensory stimuli, in that encoding principles and stimulus sensitivities can be inferred directly from behavioural experiments. Behavioural adjustments produced in response to conspecific simulated communication signals provide evidence that the receiving individual has detected the sensory stimulus.

The accurate detection of communication signals depends crucially on signal encoding by the nervous system which can be limited by internal and external noise (Schmidt et al., 2011; Waser and Brown, 1986). In the auditory and electrosensory systems, communication signals can be produced in the presence of an ongoing background signal that is a consequence of the interaction itself (Kelley and Bass, 2010; Zupanc and Maler, 1993). Different aspects of this background signal, including its frequency and contrast also provide behaviourally relevant information about social context, that is the identity and proximity of interacting individuals (Bastian et al., 2001; Engler and Zupanc, 2001; Yu et al., 2012). In this thesis the encoding of one particular communication signal on all relevant backgrounds was characterised in the electrosensory system of the weakly electric fish *A. leptorhynchus* which will be introduced in more detail in the following chapter.

[1] The rest of the introduction including *Chapter 2* is based on a text previously published in the *Journal of Physiology Paris*. The original paper is included in the appendix.

Chapter 2

The Electrosensory system

Environmental conditions involving low-light and low-electrosensory signal-to-noise ratio set a premium on efficient detection and processing of electrocommunication signals. For decades, studies examining the neurophysiological systems of weakly electric fish have provided insights into how natural behaviours are generated using relatively simple sensorimotor circuits (for recent reviews see: Chacron et al., 2011; Fortune, 2006; Marsat and Maler, 2012). Further, electrocommunication signals are relatively easy to describe, classify and simulate, facilitating quantification and experimental manipulation. Weakly electric fish are therefore an ideal system for examining how communication signals influence sensory scenes, drive sensory system responses, and consequently exert effects on conspecific behaviour.

2.1 Weakly Electric Fish

The weakly electric fish use active electroreception to navigate and communicate under low light conditions (Zupanc et al., 2001). In active electroreception, animals produce an electric field using an electric organ (and this electric field is therefore called the electric organ discharge, EOD) and infer, from changes of the EOD, information about the location and identification of objects and conspecifics in their vicinity (e.g. Kelly et al., 2008; MacIver et al., 2001). However, perturbations result not only from objects and other fish, but also from self-motion and other factors. All of these together make up the electrosensory scene. The perturbed version of the fish's own field on its skin is called the electric image (Caputi and Budelli, 2006), which is sensed via specialised receptors distributed over the body surface (Carr et al., 1982). In the following, we will describe the modulations caused by the superposition of the electric fields of two interacting fish and by the production of specific communication signals.

2.2 Electrocommunication

Electric communication signals can be analysed by measuring properties of the complex electric field that results from the interaction of nearby fish. In *A. leptorhynchus*, the dipole-like electric field (electric organ discharge, EOD) oscillates in a quasi-sinusoidal fashion at frequencies from 700 to 1100 Hz (Zakon et al., 2002) with males emitting at higher frequencies than females (Meyer et al., 1987). The EOD of each individual fish has a specific frequency (the EOD frequency, EODf) that remains stable in time (exhibiting a coefficient of variation of the interspikes intervals as low as $2 \cdot 10^{-4}$; Moortgat et al., 1998). During social encounters, wave-type fish often modulate the frequency as well as the amplitude of their field to communicate (Hagedorn and Heiligenberg, 1985). Several different types of electrocommunication signals have been identified varying in the type and the pattern of frequency and amplitude modulations of the EOD (Zakon et al., 2002; Zupanc, 2002). Communication signals in *A. leptorhynchus* have been classified into two classes: (i) chirps are transient and stereotyped EODf excursions over tens of milliseconds (Zupanc et al., 2006), while (ii) rises are longer duration and more variable modulations of EODf, typically lasting for hundreds of milliseconds to seconds (Hagedorn and Heiligenberg, 1985; Tallarovic and Zakon, 2002). As this thesis exclusively treats the encoding of chirps, rises will not be described further.

Several types of chirps have been distinguished (Zupanc et al., 2006, Types 1–6). Under most experimental conditions, the most commonly produced type is the "small chirp" (Type 2 chirp), with males producing these signals at high rates during agonistic interactions (e.g. Hagedorn and Heiligenberg, 1985; Hupé and Lewis, 2008; Larimer and MacDonald, 1968; Triefenbach and Zakon, 2008). A small chirp is traditionally defined as a short duration (10-20 ms) increase in EODf of about 60-150 Hz (Fig. 2.1A; Engler and Zupanc, 2001; Zupanc and Maler, 1993). The only other chirp type observed frequently across a number of experimental contexts and also studied electrophysiologically, is the "big chirp" (Type 1 chirp), so called because of the much larger increase in EODf (350 Hz, Cuddy et al., 2012; Engler et al., 2000; Zupanc and Maler, 1993). The big chirp is accompanied by a marked decrease in EOD amplitude that is not seen in small chirps.

Beats create an electrosensory background during communication

During the interaction of two wave-type fish, their electric fields superimpose and summate at every point in space. Measured across the skin of each fish, the combined signal consists of a carrier determined by its own EOD with a periodic amplitude modulation (AM) at a frequency equal to the difference of the two individual EODfs, the beat frequency. The beat frequency has been suggested to reflect different aspects of the social encounter (Bastian et al., 2001; Kolodziejski et al., 2007). Crucial to this idea is that EODf correlates with identifying characteristics of the emitting fish including sex and dominance status. Given that EODfs are sexually dimorphic in *A. leptorhynchus*,

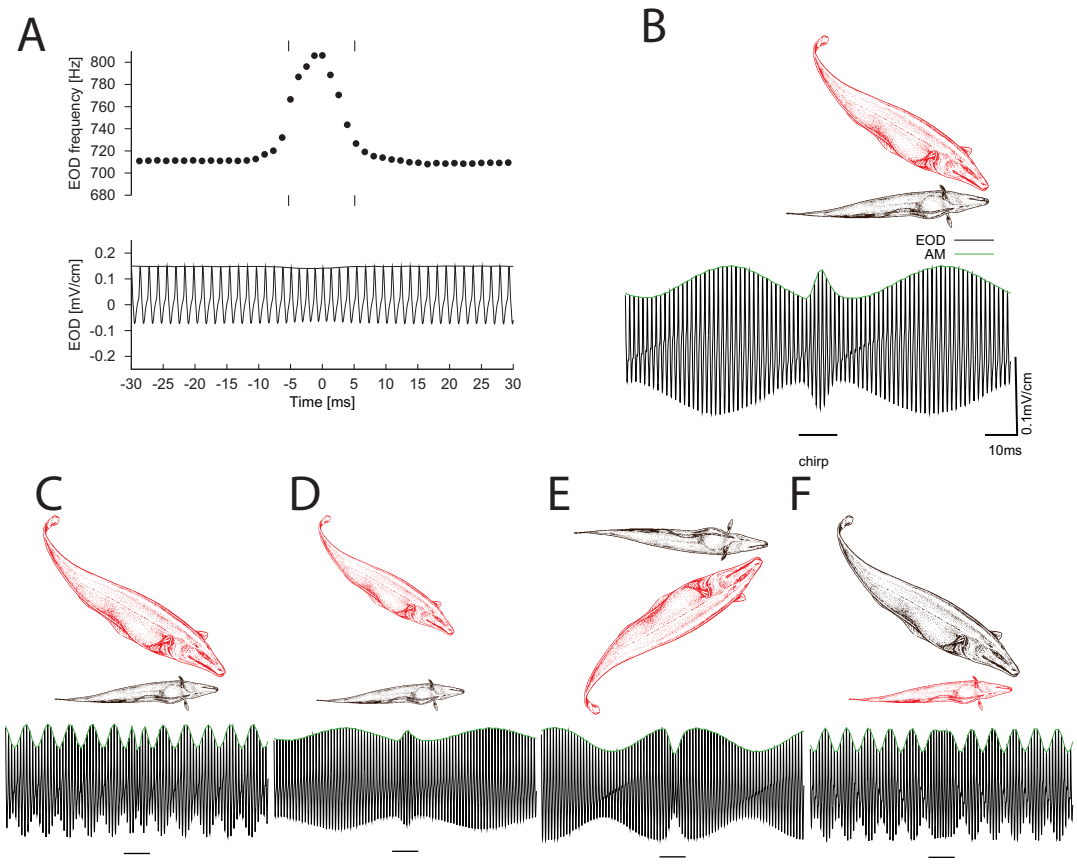

Figure 2.1: Beat modulations induced by chirps during representative encounters between different pairs of fish. A) shows one example of a small chirp. When the instantaneous EOD frequency is plotted over time (upper panel), an increase from around 710 Hz to 810 Hz is seen. The amplitude is almost unchanged during the chirp, as seen when the EOD waveform is plotted over time (lower panel). **B**–**F**) In each scenario, one fish emits the chirp shown in A, but under different simulated background conditions. The sketches of the fish demonstrate the encounter, with the chirping fish shown in red and the size of each fish reflecting its EODf (a higher EODf is indicated by a bigger size). **B**) shows the encounter with a beat frequency of 20 Hz and a contrast of about 40%; **C**) with a beat frequency of 100 Hz and 40% contrast; **D**) shows the same encounter as in B but with a contrast of 20%; **E**) shows an encounter similar to B but at a beat phase shifted 180°; **F**) as in **C**), but the fish with the smaller EODf emits a chirp (the fish sketches are modified from (Hagedorn and Heiligenberg, 1985)).

slower beat frequencies are more common in same-sex interactions. In addition, EODf has been found to be correlated with size and dominance (Dunlap, 2002; Fugère et al., 2011; Hagedorn and Heiligenberg, 1985; Triefenbach and Zakon, 2008), suggesting that the beat frequency also provides information about relative size and dominance status.

The depth of an AM signal (its peak to trough distance relative to the EOD amplitude) is referred to as its contrast. The contrast of the beat, as well as its phase, are determined by the position and orientation of the two fish with respect to each other (Kelly et al., 2008), with contrast decreasing as the distance separating two fish increases (Fig. 2.1 B and 2.1 D depict encounters of different contrast). During social interactions, fish experience increases and decreases in beat contrast due to their own movements and those of interacting conspecifics. More aggressive interactions involve more frequent and longer-lasting approach behaviours that are associated with similar changes in contrast. The contrast also depends on the amplitude of the EODs of both fish. At a given distance, fish with larger EOD amplitudes produce larger contrasts than do fish with lower amplitude EODs. The beat phase varies spatially along the fish's body in a manner that depends on their orientation (i.e. whether fish are positioned parallel or perpendicular to one another; Bullock and Heiligenberg, 1986; Kelly et al., 2008).

Chirps involve brief changes in EODf and thus directly influence the amplitude, frequency and the phase of the underlying beat (Benda et al., 2005; Zupanc and Maler, 1993). Even chirps of the same duration, identical frequency excursion and amplitude modulation can induce very different effects on the composite signal received by the other fish depending on the specific beat parameters (Fig. 2.1). Classically, a small chirp has been described in the context of a slow beat and generated by the higher frequency fish (Fig. 2.1B, for a beat frequency of 20 Hz). In the example shown it causes a fast amplitude upstroke. However, the AM looks different if the underlying beat is fast. The chirp still accelerates the beat, but now does so over multiple beat cycles (Fig. 2.1C, frequency difference of 100 Hz). Because the distance between the two fish influences the contrast, the AM caused by the chirp is smaller when fish are farther apart (compare Fig. 2.1B and D). However, the position of the chirping fish relative to the other fish also plays a critical role: the beat phase is 180°out of phase between the right and left sides of the receiving fish, so the same chirp will occur at two different phases on each side of the body (Fig. 2.1B and E). In all these cases, the chirp is produced by the fish with the higher EODf. A different picture emerges if the chirping fish emits the lower EODf because under these conditions, a chirp transiently decreases the beat frequency and decelerates the beat (Fig. 2.1F). In summary, the beat signal is not simply a static background noise source over which a chirp must be detected, but rather, it dynamically interacts with the chirp signal in a way that depends on social context. Thus, reliably detecting and encoding chirps presents a significant challenge for the electrosensory system.

Chirps are produced at slow beats

"Chirp chamber" experiments, wherein the EOD modulations produced by individual fish restrained in tubes are recorded in response to electrical stimuli (sinusoidal or EOD mimics) of varying frequency and amplitude (Dulka et al., 1995; Engler and Zupanc, 2001; Zupanc and Maler, 1993) have revealed that chirping behaviour is also influenced by the beat background. In these conditions, production rates of small (big) chirps decrease (increase) with increasing beat frequency (Bastian et al., 2001; Engler and Zupanc, 2001) regardless of the sign of the frequency difference. Beat contrast also influences the chirp production rates of fish in chirp chambers. These experiments have suggested that stimulus intensities greater than 50 μV/cm are required to elicit chirp responses in *A. leptorhynchus* (Dunlap et al., 1998; Engler and Zupanc, 2001; Zupanc et al., 2006). Further, chirp production rates of males increase with increasing stimulus intensity i.e. increasing contrast (Engler and Zupanc, 2001; Zupanc and Maler, 1993). Analyses of chirp production with respect to beat phase did not reveal any preference of fish to chirp at certain phases (Walz et al., 2012; Zupanc and Maler, 1993).

When two fish interact electrically or physically, the chirp production pattern of one fish is correlated with that of the other fish (Hupé and Lewis, 2008; Zupanc et al., 2006). Correlation analyses of the instantaneous chirp rates of fish responding to chirps suggest that following chirp reception there is a short-term inhibition of chirping (100-200 ms) which precedes a subsequent period of chirp rate enhancement (Hupé and Lewis, 2008; Salgado and Zupanc, 2011; Zupanc et al., 2006). From a sensory coding perspective, this so-called "echo response" implies that conspecific (or artificial) chirps are discriminated by the sensory system of a receiving individual amongst various background beat modulations. It is thus a convenient measure of sensory detection at the behavioural level. Using EOD playbacks, Salgado and Zupanc (2011) found that 20 ms-long chirp mimics with a frequency increase of just 1.2%, delivered with an interchirp interval of 0.6 s, were sufficient to induce a robust echo response. This indicates that the typical frequency excursion associated with small chirps (50-100 Hz) is at least five times greater than the behavioural threshold for chirp detection. These results were characterised with beat background conditions optimal for chirp encoding: in response to a signal delivered at a high stimulus intensity (mimicking an inter-individual distance of approximately 1-2 cm) with an EODf similar to that of the stimulated fish ($\pm$10 Hz) (Salgado and Zupanc, 2011).

The relationship between chirp rate and beat frequency characterised in chirp chamber studies persists across a number of behavioural scenarios (Dunlap and Larkins-Ford, 2003; Hupé and Lewis, 2008; Zupanc et al., 2006), supporting the hypothesis that small chirps are produced at high rates during stimulus conditions that represent more aggressive same-sex contexts, while big chirps are produced during conditions that signal subordinance (Cuddy et al., 2012). Given that EODf is related to indicators of dominance among males, increased production of small chirps and physical escalation are expected between more closely matched individuals. However, analysis of the chirp echo response has demonstrated that free-swimming fish reciprocate small chirps at

rates significantly greater than chance even during social pairings that result in high beat frequencies (Hupé et al., 2008). This gives evidence that small chirps can be encoded across the range of beat frequencies encountered.

To summarize, the combined signal of beat and chirp depends on both, the parameters of the underlying beat (the background) and those of the chirp. Beat frequency, contrast and phase strongly influence the EOD AM waveform caused by a chirp even of fixed parameters. Small chirps are produced most frequently if the beat frequency is low, corresponding to encounters of fish that are similar in sex and hierarchy, while the analysis of behavioural responses to chirps (echo response) revealed that they are perceived at high beat frequencies as well. Big chirps are produced most frequently when the beat is fast.

2.3 Anatomical Overview of the Electrosensory System

We now turn to the encoding of EOD signals in the nervous system. As all Gymnotiform fish, *A. leptorhynchus* possesses two kinds of electroreceptors on its skin that are activated by electric signals with different properties. Ampullary receptors are tuned to the low frequencies and DC signals associated with the passive electric sense, while tuberous receptors are tuned to the EOD frequency and comprise the active electric sense. Each electroreceptor organ is made up of several electroreceptor cells and innervated by afferents that make up the octavolateralis nerve (Zakon, 1986) projecting to the brain. Among the tuberous receptor afferents, two subpopulations can be discriminated (Scheich et al., 1973): P-type electroreceptor afferents called P-units respond by phase-locking to the EOD, firing an action potential with a probability that depends on the amplitude of the EOD received at the skin surface (Bullock, 1969; Nelson et al., 1997), while T-type electroreceptor afferents fire in response to every EOD cycle at a particular phase in the cycle.

Electroreceptor afferents project to the electrosensory lateral line lobe (ELL) of the hindbrain, the first stage in which electrosensory information is processed in the central nervous system. Here, the axons of P-unit afferents trifurcate to connect to pyramidal neurons in three different maps of the electroreceptive body surface (Carr et al., 1982; Heiligenberg and Dye, 1982), represented in regions called the centromedial segment (CMS), centrolateral segment (CLS) and lateral segment (LS), respectively. A fourth segment, the medial segment (MS) processes information carried by ampullary receptors. There are two main classes of pyramidal neurons in each segment of the ELL. E-cells receive direct input from P-units and are excited when P-units increase their rate (i.e. during EOD amplitude increases), while I-cells receive the P-unit input via disynaptic connections from interneurons and are inhibited by an increase in afferent rate (Maler, 1979; Shumway and Maler, 1989). ELL pyramidal neurons can be further categorised as superficial, intermediate and deep cells based on their morphology and physiology (Bastian and Courtright, 1991; Harvey-Girard et al., 2007).

Pyramidal ELL neurons then project to higher processing areas including the nu-

cleus praeeminentialis (nP) and torus semicircularis (TS, an inferior colliculus homologue, Maler et al., 1991; Metzner and Heiligenberg, 1991; Rose, 2004). nP provides direct and indirect (via the eminentia granularis pars posterior, EGp) feedback that is involved in reafference suppression and enhanced feature detection (Bastian et al., 2004; Berman and Maler, 1998; Bol et al., 2011; Lewis et al., 2007; Requarth and Sawtell, 2011). In the TS, the pyramidal cells of the lateral segment converge together with cells of other types and all four ELL maps (Maler et al., 1982). The TS projects to the tectum, to the diencephalic nucleus electrosensorius (nE), as well as back to nP (Maler et al., 1991; Rose, 2004). The sensorimotor nE integrates convergent electrosensory information and sends projections to two prepacemaker nuclei: the sublemniscal prepacemaker nucleus (sPPn) and the diencephalic prepacemaker nucleus (PPn) that are responsible for controlling the frequency of the EOD set by the medullary pacemaker nucleus (Pn). Spatially specific stimulation of the nE by glutamate iontophoresis results in EODf modulations (rises and chirps) via distinct inputs to the PPn (Rose, 2004). The sPPn and PPn project to the medullary pacemaker nucleus (Pn). The Pn contains electrotonically-coupled pacemaker neurons, whose endogenously oscillating membrane potential sets the EODf, and relay cells which propagate these signals to the electric organ (Smith, 2006; Smith and Zakon, 2000).

The most direct route that information can flow from sensory input to motor output is from electroreceptors to ELL, TS, nE, prepacemaker nuclei and then to the pacemaker nucleus. This direct route is indeed thought to form the basis of the jamming avoidance response (JAR Bullock and Heiligenberg, 1986; Rose, 2004), a behaviour fish show when encountering conspecifics with similar EODfs. During the JAR fish raise or lower their EODf in order to maintain sensitvity for prey induced changes of the EOD amplitude.

2.4 Encoding in the Electrosensory Periphery

In this thesis, encoding of communication signals was studied in P-units. Their response characteristics are described in more detailed now. Under baseline conditions, P-units are exposed to their own EOD of constant amplitude (see Fig. 2.2). In this situation, they fire irregularly at a certain baseline rate. Action potentials occur approximately at a certain phase of the EOD cycle, they are phase-locked to the EOD, but only with a certain probability to each cycle. The baseline rate differs from cell to cell (compare the two example cells in Fig. 2.2 A and B, Gussin et al., 2007), as does variability in their baseline discharge. The probabilistic nature of their activity leads to a high degree of noise, but the exact strength of the noise is different for each P-unit. Since tuberous receptors are distributed over the whole body and the EOD spans the whole surrounding, all P-units of a given animal are stimulated with a similar stimulus (see Kelly et al. (2008) for an exact model of the EOD). Their noise sources are, however, uncorrelated (Chacron et al., 2005b). This means, that stimuli are encoded in P-units in a heterogeneous population of cells subject to extensive neuronal noise.

The probability of emitting a spike at a certain EOD cycle depends on the ampli-

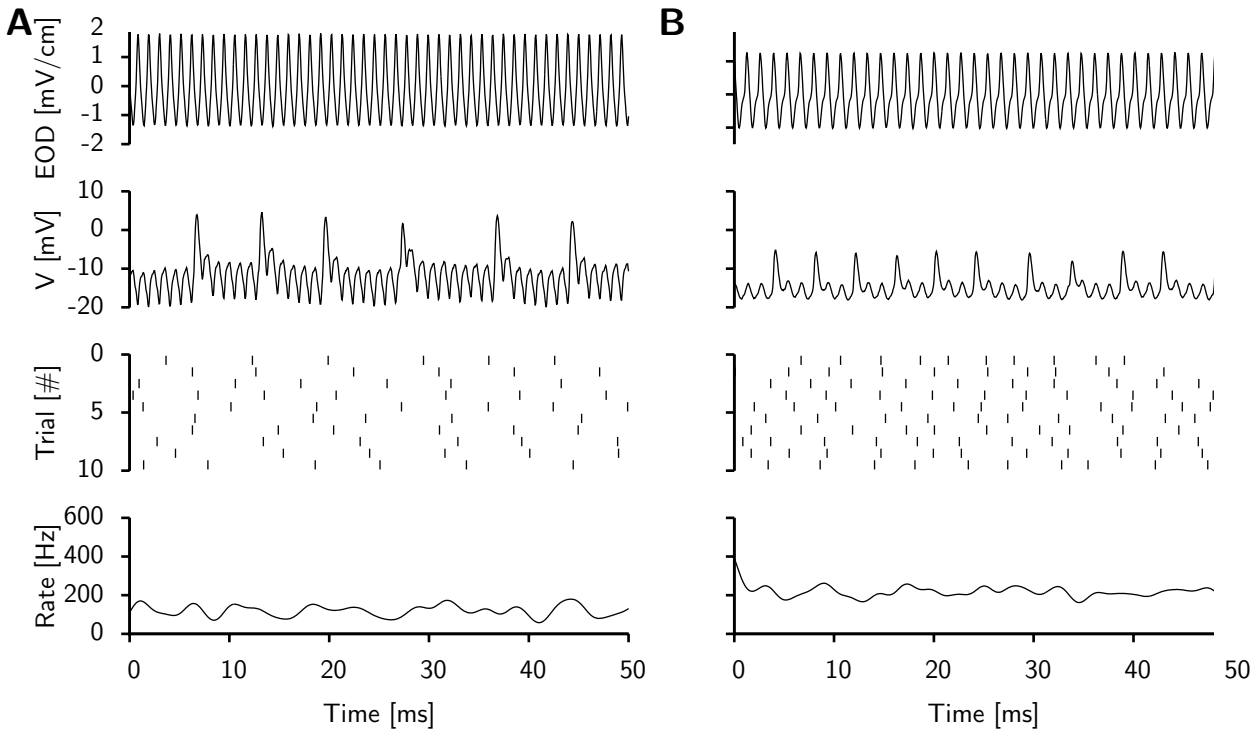

Figure 2.2: P-unit activity under baseline conditions. Two P-units (**A** and **B**) were recorded semi-intracellularly driven by their own constant EOD. The EOD is shown in the top panel, the potential recorded semi-intracellularly in the second row. From this trace, spikes are detected and different segments are aligned as trials such that the phase of the EOD is the same over trials (third row). The spiking response is convolved with a Gaussian kernel of 1 ms width and averaged over trials to obtain a rate response (fourth row). The two cells are from two different recording sessions in which the EOD differed in frequency (A:920, B:745Hz) and amplitude(A: 1.58 mV, B: 1.13 mV). The cells differ in baseline discharge rate (A: 120, B: 213 Hz) and variability (coefficient of variation of interspike interval histograms: A: 0.22, B: 0.23).

tude of the EOD making P-units responsive to amplitude modulations (Fig. 2.3). The response thereby fluctuates around a mean rate that is approximately constant. In response to a step increase in EOD amplitude, P-units exhibit pronounced spike frequency adaptation (Benda et al., 2005; Chacron et al., 2001b; Nelson et al., 1997; Xu et al., 1996). Spike-frequency adaptation involves a strong peak in firing response to the onset of a constant stimulus, followed by a decrease to a lower steady state response. Thus, adaptation acts as a high-pass filter, reducing the response to low stimulus frequencies, such as beat frequencies lower than about 25 Hz (Benda et al., 2005; Nelson et al., 1997; Xu et al., 1996). P-units therefore exhibit a band-pass tuning, i.e. they are most responsive to intermediate AM frequencies (of 30-100 Hz), while the response is weaker to lower and higher frequencies and this tuning is thought to be similar over cells (Wessel et al., 1996). Savard et al. (2011) showed that information is contained in the response at frequencies higher than the stimulation frequencies, indicating that the temporal structure of the spike trains is used to encode information about the stimulus. The synchrony in the spike responses across neurons has been shown to carry information about chirps (Benda et al., 2006; Marsat and Maler, 2010).

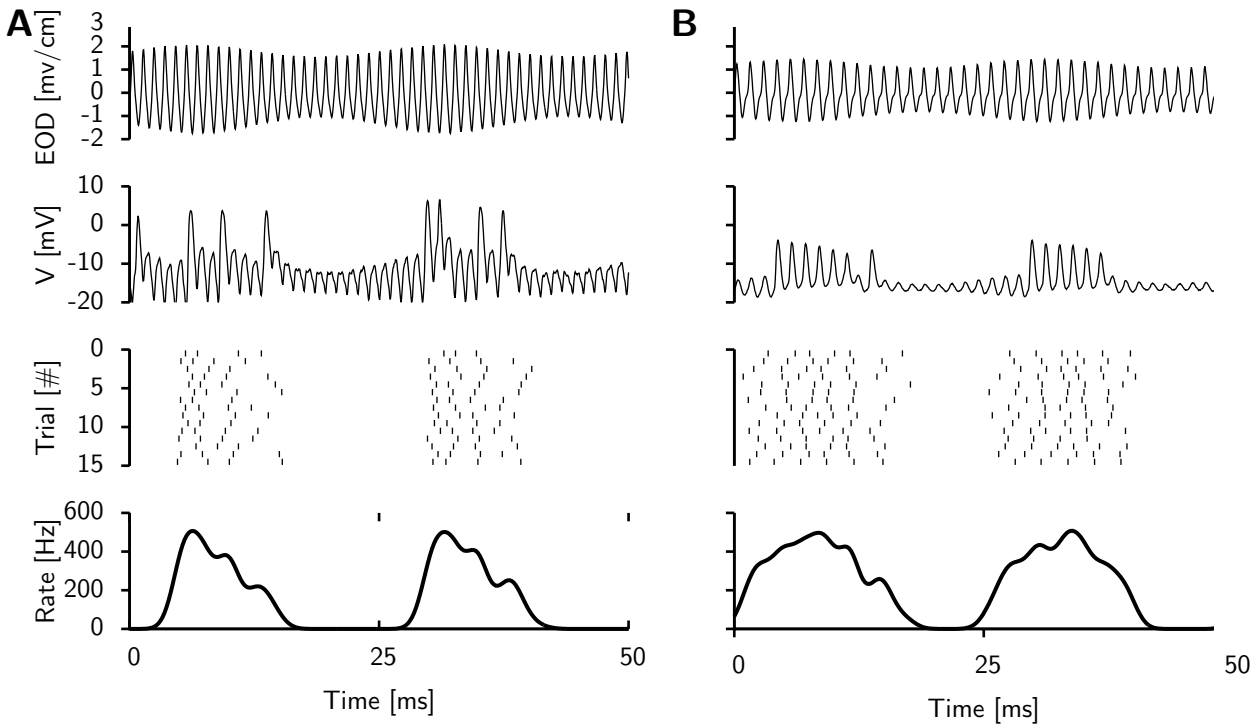

Figure 2.3: P-unit activity under stimulation. The same cells as in Fig. 2.2 were recorded under stimulation with a sinusoidal AM of $\Delta f = 40\,\text{Hz}$ and 20% contrast. The figure is organised as Fig. 2.2. The spike and rate responses of the cells follow the sinusoidal stimulus with high firing rates at the peaks and low firing rates at the troughs of the sinusoidal AM.

The information encoded by P-units is separated into different streams already at the first projection site, the ELL. Stimuli of different spacial extend are processed differently (Chacron et al., 2005b), as are those that increase or decrease P-unit activity. At sub-

sequent processing stages the information is further separated and responses become sparser (Chacron et al., 2011).

2.5 Chirp Encoding

In contrast to those in other species (Eigenmannia, see Hopkins, 1974; Metzner and Heiligenberg, 1991; Naruse and Kawasaki, 1998), *A. leptorhynchus* chirps do not contain DC components and are thus thought to be encoded by tuberous only. To date, encoding of small chirps has mainly been studied when occurring on a slow beat, i.e. the conditions of most frequent chirp production, and when emitted by the signal carrier of higher EODf. When produced by the higher frequency fish, chirps transiently increase the frequency content of the beat signal such that adaptation is transiently overcome. The result is a strong response similar to those evoked by the onset of a constant stimulus – provided the chirp is emitted during a sufficiently slow beat background. The increase of the EOD frequency associated with big chirps is so large that they decrease the rate as well as the synchrony of P-units regardless of the underlying beat frequency (although there seems to be an increase in single unit reliability at beat frequencies of less than 10 Hz, Benda et al., 2006); this effect is enhanced by the concomitant decrease in EOD amplitude typical of big chirps. The enhanced response to small chirps at slow beats, as well as the decrease in response to small and big chirps at fast beats, are seen in measures of the firing rate as well as in measures of synchronisation (Benda et al., 2006).

The next processing stage is the electrosensory lateral line lobe (ELL). As a consequence of differential ion channel distributions (Ellis et al., 2007; Mehaffey et al., 2008) as well as different connectivity to the afferent neurons (Maler, 2009), E-cells of all three segments exhibit very different response properties to P-unit inputs. From the CMS to the LS, neurons are increasingly responsive to higher frequency AMs (Krahe et al., 2008) and have larger receptive fields. Both characteristics, high-pass frequency tuning and large receptive fields, make neurons of the LS most responsive to communication signals (Marsat et al., 2009); compared to signals encountered during navigation and hunting, communication signals are much higher in frequency and more spatially broad. Not surprisingly, the LS has been shown to be crucial for communication behaviour (Metzner and Juranek, 1997). Feedback to the ELL from nP and EGp plays an important role in chirp encoding. Superficial E-cells of the LS respond with a highly reliable and synchronous burst of spikes to small chirps emitted at slow beats (Marsat et al., 2009). The second spike of the burst is not phase-locked to the EOD, indicating that it is not caused by input from P-units. The bursting mechanism relies on a depolarising after potential (DAP) that stems from backpropagating action potentials from the dendrites (Marsat and Maler, 2012; Turner et al., 2002). In these cells, the indirect feedback from EGp provides a negative image of a low frequency beat (Bastian et al., 2004). During an ongoing beat, feedback and input are antiphase but the chirp shifts the phase of the beat stimulus. When this occurs, the feedback coincides with the DAP and a spike in

response to a chirp is more likely to be followed by a second one (Marsat and Maler, 2012). Such bursts may facilitate chirp detection, similar to many systems where bursts enhance signal detection by increasing the signal-to-noise ratio (for a review, see Krahe and Gabbiani, 2004). The feedback, however, is only present in response to beats of frequencies up to 20 Hz (Bastian et al., 2004; Bol et al., 2011). The enhancement of the ELL response by feedback to small chirps is therefore likely to be even more confined to low beat frequencies than the P-unit response. Big chirps are encoded by a strong increase in firing rate in I-cells of all maps and types (superficial, intermediate and deep, Marsat et al., 2009). This is expected since they cause a decrease in the response of P-units and because, in contrast to E-cells, I-cells of different maps and morphology do not show strong differences in frequency tuning (Krahe et al., 2008).

The main target area of the ELL for further information processing is the TS. TS cells can be grouped into two categories according to their baseline firing rate and selectivity to different chirp stimuli (Chacron et al., 2011; Vonderschen and Chacron, 2011). One category, the densely coding neurons, produce responses that resemble those of ELL pyramidal cells, while cells in the other category respond much more sparsely, i.e. with a higher selectivity. Compared to the densely coding TS cells and ELL pyramidal cells, sparsely coding TS cells do not respond during the beat and respond similarly to chirps with certain attributes, but not at all to those with others (see also Fig. 2 in Vonderschen and Chacron, 2011). This population of TS cells can thus, in principle, detect the presence of certain categories of chirps and differentiates between them. How this selectivity arises is currently unknown. The synapses between ELL pyramidal cells and TS neurons show pronounced short-term synaptic plasticity that can act as a temporal filter passing low or high frequencies (Fortune and Rose, 2000, 2001 shown for Eigenmannia). This synaptic plasticity has been shown to create direction selectivity to moving electrosensory images in TS neurons (Chacron and Fortune, 2010; Chacron et al., 2009). Whether synaptic plasticity sharpens responses to chirps is unknown. Cells that respond selectively to chirps are not direction selective and *vice versa* (Vonderschen and Chacron, 2011).

Aim of this Study

The high diversity of AM patterns generated by a chirp on different background beats and the observation of recent behavioural studies that chirps are perceived by fish at all these beats (Hupé et al., 2008) was the initial point to study chirp encoding in P-units at more diverse backgrounds. This is the topic of the first research project (Chapter 3). I looked at the encoding of one small chirp at a wide range of naturally relevant beat parameters. I then reproduced the response pattern we found in this chapter by a computational model which was the subject of the second research project (Chapter 4). I focused on the frequency tuning of P-units, as this was shown to be crucial for chirp encoding. Since the model reproduces the responses of various individual P-units, I used it in the third research project to generate heterogeneous model populations that

resemble natural P-unit populations (Chapter 5). With these I then studied the effect of heterogeneity on chirp encoding in P-unit populations.

Part II. RESEARCH PROJECTS

Chapter 3

Chirp Encoding at Diverse Background Beats

3.1 Introduction

The correct decoding of communication signals in aggressive and mating contexts is crucial to an animal's survival and reproductive success. Not surprisingly, the perception of communication signals happens robustly, even though their characteristic features often only last milliseconds (e.g. Salgado and Zupanc, 2011; Vernaleo and Dooling, 2011). They occur in social situations in which interfering signals from different individuals make decoding particularly hard (Cherry, 1953; McKibben and Bass, 1998; Zupanc and Maler, 1993).

In electrocommunication of *A. leptorhynchus*, the beating background constitutes a signal that might interfere with the perception of the actual communication signal (Chapter 2, (Zupanc and Maler, 1993)). Encoding of small chirps in P-units has until now only been looked at when the chirp is emitted by a fish carrying an EOD of slightly higher EOD frequency (EODf) than the receiving fish (Benda et al., 2005, 2006; Hupé et al., 2008). This creates a background beat of low frequencies under which chirps are emitted at highest rate (Bastian et al., 2001; Engler and Zupanc, 2001). In this situation P-unit afferent neurons respond to a chirp with a strong increase in their response that can be explained by a release from adaptation (Benda et al., 2005). However, adaptation can only explain chirp responses on backgrounds of frequencies lower than 25 Hz, as the cutoff of the adaptation is around this frequency. Behavioural studies have shown that fish respond to chirps irrespective of the background (Hupé et al., 2008). The background beat influences the signal generated by an emitted chirp (Fig. 2.1, Walz et al., 2012). Together, these findings led us to ask how P-units encode small chirps at all naturally occuring backgrounds.

We start out with describing in detail the signals chirps elicit at different background beats. Our single unit as well as whole nerve recordings demonstrate that the chirp

either synchronises or desynchronises the population of P-unit receptor afferents depending on the beat frequency. This results into a division of the representation of the chirp on the receptor level into four coding regimes. We finally demonstrate that the rapid responses of the cells to chirps can be predicted based on their frequency tuning curves and that the position of the chirps within the beat only plays a role at low beat frequencies.

3.2 Material and Methods

In-vivo electrophysiology

Intracellular as well as whole nerve recordings were made from the anterior part of the lateral line nerve of 50 Brown Ghost Knifefish (*Apteronotus leptorhynchus*, Gymnotiformes) of either sex (52 in total, 46 for intracellular and 6 for whole nerve recordings, 12–16 cm body length, EOD frequency between 602-948,767.3+/-96.87). First, fish were anesthetised with MS-222 (120 mg/l; PharmaQ; Fordingbridge, UK) and a small part of the skin was removed atop of the lateral line just behind the skull under additional local anesthetics with Lidocaine (2 %; bela-pharm; Vechta, Germany). For the recordings fish were immobilised (Tubocurarine; Sigma-Aldrich; Steinheim, Germany, 25–50 µl, of 5 mg/ml solution), placed in a tank, and respired by a constant flow of water through their mouth. The water in the experimental tank ($47 \times 42 \times 12$ cm) was from the fish's home tank with a conductivity of about 300 µS/cm and kept at 28 °C. All experimental protocols were approved and complied with national and regional laws (file no. 55.2-1-54-2531-135-09).

For intracellular recordings of P-unit afferents we used standard glass microelectrodes (borosilicate; 1.5 mm outer diameter; GB150F-8P, Science Products, Hofheim, Germany) pulled to a resistance of 50–100 MΩ (Model P-97, Sutter Instrument Co., Novato, CA, USA) and filled with a 1 M KCl solution. Electrodes were advanced into the nerve using microdrives (Luigs-Neumann; Ratingen, Germany). Potentials were recorded using the bridge mode of the SEC-05 amplifier (npi-electronics GmbH, Tamm, Germany) and low-pass filtered at 10 kHz.

Spikes were detected online as peaks that exceeded a dynamically adjusted threshold value above the previous detected trough (Todd and Andrews, 1999). To track changes in amplitude of the recorded spikes, the threshold was set to 50 % of the amplitude of a detected spike, but not below a minimum threshold that was set above the noise in the recording based on a histogram of all peak amplitudes. Trials with bad spike detection were discarded from further offline analysis.

Population activity in whole nerve recordings was measured using a pair of hook electrodes of chlorided silver wire. Recorded signals were differentially amplified (gain between 200 and 2000) and band-pass filtered ($2 - 5000$ Hz passband, DPA2-FX, npi-electronics, Tamm, Germany). The strong EOD artifact in this kind of recording was

eliminated prior to further analysis by applying a running average of the size of one EOD period (Benda et al., 2006).

The EOD of the fish was recorded between its head and tail using a pair of vertical carbon rods (11 cm long, 8 mm diameter, electrophysiology), amplified 200 to 500 times and band-pass filtered ($3 - 1500$ Hz passband, DPA2-FX, npi-electronics, Tamm, Germany). These electrodes were placed isopotential to the stimulus field (see below) to eliminate contamination with the stimulus. During electrophysiological experiments the actual stimulus driving the receptor cells was estimated by recording the voltage between a pair of silver wires (1 cm apart) placed perpendicular to the trunk of the fish, thus approximating the transdermal voltage (amplification 200 to $500\times$, band-pass filtered with $3 - 1500$ Hz passband, DPA2-FX, npi-electronics, Tamm, Germany).

For online spike and EOD detection, stimulus generation and calibration, as well as pre-analysis and visualisation of the data, we used the ephys, efield, and efish plugin sets of the software RELACS (www.relacs.net) running on a Debian Linux computer. All recorded data were digitised using a data acquisition board (PCI-6229; National Instruments, Austin TX, USA) at a sampling rate of 20 kHz.

Stimulation

Electrical stimuli were applied using a pair of stimulation electrodes (carbon rods, 30 cm long, 8 mm diameter) placed on either side of the fish parallel to its longitudinal axis. Stimuli were computer-generated and passed to the stimulation electrodes after being attenuated to the right amplitude and isolated from ground (Attenuator: ATN-01M, Isolator: ISO-02V, npi-electronics, Tamm, Germany).

The EOD of a second fish can be mimicked by stimulating directly with a sine wave of an appropriate amplitude and frequency. The superposition of this stimulus with the EOD of the fish from which we recorded results in a beat (Chapter 2), a periodic amplitude modulation (AM) with a frequency given by the difference between the frequencies of the stimulus and the EOD of the fish, the difference frequency Δf_{Beat}. We set its amplitude A to 10 or 20 % of the amplitude of the fish's EOD. Chirps can be mimicked by Gaussian frequency and AM of the stimulating sine wave. The time-dependant difference frequency $\Delta f(t)$ between stimulus and EODf then follows

$$\Delta f(t) = \Delta f_{\text{Beat}} + s \cdot \exp\left(-\frac{t^2}{2\sigma^2}\right) , \tag{3.1}$$

where Δf_{Beat} is the difference frequency of the underlying beat, s is the maximal frequency excursion during the chirp (its size), and $\sigma = \Delta t/\sqrt{2\ln 10}$ sets the width of the chirp, Δt, at 10% height of the Gaussian modulation. We used chirps of $s = 60$ or 100 Hz and $\Delta t = 14$ ms. The amplitude was decreased by a Gaussian of the same width by maximally 2 % of the baseline amplitude (see Fig. 3.1 for a schema of a small chirp). The sine wave stimulus including the chirp leads to a specific AM of the EOD with a frequency following Eq. 3.1 that is encoded by the P-units.

Alternatively to the direct stimulation, any AM can be obtained by multiplying the intended AM with the fish's own EOD (multiplicator: MXS-01M, npi-electronics, Tamm, Germany) and playing the multiplied signal back via the stimulation electrodes. In order to generate the AM resulting from the superposition of the EOD of a fish emitting a chirp at time $t = 0$ and a receiving fish we computed the AM according to

$$AM(t) = A(t)\cos(\Delta\phi(t)) \quad , \tag{3.2}$$

where

$$\Delta\phi(t) = 2\pi \int_{-\infty}^{t} \Delta f(t')\, dt' = 2\pi\Delta f_{\text{Beat}} t + 2\pi s\sigma \int_{-\infty}^{t/\sigma} \exp(-z^2)dz + \Delta\phi\,, \tag{3.3}$$

is the phase of the beat as the time integral over the frequency difference of the two EODs. The first term models the beat resulting from the superposition of the two EODs with frequency difference Δf_{Beat}. The second term accounts for the Gaussian increase of the difference frequency during the chirp. $\Delta\phi$ determines at which phase of the beat cycle the chirp occurs — it is zero at the peak of a beat cycle. In addition the EOD amplitude was decreased by a Gaussian of the same width and centered at time $t = 0$ by 2 %.

A single stimulus of a given Δf_{Beat} was composed of chirps at ten different phases of the beat (every 36 °). At least 200 ms or one beat period, whichever was larger, separated the chirps. Each such stimulus of ten chirps was repeated 16 times. Then the next stimulus with a different difference frequency, contrast, or chirp size was played. After recording, chirps evoked by the same stimulus were grouped according to the measured phase of the beat at which they occurred. Because of slight changes in EODf of the fish, the phase of a chirp within a beat cycle can vary when using direct stimulation, so that instead of exactly 16 we got between 10 and 20 responses to each chirp of a given phase.

Both the direct and the AM stimuli primarily elicit responses in P-unit electroreceptors. Since we found no differences in the evoked effects on the cells, data from both stimulation paradigms were pooled (Benda et al., 2005). We also pooled data over both contrasts used (10 and 20 %), since we did not obtain different results when analyzed separately.

Chirp encoding analysis

The time course of the firing rate (the PSTH) was computed by convolving each spike train with a Gaussian kernel with a standard deviation of 1 ms and averaging over trials. We chose 1 ms as our default kernel since it corresponds to the fast excitatory component of post-synaptic potentials evoked by P-units in their target cells, the pyramidal cells in the ELL (Berman and Maler, 1998). We also tested different kernel widths and found small quantitative, but no qualitative differences (not shown).

We calculated the response during beat and chirp by averaging within two time windows, one located during the beat before the presentation of a chirp and the other one

centered around the chirp. For the size of the analysis window for responses to the beat we took the largest integer multiple of the beat period smaller than 60 ms but at least one full beat period for beat cycles longer than 60 ms. The window for chirp response analysis spanned the width of the chirp stimulus (14 ms) stretched by a factor of 1.2, and was shifted by 5 ms with respect to the time of stimulus application to account for neuronal delays. The firing rate response in each time window was assessed as the modulation depth of the firing rate, i.e. the standard deviation of the PSTH. The population activity recorded from the lateral line nerve was similarly assessed by calculating the standard deviation of the recorded voltage.

The average correlation between pairs (i, j) of spike trains, as a measure of synchrony, was quantified by means of the correlation coefficient

$$r_{ij} = \frac{\langle (s_i - \langle s_i \rangle_t)(s_j - \langle s_j \rangle_t) \rangle_t}{\sqrt{\langle (s_i - \langle s_i \rangle_t)^2 \rangle_t} \sqrt{\langle (s_j - \langle s_j \rangle_t)^2 \rangle_t}} \,, \tag{3.4}$$

where s_i and s_j are two spike trains convolved with a Gaussian kernel with a standard deviation of 1 ms (see above) and $\langle ... \rangle_t$ denotes averaging over time. The r_{ij} are then averaged over all possible pairs of spike trains recorded in one cell in response to a specific stimulus.

To assess the effect of chirps at different beats we calculated the chirp selectivity index (CSI, see Vonderschen and Chacron, 2011) as

$$CSI = \frac{r_{\text{chirp}} - r_{\text{beat}}}{r_{\text{chirp}} + r_{\text{beat}}} \tag{3.5}$$

where r_{chirp} is the response (standard deviation of the firing rate or of the population activity, or spike-train correlation) during the chirp and r_{beat} the response during the beat. The CSI is greater than zero when chirps increase a cell's response, and less than zero if they decrease the response relative to the response evoked by the beat. Note that the CSI yields qualitatively similar results to that of the chirp gain ($r_{\text{chirp}}/r_{\text{beat}}$) used in previous studies (Benda et al., 2005, 2006).

Chirp Discrimination Analysis

The distance between two spike trains was quantified using a spike train metric according to

$$d^2(s_i, s_j)_{\tau_c} = \frac{1}{\tau_c} \int_{t_1}^{t_2} [s_i - s_j]^2 \, dt \tag{3.6}$$

where s_i and s_j are two spike trains convolved with an alpha-function of width τ_c that we varied from 1 to 100 ms (van Rossum, 2001). We examined P-unit responses on two different integration intervals: one ranging from $t_1 = -10$ ms to $t_2 = 25$ ms contained only the chirp response, while the other ranging from $t_1 = -10$ ms to $t_2 = 100$ ms in addition contained the beat context.

We then asked whether the responses to chirps occurring on different beat phases are distinguishable. For this we constructed confusion matrices by assigning each spike train to the chirp stimulus at the beatphase that evoked a set of responses this spike train had the minimal distance (eqn. 3.6) to. Responses would be optimally distinguishable based on the stimulus, if each spike train was assigned to the stimulus it was evoked by and thus this matrix only had values different from zero on the diagonal. The discriminability can be quantified by the mutual information, MI, contained in this confusion matrix, which is calculated according to

$$\mathrm{MI} = \sum_{b=1}^{k} \sum_{a=1}^{k} \mathrm{p}(b|a) \log_2 \frac{\mathrm{p}(b|a)}{\mathrm{p}(a) \cdot \mathrm{p}(b)} \tag{3.7}$$

where $p(a)$ is the fraction of trials in which the chirp was delivered at a certain beat phase a and $p(b)$ is the fraction of responses that was assigned as having been evoked by beat phase b. $p(b|a)$ is the fraction of responsed that was assigned to beat phase b, although having been elicited by a. The $k = 10$ phase bins each cover $36\,^\circ$. We normalised the mutual information by its maximum, such that it ranges from zero to one, with higher values resembling better discriminability.

3.3 Results

Amplitude modulations caused by small chirps

Small chirps (Engler et al., 2000) are short EOD modulations of a small Gaussian-shaped frequency excursion ranging from a few tens up to about 150 Hz (the size of a chirp s) and lasting for around 10–20 ms (its width Δt; Bastian et al., 2001; Engler et al., 2000; Engler and Zupanc, 2001; Kolodziejski et al., 2007, see Fig. 3.1 A, B). At a receiving fish, the superposition of its own EOD with the smaller EOD of the more distant chirping fish results in a characteristic amplitude modulation (AM) of its EOD (Fig. 3.1 C).

However, the AM caused by a chirp strongly depends on the difference frequency of the underlying beat, Δf_{Beat}, indicating the social context, as well as on the phase, $\Delta\phi$ within the beat cycle at which the chirp occurs (Fig. 3.2). The time course of the AM (first and third column) is determined by the phase difference between the two EODs (middle column). During a beat the phase difference in- or decreases with constant slope. This slope is set by the difference frequency $\Delta f(t)$ between the EODf of the chirping and the EODf of the receiving fish. The absolute value of Δf_{Beat} is the frequency of the resulting beat AM. Throughout this paper we calculate Δf as the frequency of the communicating fish, EODf_2, (i.e. the frequency of the stimulus) minus the frequency of the receiving fish, EODf_1. Thus, Δf is positive if the stimulation frequency is above the EODf of the recorded fish. A chirp always constitutes an increase in EODf_2. Therefore, the transient change in $\Delta f(t)$ that a chirp induces depends on both the value and the sign of the beat Δf_{Beat}.

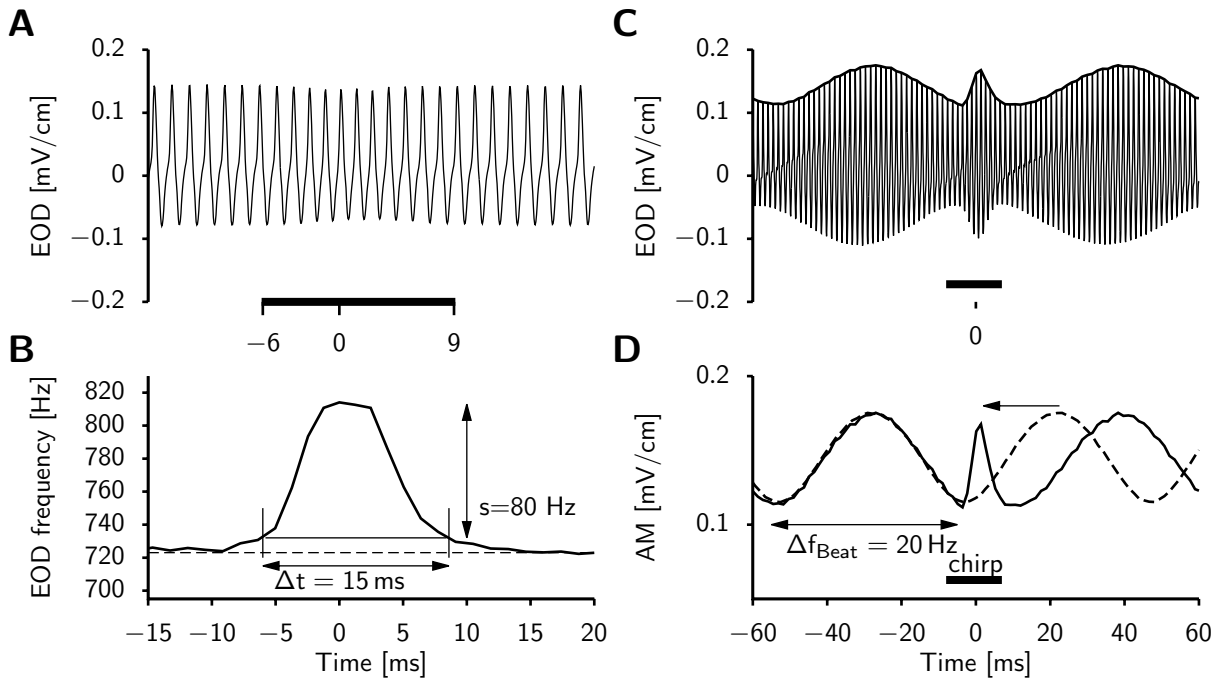

Figure 3.1: A small chirp and its effect on the amplitude modulation sensed by a receiving fish. A) EOD waveform of a single fish during a small chirp. Chirp beginning and end are defined as the times the EODf excursion exceeds $10\,\%$ of the chirp size s and are indicated by tic marks and black bar. **B**) EOD frequency during the chirp. s is the maximum deviation from baseline EODf (vertical arrow). The horizontal arrow shows the chirp width. **C**) Resulting EOD waveform close to a receiving fish that has an EOD frequency of $20\,$Hz below the chirping fish (thin line) and its amplitude modulation (AM, thick line). The chirp alters the AM form (black bar). **D**) Without the chirp the AM would be an ongoing beat (dashed line) with frequency given by the difference, Δf_{Beat}, of the two EODf. The chirp (black bar) transiently increases $\Delta f(t)$ for less than a full period of the beat (solid line).

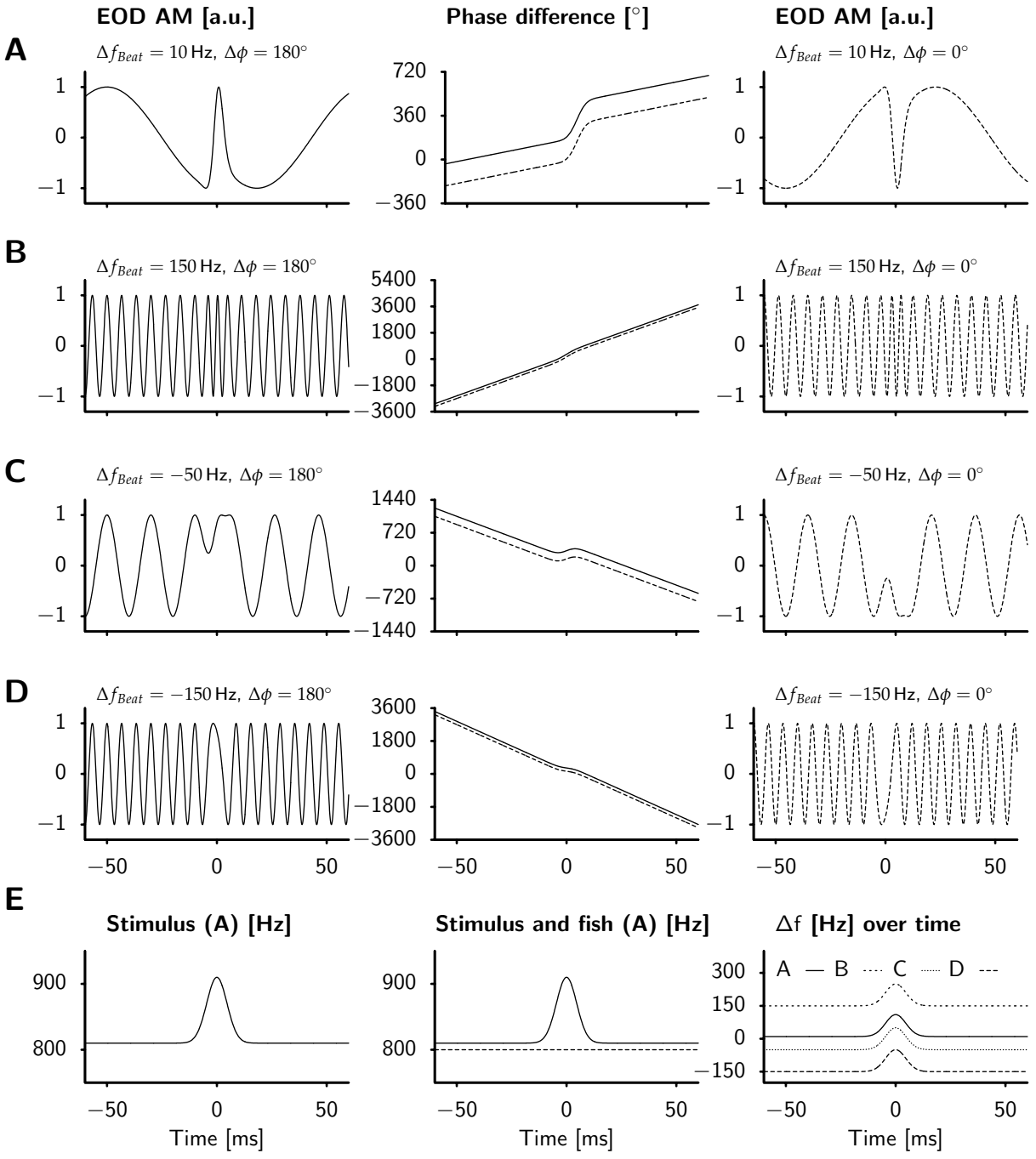
EOD AM [a.u.]
Phase difference [°]
EOD AM [a.u.]
A
$\Delta f_{Beat} = 10\,\mathrm{Hz},\ \Delta\phi = 180°$
$\Delta f_{Beat} = 10\,\mathrm{Hz},\ \Delta\phi = 0°$
B
$\Delta f_{Beat} = 150\,\mathrm{Hz},\ \Delta\phi = 180°$
$\Delta f_{Beat} = 150\,\mathrm{Hz},\ \Delta\phi = 0°$
C
$\Delta f_{Beat} = -50\,\mathrm{Hz},\ \Delta\phi = 180°$
$\Delta f_{Beat} = -50\,\mathrm{Hz},\ \Delta\phi = 0°$
D
$\Delta f_{Beat} = -150\,\mathrm{Hz},\ \Delta\phi = 180°$
$\Delta f_{Beat} = -150\,\mathrm{Hz},\ \Delta\phi = 0°$
E
Stimulus (A) [Hz]
Stimulus and fish (A) [Hz]
Δf [Hz] over time
A — B ···· C ····· D ---
Time [ms]
Time [ms]
Time [ms]

Figure 3.2: Signals caused by chirps at different beats. A–D) Characteristic AMs (left and right column) are formed by the phase difference $\Delta\phi(t)$ between two EOD signals (middle column). In all examples a chirp of width $\Delta t = 14\,\text{ms}$ and size $s = 100\,\text{Hz}$ was simulated centered around time 0 (all values corresponding to Eq. 3.3). The stimulation frequency was chosen relative to the fish's EODf to form difference frequencies $\Delta f_{Beat} = 10$, 150, -50 and $-150\,\text{Hz}$ as indicated. The left column shows the AM caused by a chirp occurring at beat phase $\Delta\phi = 180^\circ$, while the right column shows the same chirp at $\Delta\phi = 0^\circ$. The phase differences (middle column) are shown for both $\Delta\phi = 180^\circ$ (solid line) and $\Delta\phi = 0^\circ$ (dashed line). Note that the actual effects of a chirp on the AM also depend on its width and size. **E**) The time course of the EODf of a chirping fish (the "stimulus", EODf_1) with the parameters from panel A and EODf$= 810\,\text{Hz}$ (left panel), and together with the EODf of the receiving fish with $\text{EODf}_2 = 800\,\text{Hz}$ (middle column). The chirp changes the resulting time-dependant $\Delta f(t)$ (right column, solid line) which mainly determines the resulting AMs (left and right column in panel A). The $\Delta f(t)$ for panels B–D are also shown as indicated.

At positive Δf_{Beat}, when EODf_1 is greater than EODf_2, a chirp transiently increases $\Delta f(t)$ and thus briefly accelerates the beat AM (Fig. 3.1 D). At low Δf_{Beat}, the chirp leads to a fast up- or down stroke depending on the phase of the beat at which it is emitted (Fig. 3.2 A). At faster Δf_{Beat}, the chirp spans several periods of the beat and thus the beat phase at which it occurs is not as crucial anymore (Fig. 3.2 B).

When EODf_1 is lower than EODf_2, Δf is negative and $\Delta\phi(t)$ decreases with time (Fig. 3.2 C, D middle column). Now, the transient increase in EODf_1 caused by the chirp decreases $\Delta f(t)$ and thus slows down the beat. It could even invert the sign of $\Delta f(t)$. The latter occurs at Δf_{Beat} between -90 and $0\,\text{Hz}$ and results in a plateau-like signal (Fig. 3.2 C). At faster negative Δf_{Beat} the chirp leads to a few periods of a slower beat (Fig. 3.2 D).

Although the original communication signal, the chirp, is always the same (Fig. 3.2 E), it causes a huge variety of AM signals depending on the underlying beat parameters, its frequency Δf_{Beat} and phase $\Delta\phi$. In the following we demonstrate how these different signals are encoded in the electrosensory system.

Chirps increase response at slow positive difference frequencies

The AMs of both, beats and chirps, are encoded in P-unit electroreceptors. In the absence of a beat, the P-units fire randomly with a constant rate (Fig. 3.3, left column). When the cell is stimulated with a slow beat (e.g. 10 Hz in Fig. 3.3, middle column), its firing rate closely follows the stimulus. However, spike timing in between trials appears to be uncorrelated (Fig. 3.3 B).

As was shown before (Benda et al., 2005, 2006), a small chirp increases the cell's response when superimposed on such a slow beat. The peak of the firing rate during the chirp clearly exceeds that during the beat (Fig. 3.3 C), although the maximal amplitude of the stimulus is the same during chirp and beat periods (Fig. 3.3 A).

The shortest interspike interval (ISI) of the cell's response is determined by the fre-

quency of the fish's EOD. During the fast upstroke of the chirp, the cell reaches this highest possible firing rate. Here, the ISIs are on the order of one EOD period and consequently, the reliability over trials is high. The increase in firing rate is thus caused by both, an increase in instantaneous firing rate as well as an increase in reliability across trials.

Chirps decrease response at faster beats

At higher beat frequencies, for example $\Delta f_{\text{Beat}} = 100\,\text{Hz}$, the cell responds with an increased maximal firing rate of about 600 Hz to the beat (Fig. 3.3 right column). Further, action potentials are fired with a reliable 2–1-locking in response to the beat (Fig. 3.3 B, right column). In contrast to the slow beat described above the chirp now decreases the peak firing rate (Fig. 3.3 C) and the 2–1- locking breaks down during the chirp due to missing spikes (see spike raster in Fig. 3.3 B).

Population activity is either synchronised or desynchronised by chirps

Since the receptor afferents have uncorrelated noise sources (Benda et al., 2006; Chacron et al., 2005b) the effects seen over subsequent trials recorded in single cells are expected to persist at the population level as well. To test this, we measured the population response in whole-nerve recordings for the same chirp/beat combinations as used in single cell recordings. A chirp on a slow beat increases the population activity (Fig. 3.3 D, middle column), suggesting an increase in synchrony among cells. The population activity is already high in response to a faster beat (Fig. 3.3 D, right column) and is decreased by the chirp. The population activity thus resembles the effects shown for the single cell and supports the assumption that the reliability of single cells over subsequent trials mirrors the synchrony among cells in a population.

Synchronisation and desynchronisation at negative difference frequencies

At negative Δf_{Beat} that arise in interactions with an EOD of lower frequency than that of the receiving fish, the resulting beat AMs are the same as the AMs of the corresponding positive Δf_{Beat}. Consequently, the response of P-units to beats of negative Δf_{Beat} is the same as for those of positive Δf_{Beat}.

However, a chirp occurring on a beat of negative Δf_{Beat} causes quite different P-unit responses as compared to one occurring on the corresponding positive Δf_{Beat}. The chirp now decreases the absolute $\Delta f(t)$ (Fig. 3.2 D).

At intermediate negative Δf_{Beat}, where the chirp transiently inverts the sign of the difference frequency and a plateau-like signal evolves (Fig. 3.2 C), the response depends on where the plateau occurs, namely at which phase of the beat the chirp is emitted. In Fig. 3.4, middle column, we show an example where the chirp occurs more towards the trough in the beat, and the cells cease firing. They keep on firing at high levels if

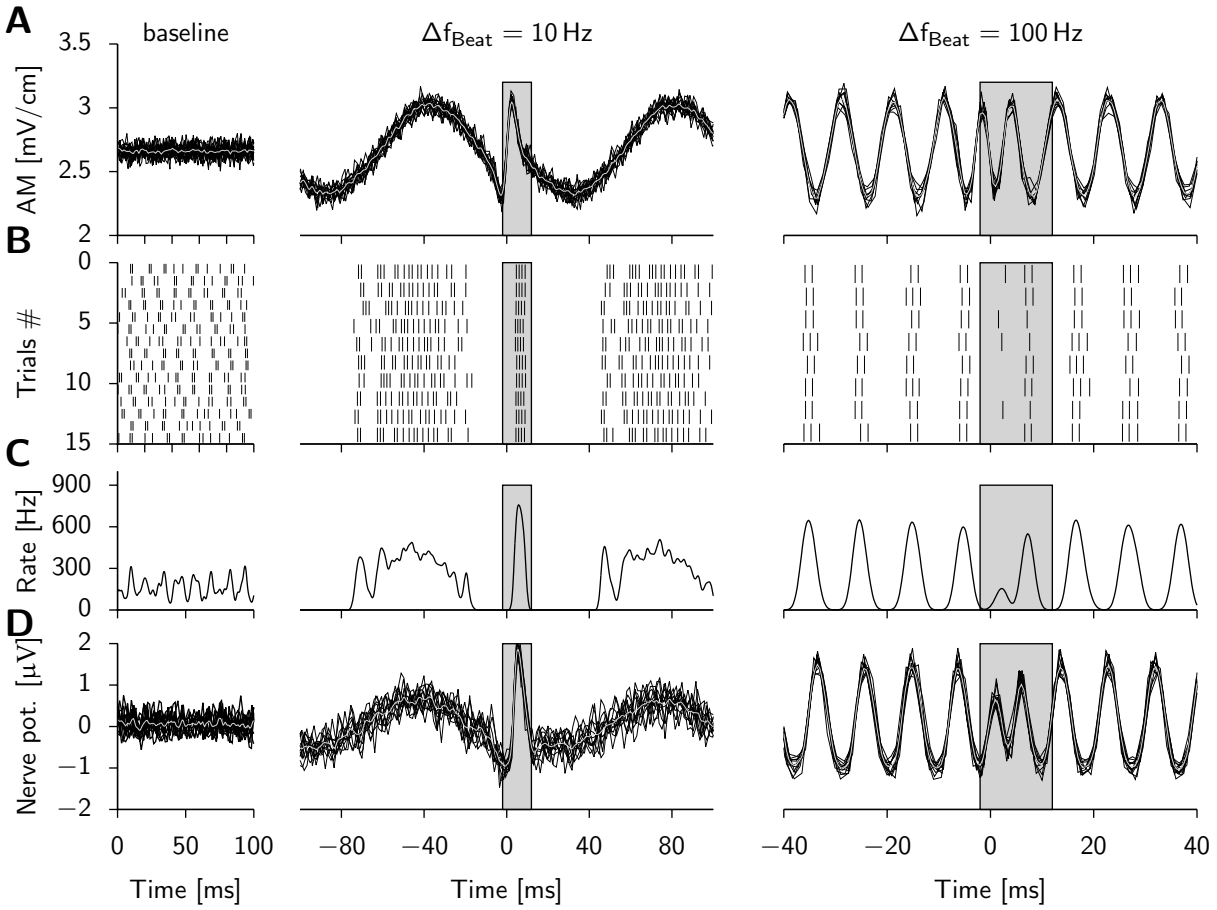

Figure 3.3: Electroreceptor activity evoked by a chirp at positive difference frequencies. A) The AM stimulus recorded at a site close to the fish's body under baseline conditions (no stimulus, left column), with a beat resulting from a difference frequency of $\Delta f_{\text{Beat}} = +10\,\text{Hz}$ (middle column) and a beat of $+100\,\text{Hz}$ (right column). A chirp of size $s = 100\,\text{Hz}$ and width $\Delta t = 14\,\text{ms}$ was delivered around time 0. Shown are individual AMs for each trial (black lines) and the average (gray line). **B**) Spike raster of a single cell recording under the respective stimulus conditions. **C**) Average firing rate computed by convolving the spike raster shown in B with a Gaussian kernel of 1 ms standard deviation and averaging over trials. The timescale of the kernel resembles the fast component of the postsynaptic potential in the target cells (Berman and Maler, 1998). **D**) Population activity as recorded from the lateral line nerve with hook electrodes. Black lines depict results from single trials, grey line their average. The gray boxes mark the time window used for analysing the responses to chirps.

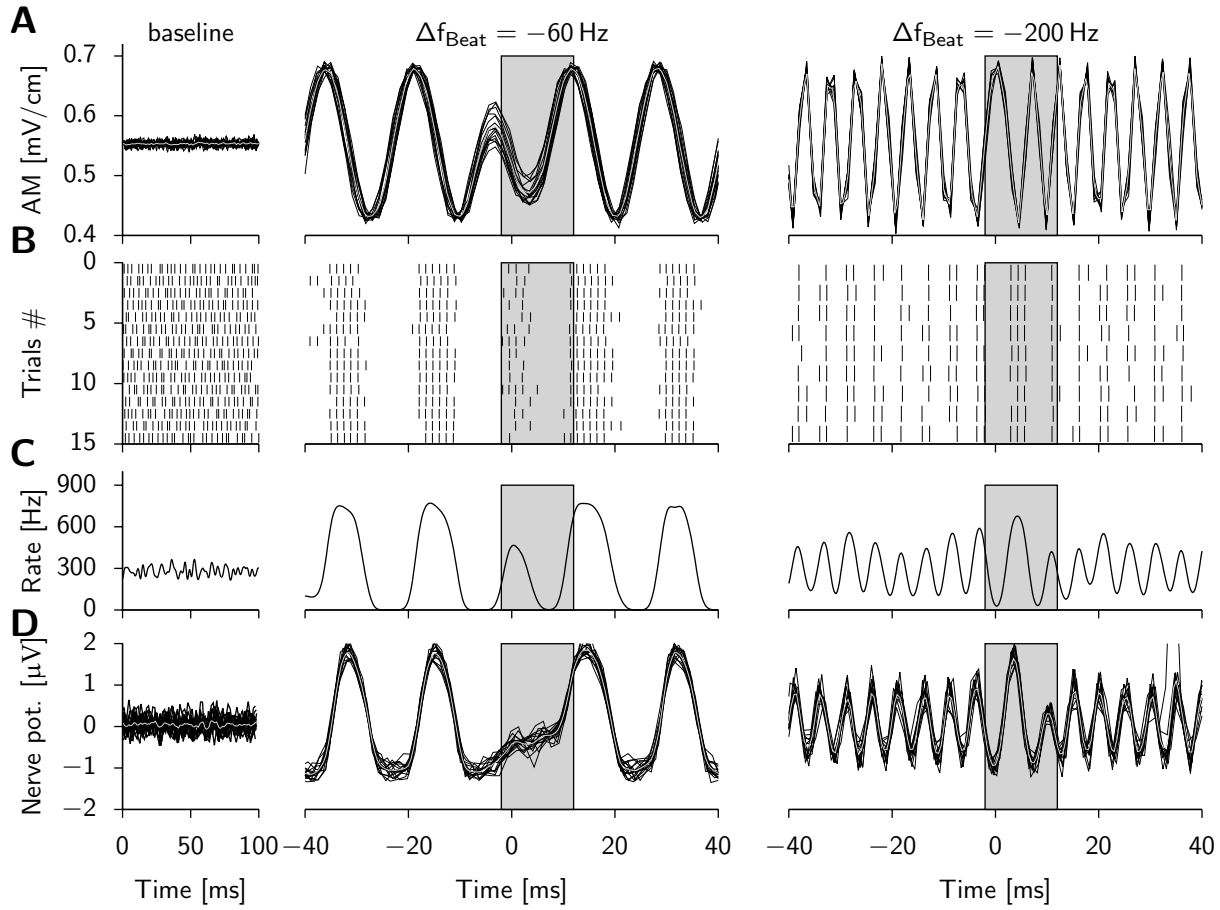

Figure 3.4: Electroreceptor activity evoked by a chirp at negative difference frequencies. The organisation of the figure is the same as in Fig. 3.3 for beats resulting from difference frequencies of $\Delta f_{\text{Beat}} = -60\,\text{Hz}$ (middle column) and $-200\,\text{Hz}$ (right column). Note that this is a different example cell from that in Fig. 3.3 and therefore exhibits a different baseline activity.

the chirp occurs at the peak of the beat (not shown). For all cases, the reliability over trials decreases in response to this slow signal. At very fast beats, where the response to beats is reduced due to the high frequency, it is now transiently increased by the chirp (Fig. 3.4, right column).

Four distinct coding regimes

The examples shown so far suggest a strong influence of Δf_{Beat} on the synchronisation or desynchronisation of the P-unit response by a chirp. In the following we systematically examine this effect and quantify the P-unit responses by the chirp selectivity index, i.e. the contrast between the responses to chirps and beats (CSI, see methods and Vonderschen and Chacron, 2011). As the response of P-units fluctuates around a mean firing rate, we determined the CSI in terms of the firing rate fluctuation and in terms of the correlation over trials.

The CSI pooled over all single unit recordings ($n = 220$ cells) as well as over all $n = 9$ population recordings confirm the impression of the example recordings shown above. There are four regimes of Δf_{Beat} in which the firing rate, the spike correlation, and the population activity are affected in the same way by a chirp of size $s = 100\,\text{Hz}$ (Fig. 3.5, left column): At large negative Δf_{Beat} (below $-100\,\text{Hz}$) the CSI is greater than zero, indicating an increase in firing rate as well as synchrony in response to the chirp. At slow negative Δf_{Beat} between -80 and $-20\,\text{Hz}$ the chirp desynchronises the P-unit responses ($CSI < 0$). For positive Δf_{Beat} the opposite happens: At low beat frequencies between about 0 and 30 Hz, the CSI is positive again (synchronisation), while all beats faster than 30 Hz lead to a CSI less than zero (desynchronisation). At these high beat frequencies, the effect is less prominent for the correlation over trials. The results at most Δf_{Beat} differ statistically significantly from zero [p-value < 0.05 and corrected with a modified Bonferroni correction, Simes method (Simes, 1986)], indicating that chirps affect the responses and that both effects, decreases as well as increases in the response, are consistent and reliable over cells. At the zero-crossings, where the CSI changes from being positive to being negative or vice-versa, values are not distinguishable from zero.

Similar results are obtained for the responses to chirps with a smaller size s of 60 Hz (Fig. 3.5, right column). However, effects are smaller at many Δf_{Beat}, especially at high positive ones. Accordingly, many values are not significantly different from zero (denoted by asterisks), particularly regarding correlation across trials. In a few Δf_{Beat}, the effect is contrary to that originating from a chirp of size $s = 100\,\text{Hz}$. At $-80\,\text{Hz}$, the 60 Hz-chirp increases the response, while the larger (100 Hz) one decreased it, at $-20\,\text{Hz}$ the former decreases it, while the response is increased by the latter chirp.

In summary, chirps are encoded by P-units over the whole behaviourally relevant repertoire of beats. However, depending on Δf_{Beat} a chirp either increases or decreases synchronisation of the P-unit population. This partitions the Δf_{Beat} in four distinct regions. In the following we analyze how the responses to chirps are generated and how cell heterogeneity and more detailed aspects of a chirp influence the response to chirps.

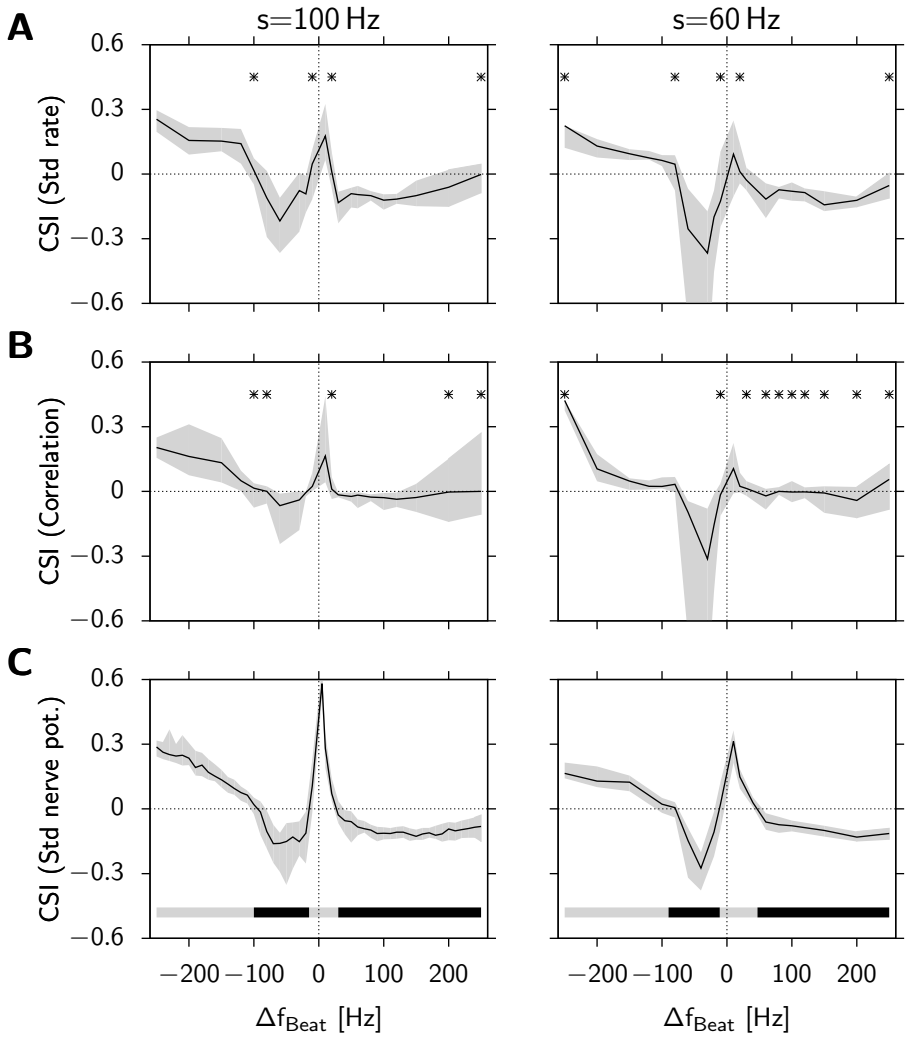

Figure 3.5: Representation of chirps by electroreceptor activity in dependence on difference frequency. The chirp selectivity index (CSI) measures the contrast between the response to the chirp and the response to the beat. **A**) The average firing rate computed in a window around the chirp (gray boxes in Figs. 3.3 and 3.4) and during the beat is used as a measure for the single unit response. Shown are the median (solid line) and the interquartile range (shaded area) of all CSI values pooled over beat phases, contrasts, and cells. **B**) CSI of single units based on spike correlation across trials. **C**) The CSI obtained from the population activity as the standard deviation of the potential recorded from the lateral line nerve. Gray and black bars indicate beat frequencies where chirps have synchronising ($CSI > 0$) or desynchronising ($CSI < 0$) effects, respectively. Difference from zero was assessed by a sign test (Bonferroni corrected) in all cases. Values that are not significantly different from zero ($p > 0.05$) are indicated by asterisks. All panels in the left column show the responses to a chirp of size $s = 100\,\text{Hz}$, in the right column to one of size $s = 60\,\text{Hz}$.

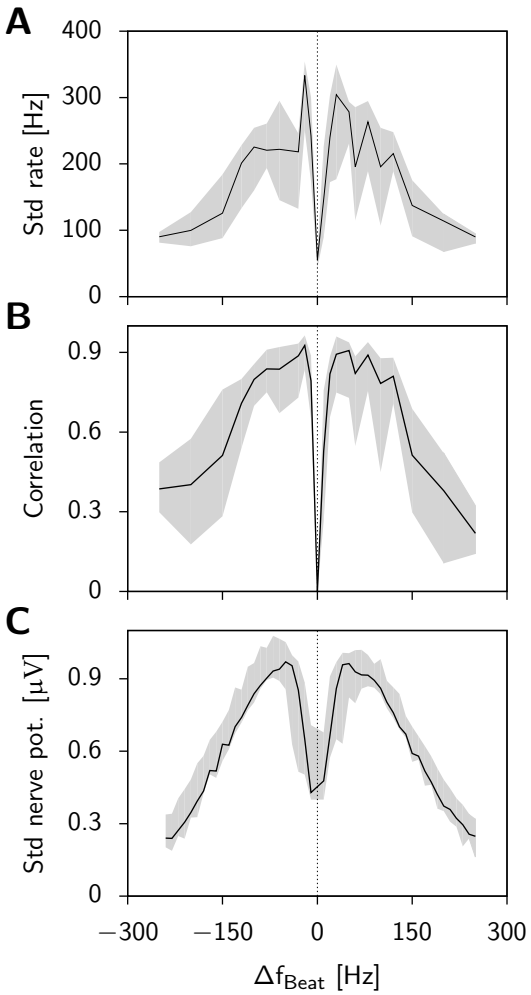

Figure 3.6: AM frequency tuning of P-units. The responses to the pure beat stimulus as a function of difference frequency Δf_{Beat} (based on the same responses as in Fig. 3.5). The responses are averages in a window during the beat of **A**) the standard deviation of the single cell firing rate as a measure for the rate modulation depth, **B**) the correlation between pairs of spike-trains as a measure of synchrony and **C**) the population activity computed as the standard deviation of the voltage recorded from the lateral line nerve. Shown are median (solid line) and interquartile range (gray).

Predicting the response to chirps from frequency tuning

As described above, a chirp increases the difference frequency $\Delta f(t)$ for a short time (Fig. 3.2) and with that transiently modulates the frequency of the resulting AM that is encoded by the P-units. The response of a P-unit to a chirp could therefore be predictable solely from its tuning to sinusoidal AMs of different frequencies, i.e. beats. The single-cell responses to sinusoidal AM stimuli show a peak in modulation depth of the firing rate as well as in correlation at intermediate AM frequencies between 50 and 80 Hz and decrease for slower and faster frequencies (Fig. 3.6 A, B). The tuning of the population response closely matches the tuning of spike-train correlations measured in single

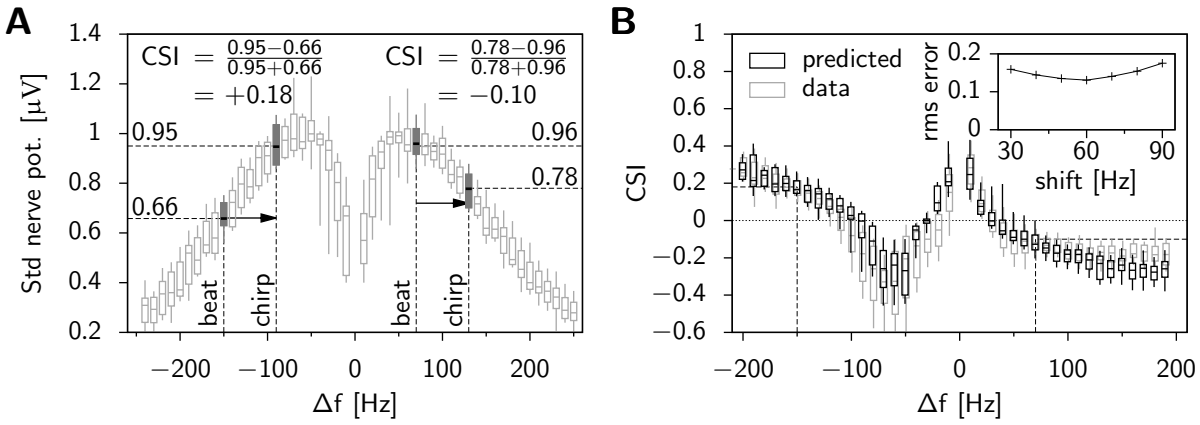

Figure 3.7: Predicting the response to a chirp solely from the AM frequency tuning. A) Prediction procedure. The average frequency excursion of a chirp with a maximum of 100 Hz over 14 ms is 56 Hz. We predicted the CSI from the response to a beat with a frequency $\Delta f_{\text{Beat}} = 60$ Hz shifted to the right with respect to the underlying beat. For example, the response to a chirp on top of a beat of $\Delta f_{\text{Beat}} = -150$ Hz was predicted to be the same as a response to a pure beat of $\Delta f_{\text{Beat}} = -90$ Hz, at a beat of $\Delta f_{\text{Beat}} = 70$ Hz the prediction was read off as the response to a beat of $\Delta f_{\text{Beat}} = 130$ Hz as demonstrated in the figure. The same applies to all other Δf_{Beat}. **B**) The predicted CSI plotted together with the measured CSI as a function of Δf_{Beat}. The inset shows the root mean squared error of the prediction for different shift values.

cells (compare Fig. 3.6 B and C). The largest modulation of the population response and thus the highest synchronicity is found at the same intermediate beat frequencies. Note that all three tuning curves are symmetrical around zero, because the AM of a beat of negative Δf_{Beat} is the same as that for a positive one.

To predict the response to a chirp with a size of $s = 100$ Hz we read off the response from the AM frequency tuning curve at 60 Hz (approximately the average change in frequency evoked by this chirp) to the right of the beat frequency (Fig. 3.7 A). With this procedure we computed the CSI for every beat frequency from the tuning curve obtained from the whole-nerve recordings. For most beat frequencies these predictions match the measured data well (Fig. 3.7 B), indicating that the cells mainly respond to the change in $\Delta f(t)$ induced by the chirp. This response to chirp-induced frequency changes is rapid since at low beat frequencies the faster Δf during the chirp shows up for less than a full period.

Small differences between prediction and data are observed for fast positive Δf_{Beat} ($>$ 120 Hz) where the measured desynchronisation is weaker than predicted, and for intermediate negative beats ($\Delta f_{\text{Beat}} \approx 30$ Hz), where higher CSI values are predicted. The latter is the region where the phase at which a chirp occurs influences the response. Phase is not considered in the prediction and the deviations are therefore not surprising. The prediction works very robustly, also for slightly different shift values (Fig. 3.7 B, inset). Computing a more precise prediction by considering the chirp's shape did not improve results (not shown).

Sources of variability

The estimates of the CSI derived from single unit responses (Fig. 3.5 A, B) show a considerable amount of variability when pooled over cells and animals. In contrast, the CSIs computed from the population rates are much more reliable, since the variability between single cells is already averaged out in the measurement (Fig. 3.5 C). In both cases, we pooled all data irrespective of the phase at which the chirps occurred within a beat cycle. Chirps at different phases $\Delta\phi$ of the beat give rise to very different AMs (Fig. 3.2, see also Walz et al., 2012; Zupanc and Maler, 1993) and thus to potentially different responses of the P-units (see below). To disentangle the influence of cell heterogeneity and phase we averaged over each factor separately and analyzed the remaining variability.

When averaging the responses over beat phases first, the remaining variability is caused by cell heterogeneity (Fig. 3.8 A) and appears to be large. The variability caused by different phases of the chirp within the beat (Fig. 3.8 B) is markedly lower except for intermediate negative beat frequencies. Comparing the standard deviation of CSI estimates when averaged over cells or over beat phases indicates that indeed the variability over cells is greater than that over phases (Fig. 3.8 C). The heterogeneity among P-units thus affects responses of single cells more strongly than the difference in stimulus shape caused by different beat phases.

Discrimination of different chirps

We next ask whether an upstream neuron could in principal distinguish chirps occurring at different phases $\Delta\phi$ of the beat. Especially at slow beats the particular phase at which a chirp occurs in a beat cycle has a strong impact on the resulting AM (Fig. 3.2). This appears to be reflected in the spike responses (Fig. 3.9 A).

For analysing the differences between spike trains evoked by chirps at different $\Delta\phi$, we performed a discrimination analysis similar to Marsat and Maler (2010) and Vonderschen and Chacron (2011) on the basis of spike distance metrics (van Rossum, 2001). For each Δf_{Beat} and each cell we constructed confusion matrices for 10 different $\Delta\phi$s (Fig. 3.9 B). The confusion matrices were averaged over cells. How well the responses to different phases can be assigned correctly, is quantified by the mutual information of the confusion matrix, that is normalised to the maximum possible value. For each Δf_{Beat} and each temporal resolution tested a single value is obtained that is color coded in Fig. 3.9 C & E (see methods for details). A high information in the confusion matrix, corresponding to a light color in Fig. 3.9 C & D, reflects a good discriminability of the responses evoked by chirps at different beat phases.

Generally, the responses to chirps occurring at different phases of the beat can be well discriminated at slow beats while discrimination becomes more difficult at higher beat frequencies (darker colors in Fig. 3.9 C, D). Discrimination performance is markedly improved at higher beat frequencies when temporal resolution of the distance measure is fine ($\tau_c = 1\,\text{ms}$, Equation 3.6). On the contrary, at slow beats good discrimination can

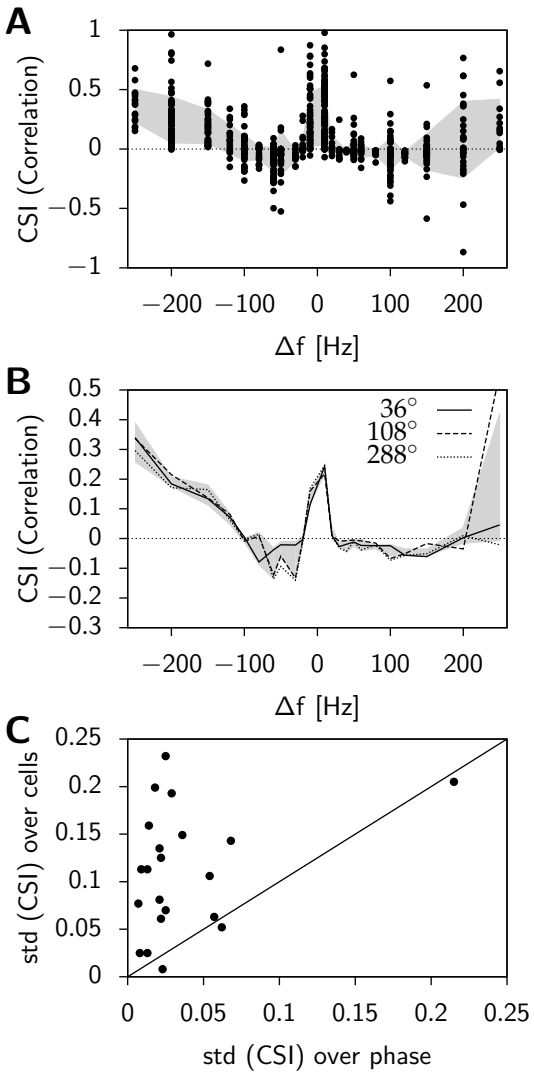

Figure 3.8: Sources of variability. A) The chirp selectivity index (CSI, based on the correlation over trials) computed from responses to chirps of $s = 100\,\text{Hz}$ in dependence on beat frequencies (same data as in Fig. 3.5 B). Here the CSI is averaged over all phases $\Delta\phi$ for each cell separately (each black circle is the average of a single cell). Gray area represents mean $\pm$ standard deviation of the CSI estimates. **B**) Same data as in A, but now averaged over cells for ten classes of beatphases $\Delta\phi$, i.e. the time of occurrence of a chirp within a beat cycle. Three phase-classes are drawn as indicated, the gray area marks the mean $\pm$ standard deviation of the ten phase classes as a function of beat frequency. **C**) Comparison of CSI variability when averaging over cells or phase. For each underlying beat frequency Δf_{Beat}, the standard deviation of the CSI estimations when averaged over cells (gray area in panel A) is plotted over the standard deviation of the estimation when averaged over cells (gray area in panel B). Points lying above the diagonal exhibit a greater variability resulting from cell heterogeneity than from different phases of chirp stimulation.

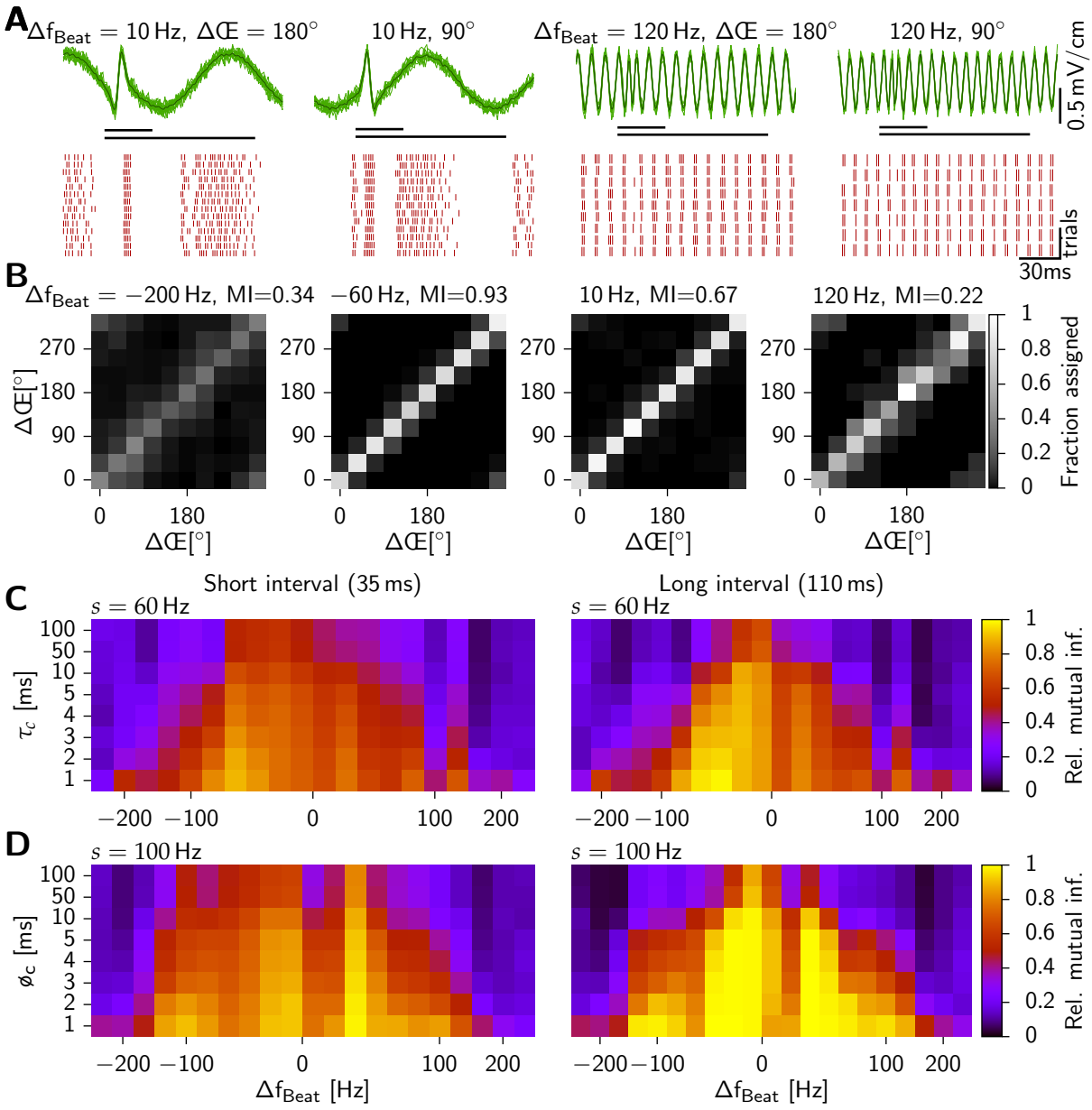
A
Δf_Beat = 10 Hz, ΔŒ = 180°
10 Hz, 90°
Δf_Beat = 120 Hz, ΔŒ = 180°
120 Hz, 90°
0.5 mV/cm
trials
30ms
B
Δf_Beat = −200 Hz, MI=0.34
−60 Hz, MI=0.93
10 Hz, MI=0.67
120 Hz, MI=0.22
ΔŒ[°]
Fraction assigned
C
Short interval (35 ms)
Long interval (110 ms)
s = 60 Hz
τc [ms]
Rel. mutual inf.
D
s = 100 Hz
øc [ms]
Δf_Beat [Hz]

Figure 3.9: Discriminability of chirp responses at different beat phases. A) top: AMs of two different beats ($\Delta f_{\text{Beat}} = 10\,\text{Hz}$ and $120\,\text{Hz}$) superimposed with chirps occurring at different phases of the beat ($\Delta\phi = 180°$Cand $90°$C). Black bars indicate the two intervals used for the discrimination analysis (short interval spanning the chirp only and long interval also including parts of the beat). Bottom: Rasterplots of the respective neuronal responses. Scale bars indicate $0.5\,\text{mV}$ in the first row and $30\,\text{ms}$ and 3 trials in the second. **B**) Confusion matrices created from assigning each chirp response (at a given phase $\Delta\phi$, x-axis) to the phase $\Delta\phi$ that had elicited a set of responses this response had the smallest distance to as estimated by Equation 3.6 (y-axis, $\tau_c = 2\,\text{ms}$). The confusion matrices were averaged over cells. From them, the mutual information was calculated (Equation 3.7). Subplots show confusion matrices for different beat frequencies Δf_{Beat} as indicated, with a τ_c of $2\,\text{ms}$ and the short analysis window. **C**) Discrimination performance (in terms of the relative mutual information) of a chirp of size $s = 60\,\text{Hz}$ as a function of Δf_{Beat} and the temporal resolution of the distance measure (Equation 3.6) for the short (left plot) and long (right plot) analysis intervals (see methods). **D**) Same as C but for responses to a chirp of size $s = 100\,\text{Hz}$. The underlying difference frequencies in **C** and **D** were -250, -200, -150, -120, -100, -80, -60, -30, -20, -10, 10, 20, 30, 50 (only for the $100\,\text{Hz}$ chirp), 60, 80, 100, 120, 150, 200 and $250\,\text{Hz}$.

be achieved with a wide range of temporal resolutions. This matches the natural time scales of the AM waveforms induced by the chirps. However, for all beat frequencies up to $100\,\text{Hz}$, the discrimination is possible at the physiologically relevant time scale which is on the order of milliseconds.

Increasing the width of the analysis interval simply increases discrimination performance since more information becomes available for the discrimination. The dependence on Δf_{Beat} and temporal resolution is, however, not influenced by the width of the analysis interval (compare left and right column in Fig. 3.9 C, D). The size s of the chirp, i.e. its maximal frequency excursion, also influences discrimination performance. Discrimination is elevated for the $100\,\text{Hz}$ chirp as compared to the $60\,\text{Hz}$ chirp (compare Fig. 3.9 D and C, respectively).

3.4 Discussion

Our data demonstrate that the very same stereotyped communication signal — the small chirp of the weakly electric fish *A. leptorhynchus* — is encoded in two opposing ways. Depending on the ongoing background signal, the beat, the chirp transiently either synchronises or desynchronises the activity of the receptor population, thereby partitioning the range of naturally occurring difference frequencies into four regimes. In contrast to a previous study where synchronisation was attributed to small chirps and desynchronisation to a different type of chirps (large chirps, Benda et al., 2006), we here focused on the neural responses elicited by a single type of chirp occurring in different social contexts that are reflected by the frequency of the background beat. We chose the small chirp as it is the most commonly emitted signal in most contexts

(Zupanc, 2002) and used background frequencies that fish are likely to encounter in the wild (Stamper et al., 2010).

Critical to a perception of signals is their representation at higher brain areas. Is the differential encoding of small chirps in dependence on the background difference frequency likely to persist at such subsequent processing stages and thus correspond to a categorial perception of these signals? P-units project with distinct convergence ratios onto pyramidal cells in three different maps of the electrosensory lateral line lobe (ELL, Chapter 2, Carr et al., 1982; Heiligenberg and Dye, 1982; Maler, 2009). As shown by lesion experiments, the lateral segment (LS) of the ELL is necessary for chirping behaviour (Metzner and Juranek, 1997). In this map about one thousand electroreceptor afferents converge onto each pyramidal cell (Maler, 2009). The resulting large receptive fields together with a readout based on coincidence detection explains their high-pass response properties (Krahe et al., 2008; Middleton et al., 2009). The pyramidal cells of the LS should therefore be sensitive to changes in the level of synchrony of the P-unit population as measured here by spike train correlations and whole nerve recordings. Indeed, LS pyramidal cells of the E-cell type encode small chirps on low difference frequencies in synchronised bursts, whereas large chirps on high difference frequencies, that desynchronise P-units (Benda et al., 2006), are encoded by I-cells (Marsat et al., 2009). We expect that depending on the beat, small chirps are encoded by E-cells whenever they synchronise the P-unit population and by I-cells in case they desynchronise the P-units. Thus, small chirps would be encoded in two different processing streams depending on the background difference frequency.

The result of four encoding regimes is largely independant of the assumed readout of the P-unit population, as the firing rate as well as correlations between spike trains give similar results. This similarity is not surprising since P-units are independant (Chapter 2, Benda et al., 2006; Chacron et al., 2005b) and their mean firing rate is the same during beats and chirps (Benda et al., 2006). In the centrolateral and the centromedial segments (CLS and CMS) of the ELL neither E-cells nor I-cells show such strong responses to chirps as in the LS (Marsat et al., 2009). In these segments, receptive field sizes are smaller. About 150 (CLS) or 40 (CMS) P-unit afferents project onto each pyramidal cell (Maler, 2009). This makes an additive readout of P-unit activity as quantified by the firing rate more likely.

Our results focus on the responses evoked by chirps directly. However, a chirp also induces a phase shift of the beat (Fig. 3.1 D, Benda et al., 2005). Superficial E-cells that encode small chirps on slow beats (Marsat et al., 2009) receive indirect feedback (Berman and Maler, 1998) that predicts and cancels responses to low-frequency ongoing beats (Bastian et al., 2004). After a chirp the beat and the feedback are out of phase, resulting in an enhanced response (Marsat and Maler, 2012). The cancellation of beat responses by the feedback only works up to AM frequencies of 20 Hz and is thus unlikely to enhance chirp responses at higher difference frequencies. Thus, at AM frequencies larger than 20 Hz that occur mostly during social encounters (Stamper et al., 2010) chirp-induced phase shifts of the beat are not processed by the indirect feedback of the ELL.

The AM waveform a chirp induces not only depends on its size, duration, and the

difference frequency, but also on the phase at which the chirp occurs during the beat (Fig. 3.2). Indeed, responses to chirps at different beat phases can be well discriminated at low difference frequencies (Fig. 3.9). This is preserved in the ELL pyramidal cells as well as in the dense coding cells of the torus semicircularis (Vonderschen and Chacron, 2011). The large differences in AM waveforms and the corresponding neural responses caused by different beat phases was demonstrated to hinder discrimination of chirps of different sizes and durations in pyramidal cell responses (Marsat and Maler, 2010). However, at difference frequencies larger than about 100 Hz P-unit responses to chirps at different beat phases become more and more similar (Fig. 3.9) thus potentially allowing to discriminate different chirp properties. This behaviourally still relevant range of difference frequencies (Stamper et al., 2010) was not tested in the mentioned ELL studies. Discrimination of chirps in P-units performed best at time constants of 1 ms in contrast to about 5 ms in pyramidal cells (Marsat and Maler, 2010; Vonderschen and Chacron, 2011), following the general pattern of less precise spike responses in upstream neurons both in vertebrates (Kara et al., 2000) and invertebrates (Vogel et al., 2005). For future analyses of chirp discrimination in P-units population responses have to be taken into account, since variability between different cells is even larger than between responses of a single cell to chirps at different beat phases (Fig. 3.8).

Because the rate of emitted small chirps strongly decreases with larger difference frequencies (Bastian et al., 2001; Engler and Zupanc, 2001) and recordings of P-unit responses suggested vanishing responses at beat frequencies beyond 60 Hz (Benda et al., 2005), all electrophysiological studies on chirp encoding considered difference frequencies only up to this frequency (Benda et al., 2006; Marsat and Maler, 2010; Marsat et al., 2009; Vonderschen and Chacron, 2011). However, large difference frequencies up to 300 Hz do occur naturally (Stamper et al., 2010) and chirps at larger difference frequencies do have significant effects on echo responses and attack behaviour (Hupé et al., 2008). Our data on P-unit responses to chirps demonstrate that chirps are indeed encoded by P-units in the full range of possible positive and negative difference frequencies.

Surprisingly, chirps as transient and stereotyped communication signals (Hupé and Lewis, 2008; Zakon et al., 2002) turned out not to be encoded by P-units irrespective of context parameters like the difference frequency. Rather the space of difference frequencies is divided into four regimes where synchronising chirp responses alternate with desynchronising responses (Fig. 3.5). Since difference frequency carries important information about social context in terms of gender (Meyer et al., 1987; Zakon and Dunlap, 1999), size (Dunlap, 2002; Zakon and Dunlap, 1999), and dominance (Dunlap, 2002; Fugère et al., 2011; Triefenbach and Zakon, 2008), our findings suggest two opposing hypotheses. Either small chirps have the same meaning at all difference frequencies, then one would expect to find neurons further upstream that respond in the same way to small chirps irrespective of difference frequency. Or different behavioural categories of chirps exist that reflect the categorical representation that we find on the receptor level.

Following the second hypothesis, we suggest that small chirps at large difference

frequencies could be used by the fish to determine the sign of the difference frequency. How fish sense the sign of the difference frequency, has been studied in detail in *Eigenmannia* in the context of the jamming avoidance response for low difference frequencies (Bullock and Heiligenberg, 1986; Kawasaki et al., 1988). However, at high difference frequencies this mechanism that is based on a comparison between amplitude and phase modulation signals evoked by the beat has not been studied yet and quite likely might not work. Alternatively, since small chirps either synchronise or desynchronise the P-unit population at large negative or positive difference frequencies, respectively, chirping could provide the necessary cue whether the fish's frequency is higher or lower than that of its opponent.

Our study on the encoding of a communication signal was triggered by behavioural observations demonstrating the utilisation of this signal on a much broader context then previously assumed (Hupé et al., 2008). The results showed a much richer response diversity on this broader space of natural stimuli. Like many recent unexpected findings from the visual system of vertebrates (e.g. Butts et al., 2007; Vinje and Gallant, 2000) and invertebrates (van Hateren et al., 2005) as well as in the auditory system (Neklen et al., 1999; Theunissen et al., 2000), this emphasises the importance of natural stimuli when studying neural function. In turn our results on the context-dependant encoding of one type of chirps by electroreceptors call for more detailed behavioural as well as electrophysiological studies that take into account the full range of natural and behaviourally relevant stimuli.

The dependence of P-unit activity on difference frequency can be explained by a simple model based on the unit's frequency tuning. As demonstrated in Fig. 3.7, the synchronisation behaviour of the P-units in response to the chirps is mainly based on their AM frequency tuning. A chirp transiently increases the difference frequency and thus modulates the AM frequency. The neuronal response rapidly follows this AM frequency shift according to the AM frequency tuning curve. The good performance of the model highlights how fast the P-units respond to changes in stimulus frequency. As the chirp width is only 14 ms and thus shorter than one period of many of our beat stimuli, P-units already respond to fractions of a beat cycle (see for example Fig. 3.3, middle column). Because P-unit action potentials lock onto the EOD (Hagiwara and Morita, 1963), their membrane time constant is likely to be shorter than a single EOD period ($\sim$ 1 ms) and thus potentially explains the P-units' ability to quickly follow such a mean-coded signal. Cortical neurons also have been shown to rapidly follow mean-coded signals (Boucsein et al., 2009; Tchumatchenko et al., 2011). A variance-coded transmission that was suggested for rapid signal transmission (Silberberg et al., 2004) is therefore not required.

The AM frequency tuning curves for both rate modulation and correlations as the basis for predicting chirp responses show a band-pass tuning with maximal values in the range of 30 to 80 Hz (Fig. 3.6). Such a band-pass frequency tuning is found in neurons of various sensory systems (auditory: Narayan et al., 1998, vestibular: Straka et al., 2005, visual: Saul and Humphrey, 1990) and is thus not a specific characteristic of P-units. The high-pass component of the P-units' tuning curve (Nelson et al., 1997) has been at-

tributed to rapid spike-frequency adaptation (Benda et al., 2005). Note that adaptation currents in general attenuate responses to low-frequency components of the stimulus thereby shaping a high-pass filter (Benda and Herz, 2003). The low-pass component could simply originate from the firing rate of the P-units (Knight, 1972a; Pressley and Troyer, 2011) that have a high baseline activity of about 100 to 250 Hz (Gussin et al., 2007).

In addition to these basic mechanisms of the spike generator the receptor current itself could already be band-pass tuned. While this is not the case for P-units, since the tuning we consider here is with respect to the amplitude modulation of a carrier signal, auditory nerve fibers, for example, are band-pass tuned by the cochlear filter to their characteristic sound frequency (Narayan et al., 1998). Many behaviourally relevant signals in acoustic communication as well as echolocation involve frequency shifts like the chirps in electrocommunication discussed here (see e.g. Bailey et al., 1993; Wang et al., 1995). The study of their encoding has been focused on more complex aspects such as the selectivity for spectro-temporal features (Zhang et al., 2003). However, the fast and robust encoding of transient signals in peripheral receptors could also be based on the simple frequency-tuning mechanism described above. This mechanism does not require unique properties in receptor cells and could therefore be a universal mechanism for a fast encoding of transient periodic signals.

Chapter 4

Predicting dynamic P-unit responses with a spiking neuron model

4.1 Introduction

When the representation of information in neural activity is known, one would also like to uncover the biophysical processes that implement it. Reproducing experimentally measured activity with theoretical models is a powerful way to reveal such mechanisms (Anderson and Kreiman, 2011). In the last chapter we have shown that P-units respond by opposite tendencies to chirp depending on the background and that these response variations can be explained from looking only at their frequency tuning and the frequency content of the stimulus. The P-unit frequency tuning therefore lies at the heart of their responses. Building on this result, we investigate the P-units' frequency tuning in this chapter by means of a computational model.

We use a leaky integrate-and-fire model to reproduce the responses of the whole P-unit receptor organs. Each P-unit is made up of one afferent neuron innervating about 25–30 receptor cells (Chapter 2). Spikes are initiated at the afferent neuron close to the receptor site, with short unmyelinated processes branching off to multiple active zones at each receptor (Bennett et al., 1989). The exact transformations of the electric organ discharge (EOD) that occur at the receptor, synapse, "dendritic" processes and spike initiation sites remain unclear, as the receptor organs are inaccessible for electrophysiology. Yet, the P-unit responses that result from these transformations, have been analysed in detail (Scheich et al., 1973; Wessel et al., 1996). As described in Chapter 2, their discharge is phase-locked to the EOD but spikes are generated in a probabilistic manner (hence "P"-unit) and the probability of spiking is dependant on the amplitude of the EOD and the frequency of the amplitude modulation (AM). The P-unit discharge is not a renewal process – successive interspike intervals (ISIs) are negatively correlated and this correlation is important for encoding electrosensory signals (Chacron et al., 2001a; Ratnam and Nelson, 2000).

Previous modelling work has greatly contributed to our understanding about the overall computations performed by P-unit electroreceptor organs. Kashimori et al. (1996) built a conductance-based model of the whole electroreceptor unit and were able to qualitatively reproduce the behaviour of different types of tuberous units. Nelson et al. (1997) constrained a stochastically spiking model by linear filters of the previously determined P-unit frequency tuning. Kreiman et al. (2000) used the same frequency filters to stimulate a noisy perfect integrate-and-fire neuron with which they investigated the variability of cell responses to random amplitude modulations (RAMs). To reproduce the probabilistic phase-locked firing and the correlations of the ISIs, Chacron et al. (2000) designed a noisy leaky integrate-and-fire model with refractoriness as well as a dynamic threshold. Benda et al. (2005) used a firing rate model with a negative adaptation current to reproduce the high-pass behaviour of P-units. These five models can roughly be grouped into studies that primarily aimed at reproducing the baseline behaviour (Chacron et al., 2000; Kashimori et al., 1996; Kreiman et al., 2000) or such which focused on the cell's responses to AM stimuli of the cells (Benda et al., 2005; Nelson et al., 1997). However, no model to date captures all aspects of P-unit encoding. We show that a model designed and calibrated to baseline characteristics can reproduce the responses to AMs that represent the naturally relevant signals with a high degree of accuracy.

In the following we will first describe the design of our model and the fit to P-unit responses to baseline conditions and step stimuli. We then describe the parameter variability underlying the fit to different cells and show how the model is altered by changing each parameter separately. Finally, we show how the models that are only constrained to response characteristics in baseline conditions and to artificial steps in EOD amplitude, can reproduce the frequency tuning of cells with high accuracy.

4.2 Methods

Experimental recordings of P-unit electroreceptors

P-unit recordings were made from the posterior branch of the anterior lateral line nerve ganglion of adult *A. leptorhynchus*. The experimental procedures were as described in detail in Chapter 3. The data in this chapter stems from recordings in seven fish (12.5 – 18.9 cm body length, 2 female, 3 male 2 not determined, EOD frequency (EODf) range 775.4 ± 73.31).

We included results of all P-units ($n = 23$) of which we had recorded baseline activity as well as responses to step and sinusoidal stimuli. We excluded all bursting cells, i.e. those in which one spike is likely to be followed by another one within one or two EOD periods. We rejected the bursting units because we suspected that, at least in some cases, such bursting may be caused by damage to the P-unit afferent fibres and so be artefactual. The tendency to burst shows up in the baseline ISI histograms as an additional peak at small intervals in addition to the peak that all cells show at the

inverse of their baseline firing rate. Therefore, we checked all ISI-histograms to have a bell-shaped form and excluded those whose histograms had more than one peak. Note that in cells with a very high baseline firing rate, the two peaks can overlap and lead to ISI-histograms with only one peak at intervals as small as one EOD cycle. We chose to be conservative and discarded such cells assuming bursting activity.

Model Simulations

P-units were modelled as noisy leaky integrate-and-fire neurons with adaptation current (LIFAC). Simulations were integrated using the Euler method with time steps of $\Delta t = 0.05\,\text{ms}$ or $0.1\,\text{ms}$ (during the fit routine). For the simulation of a stochastic noise current (ξ, see below), a normally distributed random number (N(0,1)) was drawn at every time step and divided by $\sqrt{\Delta t}$ to obtain a current with an autocorrelation function independant of the integration step size. All data acquisition, analysis and model simulations were done using custom-made C++ software. Most analysis programs are available through the RELACS package (www.relacs.net).

The membrane potential V of LIF neurons follows the dynamics

$$\tau_V \frac{dV}{dt} = -V + I + \sum(\delta(t)) \; . \tag{4.1}$$

The current is integrated and when V reaches the threshold, it is reset to 0 and a spike is listed. Because P-unit cell bodies are inaccessible in recordings and information about their membrane resistance is lacking, the current is directly integrated and carries the unit mV. It is comprised of the sum of a stimulus-dependant current I_{Input}, a bias current I_{Bias}, a spike history-dependant adaptation current I_A and a Gaussian noise current ξ, thus

$$I = \alpha I_{\text{Input}} + I_{\text{Bias}} - I_A + \sqrt{2D}\xi \; , \tag{4.2}$$

with α representing a cell-specific gain factor expressed in cm (because I_{Input} represents the EOD stimulus and carries the unit mV/cm). The adaptation current evolves over time according to

$$\tau_A \frac{dI_A}{dt} = -I_A + \Delta_A \sum(\delta(t)) \; . \tag{4.3}$$

Using the Euler integration, this corresponds to an exponentially decaying current that is incremented at every threshold crossing by

$$I_A \mapsto I_A + \frac{\Delta_A}{\tau_A} \; . \tag{4.4}$$

I_{Input} consists of an amplitude modulated sine wave that mimics the EOD. The desired waveform of the AM, $\beta(t)$, is multiplied with the EOD stimulus. EOD frequency and amplitude are taken from the recording (the amplitude is incorporated into β). The signal is then passed through a Heaviside function to include zero-clipping of the

synapse. It is low-passed filtered at about one EOD period to simulate filtering in the unmyelinated processes. Accordingly, the dynamics of the input current are

$$\tau_D \frac{dI_{\text{Input}}}{dt} = -I_{\text{Input}} + H[\beta(t) sin(2\pi f_{\text{EOD}} t)] \,. \tag{4.5}$$

Our model necessitated the fit of seven parameters, namely τ_V, α, Δ_A, τ_A, τ_D, $\sqrt{2D}$ and I_{Bias}. The first six were optimised using the simplex algorithm (Nelder and Mead, 1965). This is a standard numerical procedure for the fit of variables, in which an error function of target parameters is minimised. In our case the error function consisted of a weighted sum of four baseline parameters as well as the error between the estimated f-I-curves of model and data. The four baseline parameters were the coefficient of variation (CV) and the first serial correlation (SC) of the ISIs, the vector strength (VS) of phase-locking to the EOD and the mean firing rate. For details on how to calculate these measures see the section on *Data Analysis* below. The individual terms were weighted such that all errors were of comparable size. Since VS, for example, ranged between 0.8 and 1, its error was on the order of 0.2 and was multiplied by 5 to be about as big as the other errors. After each iteration of the simplex algorithm, I_{Bias} was adjusted such that the baseline firing rate was matched.

The fit routine risks falling into local minima, i.e. ending at a parameter combination with better results than neighbouring parameter sets, but worse results than combinations that are further away in the parameter space. To find a better overall solution, we started the fit multiple times with different starting values for each of the six model parameters. We chose 3 initial values for each model parameter and thus got a total of $3^6 = 729$ fits. The one with the lowest cost function was chosen as the best overall model fit.

Stimulation Protocols

All stimulation protocols were identical for electrophysiological experiments and model simulations. To construct f-I-curves, step stimuli of on average 14 different intensities between 80 and 120 % of the baseline EOD amplitude were used. With this intensity range we usually sampled the whole linear part of the response of the neuron or model, with only the highest and lowest values forcing it into saturation (Gussin et al., 2007). Each step was 400 ms long and was followed by a 1 s pause to guarantee that the cell was not any longer adapted to the last step. Each intensity was played back 10 times, in a sequence with the other steps such that one high intensity was always followed by a low intensity.

We stimulated with sinusoidal amplitude modulations (SAMs) to assess the frequency tuning of cells and models. SAMs ranged from 2 to 300 Hz at contrasts of 5, 10 and 20 %. We also used higher frequencies, but decided to exclude them, as the EOD is the carrier to all AMs and, following the Nyquist theorem, AM frequencies higher than EODf/2 are not represented well in the signal. Each frequency was played back between

200 and 450 times. To test cross-frequency effects, we used random amplitude modulations (RAMs). They consisted of 2 s of Gaussian white noise with a cutoff-frequency of 300 Hz and a standard deviation of 0.3 at 5 % contrast.

All stimuli were generated by multiplying the EOD with the desired AM. In the model, the phase of the EOD in each trial was randomised to account for the fact that we did not control the AM with respect to the EOD in the experiments. In general, AM stimuli can also be produced by simulating another electric signal that by superposition with the EOD of the fish generates the desired AM. In the case of SAM stimuli, for example, the EOD of a conspecific can be played back with a frequency resulting from the addition of the fish's EODf and the desired beat frequency. In the model, we tested both – direct EOD and multiplied AM stimuli – and found no differences in the resulting responses.

Data Analysis

Baseline

From each P-unit we recorded at least 30 s of baseline activity, i.e. activity in the presence of an unmodulated EOD. Likewise, we simulated 50 s of the model. From this data the four baseline parameters mean firing rate, CV, VS, and SC were extracted. The mean firing rate was calculated as the number of spikes divided by measuring time. From the ISIs the CV was calculated as their standard deviation divided by their mean,

$$CV = \frac{\sigma}{\mu}. \tag{4.6}$$

The SC_x was calculated as the correlation coefficient between successive ISIs of a particular lag, x,

$$SC_x = \frac{\langle (p_i - \langle p \rangle_t)(p_{i+x} - \langle p \rangle_t) \rangle_t}{\sqrt{\langle (p_i - \langle p \rangle_t)^2 \rangle_t} \sqrt{\langle (p_{i+x} - \langle p \rangle_t)^2 \rangle_t}}, \tag{4.7}$$

where p_i is a certain ISI and p_{i+x} the one succeeding with a lag of x intervals. $\langle ... \rangle_t$ denotes averaging over time. As a measure of the phase-locking to the EOD, the VS was calculated as

$$VS = \frac{1}{n} \sqrt{(\sum_{i=1}^{N} sin\phi_i)^2 + (\sum_{i=1}^{N} cos\phi_i)^2}, \tag{4.8}$$

where t_i is the time of the i^{th} spike and $\phi_i = 2\pi(t_i - \text{time})/\text{period}$ the phase of the EOD period at which it occurred.

f-I-curves

The time course of the firing rate response to all following stimulation protocols (the peri-stimulus time histogram) was computed by convolving each spike train with a

Gaussian kernel with a standard deviation of 1 ms and averaging over trials. 1 ms was chosen since it corresponds to the fast excitatory component of excitatory postsynaptic potential evoked by P-units in their target cells, the pyramidal cells in the electrosensory lateral line lobe (ELL, Berman and Maler, 1998).

For each step intensity we then calculated the onset response as the maximal deflection of the rate during a window of 20 ms following stimulus onset relative to the average baseline rate. The steady-state response was calculated as the average rate during the last 200 ms of stimulus application.

The slope of the steady-state f-I-curve (f_∞) was derived from a linear fit to the data. We defined the slope of the onset-f-I-curve (f_0) at the point of inflection, which we derived from a fit to the Boltzmann function,

$$y = \frac{p_0}{1.0 + \exp(-p_1 * (x - p_2))} + p_3\,, \tag{4.9}$$

where $\frac{p_0 * p_1}{4}$ gives the slope.

Sinusoidal stimuli

The response to SAM stimuli of different frequencies was characterised using two measures. First, the modulation depth of the rate was calculated as the standard deviation of the rate response. Second, the correlation over trials was assessed by the average correlation coefficient (Equation 4.7) between all pair-wise combinations of trials. From then resulting tuning curves, we also determined the cutoff frequency to both high and low frequencies as the frequency at which the response drops to half its maximal value.

Noise stimuli

To characterise the frequency response of cells and models to random amplitude modulations (RAM), we used the coherence. The coherence function between two time-varying signals $s(t)$ and $r(t)$ is given by

$$C_{sr}(f) = \frac{\|\langle SR\rangle\|^2}{\langle SS\rangle\langle RR\rangle}\,, \tag{4.10}$$

in which S and R are the signals in the frequency domain. SR is the cross spectrum and SS and RR the auto spectra. $\langle ...\rangle$ denotes averaging over trials. The spectra were calculated using Hanning windows with 50 % overlap. The coherence function can take values between 0 and 1 with high values reflecting a linear relationship between the two signals. We measured the coherence between stimulus and response as a measure of encoding linearity at different frequencies. The coherence between different trials we took as a measure of coding reliability. In both cases each spike train was convolved with a Gaussian kernel of 1 ms width. The mean was subtracted for both, response and stimulus. The stimulus-response coherence was then calculated as the coherence between the average rate response and the stimulus, the response-response coherence

as the square root of the average coherence between all pairs of trials (Roddey et al., 2000).

Goodness of fit

To quantify the goodness of fit of a certain model, we used the per cent error between the response characteristics of this model neuron and its target cell. The goodness of fit to baseline activity and f-I-curves was assessed by the errors of the baseline activity characteristics: the baseline rate, CV, VS and SC and the slopes of the f-I-curves, f_0 and f_∞.

To examine the quality of the response predictions to SAM and RAM stimuli, we as well used the per cent errors between values derived from model and cell data. The per cent error of the tuning curves to SAMs was calculated as the mean error normalised by the mean response (rate modulation or correlation averaged over frequencies). We also calculated the error of the cutoff frequencies. From the responses to RAM stimuli the per cent error was estimated of the rate response as the per cent error of the mean rate modulation (i.e. standard deviation of the rate response). The errors of the coherences were estimated as the mean error normalised by the mean coherence.

Additionally, we used the correlation coefficient between cell and model results to quantify the similarity of the shape of the frequency tuning. From the SAM responses we calculated the correlation coefficients between the response tuning curves of cell and model. The RAM prediction quality was quantified by the correlation coefficient between the rate responses as well as the coherences of cell and model.

Sensitivity Analysis

To assess the influence each parameter has on the activity of the model, we changed the parameters one by one in a relative fashion from 0.5 to 1.5 of their value, and compared the response properties of the altered models to the default model. For each realisation we adjusted I_{Bias} to match the baseline firing rate and to avoid confounding effects of different firing rates. All relations between parameter and property were significantly linearly correlated (p-value < 0.05). However, the size of the effect varied strongly. We quantified it by the normalised sensitivity coefficient $S(C, P)$ between a certain response characteristic C and the parameter P according to

$$S(C,P) = \frac{dC/C_{\text{default}}}{dP/P_{\text{default}}}\,. \tag{4.11}$$

Specifically, we calculated $S(C, P)$ as the slope of a linear regression between dC and dP, given by

$$\frac{dC}{C_{\text{default}}} = S(C,P) * \frac{dP}{P_{\text{default}}} + X\,. \tag{4.12}$$

The response characteristics C we used in the sensitivity analysis were the same six baseline characteristics as before. However, the Boltzman fit was too unstable to derive

f_0 from it, and we derived it from a linear fit of the middle part of the f-I-curve. For the analysis of changes in SAM response predictions, we used the correlation coefficients between the tunings of the modified model and the reference model, as well as the mean errors between the two data series. For the RAM responses, the correlation coefficients and the errors of the rate response fluctuations (i.e. standard deviations) and of the coherences were evaluated.

4.3 Results

We here present a model of P-unit electroreceptors. Our aim with the model was twofold: To investigate the variability in biophysical parameters underlying population heterogeneity in these neurons and to examine their frequency tuning. Specifically, we examined whether a model constrained to baseline discharge characteristics is able to reproduce the frequency tuning to simple and complex stimuli.

The model is designed and fit to baseline activity

We start with the description of the response characteristics of P-units that form the basis of our model. A complete characterisation of their activity has been the subject of previous studies (Gabbiani et al., 1996; Gussin et al., 2007; Scheich et al., 1973; Wessel et al., 1996; Xu et al., 1996; Zakon, 1986). Under baseline conditions, P-units are stimulated by a constant EOD, to which they respond with a constant baseline rate, but high interspike interval (ISI) variability (Fig. 4.1 A). This variability is reflected in a broad ISI histogram (Fig. 4.1 B) that is discrete because of phase-locking to the EOD. Successive ISIs are negatively correlated at first lag (Fig. 4.1 C), a prominent feature of P-units resulting from their strong spike-frequency adaptation (Chacron et al., 2001a; Farkhooi et al., 2009; Ratnam and Nelson, 2000). Overall, the baseline activity of single cells can be described by the well-established measures baseline firing rate, coefficient of variation (CV) and first serial correlation (SC) of ISIs as well as vector strength (VS) of EOD coupling. Note that we ignore possible positive correlations among ISIs at longer time scales that have been described in P-units before (Chacron et al., 2001a). Such positive correlations show up as an increase in the Fano factor for long analysis windows, a feature that we only saw inconsistently in some of our cells and therefore chose to disregard.

The probability with which P-units fire at each EOD cycle depends on the amplitude of the EOD. Upon a step in amplitude the cells show a strong initial response that decays to a steady-state upon constant stimulation (Fig. 4.1 D). The response can also be a reduction of activity and increase to a steady-state if the EOD amplitude is decreased (as upon termination of the step in Fig. 4.1 D). Cells with such a behaviour to step stimuli can be described by two f-I-curves (relationships between firing rate and stimulus strength, Fig. 4.1 E, Benda et al., 2005, 2010). One is derived from the maximal response at stimulus onset for steps of different amplitudes, the other as the steady-state response

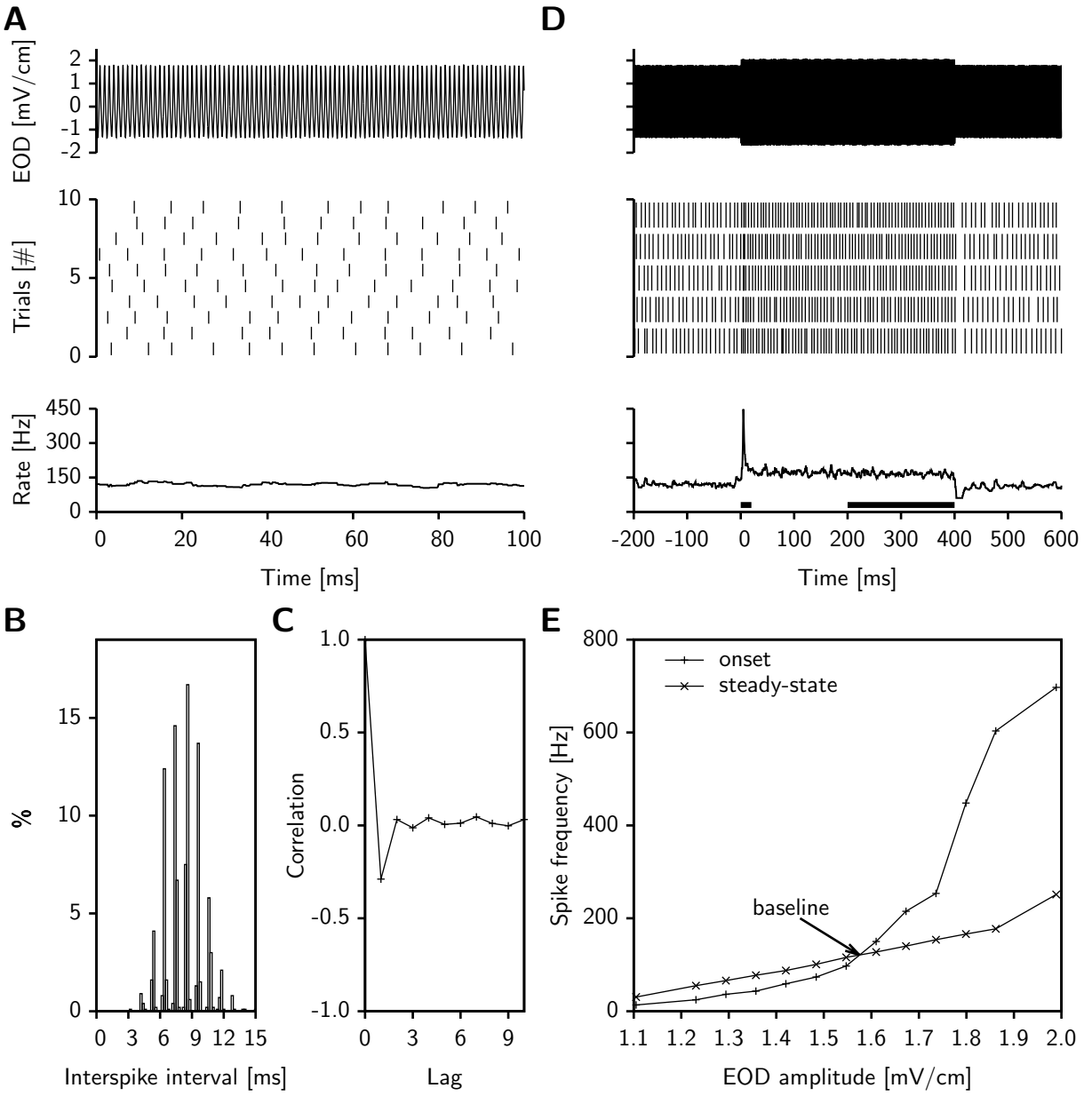

Figure 4.1: Baseline activity and f-I-curves of P-units. **A**) Stimulus and response of a representative P-unit under baseline conditions, when the EOD amplitude is constant. The EOD is shown in the top panel, the spiking response in the middle panel and in the third panel the rate as obtained by convolving the spiking response with a Gaussian kernel of 1 ms width. **B**) and **C**) show the interspike interval (ISI) histogram and the correlations of successive ISIs derived from the baseline activity in A, respectively. **D**) shows the activity of the example cell under step stimulation. The organisation of the panels is the same as in A. **E**) Two f-I-curves are calculated from the responses to step stimuli of different intensities: The onset f-I-curve is generated by taking the maximum in a window after stimulus onset and the steady-state f-I-curve by averaging in a second window in the last second half of the stimulus (the windows are indicated in D as black bars). At the baseline EOD amplitude, the two curves intersect.

after adaptation to each step. The slopes of the two f-I-curves, f_0 (onset) and f_∞ (steady-state), indicate the firing rate sensitivity of the cells, as higher slopes indicate a bigger change in firing rate associated with a certain change in EOD intensity.

Based on these characteristics, we designed the model (Fig. 4.2): We chose a simple form of spike generator, the noisy leaky integrate-and-fire model, that integrates the stimulus with a low-pass filter of time constant τ_V and a noise current of strength $\sqrt{2D}$ until it reaches a threshold and a spike is noted (Lapicque, 1907). The adaptation was modelled as a negative adaptation current that is incremented at every spike by Δ_A and relaxes back to zero exponentially with a certain time constant τ_A (Benda and Herz, 2003). We designed the stimulus as a modulated EOD to preserve phase-locking to the EOD. The stimulus was passed through a nonlinearity that clipped it at zero as well as a low-pass filter with time constant τ_D simulating processes at the synapse and the unmyelinated dendritic processes, respectively. The gain factor α and offset I_{Bias} account for the different sensitivities and baseline rates of different cells.

The model has the seven parameters τ_D, α, I_{Bias}, τ_V, $\sqrt{2D}$, Δ_A and τ_A. When these are constrained in a fit routine to match a cell's mean firing rate, CV, VS, SC and f_0 as well as f_∞, the model reproduces the full baseline ISI histogram (Fig. 4.3 A), all serial correlations (Fig. 4.3 B) as well as the full onset- and steady-state f-I-curves of the target cell (Fig. 4.3 C). We repeated the fit for all 23 P-units (baseline rate$=$ 144.14 Hz$\pm$32.5; $CV = 0.281 \pm 0.05$) of which we had recorded baseline activity and responses to step and SAM stimuli. The fit was successful for all target data sets showing that the result is not specific for one example neuron. The rate, CV and VS lie within 10 % range of the target values, only the SC is matched poorer (Fig. 4.3 D). The errors of f_0 and f_∞ are also higher and lie between $\pm$20 %. The error values of the example cell (points in Fig. 4.3 D) lie well within the range of those of the other cells, demonstrating that such error values correspond to a very good match of the entire shapes of ISI histogram, ISI correlations and f-I-curves.

In order to test the necessity of the dendritic low-pass filter we also fit the model without such a filter to the data. This reduced model matches the shape of the ISI histogram, but fails to match its peak height (Fig. 4.4 A). The f-I-curves of cell and model correspond nicely (Fig. 4.4 B). The mismatched histogram peak is reflected in a mismatch of VS. The model without the filter consistently leads to strong phase-locking and therefore only produces activity with high VS (Fig. 4.4 C).

The model reproduces the heterogeneity of P-units

Our sample of 23 P-units differs in all four baseline response characteristics as well as in the slopes of the f-I-curves (see Fig. 4.5 A–F, distributions of cells in grey). It approximately covers the range that has been described for these neurons, although the baseline firing rates are lower than seen in previous studies (Nelson et al. (1997) report firing rates around 320 Hz, Gussin et al. (2007) around 200 Hz). This might be caused by the rigorous criterion that we applied to leave out bursting cells (see Sec. 4.2). Bursting

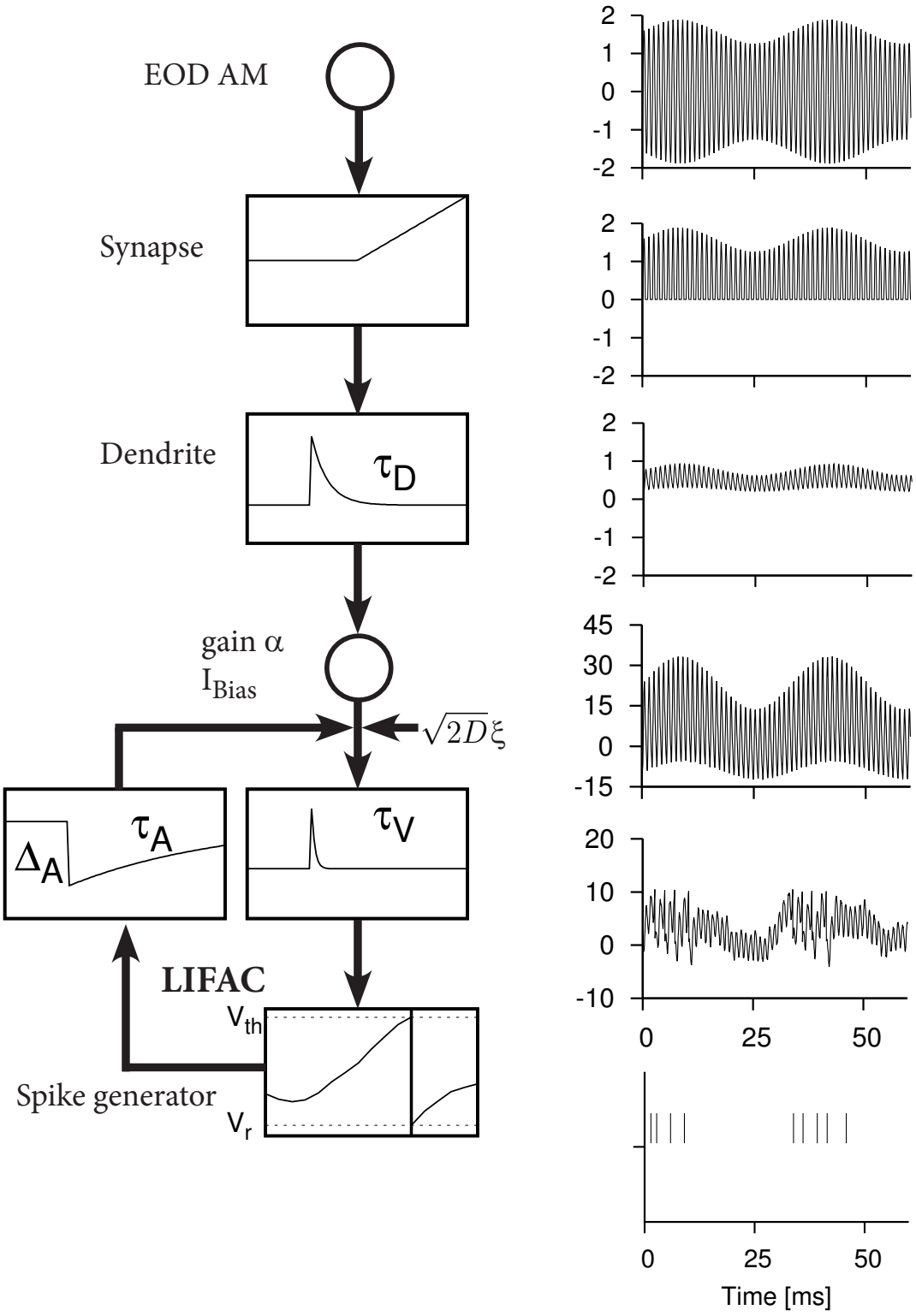
EOD AM
Synapse
Dendrite
τ_D
gain α
I_{Bias}
$\sqrt{2D}\xi$
τ_A
Δ_A
τ_V
LIFAC
V_{th}
V_r
Spike generator
2
1
0
-1
-2
45
30
15
0
-15
20
10
0
-10
0
25
50
Time [ms]

Figure 4.2: P-unit model. The EOD and possible AMs are sensed by tuberous receptors (top panel on the right). The synapse between receptor and afferent clips the signal at zero (second panel). This zero-clipped signal is low-pass filtered in the dendritic processes with a certain time constant τ_D (third panel) and enhanced by a gain (α) and offset (I_{Bias}) at the cell (fourth panel). The processes at the cell body are modelled by a leaky integrate-and-fire model with an adaptation current (the integrated input is shown in the fifth panel). When it reaches the threshold, a spike is noted (sixth panel) and the voltage is reset to zero. Also, the adaptation current is incremented by Δ_A and relaxes back to zero with a time constant τ_A. All left panels schematically depict the mathematical operations: Heaviside function, low-pass filtering, leaky integration, reset at threshold, and the feed-back of the negative adaptation current.

is positively correlated with firing rate (not shown), we thus underestimate the firing rate.

The model can not only be fit to all different P-units regardless of their characteristics, it also reproduces the distributions of these characteristics (see Fig. 4.5 A–F, distribution of model values in black). Furthermore, over cell and model population the response characteristics exhibit the same correlations. Cells and model with higher rates also show higher SCs, those with higher CVs also have higher slopes of both their f-I-curves and the slopes of the two f-I-curves are correlated as well. The model population thus resembles the heterogeneity of the P-unit population in terms of both, variability and correlation of the response characteristics.

Parameter variability underlies heterogeneity

Causing the heterogeneity in the model is a high variability of parameter values over fits to different target cells (Fig. 4.6). The distributions of values for each parameter are of different shape and width. We determined the degree of variation as the percentage of the median value that the semiquartile range took up. The latter is defined as half the difference between first and third quartile. The semiquartile range spans from 11 % (for τ_A) to 78.5 % (for the I_{Bias}, see Table 5.3) of the median value. This means that half the values of the different models are spread over 22–157 % of their median value, demonstrating that the models vary greatly in the values of their parameters.

In addition to heterogeneity compensatory effects can also cause variation in parameter values, when two parameters are jointly varied without affecting the outcome. Compensations lead to correlations between parameters. In the model only the following are significantly correlated: Δ_A, τ_V and $\sqrt{2D}$ (see Table 5.3), implicating that there are little compensatory effects.

Sensitivity analysis relates parameters with model activity

The basis for the heterogeneity in baseline characteristics thus lies in the variability of the model parameters. But which parameter influences which characteristic? We addressed this question in a so-called sensitivity analysis. We varied the model parame-

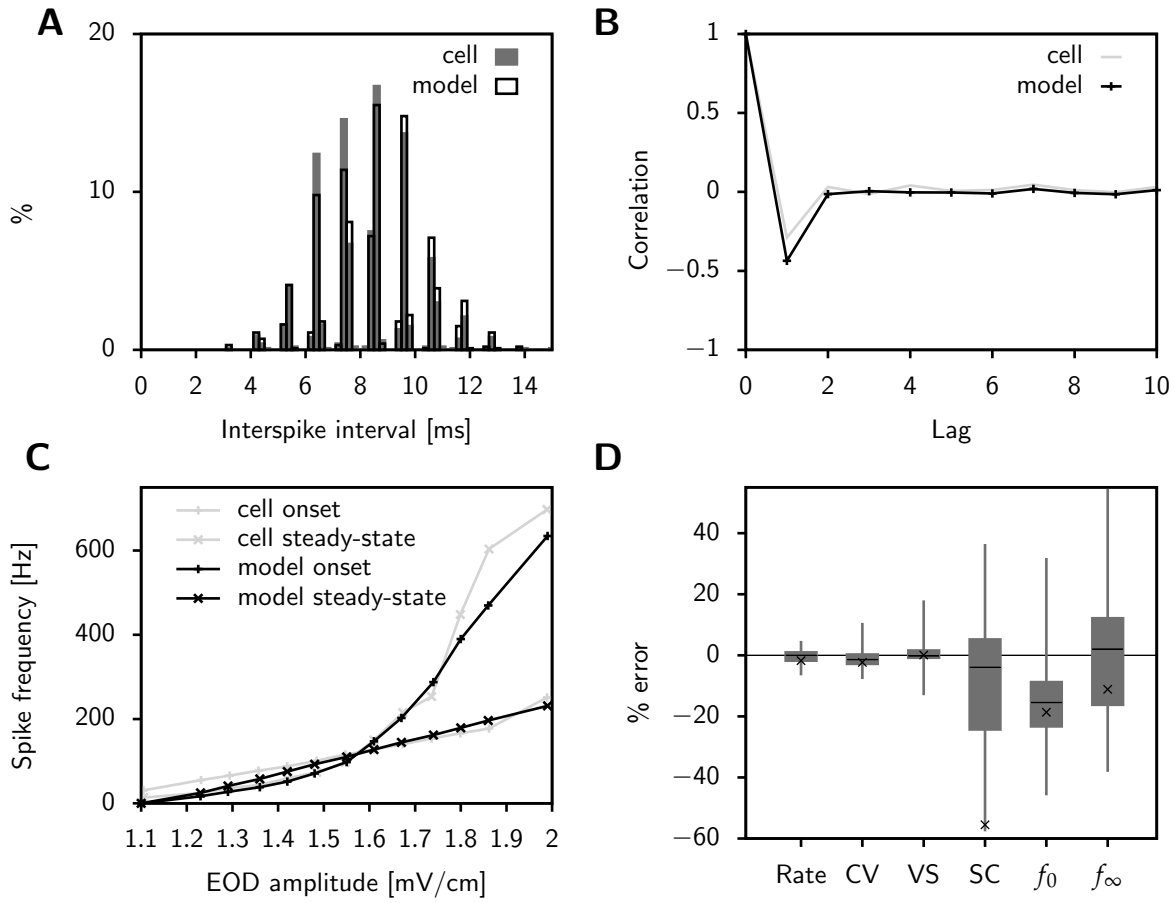

Figure 4.3: Fit of the model. **A**) The ISI histogram of one representative P-unit (the same as in Fig. 4.1) is shown together with that of the corresponding model. **B**) The serial correlations between successive ISIs and **C**) the f-I-curves for the same cell and model. **D**) shows the per cent errors of all 23 fits for the baseline rate, the coefficient of variation, CV, and the first serial correlation, SC, of the ISIs, the vector strength of phase-locking to the EOD period, VS, and the slopes of the f-I-curves, f_0 and f_∞, indicated as medians, interquartiles and maximal values. Points show the values of the example cell from A–C.

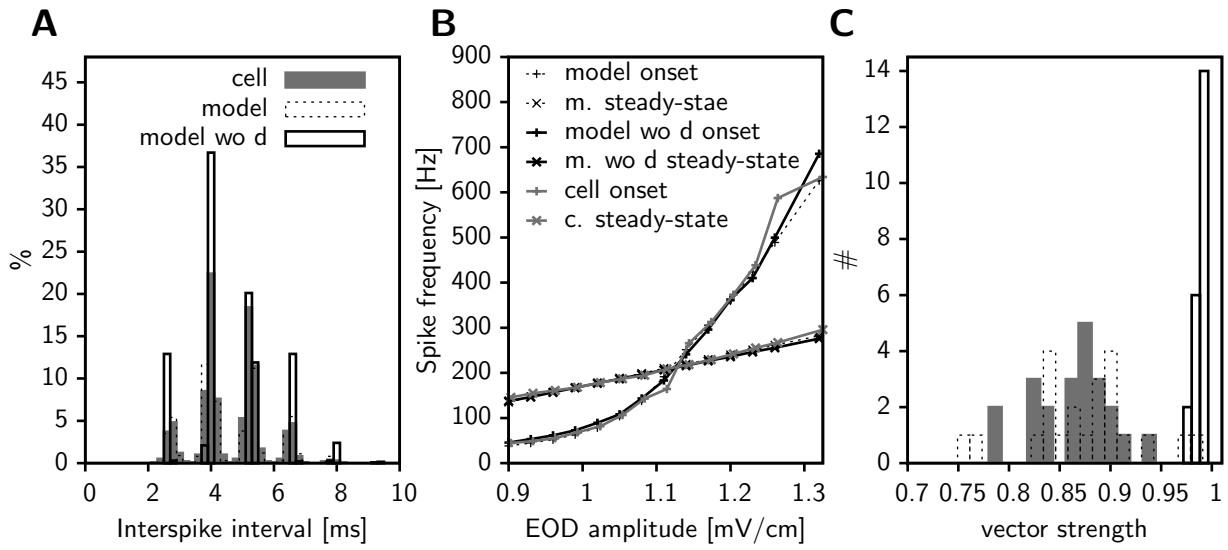

Figure 4.4: Effect of the dendritic low-pass filter. **A**) shows the baseline ISI histogram for the example cell ("cell") and the results of the corresponding model with ("model") or without ("model wo d") a dendritic low-pass filter (same fitting procedure was used). The latter can match the shape of the histogram, but fails to match its peak height. **B**) shows the f-I-curves for the same cell and models. **C**) The model without the filter was fit to all 23 cells. This panel shows the distribution of VS for the cells, the model with a low-pass-filter as well as without the low-pass filter (the legend is the same as in A). The reduced model consistently leads to strong phase-locking reflected in high VS.

ters in a relative fashion between 0.5 and 1.5 of their default value and measured the corresponding relative change in the response characteristics. To eliminate confounding effects by different baseline rates, the rate was adjusted via I_{Bias} and this parameter therefore left out of the analysis. In the following, we describe the changes in the six response characteristics caused by changing each of the model parameters. We restrict the descprition to those relations in which doubling the value of a parameter led to a change in response characteristic of at least 10 % corresponding to a sensitivity coefficient S (see Eq. 4.11) of at least 0.1 (relations shown in Fig. 4.7 and Table 4.2).

Increasing the gain factor α most strongly influences f_∞ and f_0, but it also increases VS (Table 4.2, first row, Fig. 4.7 C, D and F, first panels). These effects are expected, since increasing α will increase the effective stimulus strength and thus the sensitivity of the cells to the EOD stimulus. Increasing noise strength $\sqrt{2D}$ has the opposite effect and predictably increases the CV and decreases the SC as well as the VS (Table 4.2, second row, Fig. 4.7 A and B first panel, C second panel). The CV is a measure of discharge variability, while the SC and VS rely on response regularity with respect to the ISIs and the phase of the EOD, respectively.

Lengthening the membrane time constant τ_V decreases the CV, the SC and f_∞ and, particularly, f_0 (Table 4.2, third row; Fig. 4.7 A, B and D, second panels). Its influence on the CV and on f_0 results from its low-pass filter effect. The first is decreased because fast components and thus the effective amplitude of the Gaussian noise are reduced. The

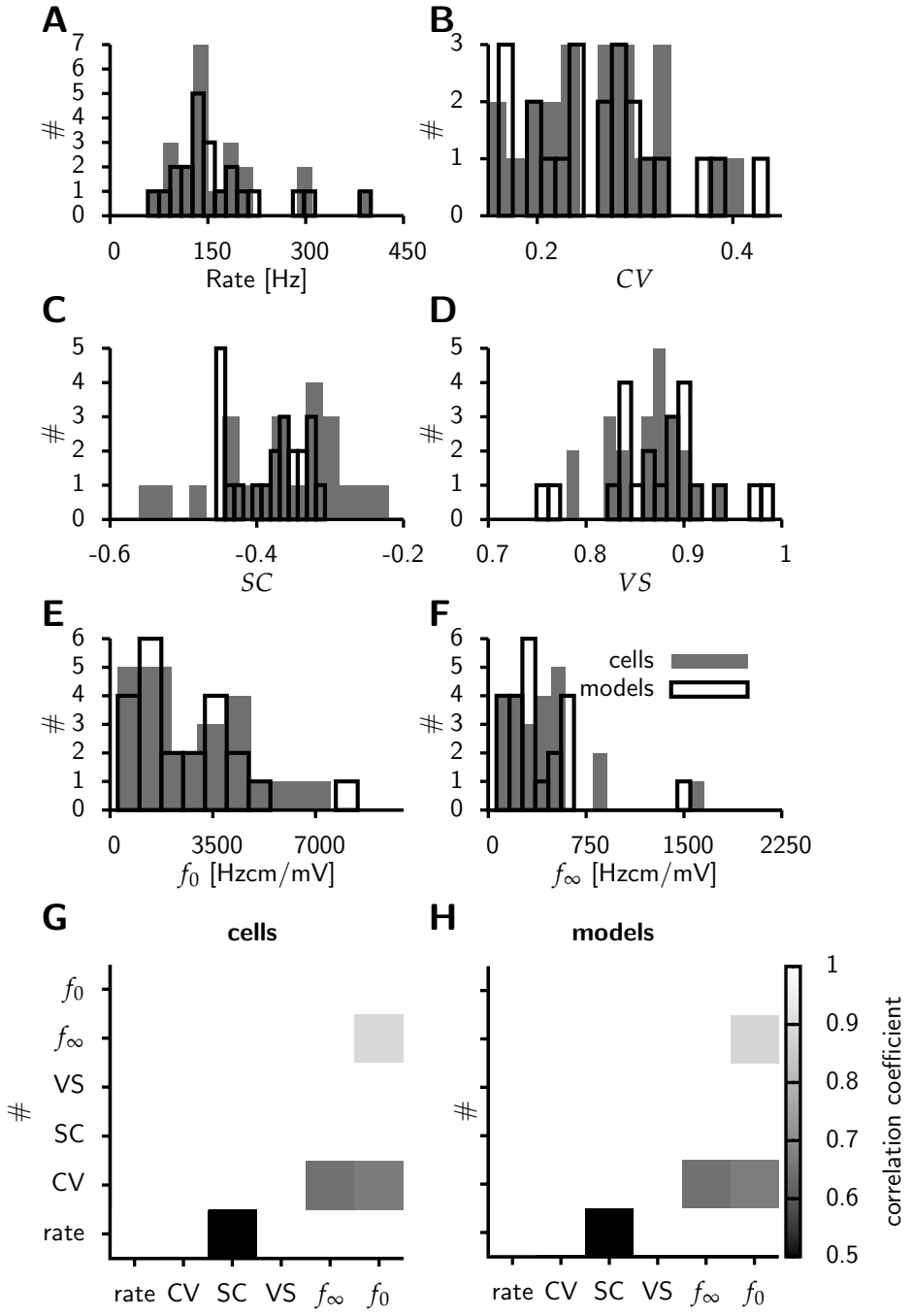

Figure 4.5: Distributions of response characteristics of cells and models. Shown are the distributions of cells (grey, filled boxes) and model fits (black, empty boxes) for the following response characteristics: **A**) baseline rate, **B**) CV, **C**) SC, **D** VS, **E**) f_0 and **F**) f_∞. Correlations between these six response characteristics are shown in **G**) for the values from the recorded cells and in **H**) for the corresponding values. Shown are those correlation coefficients that are statistically significant (p-value < 0.05, Bonferroni corrected).

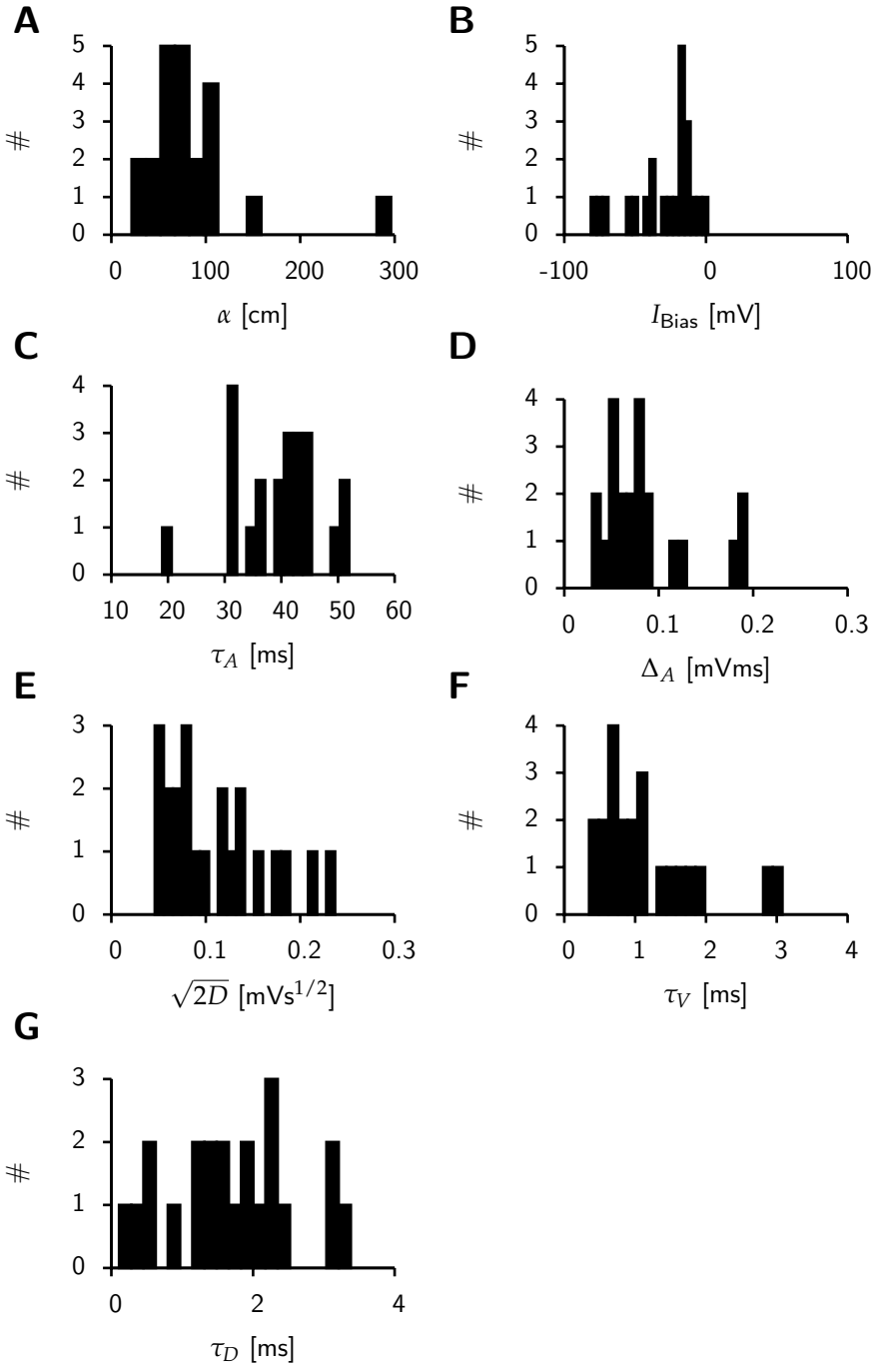

Figure 4.6: Distribution of model parameters. Shown are the distributions of the seven parameters that were adjusted during the fit routine: **A**) gain factor α and **B**) offset I_{Bias} of the input current, **C**) time constant τ_A and **B**) increment Δ_A of the adaptation current, **E**) strength $\sqrt{2D}$ of the noise current, **F**) time constants of the membrane τ_V and **G**) dendritic low-pass-filter τ_D. Shown are the values that were the result of the best fit for 23 cells.

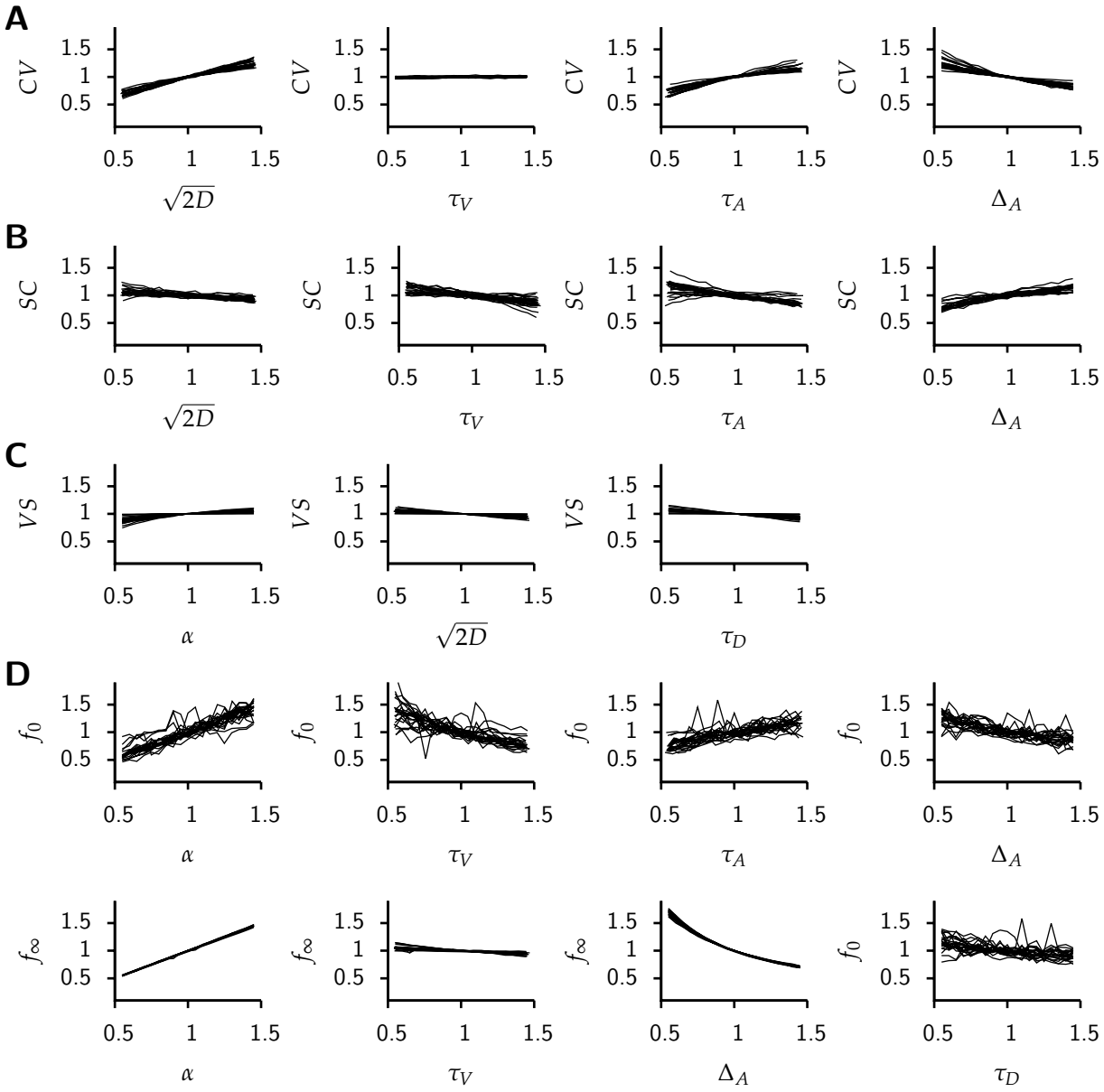

Figure 4.7: Sensitivity of baseline characteristics. The relative change of different baseline parameters as a result of changing a certain model parameter is shown. For example, by increasing the noise strength $\sqrt{2D}$ by half, the CV is increased by half, while it is increased only slightly when increasing the membrane time constant τ_V (first and second panel in the top row). The reference value is the default model, the different lines show the relation for the 23 fits. All relations whose slope lies above 0.1 are shown for effects on **A**) the CV **B**) the SC, **C**) the VS and **D**) the slopes of the f-I-curves. The order of the underlying parameters from left to right are: α, $\sqrt{2D}$, τ_V, τ_A, Δ_A and τ_D. If a parameter did not have an effect, the panel for the next one is shown in its place (as for example α did not have an effect in A, the relation with $\sqrt{2D}$ is shown in the first panel).

Table 4.1: Distributions of model parameters. From the distributions shown in Fig. 4.6 median values and semiquartile ranges are shown in the second column. To quantify the dispersion of values, the semiquartile ranges are given in the second column as percentages of the median. The semiquartile range is defined as half the difference between first and third quartile. The right part of the table shows the correlations between optimal model parameters. Only significant correlations are shown ($p < 0.05$, Bonferroni corrected).

parameter	median value	per cent	α	I_{Bias}	$\sqrt{2D}$	τ_V	τ_A	Δ_A	τ_D
α [cm]	77.9±20.58	26.4	1.0						
I_{Bias} [mV]	−17.19±13.49	78.5		1.0					
$\sqrt{2D}$ [mVs$^{1/2}$]	0.098±0.04	41.1			1.0	0.91		0.84	
τ_V [ms]	0.95±0.46	48.4			0.91	1.0		0.72	
τ_A [ms]	41±4.5	11					1.0		
Δ_A [mVms]	0.0768±0.0246	32			0.84	0.72		1.0	
τ_D [ms]	1.804±0.55	30.7							1.0

Table 4.2: Sensitivity Analysis of Baseline Response Characteristics. Shown are the sensitivity coefficients $S(C,P)$ (see Eq. 4.11) of the relations between changes in model parameters P and resulting changes in response characteristics C (full relations shown in Fig. 4.7). All $S(C,P) > 0.1$ are bold. They correspond to a 10 %-change in response characteristic C, when changing the model parameter P by 100 %, and are discussed in the text.

param.	CV	SC	VS	f_∞	f_0
α	−0.02±0.02	−0.01±0.03	**0.17**±0.09	**1.00**±0.01	**0.90**±0.18
$\sqrt{2D}$	**0.62**±0.11	−**0.15**±0.09	−**0.12**±0.06	−0.04±0.02	−0.07±0.07
τ_V	−**0.64**±0.21	−**0.27**±0.16	−0.07±0.03	−**0.12**±0.06	−**0.64**±0.27
τ_A	**0.47**±0.12	−**0.31**±0.20	0.02±0.01	0.01±0.01	**0.44**±0.17
Δ_A	−**0.44**±0.15	**0.37**±0.14	−0.02±0.01	−**1.03**±0.05	−**0.43**±0.14
τ_D	−0.01±0.02	0.01±0.03	−**0.15**±0.08	−0.04±0.03	−**0.25**±0.19

second effect is confined to high intensity steps (not shown), to which the maximal firing rate of the model is decreased. The dependency with the SC exhibits a different shape for different models. The SC has a maximum when the time scale of adaptation exactly matches the baseline firing rate (Benda et al., 2005). In Fig. 4.7 B, second panel, some curves have a slightly positive slope in contrast to the negative slope seen on average. For most models the SC would be greater for a smaller τ_V while it is too long for others.

Stronger adaptation, thus an increase in Δ_A, decreases the CV, increases the SC and decreases f_0 as well as f_∞ (Table 4.2, fifth row, Fig. 4.7 A, B and D, fourth panel, last row third panel). The influence of adaptation on ISI variability depends on the adaptation time scale (Liu and Wang, 2001; Schwalger and Lindner, 2013). When the adaptation time scale is on the order of the mean firing rate, it decreases the variability (Benda et al., 2010; Liu and Wang, 2001) and thus the CV. It has also been shown that adapta-

tion leads to negative ISI correlations (Chacron et al., 2001a) and that this correlation is increased by increasing the strength of adaptation (Liu and Wang, 2001), which explains the effect on the SC. The negative adaptation current decreases the effective stimulation current and thus decreases the f-I-curve slopes. The effect is stronger on f_∞ which is in accordance with its high-pass filter effect (Benda et al., 2005).

The adaptation time constant, τ_A, increases the CV and f_0, while it decreases the SC (Table 4.2, fourth row, Fig. 4.7 A, B and D, third panels). When the adaptation current is incremented by Δ_A at each spike, it is normalised by τ_A (Eq. 5.3) as a result from the Euler integration method. Increasing τ_A therefore at the same time decreases the magnitude of the adaptation current. As a consequence f_∞ is constant upon changes in τ_A, because the effect of lengthening the relaxation of the adaptation current cancels out that of decreasing it maximal strength. The normalisation also leads to effects on the CV, the SC and f_0 that oppose the effects of Δ_A. However, previous studies have also shown that increasing τ_A increases the ISI variability (Liu and Wang, 2001; Schwalger and Lindner, 2013). The effect of τ_A on the SC seems to be nonlinear, in the same way as shown for τ_V, as the SC is highest when τ_A matches the baseline firing rate (Benda et al., 2010). In Fig. 4.7 B, third panel, some curves exhibit a positive slope in contrast to the negative slope of the average.

It was shown above (Fig. 4.4) that the dendritic low-pass filter is needed to reduce the phase-locking to the EOD. Increasing its length by increasing τ_D decreases the VS (Table 4.2 sixth row, Fig. 4.7 C third panel). It also has an effect on f_0 which it decreases (Fig. 4.7 last panel). By filtering out high frequencies, the fast onset of the step stimulus is washed out and the onset response is decreased.

Models predict responses to sinusoidal stimuli

We now turn to the second aim of our study which is the investigation of the frequency tuning of our P-unit model. When stimulated with sinusoidal amplitude modulations (SAM), P-units respond with an increased rate during the peaks, while the rate is decreased during the troughs (Fig. 4.8 D, Chapter 3, Wessel et al., 1996). The magnitude of rate modulation depends on the frequency of the SAM, being strongest for intermediate frequencies between about 50 and 150 Hz and decaying for both lower and higher frequencies (Fig. 4.8 E). The pattern of how P-units respond reliably to the stimulus, as seen in the correlation over trials, is similar (Fig. 4.8 F). The model cell reproduces the behaviour of its real-cell counterpart in both the time course of the spike and rate response to single frequencies (Fig. 4.8 C and D, except for the axonal delay (Heiligenberg and Dye, 1982; Nelson et al., 1997) that is not included into the model) as well as the shape and the height of the frequency tuning in terms of rate modulation (Fig. 4.8 E) and correlation over trials (Fig. 4.8 F). Since the model was neither designed nor calibrated to reproduce the frequency tuning of P-units, this is an emergent property from their responses to baseline condition and step stimuli.

The rate mainly fluctuates around an average firing rate which does not depend much on the stimulus frequency (Fig. 4.8 G). However, P-units show an enhanced re-

sponse to AMs with a frequency close to their baseline frequency or multiples thereof. This nonlinear effect is reproduced by the model (Fig. 4.8 G, this cell fired at 210 Hz. See also Brunel et al., 2001; Fourcaud-Trocmé et al., 2003; Knight, 1972b). However, the locking is smaller in the model than in the cell, indicating that our model for the neuronal noise is not optimal (Brunel et al., 2001; Fourcaud-Trocmé et al., 2003).

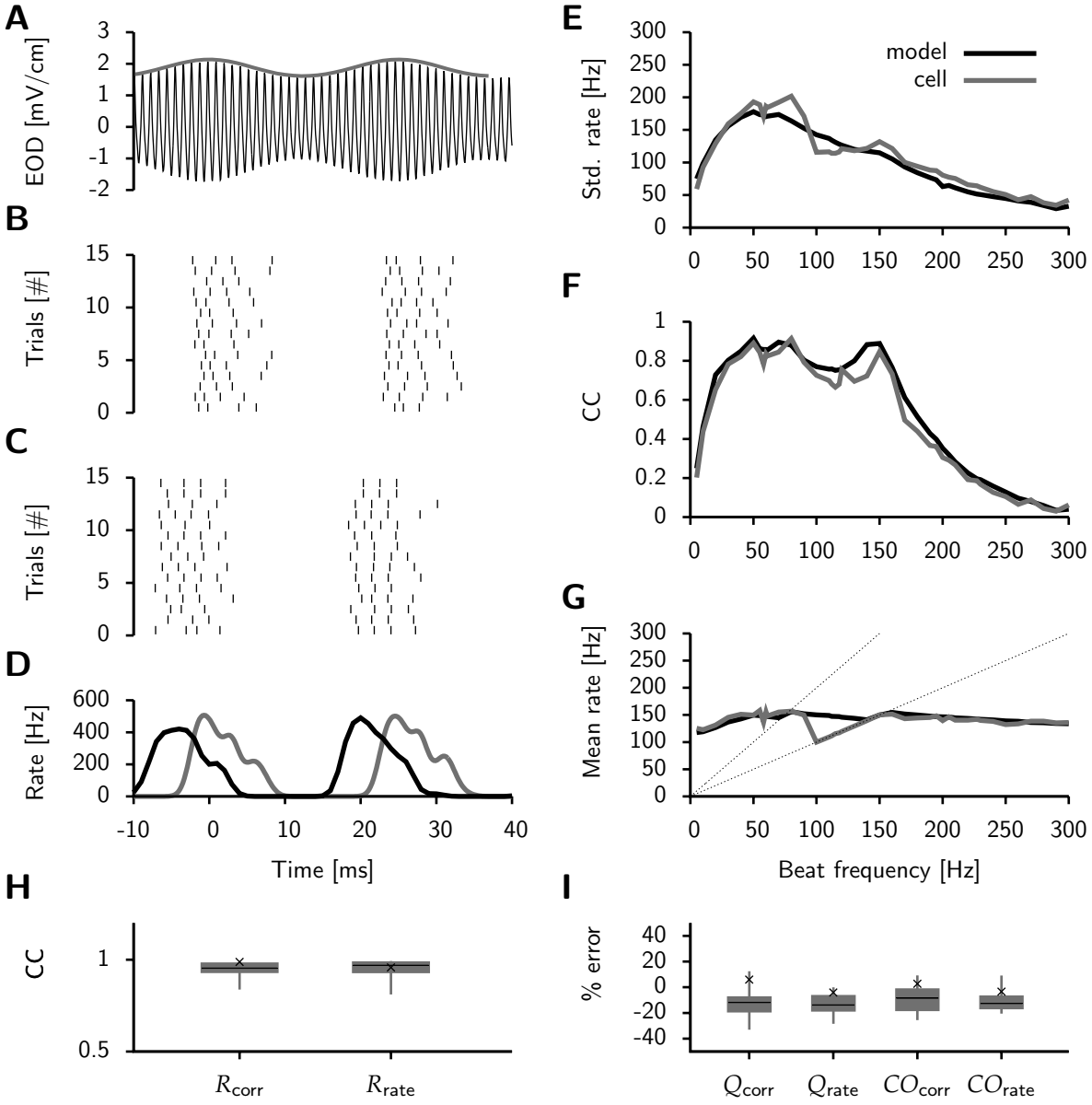

Figure 4.8: Response of cell and model to sinusoidal stimuli. A) Cell and model were stimulated with sinusoidally amplitude modulated EODs of 40 Hz and 20 % contrast. The EOD is shown in black, its amplitude modulation in grey. **B**) shows the spiking response of the representative P-unit (the same as in Fig. 4.1 and 4.3) over different trials, **C**) the spiking response of the corresponding model. **D**) The spiking responses were convolved with a small Gaussian kernel (1 ms width) and averaged. Shown are the rate responses of the cell (black) and model (grey). **E**) The same cell and model were stimulated with sinusoidal AMs between 5 and 300 Hz (at 20 % contrast). From the rate response, the standard deviation as a measure of modulation depth was calculated. This is plotted over the stimulation frequency. **F**) The correlation coefficient over trials was also calculated and plotted over stimulation frequency. **G**) shows the mean rate of responses to all frequencies. The dashed lines show the bisecting line and twice the bisecting line. P-units show enhanced responses to AMs of their baseline firing frequency. They show up as peaks on the bisecting line as here seen primarily in the cell data. **H**) and **I**) summarise the prediction performances for all 23 modelled cells. H shows correlation coefficients between the frequency tunings of cell and model as derived from the correlation over trials (R_{corr}, derived from the values shown in F) and standard deviation of the rate (R_{rate}, derived from E), I shows per cent errors (Q_{corr} and Q_{rate}) and the cutoff frequencies (CO_{corr} and CO_{rate}) of these. The cutoff frequencies were calculated as the frequencies at which the response drops to half its maximum. We here only show high cutoff frequencies, because for many cells (as for our example cell), the lower cutoff lay below the frequencies we had used in our stimulation protocol. Shown are median, interquartiles and maximal values, the points show the values of the example cell.

The model reproduces SAM responses of different P-units as well as the population response

The prediction of the responses to SAMs worked well for all 23 cells. We calculated the correlation coefficients between the frequency tuning of each pair of cell and model to quantify how well the model reproduces the shape of the frequency tuning, and the per cent error as a measure of the reproduction of the exact magnitude. The shape of the frequency tuning is reproduced almost perfectly in the models, resulting in correlation coefficients between cells and models close to one (Fig. 4.8 H). The per cent errors lie within 20 % (Fig. 4.8 I).

The correlation over trials to SAM stimuli depends on the contrast of the stimulus. Different models reproduce the behaviour of their target cells for different contrasts (Fig. 4.9 A–C for contrasts from 5–20 %). The population response of the 23 models also matches the population response of the corresponding P-units at two different contrasts (Fig. 4.9 D and E). Interestingly, this population response does not exhibit resonances as the single neuron responses. Because each P-unit locks to a different frequency – its baseline rate, averaging smoothes out the peaks (Fig. 4.9 D and E). Similarly, the summed potential of all P-units in a nerve does not show peaks, but rather smooth band-bass tuning to SAMs (Fig. 4.9 F).

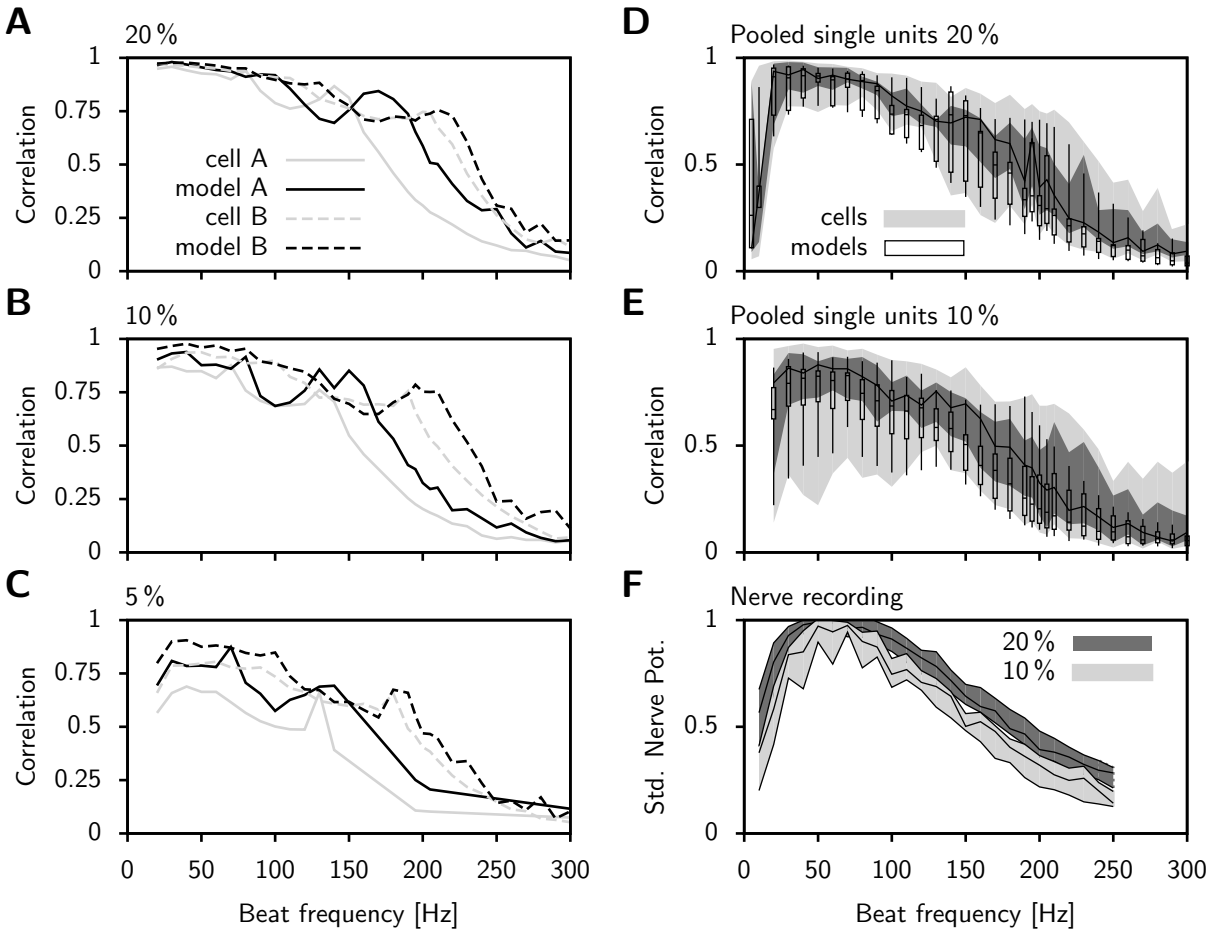

Figure 4.9: SAM responses to different contrasts and averaged over population. **A**) The responses to SAMs in terms of the correlation over trials (as plotted in Fig. 4.8 F), for two different cells and their corresponding models at 20 % contrast. **B**) and **C**) show the responses of the same cells to lower contrasts, 10 % and 5 %, respectively. **D**) The correlation over trials in response to SAMs of 20 % is averaged over cells and models. Candlesticks depict medians, quartiles and maxima of the model responses, the line and grey areas depict the medians (line) quartiles (darker grey) and maxima (lighter grey) of cell responses. **E**) The same as in D, but to SAMs at 10 % contrast. **F**) The population response of P-units as measured in whole nerve recordings to SAMs of 20 and 10 % contrast (the data for 20 % is the same data as shown in Fig. 3.6 C).

Table 4.3: Sensitivity of response predictions to SAM stimuli. The normalised sensitivity coefficient between parameter changes and alterations of the results as calculated by the slope of their relation. They are shown for the correlation coefficient (R_{Corr}) and the mean deviation (Q_{Rate}) between the frequency responses of model and target cell in terms of correlation over trials. For the rate modulation, the coefficients are shown only for the deviation (Q_{Rate}), as the correlation coefficient did not change when changing any of the parameters. The right two columns show the sensitivity coefficients for the errors of low and high cutoff frequencies as estimated from the rate response (low CO_{Rate} and high CO_{Rate}).

param.	R_{corr}	Q_{Corr}	Q_{Rate}	low CO_{Rate}	high CO_{Rate}
α	0.01 ± 0.01	$\mathbf{0.36}\pm0.15$	$\mathbf{0.29}\pm0.09$	-0.07 ± 0.25	-0.06 ± 0.06
$\sqrt{2D}$	0.01 ± 0.01	$-\mathbf{0.23}\pm0.11$	-0.09 ± 0.05	0.03 ± 0.15	-0.04 ± 0.04
τ_V	-0.00 ± 0.02	-0.04 ± 0.13	$-\mathbf{0.12}\pm0.06$	-0.02 ± 0.08	0.03 ± 0.08
Δ_A	-0.01 ± 0.01	-0.09 ± 0.06	$-\mathbf{0.13}\pm0.08$	$\mathbf{0.15}\pm0.57$	0.06 ± 0.04
τ_A	0.02 ± 0.03	0.09 ± 0.05	$\mathbf{0.12}\pm0.07$	-0.06 ± 0.22	-0.03 ± 0.07
τ_D	-0.00 ± 0.02	$-\mathbf{0.15}\pm0.08$	$-\mathbf{0.10}\pm0.06$	-0.01 ± 0.03	-0.06 ± 0.08

The height of the frequency tuning is senstive to changes in the parameters

We next examined how sensitive the prediction of SAM responses is to parameter changes. None of the parameters influences the shape of the frequency tuning strongly (Table 4.3), the correlation coefficient stay high), indicating that the band-pass tuning is a robust phenomenon of the model. This is not surprising as LIFAC models are known to be band-pass tuned (Benda et al., 2010). However, all parameters had an effect on the height of the tuning curves either in terms of the correlation over trials or in terms of the rate. Increasing α strongly increases the response to all frequencies (not shown) resulting in increases in the correlation over trials as well as in the rate modulation (Table 4.2 first row). This is due to an increase in signal-to-noise ratio, as I_{Input} becomes stronger while ξ is unaffected. In contrast, increasing the noise strength $\sqrt{2D}$ decreases the signal-to-noise ratio, thereby decreasing the tuning in terms of correlation over trials (Table 4.2 second row). The low-pass filter of the membrane, τ_V decreases the response to high frequencies, thus decreasing the responses in both correlation over trials and the rate (Table 4.2, third row).

Only the strength of adaptation Δ_A influences the cutoff frequencies. It has an effect on the low cutoff frequencies. It has been shown before that the cutoff frequency and the adaptation are inversely related (Benda and Herz, 2003; Benda et al., 2010). Surprisingly, τ_A does not influence the cutoff frequency as strongly. However, it decreases the response in terms of rate modulation (Table 4.2 fourth row) and does so by affecting mainly the responses to low frequencies (not shown). The negative effects of τ_D on the tuning in both correlation over trials and rate modulation can be explained by its low-pass filter-effect and the resultant response decrease to high frequencies.

The model predicts responses to noise stimuli

To check for cross-frequency effects on the encoding of different frequencies we now look at the responses of cells and models to random amplitude modulations (RAM). RAMs contain all frequencies in all possible combinations, but despite this complexity, the model reproduces RAM responses well (Fig. 4.10). The spiking and rate responses of cell and model are very similar (Fig. 4.10 B–D), apart from the small delay in the rate of the cell with respect to the model that we had seen in the responses to SAMs as well.

Models and cells exhibit similar coding linearity

We used the coherence function to estimate nonlinearities in the encoding in both cells and models. The coherence function measures frequency-dependant correlations between two time series. It reaches its maximal value, 1, if the relationship is purely linear, and takes on smaller values in the presence of noise or nonlinearities. We quantified the coherence between stimulus and response for both, the response of the cell and the corresponding model. We found great similarity between the two (Fig. 4.10 E). This suggests that the model adequately captures the nonlinearities and the noise inherent in P-unit responses.

To determine the maximal coherence that can be reached in the presence of noise, we also calculated the coherence between different trials. Again, the model yields similar values as the cell (Fig. 4.10 F) indicating that the neuronal noise can be adequately modelled by Gaussian white noise. Furthermore, this response-response coherence is only slightly higher than the stimulus-response coherence. This shows that stimulus encoding in P-units is mainly linear, because the lower coherence values result mainly from noise and not from nonlinearities.

We had recorded the response to noise stimuli in eleven P-units. As in examining the SAM responses, we calculated the correlation coefficients and per cent errors between the rate responses and the coherences of the models and the cells to examine the similarity of their shape and absolute values. All eleven pairs show only small deviations in shape (Fig. 4.10 G) and values (Fig. 4.10 H).

Changes in the parameter alter the magnitude of RAM responses

We also examined the sensitivity of RAM response predictions to changes in our model parameters. The shapes of the rate response and the coherence functions are not strongly influenced by changing the parameters (first, third and fourth column in Table 4.4), as we do not see changes in correlation coefficients upon changing the parameters. However, almost all parameters have an influence on the actual magnitude of the rate as well as the coherences. The magnitude of the rate response was calculated as the ratio of the standard deviations of cell and model responses. It is increased by an increase in α (Table 4.4, first row) and decreased by an increase in $\sqrt{2D}$ (Table 4.4, second row), due to an increase and decrease in signal-to-noise ratio, respectively. The two effects are also

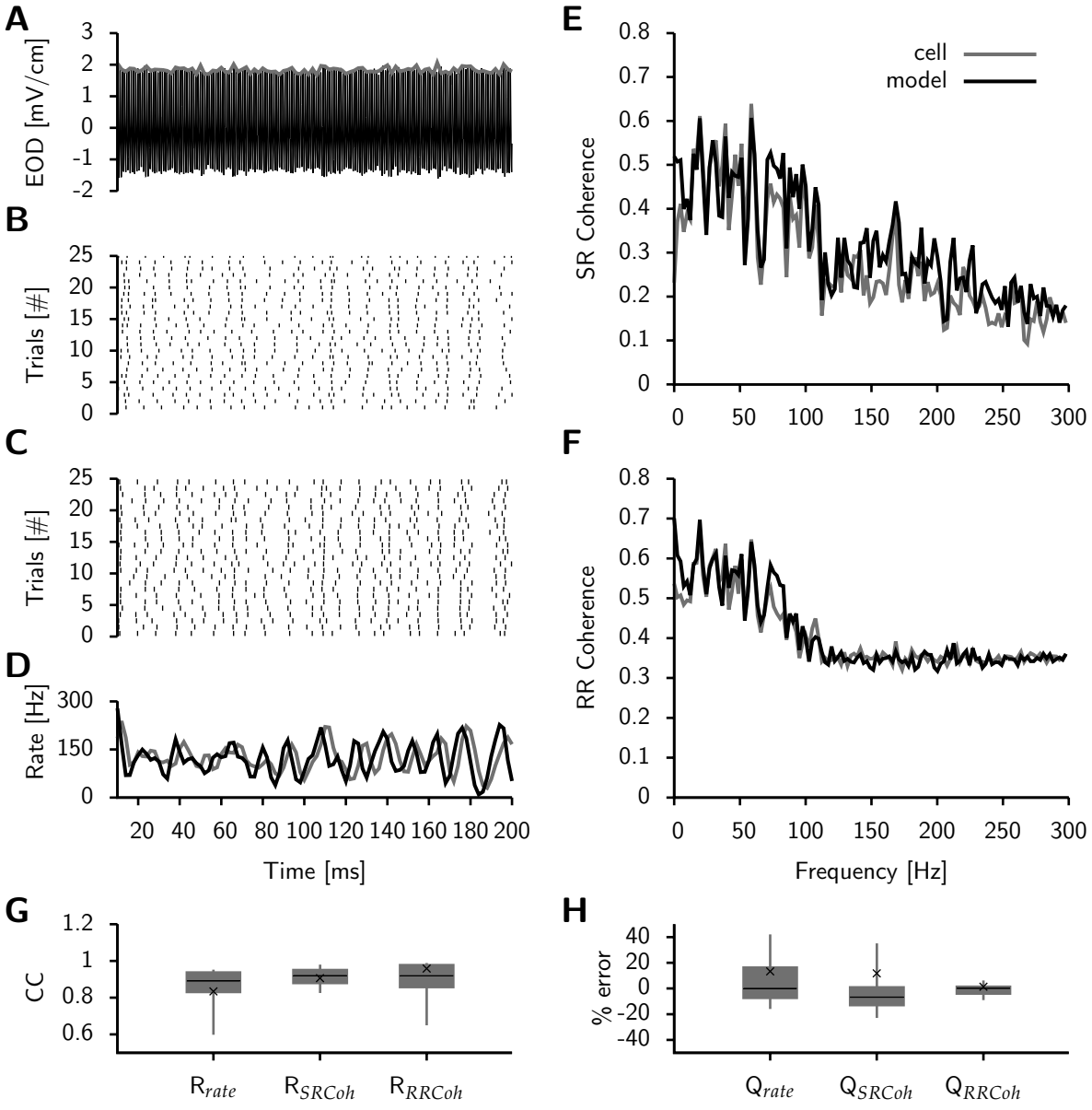

Figure 4.10: Response of cell and model to RAM stimuli. The response of the example cell and model (the same as in Fig. 4.8, 4.1 and 4.3) is shown to random amplitude modulations of the EOD (RAM stimuli). **A**) shows the stimulus with the EOD in black and the AM in grey. In **B**) the spiking response of the cell is shown, in **C**) that of the model. **D**) shows the rate responses of both the cell (black) and the model (grey). **E**) The coherence between response and stimulus (SR Coherence) is shown for frequencies up to the stimulus cutoff (300 Hz) for both cell and model. **F**) shows the same for the coherence between different trials (RR Coherence). **G**) and **H**) demonstrate the average performance of all models in predicting the responses of their target cells (11 in this case as we had recorded noise responses of only 11 cells). In G it assessed as the correlation coefficients of the rate (R_{rate}, calculated from the data shown in D, the stimulus-response coherence and the response-response coherence (R_{SRCoh} and R_{RRCoh}), derived from the data plotted in E and F). In H it the performance is quantified as the per cent errors (Q_{rate}, Q_{SRCoh} and Q_{RRCoh}). Depicted are again medians, interquartiles and maxima.

reflected in an increase (and decrease) in the coherence for α (and $\sqrt{2D}$). τ_V decreases the rate response by filtering out fast fluctuations.

Increasing the adaptation strength Δ_A also decreases the rate response and the stimulus-response coherence by reducing the effective stimulus strength, especially for low frequency stimuli (Table 4.4, fourth row). τ_A increases the modulation of the rate response (Table 4.4, fifth row), in correspondence with its effect on the CV (Table 4.2). τ_D decreases the rate response as well as both the stimulus-response coherence as well as the response-response coherence, again affecting mainly the response to high frequencies (Table 4.4, sixth row).

Table 4.4: Sensitivity of response predictions to RAM stimuli. The normalised sensitivity coefficients between parameter changes and alterations of the outcome are shown as the slopes of the linear relations. They are shown for the correlation coefficient and per cent error for rate response and coherence function in response to noise stimuli. R's denote correlation coefficients between model and cell data for the rate response (first column, R_{rate}) and the stimulus-response coherence (third column, R_{SRCoh}). There were no significant effects on the correlation coefficients between the response-response and stimulus-response coherences, R_{RR} R_{SRCoh}, and and we here only show R_{SRCoh} representative for both. To quantify the deviation of the actual magnitude, the ratios were calculated (all Q's), for the standard deviation of the rate (second column, Q_{rate}), the stimulus-response coherence (fourth column, Q_{SRCoh}) and response-response coherence (fifth column, Q_{RRCoh}).

param.	R_{rate}	Q_{rate}	R_{SRCoh}	Q_{SRCoh}	Q_{RRCoh}
α	0.05 ± 0.02	$\mathbf{0.51}\pm0.12$	0.02 ± 0.02	$\mathbf{0.62}\pm0.16$	$\mathbf{0.34}\pm0.12$
$\sqrt{2D}$	0.01 ± 0.02	$-\mathbf{0.15}\pm0.07$	-0.00 ± 0.01	$-\mathbf{0.42}\pm0.16$	$-\mathbf{0.28}\pm0.12$
τ_V	-0.02 ± 0.03	$-\mathbf{0.31}\pm0.15$	0.01 ± 0.01	-0.06 ± 0.11	0.01 ± 0.07
Δ_A	-0.00 ± 0.03	$-\mathbf{0.20}\pm0.14$	-0.00 ± 0.01	$-\mathbf{0.14}\pm0.07$	-0.03 ± 0.03
τ_A	0.05 ± 0.04	$\mathbf{0.48}\pm0.15$	0.01 ± 0.02	0.07 ± 0.05	0.04 ± 0.03
τ_D	-0.01 ± 0.03	$-\mathbf{0.15}\pm0.11$	0.01 ± 0.01	$-\mathbf{0.27}\pm0.12$	$-\mathbf{0.1}\pm0.08$

4.4 Discussion

The leaky integrate-and-fire model is one of the simplest models of spike generation and has been shown insufficient to reproduce responses of many neuron types (Izhikevich, 2004). Here, we show a case where, when supplemented by appropriate data-derived filters and adaptation, it successfully provides a realistic description of the activity of not only a single cell but a whole receptor-afferent organ. We calibrate the model to responses to baseline conditions and artificial step stimuli and show that these models inherently have the same frequency tuning as the receptor organs.

We thereby ignore the nonlinear processes taking place at the receptor's basilar membrane, as described by Kashimori et al. (1996), and replace it by a linear gain in amplitude. This simplification is possible, because in response to only one frequency – the

EOD frequency – the system can be approximated as a damped oscillator. Our model builds most strongly on that of Chacron et al. (2000). In their model spike-frequency adaptation was obtained by a dynamic threshold. Benda et al. (2010) showed that the dynamic threshold and the negative adaptation current have different effects on the onset f-I-curve at different preadaptation levels. The dynamic threshold has a divisive effect, reducing f_0 – the slope of the onset f-I-curve – for higher preadaptation, while with a negative adaptation current, the curve is merely shifted with stable f_0. P-units exhibit the latter subtractive effect (Benda et al., 2005), which is why we used an adaptation current. However, we fit our model as well as an identical one with a dynamic threshold (LIFDT) to data where we had determined f-I-curves at different preadaptation states, and got statistically indistinguishable results. The constant carrier in form of the EOD seems to change the signal processing properties of the LIFDT such that they more closely resemble those of the LIFAC. Note that with this simple model of adaptation, we neglect the multiple time scales demonstrated by Nelson et al. (1997) and still reproduce the responses well, because the additional time scales of adaptation are on a longer ($> 1\,\mathrm{s}$) time scale than those analysed in our study.

The most substantial difference of our model to previous ones is the low-pass filter that we apply after rectifying the EOD signal. Without the low-pass filter, the model responses lock too strongly to the EOD (Fig. 4.4), despite an otherwise comparably good reproduction of baseline ISIs and f-I-curves. Various other mechanisms could also lower the phase-locking, such as for example a second noise term (Chacron et al., 2000). However, most of them also decrease the sensitivity to AMs, which is in contrast to the observation that in P-units low vector strengths are not correlated with low sensitivity. We also need the filter to get correct response predictions to RAM and SAM stimuli (sensitivity of predictions to changes in this parameters seen in Table 4.3 and 4.4). This demonstrates that the filter is an essential component of the correct description of the electroreceptor unit.

The filter allows us to obtain the right sensitivity to both the AM and its EOD carrier. Sensitivity to envelopes of signals while preserving the response to the signal itself has recently been demonstrated for higher order envelopes by exactly the same mechanism, i.e. rectifying and subsequent low-pass filtering the signal (McGillivray et al., 2012; Savard et al., 2011). Our filter could thereby represent processes at the receptor, the synapse or at the dendritic processes that precede the spike-generation in the axon. Important is that the low-pass filter comes after rectifying the signal. It is thus more likely to represent postsynaptic processes.

The simplifications underlying our model prohibit assessment of realistic parameters such as ion channel conductance or time course, as would be possible with a full conductance-based model of the Hodgkin-Huxley type (Jaeger et al., 1997; Roth and Häusser, 2001). Since it is not possible to intracellularly record from electroreceptors or the dendrites of their innervating axons, constraining such more realistic parameters remains impossible. However, our model parameters are biophysically motivated and examining their variability and their influence on the model performance allows predictions on the nature of P-unit population response to sensory input.

P-units show a high diversity in various response characteristics (Gussin et al., 2007). The high variability and infrequent correlations of the parameters, that we obtain by modelling a number of cells in an automatic fit routine, suggest that the heterogeneity can not be modelled by only changing one parameter, in contrast to suggestions of previous studies (Savard et al., 2011). This finding is confirmed by the sensitivity analysis, in which we find effects of all parameters on the response of the model. None of the parameters affected all response characteristics that underlie the heterogeneity.

In the second part of our model analysis we focused on the reproduction of the P-units' frequency tuning. Periodic AMs form the basis of signals fish receive in the wild. When two fish interact, their EODs superimpose to create a beat, a quasi-sinusoidal AM at the difference frequency (Chapter 2 and *3*). Since EOD frequencies in *A. leptorhynchus* range from 700–1000 Hz, SAMs of up to 300 Hz are common stimuli for the fish (Stamper et al., 2010). Communication signals are often comprised of changes in EOD frequency (Chapter 2, Zakon et al., 2002) which consequently show up in changes in the AM frequency (Chapter 3, Benda et al., 2005). Self-motion on the other hand induces perturbations of the field that can be modelled by RAMs (Yu et al., 2012). We here show that the exact frequency tuning that underlies responses to such stimuli is intrinsically characterised already by responses to step and constant stimuli.

This emphasises the effectiveness and also the importance of choosing the right stimulus when characterising a neuron. Step stimuli have been shown effective to constrain a model (Druckmann et al., 2011) and aspects of the frequency tuning are inherent in such stimuli. The "adapted f-I-curves" describe cell dynamics at two separate time scales (Benda and Herz, 2003; Benda et al., 2010), with the onset f-I-curve capturing responses to fast stimuli and the steady-state f-I-curve determining the effective mean input. If the ISI's are shorter than the adaptation time constant, these two dynamics can formally be separated and the cutoff-frequency of the high-pass filter as induced by the adaptation current can directly be determined from the f-I-curves (Benda et al., 2010). The maximal gain to SAM stimuli then corresponds to f_0.

The integrate-and-fire model has been introduced with different voltage-dependant functions in place of the leak term, such as an exponential (Brette and Gerstner, 2005; Fourcaud-Trocmé et al., 2003, EIF) or quadratic one (Ermentrout, 1996, QIF). In a previous study, the choice of this function influenced the filtering properties of the model, especially its response to high frequencies (Fourcaud-Trocmé et al., 2003). We fit an EIF and QIF in the same way as the LIF to our data and did not see such a difference (not shown), probably because of the noise, which causes these models to behave similarly (Lindner et al., 2003).

Previous studies have shown that IF models exhibit resonances in the firing rate response to frequencies that are multiples of their baseline rate (Brunel et al., 2001; Fourcaud-Trocmé et al., 2003; Knight, 1972b), if the noise is sufficiently low. These resonance peaks had not been reported in P-units before, probably because previous studies averaged over a number of cells (Benda et al., 2006). Such averaging smoothes peaks, because different cells exhibit them at different frequencies (Fig. 4.9, also see Knight, 1972b). As we showed in Chapter 3, stimuli are encoded by sweeps on the cells' tuning

curves. Smooth tuning curves might therefore be beneficial and constitute one advantage of heterogeneity in these cells.

For the readout of a population of P-units, recent studies have proposed a synchronisation-desynchronisation code (Benda et al., 2006; Middleton et al., 2009). The degree of synchronous activity in a population can be read out easily by upstream neurons (Softky and Koch, 1993) and propagated through layered networks of neurons (Diesmann et al., 1999). P-units have been shown to synchronise to different degree depending on the stimulus frequency, suggesting that a synchrony code could transmit the information about the frequency content of the stimulus (Benda et al., 2006). However, many open questions remain, such as, e.g., about the number of neurons needed to fire synchronously to encode stimuli of different contrasts, the effect of heterogeneity on such a code etc. Since our model reproduces the frequency tuning in terms of correlation of spike trains for different contrasts (Fig. 4.8, Fig. 4.9), it can now be used to tackle such questions.

Under the naturalistic conditions that occur during navigation, prey capture or electrocommunication, large populations of P-units will be stimulated. It is only possible to record from single P-units at a time and extrapolation to the entire population is not readily achieved. There are now good models that describe the effective electrosensory stimuli for both electrolocation (Babineau et al., 2007; Chen et al., 2005) and electrocommunication (Kelly et al., 2008; Yu et al., 2012). Our model, combined with our understanding of electrosensory stimuli, will allow us to predict the effects of complex stimuli on the activity of the entire population of P-units. This will make studies possible on fundamental questions about receptor populations, such as on the ability of cells to detect and discriminate different signals, on the role of heterogeneity in the population and, especially, on the neuronal population codes that might be important for electroperception.

Chapter 5

Population Coding of Chirps

5.1 Introduction

Sensory signals are encoded distributed across neuron populations rather than in single neurons (Pouget et al., 2000, Chapter 1). Signal encoding is therefore best studied in populations. Because it is often impossible or tedious to record from many neurons, it is highly desirable to build neuron model populations to replicate natural populations (Marder and Taylor, 2011). In Chapter 4 we investigated in detail a model of P-unit electroreceptors that could be fit to a number of cells of different characteristics. The model can therefore be used to build a heterogeneous model population that resembles natural P-unit populations. Building on that we here use it to investigate the effect of heterogeneity on population coding.

Heterogeneity is a ubiquitous feature of neuronal populations (Chapter 1, Chelaru and Dragoi, 2008; Hospedales et al., 2008; Padmanabhan and Urban, 2010; Ringach et al., 2002). It has been shown in theoretical (Shamir and Sompolinsky, 2006) and experimental studies (Chelaru and Dragoi, 2008; Padmanabhan and Urban, 2010) to decorrelate the activity of cells, thus decreasing redundancy and increasing the capacity of the population to transmit information. These studies used simplified descriptions of the population heterogeneity (Chelaru and Dragoi, 2008) or investigated the encoding of artificial stimuli (Padmanabhan and Urban, 2010). With our model and the detailed knowledge of signals involved in electrocommunication, we are able to study the effect of heterogeneity on encoding a behaviourally relevant signal in model populations that closely resemble their natural counterparts.

At the projection site of P-units, the electrosensory lateral line lobe (ELL), pyramidal cells pool over around 1000 afferent neurons to process the high-frequent communication signals (in the lateral segment; Chapter 2, Krahe et al., 2008; Maler, 2009). Tuberous receptors are distributed across the whole fish body (Carr et al., 1982) and in communication contexts many receptor cells are stimulated by the same signal (Chacron et al., 2003). Interestingly, P-units are diverse in the rate and variability of their baseline dis-

charge (Gussin et al., 2007, Chapter 2), but are believed to exhibit similar frequency tuning (Wessel et al., 1996). They are neither connected among each other nor receive shared feedback. All correlated activity results from stimulus correlations. We specifically ask how heterogeneity in baseline activity can aid the encoding of signals in a population of cells that receive the same stimulus to which they are presumably equally sensitive.

A detailed characterisation of the parameter distributions underlying the model fits from Chapter 4 sets the basis for modelling the population. It will be subject of the first part of this chapter. From the distributions we draw representative parameters and use them to simulate a heterogeneous population. We show that the population reproduces natural P-unit population activity in baseline conditions as well as under stimulation with communication signals (beats and chirps, Chapter 2). In the last part we investigate how model neurons of distinct characteristics respond to the communication signals in order to assess the effect of heterogeneity on stimulus encoding.

5.2 Methods

Experimental Recordings

All experimental data used in this chapter is the same as in the preceding two chapters. The investigations of the parameter variability and the variability of baseline response characteristics are based on the 23 data sets presented in Chapter 4. The comparison of chirp encoding in a model population and a natural cell population (Fig. 5.5, 5.8) is done using the data presented in Chapter 3, which comprises recordings from 220 P-units. All experimental procedures were as stated in detail in Chapter 3.

Model of Electroreceptors

P-units were modelled as leaky integrate-and-fire neurons with an adaptation current (LIFAC) to account for spike-frequency adaptation and negative interspike interval (ISI) correlations. The model has been extensively investigated in Chapter 4. Since the parameters and their distributions are a central topic of this project, we restate the equations that underlie the dynamics of the model. The membrane potential V follows the dynamics,

$$\tau_V \frac{dV}{dt} = -V + \alpha I_{\text{Input}} + I_{\text{Bias}} - I_A + \sqrt{2D}\xi + \sum(\delta(t)) \;, \tag{5.1}$$

with τ_V being the membrane time constant, α a cell-specific gain factor, I_{Input} an external input current, I_{Bias} a cell-specific constant offset current, I_A the adaptation current and ξ a Gaussian white noise of strength $\sqrt{2D}$. The current is directly integrated, because the membrane resistance of P-units is unknown. The current therefore carries the unit mV. Whenever the membrane potential reaches the threshold (10 mV in our case), a spike is

noted and I_A is incremented by Δ_A. It then relaxes back to zero with

$$\tau_A \frac{dI_A}{dt} = -I_A + \Delta_A \sum(\delta(t)) \,, \tag{5.2}$$

where τ_A is the adaptation time constant. Within the Euler integration routine, this corresponds to an increment of the current at every spike by

$$I_A \mapsto I_A + \frac{\Delta_A}{\tau_A} \,. \tag{5.3}$$

The external input current I_{Input} is an amplitude modulated EOD current that is passed through a Heaviside function to include zero-clipping of the synapse between electroreceptor and afferent neuron. It is low-pass filtered at about one EOD period to simulate filtering processes in the dendritic processes of the afferent. Together, this gives

$$\tau_D \frac{dI_{\text{Input}}}{dt} = -I_{\text{Input}} + H[\beta(t) sin(2\pi f_{EOD} t)] \,, \tag{5.4}$$

where $\beta(t)$ is the desired AM waveform and τ_D the time constant of the dendritic filter. The baseline amplitude of the EOD is set to 1.0 mV/cm, its frequency to 700 Hz. Because I_{Input} resembles the EOD stimulus and carries the unit mV/cm, the gain factor α is expressed in cm.

The six parameters α, τ_V, $\sqrt{2D}$, τ_A, Δ_A, and τ_D were calibrated using a simplex fit as described in Chapter 4. The cost function consisted of a weighted sum of the errors of six basic measures describing the response of cells to constant EOD amplitude and step stimuli. These were the mean firing rate, the coefficient of variation (CV) and the first serial correlation (SC) of the ISIs and the vector strength (VS) of phase coupling to the EOD in response to constant baseline EOD. From the responses to step stimuli the slopes of two f-I-curves were measured: f_0 of the relation between stimulus intensity and onset response, and f_∞ between stimulus and steady-state response (see section on *Data Analysis* for details). I_{Bias} was adjusted after each fit iteration such that the model matched the mean firing rate. The model was calibrated to match responses of a target data set to constant EOD and step stimuli.

In order to avoid local minima of the error function, we fit the model to each target data set using three different initial values for each parameter. We varied the initial values systematically, yielding $3^6 = 729$ different fits. Each of these fits yields one optimal parameter combination. However, since the fit routine depends on the initial conditions, the resulting parameters vary. From the 729 parameter sets for each cell we took the best 10 % when ranked according to their cost function for further analysis. These are referred to as the "best 10 %" in the following. We also selected the best fit for each target data set.

The three initial values for each parameter were chosen from good fits that we had obtained beforehand. For this purpose the 23 target data sets were fit with a simplex fit in which the initial conditions were hand-tuned to obtain reasonable results. From the resulting 23 parameter combinations, we took the mean and maximal values as the three initial values. They are stated in Table 5.1.

Table 5.1: Initial values of parameters. Fits were run with all 729 combinations of these values as initial values.

parameter	initial values
α[cm]	50, 200, 450
$\sqrt{2D}$[mVs$^{1/2}$]	0.1, 0.2, 0.3
τ_V [ms]	0.1, 0.5, 1
τ_A [ms]	20, 30, 40
Δ_A [A]	0.1, 0.3, 0.6
τ_D [ms]	1, 2, 3

Constructing Heterogeneous populations

In order to construct heterogeneous populations of model neurons that resemble the variability found in natural populations, we first characterised in detail the variability exhibited by the parameters resulting from different fits. For this purpose, we pooled the parameters over the fits to different target data sets. The 23 target data sets originated from recordings of fish that potentially had different EOD frequencies (EODf) and amplitudes. To pool the values, we first converted those that are affected by EODf or EOD amplitude. We assumed that all time constants were related to the EODf and converted them such that they were expressed in multiples of the EOD period by multiplying them with the EODf. Further we expected the gain factor α being associated with the EOD amplitude and normalised it by the corresponding EOD amplitude.

Next, we estimated the types and moments of the pooled parameter distributions to be able to later draw new realistic parameter sets. We fit normal, lognormal and gamma distributions of different order. Best fits yielded the normal distribution given as

$$g(x) = a \exp \frac{-(x-\mu)^2}{2\sigma^2}, \tag{5.5}$$

where μ corresponds to the expectancy value and σ to the variance, and the lognormal distribution with

$$gn(x) = \frac{a}{\sigma x\sqrt{2\pi}} \exp -\frac{(\log(x)-\mu)^2}{2\sigma^2}. \tag{5.6}$$

The expectancy value of the lognormal distribution is then given by

$$E(x) = \exp \mu + \frac{\sigma^2}{2} \tag{5.7}$$

and the variance by

$$Var(x) = \exp 2\mu + \sigma^2(\exp \sigma^2 - 1). \tag{5.8}$$

We transformed all lognormal distributions to normal distributions by taking the logarithm of the corresponding values. We thus obtain a multivariate Gaussian distribution from which we are able to draw new values. However, we first have to account

for correlations between the parameters. Such correlations demonstrate compensatory effects between parameters. Since we were interested in compensations involved in simulating a population of cells rather than one particular cell, we only included the best parameter combination for the 23 target data sets in the following steps.

We first determined the covariance matrix Σ of the 23 parameter sets. Σ is given by

$$\Sigma_{ij} = E[(X_i - \bar{X}_i)(X_j - \bar{X}_j)]\,, \tag{5.9}$$

where X are the parameters and $E[...]$ denotes averaging over the different data points. Since we only had 23 data points for $n(n+1)/2 = 28$ degrees of freedom (since the covariance matrix is quadratic, but symmetrical with $n = 7$), we cross-validated our sample by a leave-one-out analysis. We took all 22 combinations of data points when leaving one out and calculated Σ for each of these. We then compared the estimations of Σ by calculating the cosine between all pairs of matrices. All values were well above 0.95 (with 90 % above 0.99) indicating that the estimations did not differ. The covariance matrix was thus a valid estimate regardless of the small sample of data points.

To generate a multivariate Gaussian distribution that exhibits the same covariance matrix, one first draws uncorrelated random numbers and then multiplies the resulting matrix with a Cholevsky decomposition L of Σ. L is defined as

$$L^T L = \Sigma\,. \tag{5.10}$$

In line with this approach, we generated 2000 parameter combinations by drawing a 2000×7 matrix of random numbers and multiplied it by L calculated from the data. Finally, we added the mean and multiplied the standard deviation of each parameter. That way we generate distributions of parameters that resemble those obtained from the calibration to real data in their mean, standard deviation and covariance matrix.

Whenever we calculated correlations between parameters or response characteristics, we used the Pearson's correlation coefficient according to

$$r = \frac{\sum_{i=1}^{n}(X_i - \bar{X})(Y_i - \bar{Y})}{\sqrt{\sum_{i=1}^{n}(X_i - \bar{X})^2}\sqrt{\sum_{i=1}^{n}(Y_i - \bar{Y})^2}}\,. \tag{5.11}$$

We assessed the significance level via the Pearson's test. Only those pairs of parameters were regarded as correlated whose p-values were below 0.05 (Bonferroni corrected).

Stimulation

The AM waveforms used to stimulate models or cells were the same. For details on the generation of stimuli in electrophysiological experiments, see the corresponding sections in Chapter 3 and 4. We here describe the generation of stimuli for the model simulations. The baseline stimulus consisted of a constant sine wave of 700 Hz at 1 mV/cm that mimics a constant EOD stimulus. For the analysis of the baseline response characteristics, 100 s of model activity in response to this stimulus were simulated.

All stimuli consisted of AMs of this EOD mimic and were generated by multiplying it with the desired waveform. F-I-curves (relations between firing rate and stimulus intensity) were generated by stimulating with step stimuli, during which the EOD amplitude was in- or decreased for 200 ms. We used eleven different steps in which the intensity was changed to a value between 0.5 and 1.5 of the baseline EOD amplitude. Each step was repeated 300 times.

Chirps were superimposed on beats. Beats are formed when two EODs superimpose and constitute sinusoidal AMs of the frequency difference between the two signals. We denote beat frequencies as Δf_{Beat}. We calculate it as the frequency difference between the EODf of the communicating fish (or the stimulus), EODf_2, and the EODf of the receiving fish (or recorded or simulated fish), EODf_1, according to $\text{EODf}_2 - \text{EODf}_1$. It can be positive and negative, depending on which EOD is of higher frequency. The AM during the beat is given by

$$AM(t) = A(t)\cos(2\pi\Delta f_{\text{Beat}}t)\ , \tag{5.12}$$

where A(t) is the amplitude of the stimulus which we set to values between 0.01 and 0.4 (resembling contrasts from 1 to 40 %). The beat was simulated from $t = -250$ to 250 ms with a Δf_{Beat} between -250 to 250 Hz ($\pm 5, 10, 20, ..., 100, 120, ..., 200, 225, 250$).

The phase of the beat $\Delta\phi(t)$ is the time integral over the frequency difference between the two signals. It advances with a constant rate in the case of a normal beat. Chirps were modelled as modulations of $\Delta\phi(t)$ originating from the superposition of the EOD with another EOD whose frequency is transiently increased. The frequency increase due to the beat was modelled as a Gaussian of maximal frequency excursion s and width Δt. The phase modulation yields

$$\Delta\phi(t) = \sigma\int_{-\infty}^{t}\Delta f(t')\,dt' = \Delta f_{\text{Beat}}t + s\sigma\int_{-\infty}^{t/\sigma}\exp(-z^2)dz + \Delta\phi\ . \tag{5.13}$$

The first term models the beat while the second term accounts for the Gaussian increase of the difference frequency during a chirp centered around $t = 0$. The width of the Gaussian frequency increase is modelled by $\sigma = \Delta t/\sqrt{2\ln 10}$, such that the chirp has its width Δt at 10 % of its size s. $\Delta\phi$ determines at which phase of the beat cycle the chirp occurs – it is zero at the peak of a beat cycle. In addition, the EOD amplitude A(t) was decreased by a Gaussian of the same width and centered at time $t = 0$ by a. We used chirp parameters of $s = 50, 100, 150$ Hz, $\Delta t = 15, 50$ ms, $\Delta\phi = 36, 72, ...360^\circ$ and $a = 2, 20$ %.

Data analysis

The response characteristics of the model populations were evaluated by assessing several quantities from the baseline activity, the f-I-curves and the response to chirps and beats.

From the baseline activity, four measures were derived: The rate, the CV, SC and VS (for details on how to calculate them, see Chapter 4). From the response to step stimuli, two f-I-curves were constructed: The onset f-I-curve, that relates the maximal response to the stimulus onset with stimulus intensity and the steady state f-I-curve of the average response after adaptation. To construct these, the onset and steady-state rate in response to each step was measured and plotted over the intensity of the step. The onset rate was determined as the maximal deviation of instantaneous to mean rate during the first 100 ms upon stimulus onset. The instantaneous rate is given by the inverse of the ISIs. The steady state rate was calculated as the mean firing rate in the second half of stimulation, i.e. between 100 ms and 200 ms after stimulus onset. The slopes of the f-I-curves were derived from linear fits to the full f-I-curve in the case of the steady-state, yielding f_∞, and to the middle part of the onset f-I-curve, yielding, f_0. The two slopes together with the four baseline response characteristics were matched during the fit routine (see above).

Beat and chirp responses were analysed by calculating the response in a time window during the beat and around the chirp, respectively. The analysis window for beat responses spanned the time of the beat stimulation following the chirp stimulus, i.e. from $t = \Delta t/2$ (since the chirp stimulus of width $\Delta t/2$ was centered around 0) to the end of stimulation at $t = 250$ ms. The window size was adjusted such that it spanned integer multiples of the respective beat period. For analysing the response to chirps, an analysis window was set from $t = -\Delta t/2$ to $t = \Delta t/2$. The effect that a chirp had on the response compared to the underlying beat, was assessed by the contrast between chirp and beat response, the so-called chirp selectivity index CSI (Vonderschen and Chacron, 2011), given by

$$CSI = \frac{r_{\text{chirp}} - r_{\text{Beat}}}{r_{\text{chirp}} + r_{\text{Beat}}}, \tag{5.14}$$

where r_{chirp} and r_{Beat} are the responses in the chirp and beat analysis windows, respectively.

As the response of P-units mainly fluctuates around a mean rate, the response was calculated as the standard deviation of the rate. Each model (and neuron, see Chapter 3 for more details), was stimulated 15 times with the same chirp/beat stimulus. Each single trial spike train was then convolved with a Gaussian kernel of width $\sigma = 1$ ms (to resemble the fast excitatory component of the postsynaptic potential in the projection cell Berman and Maler, 1998). The rate was averaged over the 15 trials and this average fed into the subsequent analysis.

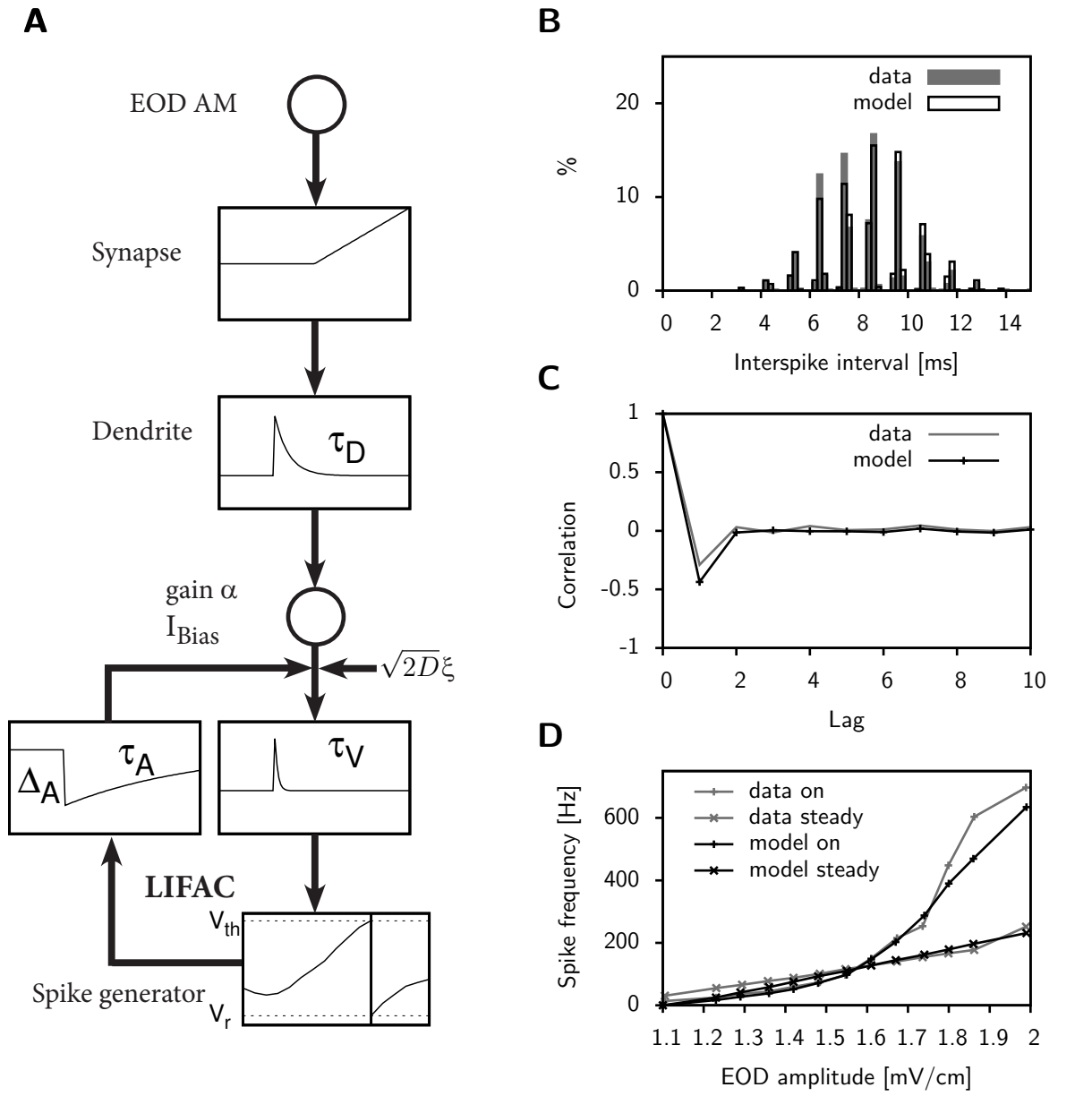

Figure 5.1: P-unit model. A) Sketch of the P-unit model. The stimulus is an amplitude modulated EOD current (EOD + AM). It is rectified and low-pass-filtered to represent processes at the synapse between receptor and afferent neuron and the dendritic processes of the neuron, respectively. The signal is scaled with a gain factor α and shifted by an offset I_{Bias}. The membrane potential then integrates the current together with an independant noise ξ and the negative adaptation current. A spike is fired whenever the membrane potential reaches the threshold. It is then reset to zero and the negative adaptation current is incremented by Δ_A. The adaptation current subsequently exponentially relaxes back to zero with τ_A (panels on the left, clockwise from top, as indicated by the arrows). The model is designed to match baseline activity and f-I-curves shown on the right for one representative P-unit and the corresponding model. **B**) The histogram of interspike intervals (ISIs). **C**) The serial correlations between succeeding ISIs of different lag. **D**) F-I-curves as derived from responses to step stimuli of different EOD amplitude. From each step the maximal response upon stimulation onset is extracted as well as the average response after the response is adapted to this step. Plotting the two over the step intensity yields the onset and steady-state f-I-curves of slope f_0 and f_∞, respectively.

5.3 Results

The model is designed to reproduce baseline characteristics and f-I-curves of P-units

In Chapter 4 we introduced a leaky integrate-and-fire (LIF) model that reproduces the behaviour of P-units of distinct response characteristics in great detail. We here briefly recapitulate the results as they set the basis for the following investigations. The well informed reader may skip this section and move on to the next one on *Characterising parameter distributions*.

The input to the model is a sinusoid whose amplitude is modulated by the desired stimulus waveform, representing an amplitude modulated EOD. It is rectified and low-pass filtered with time constant τ_D to simulate processes at the synapse and dendritic processes, respectively. To account for different sensitivities and operating points of different P-units, it is multiplied by the gain factor α as well as shifted by the offset current I_{Bias} (Fig. 5.1 A, upper part). A Gaussian noise current ξ of strength $\sqrt{2D}$ is added to model neuronal variability. The adaptation current I_A is subtracted to account for spike-frequency adaptation. The combined current is integrated with time constant τ_V (Fig. 5.1A, middle part). Spikes are noted when the membrane voltage reaches a certain threshold (Fig. 5.1A, right bottom part). At this point in time the membrane voltage V is reset to zero and the adaptation current I_A is incremented by Δ_A and exponentially relaxes back to zero with time constant τ_A (Fig. 5.1 A, left bottom part).

The model reproduces the activity of P-unit electroreceptors under various condtions (Fig. 5.1 B–D, results for the example cell shown in grey, results for the corresponding model in black). Under baseline conditions – when stimulated with a constant EOD – P-units fire irregularly with a high baseline rate (144.14 Hz$\pm$32.5 in our sample of 23 cells). Since they phase-lock to the EOD, a distribution over the interspike intervals (ISI) is broad and discrete (Fig. 5.1 B). Their strong spike frequency adaptation leads to a negative correlation between successive ISIs (Fig. 5.1 C) and strong transient changes in their firing rate to step stimuli, referred to as the onset rate. Upon stimulation, the response relaxes to a steady state. Onset and steady-state f-I-curves describe the relation between these two responses and the step intensity (Fig. 5.1 D).

Based on these features, different cells are well characterised by six measures: baseline firing rate, coefficient of variation (CV) and first serial correlation (SC) of ISIs, vector strength of phase-locking to the EOD (VS), and the slopes of the onset and steady-state f-I-curve, f_0 and f_∞, respectively. All six measures differ from cell to cell (Chapter 4) demonstrating the population heterogeneity in P-units (Gussin et al., 2007).

Characterising parameter distributions

The model comprises seven parameters in total: α, I_{Bias}, $\sqrt{2D}$, τ_V, Δ_A, τ_A and τ_D. Different values of these parameters give rise to models with different response character-

istics. The basis for the simulation of heterogeneous model populations therefore lies in a reproduction of the parameter variability underlying fits to distinct P-units. For this purpose, we now examine in detail the distributions of values underlying the model fits from Chapter 4. We distinguish between two sources of parameter variability: The uncertainty of choosing parameters for one target data set and the distribution of values across fits to different target data sets.

Multiple fits to one target data set are variable

Table 5.2: Variability of model parameters. To quantify the dispersion of parameter values, the semiquartile range is given in per cent of the median value for each parameter. The semiquartile range is half the difference between the first and third quartile. The middle column gives the measure across fits to different target data sets. The right column shows it for the values of the 10 % best fits to one target data set. The latter was calculated for each target data set separately and then averaged.

parameter	dispersion cells [%]	dispersion fits [%]
α	34.1	19.4
I_{Bias}	78.5	18.7
$\sqrt{2D}$	41.1	24.8
τ_V	39.63	13.4
τ_A	10.14	14.6
Δ_A	53.4	19
τ_D	38.7	25

To avoid local minima, we fit each target data set with a different set of initial conditions. From this approach we yield 729 fits from which we take the best 10 % into the following analysis of the variability arising from fit uncertainty. They reproduce the baseline characteristics well (per cent errors in Fig. 5.2 H for the example cell). The distributions are steady without distinct local minima, but they show a high variability (grey distributions in Fig. 5.2 A–G). We quantified the degree of variability by calculating the ratios between the semiquartile range and the median. The semiquartile range is defined as half the difference between first and third quartile. It takes up from 13.4 to 25 % of the median for different parameters (Table 5.2), implying that half of the values resulting from different fits to the same target data set spread over 27-50 % of their median value.

Parameter correlations reveal compensatory effects

How can such different values generate models that are very similar in their activity? The parameter values of the 10 % best fits are highly correlated (Fig. 5.2 I). This shows that alterations in model performance caused by changing one parameter are compen-

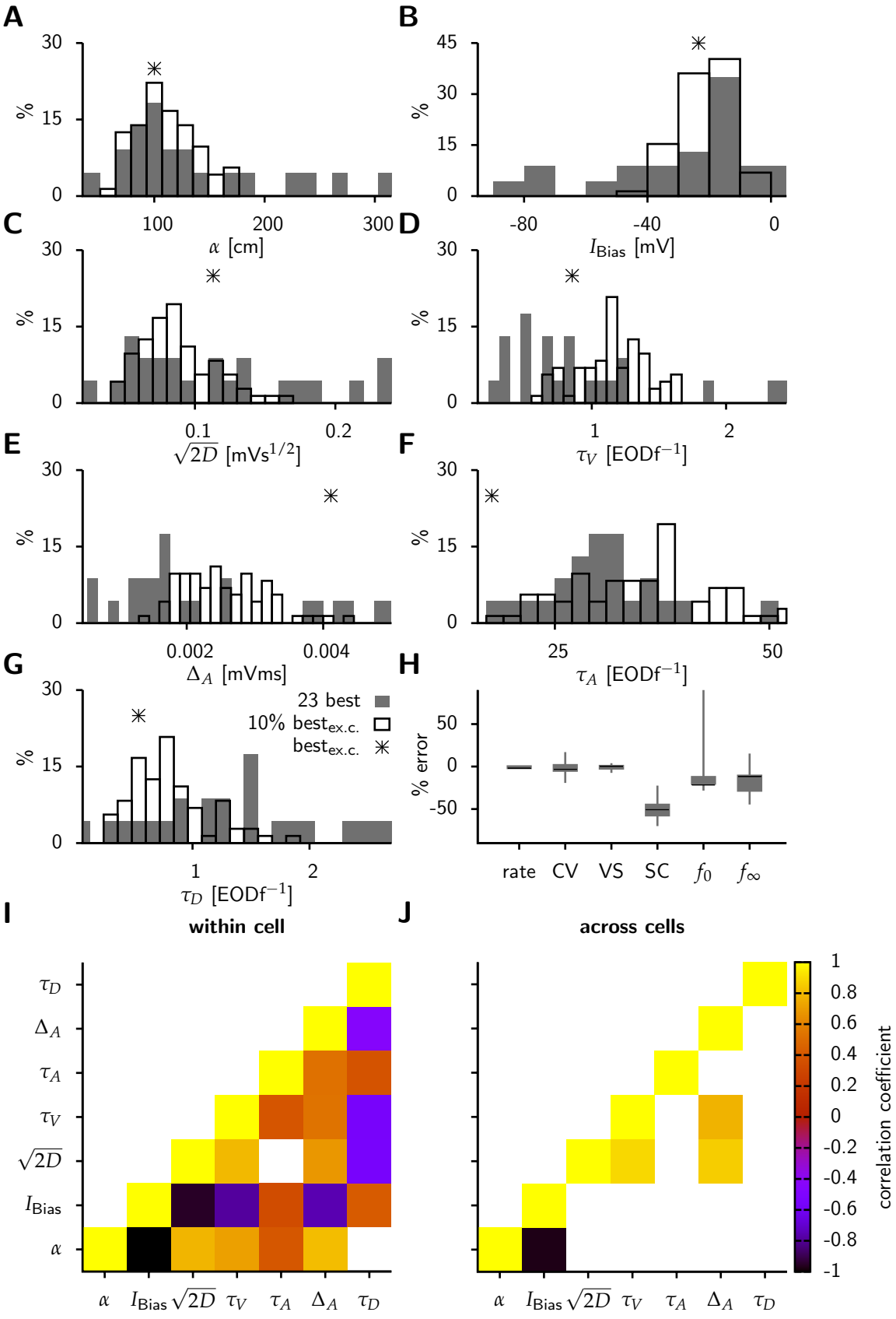
A
B
C
D
E
F
G
H
I
J
%
α [cm]
I_{Bias} [mV]
$\sqrt{2D}$ [mVs$^{1/2}$]
τ_V [EODf^{-1}]
Δ_A [mVms]
τ_A [EODf^{-1}]
τ_D [EODf^{-1}]
23 best
10% best$_{ex.c.}$
best$_{ex.c.}$
% error
rate
CV
VS
SC
f_0
f_∞
within cell
across cells
correlation coefficient

Figure 5.2: Variability of parameter estimation. The distributions of parameter values originating from fits to different target data sets (grey), and from different fits to the same target data set (10 % best of the example cell, ex.c.,black) are shown for the seven model parameters: gain factor α (**A**), offset I_{Bias} (**B**), noise strength $\sqrt{2D}$ (**C**), membrane time constant τ_V (**D**), adaptation strength Δ_A (**E**) and time constant τ_A (**F**) and time constant of dendritic low-pass filter τ_D (**G**). The value of the best parameter set for the example cell is shown as the asterisks on top the distributions. **H**) The estimation errors of the six baseline response characteristics of the 10 % best fits to the example cell. Indicated are median and quartiles as well as maximal values. **I**) Correlations between parameters of the 10 % best fits. **J**) Correlations between parameters from the best fit for each different target data sets.

sated by changing another. This also explains why the parameter values of the best fit often lie outside the center of their distributions (asterisks in Fig. 5.2 A–G).

Parameter fits to different target data sets are variable

We quantify the variability of parameter values across a population of cells via the best parameter sets for the 23 target data sets. The distributions of these parameter sets have been reported before (Fig. 4.6, values might deviate they are normalised by EOD frequency and amplitude). Their dispersion is greater than that for different fits for one cell, which is reflected in wider distributions in Fig. 5.2 A–F and bigger percentage quartile ranges in Table 5.2. However, the values are only seldom correlated (Fig. 5.2 J).

Table 5.3: Distributions of model parameters. The types and moments of the parameter distributions shown in Fig. 5.3. The types (Distr. type.) are stated in the second column, the mean values and the standard deviations in the third and fourth, respectively. For the normal distribution the mean and variance are directly given by probability density function fit to the data (μ and σ), in the lognormal they are derived according to Eq. 5.7 and 5.8.

parameter	Distr. type	$E[x]$	$\sqrt{Var[x]}$
α[cm]	lognormal	121.4	84.7
I_{Bias}[mV]	lognormal	-22.05	42.1
$\sqrt{2D}$[mVs$^{1/2}$]	lognormal	0.095	0.069
τ_V[EOD^{-1}]	lognormal	0.813	0.423
τ_A[EOD^{-1}]	normal	28.12	2.61
Δ_A[mVms]	lognormal	0.00194	0.00078
τ_D[EOD^{-1}]	normal	1.099	0.838

Populations can be constructed from parameter distributions

In order to reproduce the parameter variability, we have to define distributions from which we can draw parameter values in the next step. Smooth distributions are ob-

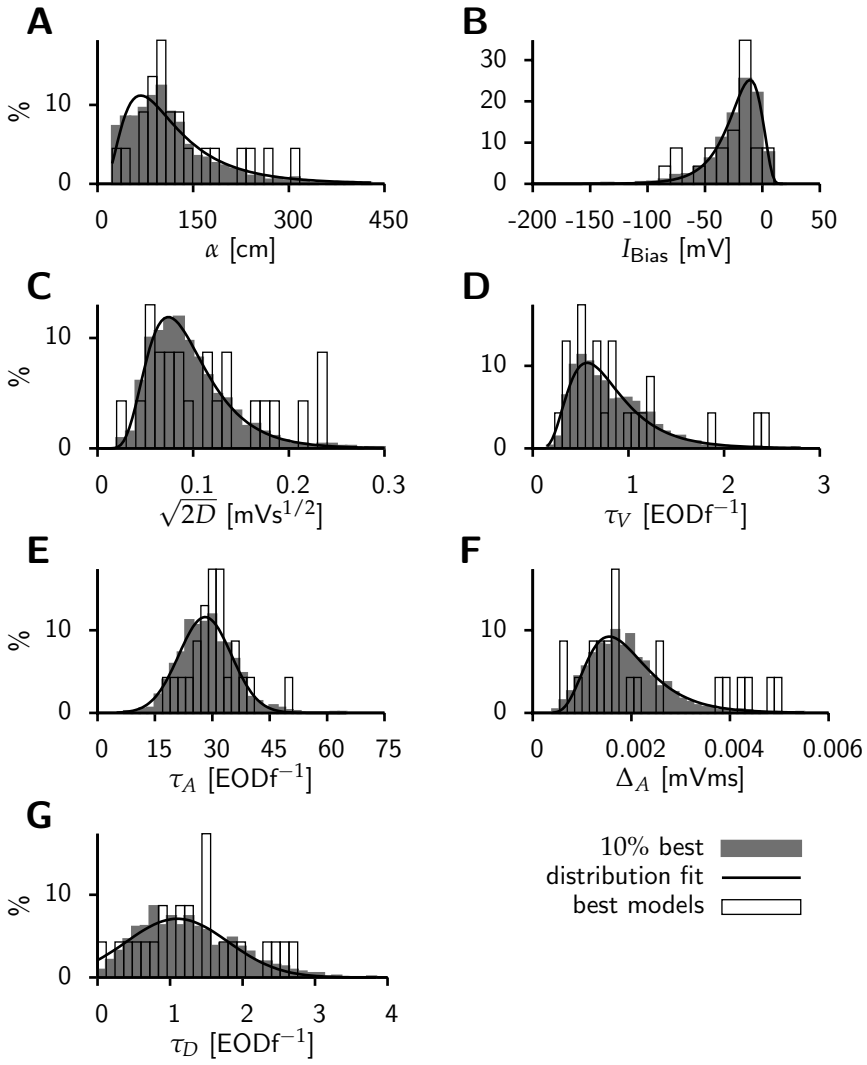

Figure 5.3: Estimated distributions of model parameters. Pooling the 10 % best parameter sets over all cells reveals smooth distributions (grey filled bars). The type and moments of these distributions can unambiguously be determined (black line). The parameter sets for the best fits to different target data sets lie within them (black open bars). As in Fig. 5.2, the histograms and the fitt distributions are shown for the seven model parameters: gain factor α (**A**), offset I_{Bias} (**B**), noise strength $\sqrt{2D}$ (**C**), membrane time constant τ_V (**D**), adaptation strength Δ_A (**E**) and time constant τ_A (**F**) and time constant of dendritic low-pass filter τ_D (**G**). The fit distributions are lognormal for A, B, C, D, and F and normal for E and G.

tained when the 10 % best parameter sets for all target datasets are pooled (Fig. 5.3, grey distributions). The distributions of the single best parameter sets correspond to the distributions of the 10 % best in terms of the shape and moments (Fig. 5.3, black distributions). For five of the parameters, the distribution was modelled best as a log-normal distribution. These were: α, τ_V, $\sqrt{2D}$, Δ_A and τ_D. The distributions of I_{Bias} and τ_A were best modelled as a normal distribution (Table 5.3). All distributions could be clearly defined by their first and second moment (Table 5.3).

From the distributions we now drew 2000 new representative values. To account for compensatory effects (Fig. 5.2 I and J), we matched their covariance to the covariance of the 23 best parameter sets. The population of 2000 model neurons resembles the P-unit population in terms of baseline rate, CV, SC and f_0 as well as f_∞. Only the distribution of VS differs between model and neurons (Fig. 5.4). This demonstrates that the model population exhibits a similar heterogeneity as the P-unit population. A difference lies in the correlations between the different characteristics. Among the model population, they are highly correlated (Fig. 5.4 G). In fact, only the rate and the CV are not correlated. This is in contrast to the cell population where only few combinations are correlated (Fig. 5.4 H).

Population coding of communication signals matches that of the natural population

With the model population that resembles natural P-units in terms of baseline characteristics, we want to investigate the encoding of communication signals. As described in Chapter 2 and Chapter 3 chirps are transient increases in EOD frequency emitted in communication situations. Thus, chirps occur on top of beats, AMs formed by the superposition of two EODs that periodically oscillate at the difference frequency Δf_{Beat} between the two individual EODs (Chapter 2). We have shown in Chapter 4 that the model faithfully reproduces the frequency tuning of P-units to beat stimuli.

We here show that the model also reproduces chirp responses on the single cell as the population level (Fig. 5.5). A chirp interrupts the periodic beat response (Fig. 5.5 A). In the case of a chirp superimposed on a slow beat ($\Delta f < 30\,\text{Hz}$), the maximal spike frequency as well as the rate are higher in both, model and P-unit, during the chirp than they are during the beat background (Fig. 5.5 B and D). The rate response of the cell lags the response of the model with a few milliseconds, probably due to an axonal conduction delay that is not included in the model.

Depending on the frequency of the beat, a chirp might also decrease the response (Fig. 5.5 F, Chapter 3). The chirp selectivity index, CSI, measures the contrast between chirp and beat response. It is negative when the chirp decreases the response and positive if it increases it. The behaviour of P-units in response to chirps has been extensively investigated in Chapter 3. Here it suffices to say that chirp responses are different depending on the background beat. The sign as well as the value of the CSI depend on

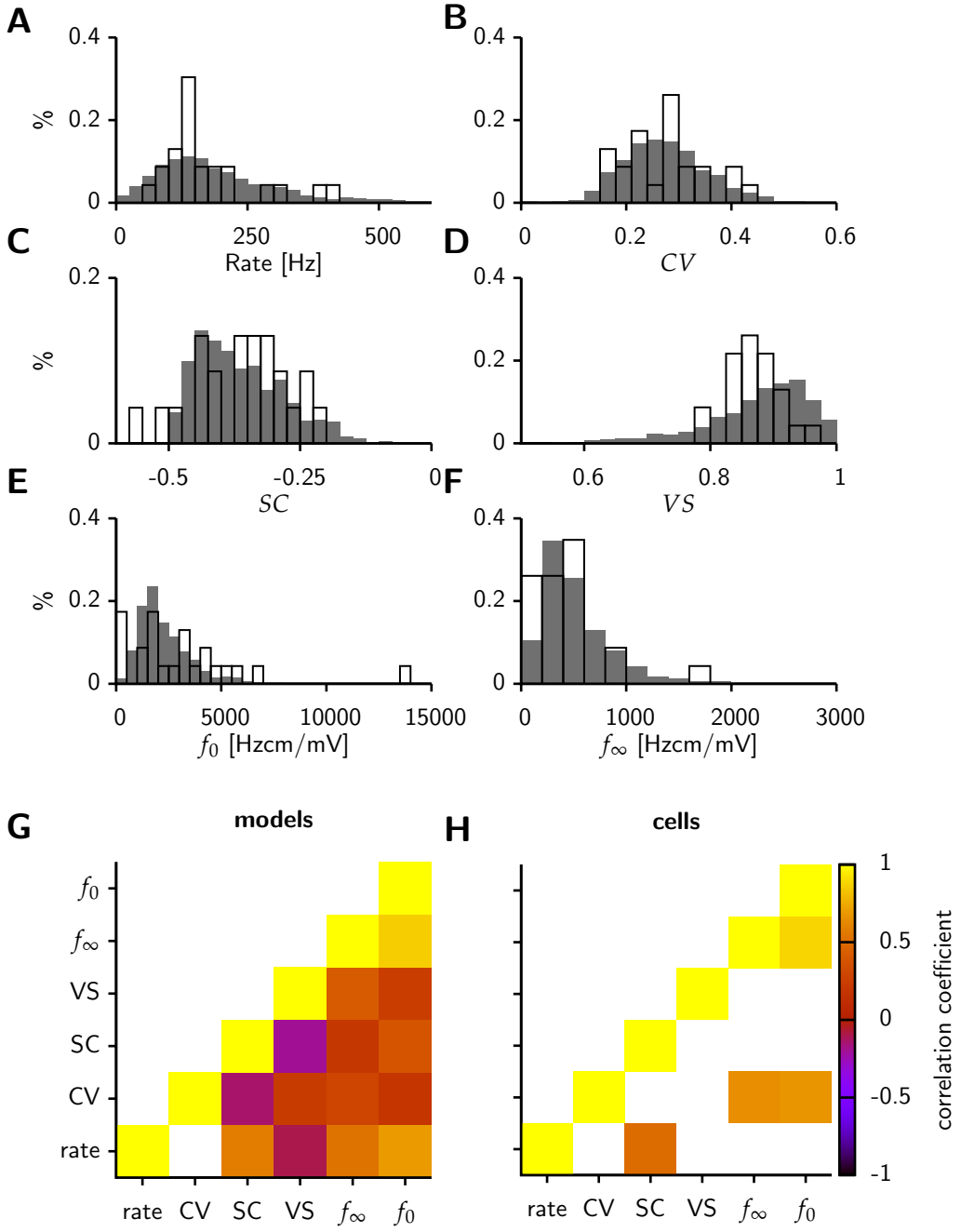

Figure 5.4: Response characteristics of cell and model population. From the estimated distributions of parameter values shown in Fig. 5.3 2000 parameter combinations were drawn and models were simulated with constant EOD as well as EOD steps of different intensities. From these responses (grey) as well as from the responses of 23 P-unit recordings (black), the baseline rate (**A**), the coefficient of variation (CV, **B**) and the serial correlation (SC, **C**) of the ISIs, the vector strength of EOD phase-locking (VS, **D**) and the slopes of the onset f-I-curve (f_0, **E**) and the steady-state f-I-curve (f_∞, **F**) are derived. Correlations between the response characteristics within the model neuron population in **G** and within the sample of P-unit recordings in **H**.

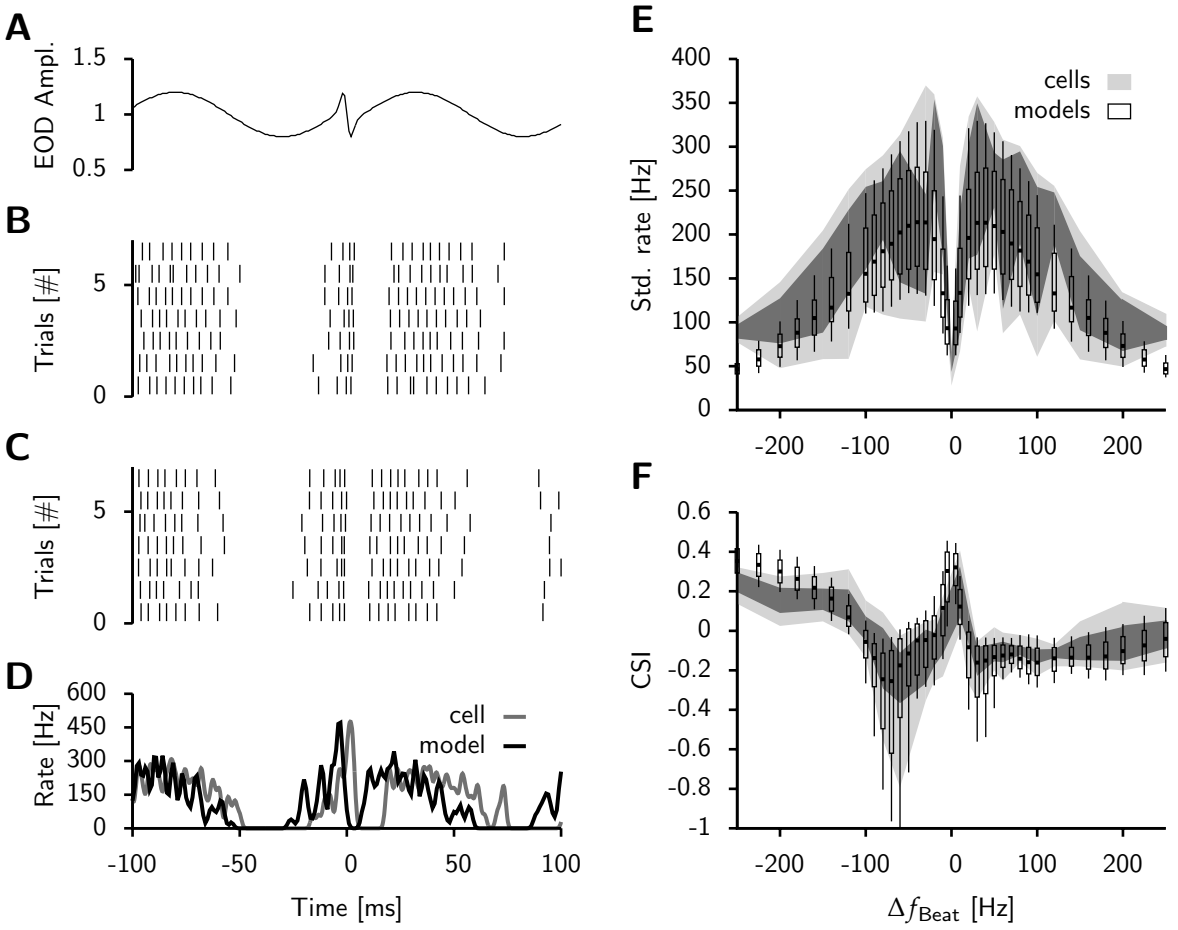

Figure 5.5: Population responses to chirps and beats. The model reproduces the chirp responses of recorded P-units on the single cell as well as on the population level. **A**) shows the AM stimulus of a chirp of size $s = 100\,\text{Hz}$, width $\Delta t = 15\,\text{ms}$ EOD amplitude drop of 2 %, superposed on a beat of frequency $\Delta f_{\text{Beat}} = 10\,\text{Hz}$ and phase $\Delta\phi = 240^\circ$. **B**) The spiking response of the example cell and **C**) the spiking response of the corresponding model. **D**) The spiking responses are convolved with a Gaussian kernel of 1 ms width corresponding to the fast excitatory component of the post-synaptic potential at the projection site, and then averaged over trials. The rate response of the cell (grey) lacks that of the model (black) because of axonal delays. **E**) The rate modulation as the rate's standard deviation in response to beats is analysed for single P-units and single model neurons and then averaged over the population. It is plotted over the frequency of the beat stimulus Δf_{Beat}. **F**) From the responses to beats and chirps, the chirp selectivity index (CSI) is calculated for chirps on the different background beats. Shown are median, interquartile ranges and extrema for the model population, and interquartile ranges and extrema in dark and light grey, respectively, for the recorded P-unit population.

Δf_{Beat}. Importantly, the different responses are matched well by a population of model neurons for all frequencies except $\Delta f = -250\,\text{Hz}$ (Fig. 5.5 F).

SAM responses of model neurons exhibit different gains, while chirp responses do not differ systematically

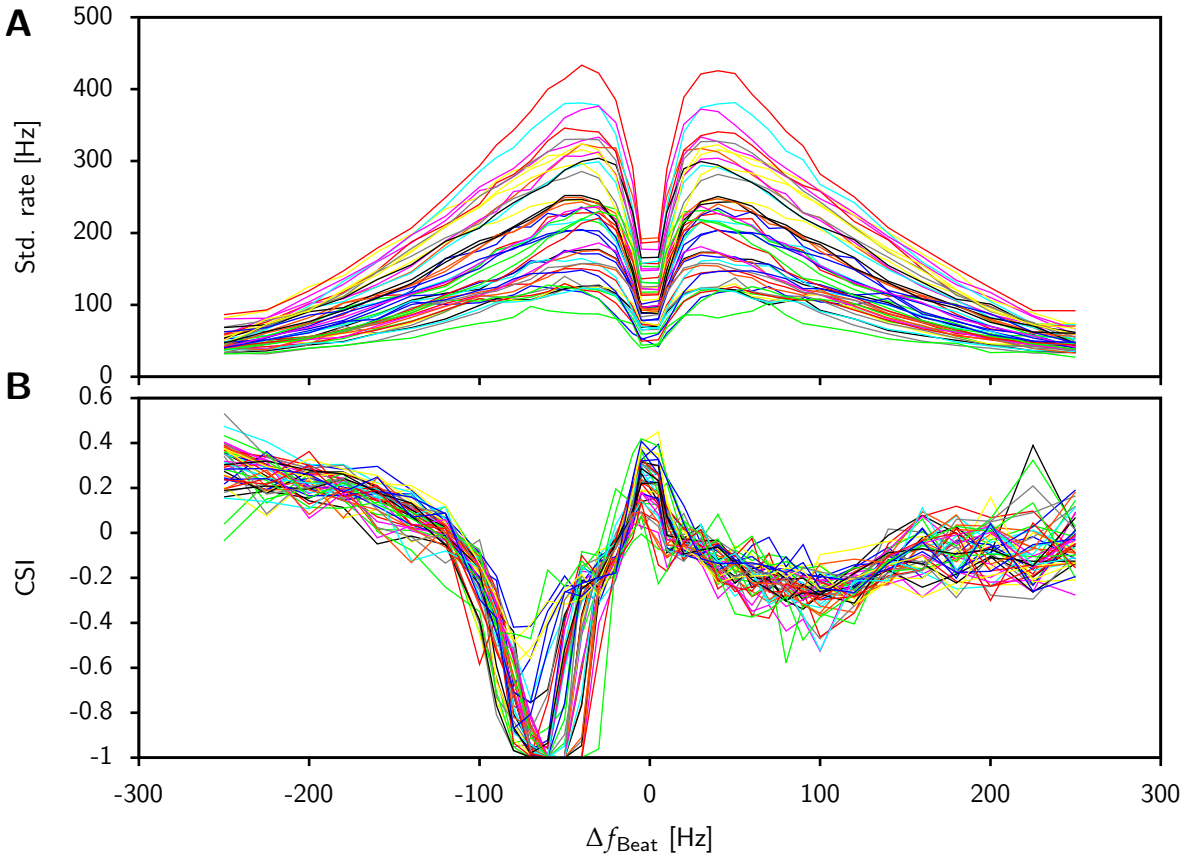

Figure 5.6: Beat and chirp responses of single model neurons. A) The responses of single model neurons to beats is calculated as the standard deviation of the rate response. It is plotted over the difference frequency Δf_{Beat} of the beat Δf_{Beat}. Each colour represents a specific model neuron. **B**) The CSI of the same model neurons to a chirp of the same characteristics as indicated in Fig. 5.5 superimposed on beats of different Δf_{Beat}.

With the model population we can now look at responses of different single neurons to the whole range of beats and chirps (Fig. 5.6). This is not feasible in P-unit recordings, because the length and number of experiments is limited. The band-pass tuning to beats is conserved across different model neurons as are slight non-uniformities from the resonances to their baseline frequencies (Fig. 5.6 A). However, the magnitude of the maximal response varies strongly. It ranges from 50 Hz in models with weak responses to up

to 450 Hz in those that respond strongly. The responses to a chirp superimposed on the beats, on the other hand, do not vary systematically (Fig. 5.6 B). In general the pattern of CSI over Δf_{Beat} of single models exhibits more variability than that of the population. However, no systematic trends can be made out among model neurons (Fig. 5.5 B).

Model neurons of different onset gain perform better at encoding a chirp depending on the background

We have demonstrated that the model population exhibits natural-like heterogeneity and that it reproduces responses to a behaviourally-relevant signal. To examine the effect of heterogeneity on the population encoding of chirps, we look at the differential encoding of chirps by model neurons of distinct response characteristics. We use the absolute CSI as it reflects, how strong the chirp changes a response, and start out by relating the CSI to the onset gain (Fig. 5.7).

The CSI is strongly correlated with f_0, demonstrating that model neurons of particular onset gain encode a chirp better than others. However, this correlation depends on the parameters of the underlying beat. At low positive Δf_{Beat} (10 Hz) a chirp is encoded better by cells with high f_0 if the contrast is low (Fig. 5.7 A), while the opposite is true at high contrast (Fig. 5.7 B). On the other hand, at a high contrast and a fast negative Δf_{Beat} (-200 Hz) cells with a high f_0 again outperform those with low f_0 (Fig. 5.7 C and D). At some Δf_{Beat} it depends on the phase of the beat $\Delta\phi$ at which the chirp is occurs which cell encodes it most strongly. At low Δf_{Beat} and intermediate contrast, a higher f_0 is beneficial when the chirp is emitted at the peak of a beat, while there is no effect of f_0 if it is emitted at the trough of the beat (Fig. 5.7 E and F). Together, these relations show that it is beneficial for a population exposed to chirps at different backgrounds to encompass cells of different f_0.

Recordings indicate that different P-units encode chirps better than others

To see whether such effects are also seen in natural cell populations, we correlated chirp responses with responses to firing rate sensitivity in our recordings (Fig. 5.8 A). We took the cells' beat response as a measure of firing rate sensitivity. The gain of cells to SAMs is correlated with their f_0 (Benda et al., 2010). At high contrast, there is a negative relation between chirp response and firing rate sensitivity (Fig. 5.8 A). This reproduces the relation seen in the model neurons (Fig. 5.7 B). The relation becomes weaker for lower contrasts (Fig. 5.8 B and C) indicating that different P-units encode chirps better at different backgrounds. However, it never reverses as in the model population (Fig. 5.7 B).

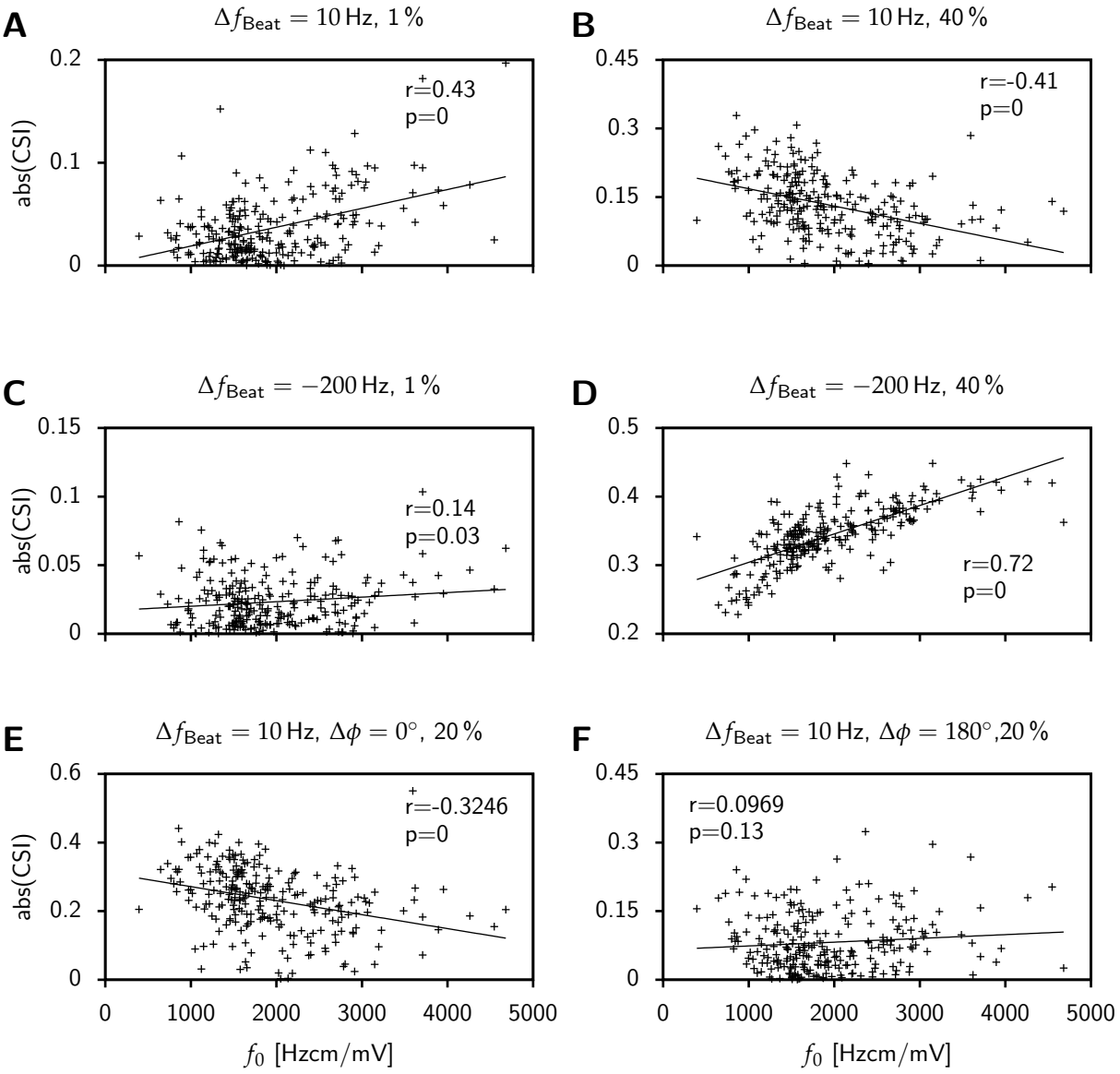

Figure 5.7: Relation between chirp encoding and firing rate sensitivity in the model population. Different model neurons are simulated 15 times in response to different chirp/beat combinations. From the responses, the CSI is calculated, and plotted over f_0 of the same model. Each dot represents the result for one model neuron. For different chirp/beat combinations, the relations differ in sign or strength, as indicated by a linear regression (black) and the correlation coefficient (r) with corresponding p-value (p). The relations are shown for a chirp on a slow beat ($10\,\text{Hz}$) at low contrast ($1\,\%$) in **A**) and at a high contrast ($40\,\%$) in **B**). **C**) and **D**) show the relations at low and high contrast, respectively, at a fast negative Δf_{Beat} ($-200\,\text{Hz}$). In **E**), Δf_{Beat} is again low as in A and B, but now the phase of the beat is shifted to $0°$, while it is $180°$again in **F**). All parameters that are not listed had the following default values: The beat had a $\Delta f = 10\,\text{Hz}$ at $20\,\%$ and a chirp of $s = 100\,\text{Hz}$, $\Delta t = 15\,\text{ms}$, $a = 2\,\%$ was emitted at $\Delta\phi = 180°$

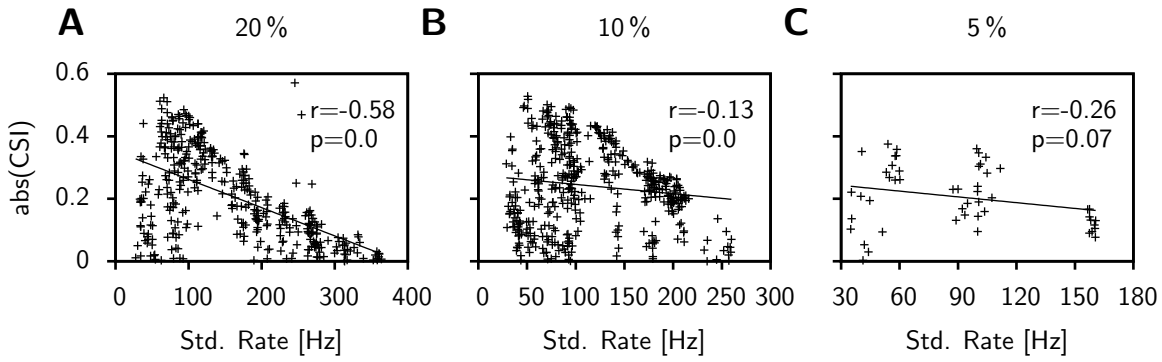

Figure 5.8: Relation between chirp encoding and firing rate sensitivity in recorded P-units. The CSI to a chirp of $s = 100\,\text{Hz}$, $\Delta t = 14\,\text{ms}$ and $\Delta A = 2\,\%$ on a beat of $\Delta f = 10\,\text{Hz}$ are derived and plotted over the response to the underlying beat alone. Both responses are calculated in terms of the standard deviation of the rate. The contrast of the stimulus was 20 % in **A**), 10 % in **B**) and 5 % in **C**). The relations become weaker for increasing contrast, indicating a similar relationship in neurons as seen in the model in Fig. 5.10.

Different baseline characteristics are needed for good chirp encoding on different backgrounds

There does not seem to be an optimal f_0 for chirp encoding when all backgrounds are taken into account. But might there be an optimal value for the baseline characteristics? Exemplary relations between CSI and all four baseline characteristics demonstrate as well that they have opposing effects depending on the background beat (Fig. 5.9). A high baseline rate is beneficial for chirp encoding on fast positive Δf_{Beat} (Fig. 5.9 A), while cells with high baseline rate perform slightly worse than others at intermediate negative Δf_{Beat} (Fig. 5.9 B). For the CV there is a slightly negative correlation with CSI at low positive Δf_{Beat} at low contrast (Fig. 5.9 C), while there is a positive correlation at intermediate negative Δf_{Beat} (Fig. 5.9 D). Stronger SC (i.e. greater negative correlations) are beneficial for encoding a chirp at low positive Δf_{Beat} (Fig. 5.9 E), while they deteriorate encoding at fast positive Δf_{Beat} (Fig. 5.9 F). For the VS the relation is positive at low positive Δf_{Beat} and low contrast (Fig. 5.9 G), while the relation is conversed at high contrast (Fig. 5.9 H).

Overall, these results show that there is not a single neuron in a population that encodes chirps optimally at every background. For every chirp/beat combination a different cell is best suited. The variability of naturally occurring signals makes it beneficial for a population to exhibit heterogeneity in their baseline properties (Fig. 5.9) and f-I-curves (Fig. 5.7).

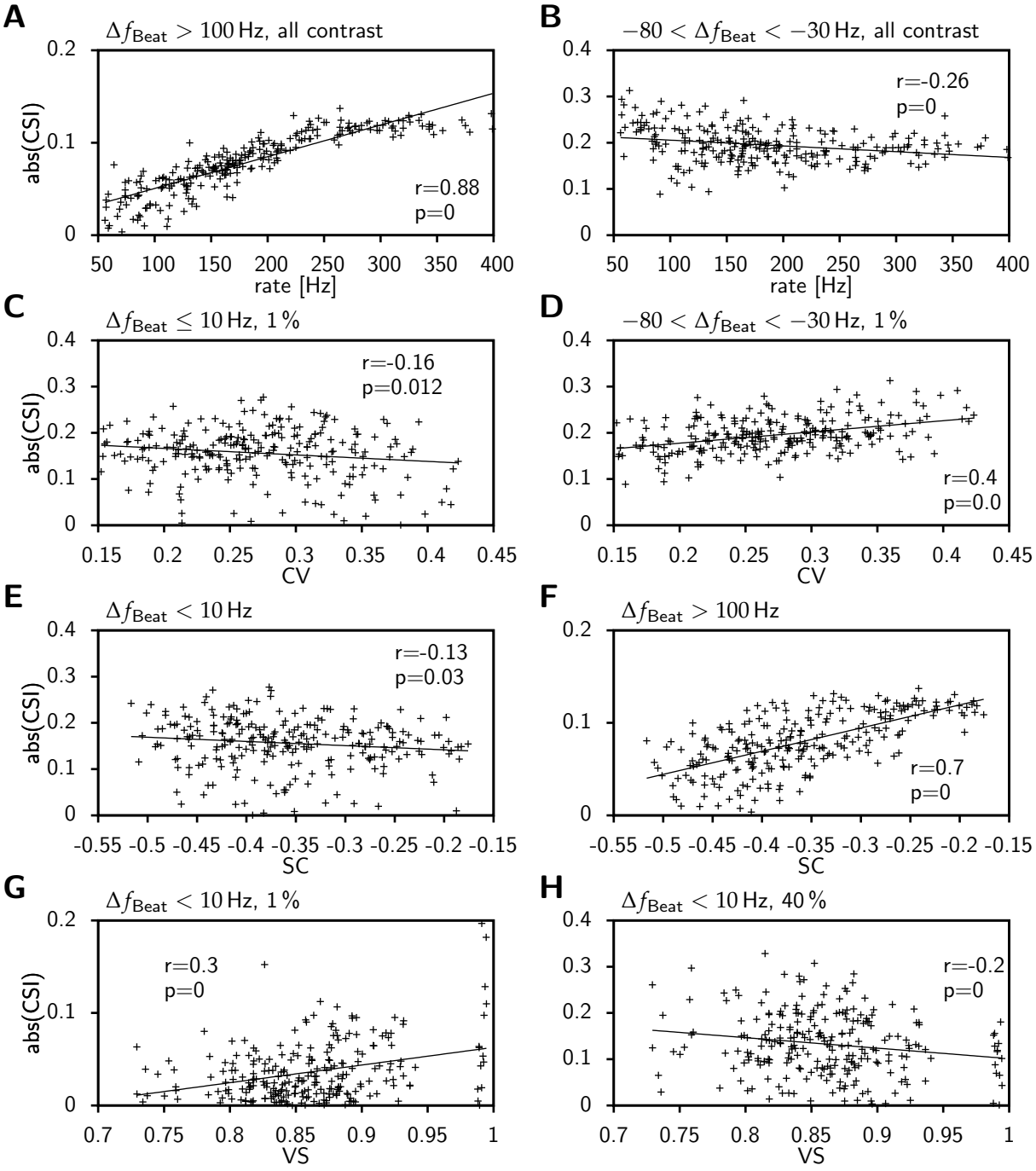

Figure 5.9: Relation between chirp encoding and baseline characteristics in the model population. From the same data as used in Fig. 5.7 the absolute CSI in response to different chirp/beat stimuli is related with different baseline characteristics of the model neurons. **A**) and **B**) The CSI in relation to the baseline firing rate. The chirp stimulus was superimposed on high, negative Δf_{Beat} ($> 100\,\text{Hz}$) in A and on intermediate negative Δf_{Beat} (between -80 and $-30\,\text{Hz}$) in B. **C**) and **D**) The relation between CSI and CV. The chirp stimulus was on a beat of low positive Δf_{Beat} ($\leq 10\,\text{Hz}$) in C and on intermediate negative Δf_{Beat} (between -80 and $-30\,\text{Hz}$) in D. **E**) and **F**) show the relation with SC for a chirp on low ($< 10\,\text{Hz}$) in E and fast positive Δf_{Beat} ($> 100\,\text{Hz}$) in F. **G**) and **H**) The relation between CSI and VS for a chirp superimposed on a beat of low positive Δf_{Beat} ($< 10\,\text{Hz}$) at low contrast in G and high contrast in H.

5.4 Discussion

We here investigated the heterogeneity of electroreceptor populations and its effect on encoding communication signals. For this purpose, we rebuilt a natural population by means of model neurons. We reproduced the population heterogeneity by distributing the underlying parameters according to the variability found in fits of our model to different target data sets.

To do so we first analysed the distributions of and correlations between parameters underlying good fits of the model to target data sets. We got smooth distributions of parameters that could be characterised in their type and moments. We distinguished between variability caused by the uncertainty of fitting one target data set and the variability obtained when fitting different target data sets. While both caused similar parameter distributions, we frequently observed significant correlations between parameters only when looking at the repeated fits to one target data set. Parameters resulting from fits to different target data sets were not correlated.

Correlations between parameters reveal compensatory effects between them, i.e. relations in which the effect of changing one parameter can be compensated by changes in another (Olypher and Calabrese, 2007). In such a case many different parameter combinations can produce the same behaviour (Prinz et al., 2004). The variability and correlations between parameter combinations to one particular target data set reveal that cells are not represented by single points in the parameter space, but rather by hyperdymensional planes (Goldman et al., 2001). Furthermore, the fact that pooling the parameters over all target data sets yields smooth distributions indicates that there is a continuous region in the parameter space that underlies all different fits.

Our approach leads to very few models that do not produce realistic P-unit activity. Furthermore, discrepancies only appear in one of six response characteristics (the strength of phase-locking to the carrier signal, VS). The five remaining response characteristics are matched well both in value and in the distribution of values. A previous study reported the lognormal distribution of baseline firing rates (Gussin et al., 2007) and hypothesised that it originates from the nature of the P-unit electroreceptor organ, in which 25-30 receptor cells are innervated by one afferent nerve fibre. Our model now allows more detailed investigations on the possible causes as well as on potential benefits for signal encoding imposed by the distributions of baseline characteristics underlying P-unit heterogeneity.

The model population differs substantially from the cell population in the correlations between their response characteristics (Fig. 5.4). This could have different causes. The sample of 23 recordings might be too small to elucidate existing correlations between response characteristics in the natural population. On the other hand, the covariance matrix we use to draw correlated parameters for the model population might not be a valid estimation of the true covariance between parameter sets. However, we tested for the robustness of the correlation matrix between response characteristics as well as of the covariance matrix of parameters in leave-one-out analyses and found that

both are robustly defined. Most likely, the uncertainty in fitting each target data set hinders the exact estimation of the covariance matrix of the parameters. The covariance matrix is calculated between the 23 parameter sets that yielded the best fit for each cell. However, this selection seems delicate considering the good performance of the 10 % best parameter combinations for each individual target dataset. A more detailed analysis of the relations between planes in the parameter space underlying these fits could allow for a better estimation of the covariance between parameters. However, this was not the focus of the study at hand, and we therefore used this population regardless of this discrepancy for further analyses.

In the face of the ubiquity of population coding to rebuild natural populations by computational models has gained much attention during the past years. In cases in which model parameters can be derived from physiological experiments, such as conductances in conductance-based models, average or maximal values are derived from these and a simple distribution is assumed to underlie population diversity (Butera et al., 1999; Golomb and Rinzel, 1993). Using physiological data certainly allows for more realistic models, however, there are also limitations to this approach. First, the distribution of the parameters across a population is usually not known since experimental data is often too scarce. Second, each parameter value is usually derived from recordings in a different cell and putative compensations between them are thus inaccessible.

A different approach is to sample a big parameter space and to select those models that reproduce the normal behaviour (Prinz et al., 2004; Taylor et al., 2009). Correlations and distributions of the parameters are then derived from the successful fits. Similar to the second approach, we sample the whole parameter space during the fitting procedure and select those models that reproduce the data well. However, we then do not restrict our analysis to these selected models, but go one step further and extrapolate from the derived parameter distributions a population that resembles a heterogeneous cell population. Our approach thus combines the two approaches described above.

When populations were built in previous studies to investigate the effect of heterogeneity, the analysis was often restricted to varying one parameter (Chelaru and Dragoi, 2008; Hospedales et al., 2008; Mejias and Longtin, 2012; Savard et al., 2011). This alleviates the systematic analysis of the mechanisms and causes of heterogeneity effects. However, it builds on strong assumptions about the underlying diversity. On the contrary, we here model heterogeneity in several baseline characteristics. A detailed examination of the exact mechanisms why one population performs better than another is therefore not feasible. However, our population is less likely to miss important aspects of natural heterogeneous populations.

With our model population we studied the encoding of a behaviourally relevant natural signal – the chirp. The model had not been constrained to reproduce chirp responses, but reproduces such responses in the single cell as well as on the population level. This finding is in line with the good model predictions of the neurons' frequency tuning to SAM and RAM stimuli (Chapter 4). The frequency tuning had earlier been shown to lay the basis for responses to chirps. Chirps are transient changes in AM

frequency and P-units had been shown to respond without further processing to this change in frequency (Chapter 3).

We were able to investigate the effect of natural-like heterogeneity on chirp encoding. When correlating the variations in each of the heterogeneity characteristics (f_0, baseline rate, CV, SC or VS) with chirp encoding, we found that different values of each characteristic were optimal for the encoding of different stimuli. This shows that it is beneficial to have cells of different characteristics and suggests that a heterogeneous population performs better in response to the whole stimulus ensemble. In a previous study about heterogeneity and signal encoding in P-units Savard et al. (2011) have shown that cells with lower baseline rates, higher CV and higher f-I-curve slopes encode the envelope of a stimulus better. For the encoding of envelopes a homogeneous population of the responsive cells would suffice. In contrast we show that for encoding different stimuli different neurons might be needed. This is a stronger implication on the benefit of heterogeneity than was shown before.

Crucial for our analysis is a correct approximation of the distribution of naturally occurring stimuli. We used beat backgrounds of various phases and Δf_{Beat}. Fish have been shown to chirp at random at any phase of the beat (Walz et al., 2012; Zupanc and Maler, 1993). They are most frequently emitted in encounters of low Δf_{Beat}. However, behavioural studies have shown that fish respond well to chirps emitted at higher Δf_{Beat} as well (Hupé et al., 2008). Our stimulus ensemble is based on current knowledge of chirping behaviour.

But why do the model neurons respond differently to a chirp on different background beats? In contrast to earlier studies (Wessel et al., 1996) who described the frequency tuning of P-units to be similar across cells, we see subtle differences in the response to SAM stimuli (Fig. 5.6 A). Different model neurons show different overall gains in the tuning curve, but also slightly different shapes. The different chirp responses are most likely resulting from the differences in the frequency tuning of the neurons.

Heterogeneity has been shown before to have a benefit for stimulus encoding. It can reduce the likelihood of populations to entrain to high frequencies and thus increase the tuning bandwidth (Hospedales et al., 2008). Another well-known effect of heterogeneity is that it decorrelates cell activity. This reduces redundancy and increases the information content stored in a population (Chelaru and Dragoi, 2008; Padmanabhan and Urban, 2010; Shamir and Sompolinsky, 2006). Correlated activity arises from shared input that can either originate from the stimulus or from shared noise (Kohn and Smith, 2005; Zohary et al., 1994). P-units are not connected and have independant noise sources (Benda et al., 2006; Chacron et al., 2005a). However, they receive shared input. Their responses are therefore correlated by the stimulus and a decorrelation could improve stimulus encoding. Our analysis does not assess this question, as we analyse the chirp responses on the single cell level only. However, our results point into a similar direction: we find that single neurons respond differently well to certain stimuli thereby potentially increasing the information the population response carries about a stimulus.

It is ubiquitous in the nervous system that stimuli are encoded by populations of

neurons rather than single cells (Fitzpatrick et al., 1997; Georgopoulos et al., 1986; Kilgard and Merzenich, 1999; Wilson and McNaughton, 1993). This implies that evolution might not optimise single cells but rather populations of cells (Marder and Goaillard, 2006). We here find that it might be beneficial for populations to hold a wide set of strategies – in our case a set of response characteristics – to be able to respond to big ensembles of stimuli as encountered in the wild. Heterogeneity might be a result of a selection pressure to encode the whole natural ensemble of stimuli.

5.5 Perspective: Modelling a Population Response

In the last part of the results section of this chapter we analysed the effect of heterogeneity on chirp responses. For this purpose, each model neuron was stimulated 15 times with the same chirp stimulus and the rate modulation to beats and chirps were averaged over trials. However, a downstream neuron does not have access to multiple responses of one neuron. Rather, it has information about one response of each projecting cell and has to average over a population of such single trial responses. In the following we apply an analysis that more realistically resembles such a situation. Because some aspects of this analysis remain delicate (see below), I decided to include it as a separate section rather as part of the result section.

In th following we take one trial of a response of a model neuron, analyse it and then pool over a population (Fig. 5.10). The rate response of single trials is calculated as the instantaneous rate given by the inverse of the ISIs (Fig. 5.10 A and B, third row). The response to the beat and chirp is then derived as the standard deviation in time windows during beat and chirp as described in Section 5.2. In contrast to the previous analysis, these measures are not derived from averaged responses, but from single trials.

We now average these responses over populations of 100 different model populations. In order to simulate heterogeneous populations, we pool single trials of models with different parameter sets (Fig. 5.10 A). Multiple trials of a model instance are used to form homogeneous populations (Fig. 5.10 B). Different heterogeneous populations respond similarly to beats and chirps (Fig. 5.10 C and D, grey curves). In contrast, different homogeneous populations perform differently (Fig.‘5.10 C and D, coloured curves, every colour represents a different homogeneous population).

In response to one stimulus there are homogeneous populations that perform better than all heterogeneous populations, but also some that perform worse. Heterogeneous populations show moderate responses and they behave very similarly. One advantage of heterogeneity could be to minimise the likelihood of very poor encoding performance.

We now ask whether homogeneous populations that are good for encoding one chirp, remain good in encoding chirp stimuli of other parameters. Chirps can be of different size s, width Δt and amplitude decrease a. All these change the waveform of the AM caused by the chirp and thus influence the cellular response. So far we used a “standard chirp” that was generated with $s = 100\,\mathrm{Hz}$, $\Delta t = 15\,\mathrm{ms}$ and $a = 2\,\%$ and

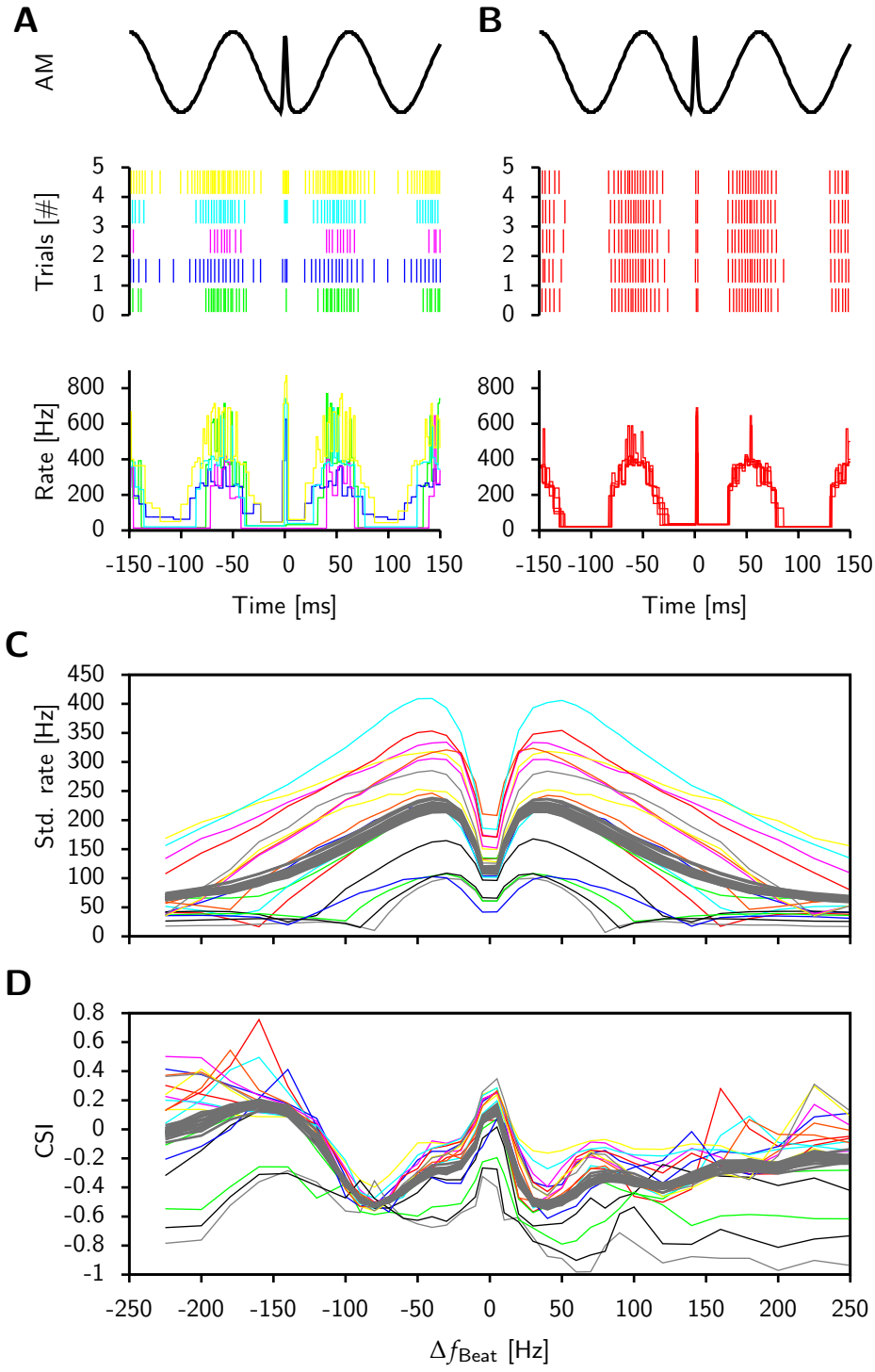
A
B
AM
Trials [#]
Rate [Hz]
Time [ms]
Time [ms]
C
Std. rate [Hz]
D
CSI
Δf_{Beat} [Hz]

Figure 5.10: Chirp encoding in heterogeneous and homogeneous populations. population responses to chirp stimuli are simulated for 100 model neurons of different parameter sets (heterogeneous population, **A**) or as 100 repetitions of the same parameter set (homogeneous population, **B**). The top row shows the chirp AM stimulus, the second row the spiking responses, the third row the instantaneous rate as derived as the inverse of the spiking response of single trials in B. **D**) From this rate response the standard deviation in a window during the beat was calculated and averaged over a heterogeneous (grey) or homogeneous population (colour, different colours represent different populations). **D** Accordingly, the CSI was derived from the rate response for each model simulation and averaged. The chirp had the default width and size, the stimulus contrast was 20 %.

was emitted on a beat of $\Delta f = 10\,\mathrm{Hz}$ at 20 % contrast, if not indicated differently. From the responses to the "standard chirp" we select the best and worst homogeneous populations, and stimulat it with chirps of other parameters. The best population shows moderate responses to other chirp types (Fig. 5.11 B), while the worst population performs well on some chirp stimuli as well (Fig. 5.11 D).

However, even over the whole range of chirp stimuli that we include in our analysis, the best homogeneous population remains better than a representative heterogeneous population. This seems to contradict our finding of the result section of this chapter stating that distinct models encode different kinds of chirps well (see Fig. 5.7 and Fig. 5.9). One would suspect that the heterogeneous population comprises individual neurons that give a good response for each chirp stimuli and thus performs better than a homogeneous population that presumably fails at encoding a range of chirp stimuli.

The "best" homogeneous population is worse than the heterogeneous in only a few of the chirp stimuli. To generate the heterogeneous population response, we sum the absolute CSI of individual models. Good responses of some models could be covered by a bulk of bad responses. On the other hand, the good homogeneous population might perform worse than some other models for individual chirp stimuli, but still better than average. The best homogeneous population comprises the model with the highest f_0 (turquoise population in Fig. 5.10). In Fig. 5.7 we have seen that a high f_0 is detrimental for encoding several chirp stimulus. However, the slopes of the relations differ and the positive correlations usually have a higher slope. This could mean that in Fig. 5.11 C, the CSIs in which the homogeneous population performs better, are higher and further separated from the heterogeneous population and cause a visual bias when looking at this figure.

The addition of absolute, individual CSI to generate the population response is based on three assumptions about the read-out of P-unit responses in the ELL. First, we decided to sum the CSI, because individual models usually have a CSI of similar magnitude. On the contrary, cells of higher f_0 have much higher individual responses to beats and chirps, thus have a higher impact than cells on a sum of these responses. However, an upstream cell more likely integrates beat and chirp responses and compares the averaged responses in a form of CSI.

Second, individual models possibly have CSIs of different sign in response to the

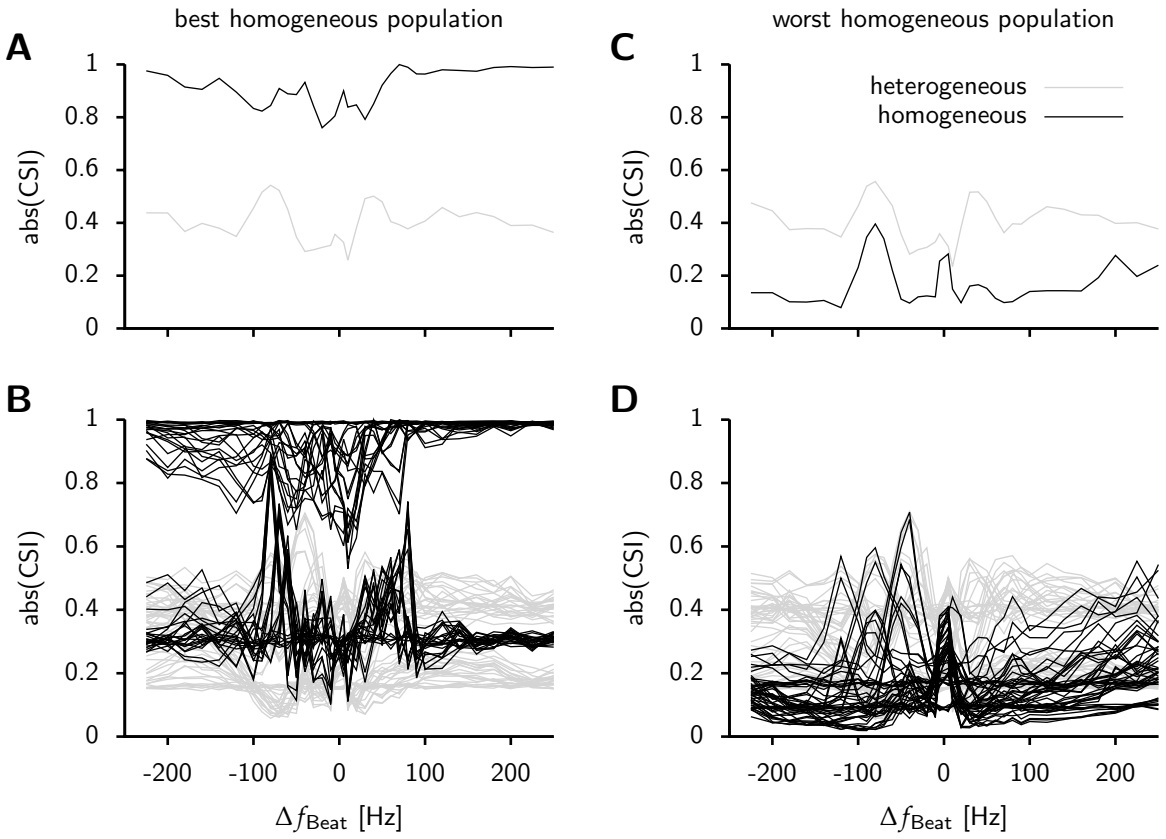

Figure 5.11: Population responses to different chirps. **A**) The best homogeneous population is chosen as the one exhibiting the largest absolute CSI from the data shown in Fig. 5.7. Its response is plotted together with a representative heterogeneous population. **B**) Both populations are stimulated with chirps of different parameters ($s = [50, 100, 150]$ Hz, $\Delta t = [15, 50]$ ms and $\Delta A = [2, 20]$ %, resembling the diversity of chirps found in Kolodziejski et al. (2007)). Each line represents one chirp of fixed characteristics. The responses of the homogeneous population are plotted in black, those of the heterogeneous in grey. **C**) Similarly as in A, the chirp responses of the worst homogeneous population are plotted together with a random heterogeneous population. **D**) As in B, the "worst" homogeneous and the heterogeneous population are stimulated with chirps of different parameters.

same chirp stimulus. We assume that the downstream cell takes into account the magnitude of the *CSI* only and we therefore use the absolute *CSI*. We do not make a prediction how this could be implemented in ELL pyramidal cells. Third, we assume an equal summation of all P-units. While this is the simplest possibility of how information could be read out of the population, the strength of synapses and their position within the dendritic tree could weigh different P-unit inputs differently.

The instantaneous rate of single trials fluctuates heavily (Fig. 5.10) and this can lead to an unstable estimation of the *CSI*. Overall, the estimation of the *CSI* as well as the justification of the read-out assumptions are fragile and should be elaborated on in future research. Nevertheless, in case the results persist, one can ask, why natural P-unit populations are heterogeneous and do not resemble an optimal homogeneous population. One reason could be that the calibration of a homogeneous population to the optimal case was too costly in evolution and a mediocre heterogeneous population was better than a bad homogeneous one. Another reason could be an incompleteness of our parameter space. P-units also encode signals that are of completely different statistic for tasks such as localisation and prey capture. Including those might enhance the equalising effect that we see for increasing the parameter space. Heterogeneous and homogeneous populations might then perform the same when the whole parameter space is taken into account. Again, heterogeneous populations would then have the advantage that they do not have to be calibrated as strongly a homogeneous population.

Part III. DISCUSSION

Chapter 6

Conclusions

Signal encoding in heterogeneous populations of receptor neurons was the subject of this thesis. Its investigation was based on the encoding of an electrocommunication signal – the chirp – in P-type electroreceptors. Various complementary approaches were employed ranging from electrophysiological experiments to computational modelling. In the following, I recapitulate the conclusions of the three research projects separately and then combine the findings with respect to their implications for information coding. Finally, I present an outlook on follow-up research questions.

Chirps occur on top of beats, periodic amplitude modulations (AMs) of the electric organ discharge (EOD) due to the superposition of the EODs of two fish. Behavioural studies have shown that fish readily respond to chirps at beats of a wide range of difference frequencies (Hupé et al., 2008). In Chapter 3 I studied the responses of P-units to chirps at beats of different parameters via electrophysiological recordings. The results were as follows:

- The AM waveform is the relevant signal for P-units. Its frequency is given by the frequency difference between the EODf of a receiving and the EODf of a communicating fish and is affected by both the initial difference frequency of the beat and the transient frequency change of the chirp. The signal therefore depends on both beat and chirp.

- The P-unit response to a chirp depends on the difference frequency of the underlying beat, partitioning the range of occurring difference frequencies in four distinct regimes: beats of high negative and low positive frequencies elicit an increased response, while low negative or high positive ones decrease the response.

- The response increases and decreases are reflected in changes in synchronisation as measured by the correlation over trials and in the modulation depth of the rate.

- Whether P-units respond by synchronisation or desynchronisation to the chirp can be predicted by taking into account only the frequency of the signal and the

frequency tuning of the cells, although the duration of a chirp is often shorter than a full period of the frequency it elicits.

The great informative value of the cells' frequency tuning with respect to their chirp responses led us to investigate this tuning in Chapter 4 by means of a computational model. I constructed a leaky integrate-and-fire model with data-derived dendritic filter and adaptation current. The model showed the following:

- A P-unit's baseline activity and responses to step stimuli can be reproduced with high accuracy when the model parameters are calibrated to replicate characteristics of these responses.
- Heterogeneous baseline discharges of P-units can be simulated by varying the model parameters. The model can reproduce successfully the responses of all P-units we had recorded from and thus produce activity of different baseline characteristics reflecting the heterogeneity found in P-unit populations.
- The frequency tuning to sinusoidal and noise AM stimuli is an emergent property from the responses to step stimuli and the constant EOD. Even when calibrated to the latter, the model responds to sinusoidal and noise AMs in a similar way as the target P-unit.

The ability of the model to reproduce responses of distinct P-units allowed for a simulation of a heterogeneous model population that resembles the natural P-unit population. I characterised the parameter variability and correlations underlying the fits to distinct P-units in order to generate new representative parameter combinations. With these I built model populations that led to the following conclusions:

- The distributions of parameter values are a sufficient foundation to produce natural-like heterogeneity. The model population resembles the natural population in terms of baseline characteristics, even though it encompasses models that are not fit directly to P-units, but whose parameters are drawn from the characterised distributions.
- The model also reproduces chirp responses. A single model neuron responds to chirps as its target P-unit, and the population responds to chirps like the P-unit population virtually at the full range of background beats.
- The single models in the population exhibit a frequency tuning of varying magnitude, but similar shape in response to sinusoidal AMs. No systematic differences can be made out in their chirp encoding.
- For a single chirp stimuli the responses of different model neurons are correlated with certain baseline response characteristics. P-units of a certain characteristic encode a chirp more strongly, but different P-units optimally encode different chirps.

This suggests that a heterogeneous population is better suited to encode the natural range of chirps than a homogeneous population, because it possesses strong responses to all chirp stimuli.

The findings allow for implications on the strategies of information coding applied in the electrosensory system. Before I now go in detail into these implications, I here combine the results of the different projects:

- The coding of chirps in P-units is context-dependant. This challenges behavioural theories about these signals and shows how a detailed physiological description can make predictions concerning the behaviour of an animal.
- The synchrony response of P-units is fast and linear. Since it does not require unique encoding mechanisms, this could constitute a universal strategy of receptor cells to encode fast, transient signals.
- A simple model of spike generation can predict responses to complex dynamic stimuli even if calibrated to responses to simple stimuli. It therefore constitutes a general description of the natural neuron. This demonstrates the power of simple models when they are carefully designed and calibrated.
- Different individual model neurons respond optimally to chirp stimuli of different characteristics suggesting an advantage of a heterogeneous population in the encoding of variable natural signals. It indicates that the whole stimulus ensemble might put a selective pressure on the development of populations of sensory neurons.
- Careful examinations of the signals caused by different chirps on different contexts lay the basis for understanding the response in receptor cells. Main findings of this thesis were only revealed when the whole stimulus space was taken into account. This underlines the importance of a detailed knowledge of the natural sensory environment when characterising a neuronal system.

Chapter 7

Implications for Information Coding in the Electrosensory System

7.1 Context-dependency of Responses to Communication Signals

Perception does not strictly mirror the stimuli from the external world, but rather originates from the construct that the nervous system forms of them (Zeki, 2001). Otherwise, phenomena such as colour or shape constancy would not exist, in which our perception is not linearly related to the physical stimulus. The nervous system creates new "qualities" from the physical information present in the external world. That is, it forms categorisations of the stimuli that differ from those that are present in physical world. We perceive red as red in a number of different light conditions, in which the physical stimulus – the absolute intensities of the different wavelengths reflected by a surface – is very different, as it depends on the properties of both the surface and the light elucidating it. We do so by taking into account the composition of the light source also by comparing the light reflected by all surfaces. If the perception was based solely on the stimulus' magnitude, we would have distinct colour percepts in differing light conditions.

Such mapping of a physical stimulus to a perceptual category plays a crucial role in communication. Here, communication signals are perceived as distinct categories, albeit often consisting of continuously variable acoustic signals (e.g. in humans, Holt and Lotto, 2010, monkeys, May et al., 1989, or birds, Nelson and Marler, 1989). Recent studies have revealed neural correlates of this mapping from variable sensory stimuli to perceptual categories (Gifford et al., 2005; Prather et al., 2009). In contrast I show in Chapter 3 that the responses of single P-units are influenced by the background beat in a way that does not correlate to a known behaviour. A chirp either synchronises or desynchronises the P-unit responses depending on the beat background creating four different encoding regimes. This partition persists on the population level (Chapter 5).

Although P-units are just the first stage of sensory information processing and perceptual phenomena are the result of extensive parallel and interconnected processing (Nassi and Callaway, 2009), our findings suggest that the nervous system categorises chirps as distinct when they occur on different backgrounds.

P-units respond to amplitude modulations (AMs) of the EOD by in- or decreasing the ongoing baseline response. An increase of population activity is read out by E-type pyramidal cells in the electrosensory lateral line lobe (ELL), while a decrease activates I-type pyramidal cells (Chapter 2, Shumway and Maler, 1989). Whether or not this separation of information persists up to a perceptual level, remains unknown. However, it has been suggest that E- and I-cells form encoding streams that process information about conductors (prey) or insulators (rocks) in parallel (Chacron et al., 2011). In the context of communication signals this separation has been suggested to underlie the distinction between big and small chirps (Marsat and Maler, 2010).

Assuming that the separation of the encoding persists and results in a distinct perception of small chirps depending on the background, the question arises whether the communication behaviour is influenced by this distinction. More specifically, the differential encoding challenges two assumptions about small chirps. First, behavioural studies on small chirps suggested that they convey the same information regardless of the background (Bastian et al., 2001; Cuddy et al., 2012; Engler and Zupanc, 2001; Hupé et al., 2008; Salgado and Zupanc, 2011). This is consequential considering the stereotypical form of the chirp independant on the background (Zupanc et al., 2006). However, the various AM forms elicited by a chirp at different backgrounds (Fig. 2.1 and Fig. 3.2) and the differential encoding in P-units suggests that the behavioural meaning of the small chirp differs depending on the background.

Second, a clear distinction between small and big chirps is suggested in terms of their behavioural relevance (Bastian et al., 2001; Engler and Zupanc, 2001; Salgado and Zupanc, 2011). The correlate of this distinction at the physiological level has been thought to be the encoding of small and big chirps by synchronisation and desynchronisation of P-units, respectively (Benda et al., 2006), that persists at the level of the ELL by encoding in E- and I-cells (Marsat and Maler, 2010). Our results show that small chirps are also encoded by desynchronisation of P-units at certain backgrounds and thus question the clear distinction between big and small chirps at these backgrounds, namely high positive difference frequencies.

Overall perception in an organism can ultimately only be probed by behavioural studies. While cognitive phenomena such as colour and shape constancy are accessible via introspection or psychophysical methods, perceptual experiments are more difficult to perform with animals. Communication signals are an exception in that their perception can well be assessed by studying the behavioural response (Chapter 1, Walz et al., 2012). While a behavioural examination was beyond the scope of this thesis, future studies could explore chirp encoding on different backgrounds by looking at behavioural responses to these signals. This could then clarify whether a new quality is formed and perception indeed categorises chirps according to the background they occur on.

7.2 Frequency Tuning in P-units

Temporal and rate coding describe two modes of embedding information in neuronal responses that differ in the way information is represented in the activity of single neurons or neuronal populations and in the way it is propagated over nuclei and regions in the nervous system (Chapter 1). Several previous studies have concluded that the early electrosensory system uses a temporal rather than a rate code (Berman and Maler, 1999; Nelson et al., 1997). The phase-locking of P-units to the EOD and the short excitatory postsynaptic potential observed in ELL pyramidal cells appears appropriate to read out information using synchrony among P-units on time scales of the EOD period (Berman and Maler, 1999).

Information about prey and communication is thought to be encoded in parallel in the electrosensory system as prey gives rise to locally restricted, low-frequency stimuli, while communication signals stimulate receptors on the whole body of a fish and contain high frequencies (Chacron et al., 2005c; Middleton et al., 2009). The two classes of stimuli elicit responses in different maps of the ELL (Chapter 2). In both cases a temporal code has been postulated to underlie the read-out of P-unit responses in the ELL. The small rate increase in single P-units, as induced by prey, seems to be too small to be detectable on the background noise. Since it affects several P-units, Nelson et al. (1997) suggested that it should be read out via the synchrony among P-units. The cells in the ELL that respond to communication signals (pyramidal cells of the lateral segment, Chapter 2, Krahe et al., 2008; Marsat et al., 2009; Metzner and Juranek, 1997) have particularly large receptive fields and a high spike threshold. These characteristics make them particularly well suited for the detection of high-frequency, synchronous activity (Middleton et al., 2009).

Throughout *Part II* we measure P-unit activity either in terms of the correlation over trials or the rate modulation. For both measures we convolve the spike trains with a Gaussian kernel of 1 ms width. Although we do not apply a rigid time window for calculating the correlation or rate, this kernel resembles our choice of an "encoding window", as information on a finer time scale is smoothed out by the convolution. The kernel width corresponds to the width of the excitatory postsynaptic potential in ELL pyramidal cells (Berman and Maler, 1998), the read-out of sensory inputs is therefore likely to discard information on finer time scales as well.

Since P-units have independant noise sources (Chacron et al., 2005b), the population activity can directly be inferred from the single cell's activity. In a homogeneous population the population rate corresponds to the single cell's rate and the synchrony to the correlation across trials. This allows a direct comparison of information encoding when a rate code is implied and when a temporal code is implied. Qualitatively, both measures yield the same results: the rate as well as synchrony response is strongest to beats of intermediate frequencies and fall off at higher and lower frequencies (Fig. 3.6).

Chirps as well have the same effects on rate and synchrony (Fig. 3.5): they increase rate and synchrony at low positive and fast negative beats, and both measures decrease

at fast positive and low negative beats. Quantitatively, the rate is more sensitive to chirps than is the correlation (Fig. 3.5). A chirp of size 60 Hz affects the rate response significantly on beats of difference frequencies at which the correlation is not affected significantly. We additionally performed whole-nerve experiments in which the strength of the signal represents the degree of synchrony in the whole population of P-units in the nerve. For this kind of experiment, the effect of a chirp is significant on all background beats (Fig. 3.5 C). The information embedded in the synchrony of the whole population is thus sufficient to encode all chirp-beat combinations.

The whole-nerve recordings also show that the synchrony across a population is modulated very fast upon changes in the stimulus. With them I could predict from the frequency of the stimulus together with the frequency tuning of the P-units whether they would respond by synchronisation or desynchronisation to a chirp (Fig. 3.7). A chirp increases the frequency of the stimulus by on average 55 Hz for about 14 ms (for the parameters we used). On low beat frequencies (e.g. 10 Hz) this means that its duration is on the order of just one period of the frequency we used to predict the response ($10 + 55 = 65$ Hz in our example, corresponding to a period of 15.4 ms). The good match between prediction and data shows that the synchrony response is very fast.

The prediction also shows that the response is linear. I used an average of the frequency, although in reality the chirp constitutes a Gaussian-shaped frequency excursion. The response thus changes in response to the combination of multiple frequencies as it would do to each one of them separately. The simple nature of the synchrony response is further supported by the finding that a population of leaky integrate-and-fire model neurons shows exactly the same responses in terms of correlation over trials. It does not only reproduce the shape of the tuning curve, but also the exact magnitude of synchrony to different frequencies (Fig. 4.8) and further generalises for different contrasts (Fig. 4.9). The exact match of the synchrony response is more surprising than that of the rate response, as to generate it, one needs an additional nonlinear step. To calculate the correlation coefficient over trials, for example, one first multiplies the two time series. The reproduction of the synchrony response with the model allows for very important simulation experiments on the encoding of signals that are small (prey) and transient (communication) in neuronal populations that were not possible to date.

7.3 P-unit Modelling

Since the beginning of neuroscience (Lapicque, 1907), mathematical modelling has been used as a powerful way to reveal mechanisms of information encoding in single neurons and neuronal networks (for reviews on single cell modelling, see Herz et al., 2006; Koch and Segev, 2000, for network modelling Averbeck et al., 2006; Gerstner, 2000). Theoretical models allow to characterise in detail which aspects of the external world are represented by the nervous system and how this representation is influenced by changes in the encoding process. One can even perform novel "in silico" experiments that are difficult or impossible to perform on biological neurons or neural networks,

or use models to generate inputs for neural prostheses (Chen and Zhang, 2007; Humayun et al., 1999). While for many modelling tasks a qualitative reproduction of the behaviour of natural cells is sufficient, a quantitative examination is mandatory for the latter. Also, "in silico" experiments and neural prostheses require predictive power, that is models have to reproduce cell responses not only to those stimuli used during the model fit, but also to novel ones.

Modelling includes two steps in which target data is needed: Calibration and validation. During calibration, the model is designed and the parameter values are constrained in order to best match a target data set. During validation, a different data set is used to test the performance of the model. Essentially, the choice of the validation data determines whether or not predictive power of a model is tested. Despite the relevance of models with quantitative predictive power, they remain rare. Only over the past ten years, such models have been introduced (Brette and Gerstner, 2005; Jolivet and Gerstner, 2004; Jolivet et al., 2008; Keat et al., 2001; Pillow et al., 2005; Schaette et al., 2005).

Keat et al. (2001) were able to reproduce the exact timing of the spiking responses of cells in the early visual system with a model comprised of a linear filter followed by a nonlinearity and a negative feedback. A leaky integrate-and-fire model has been shown to accurately reproduce the mean firing rate of cortical cells recorded *in vitro* in response to noise stimuli with varying standard deviation (Camera et al., 2004; Rauch et al., 2003) and follow-up studies showed that this model also reproduced the membrane potential fluctuations Clopath et al. (2007) and the exact timing of spikes (Jolivet et al., 2006).

However, the validation data sets of these studies were taken from the same stimulation paradigm as the calibration data. Validation to stimuli of novel statistics has been used to test how well simple models can reproduce the dynamics of more complex ones that are thought to resemble more natural activity (Brette and Gerstner, 2005; Jolivet and Gerstner, 2004). A quantitative prediction of experimental responses to novel stimulation paradigms was employed by Schaette et al. (2005), who predicted responses to noise stimuli by a stochastic neuron model fit to responses to step stimuli, and Pillow et al. (2005), who could reproduce responses to brief impulse-like stimuli by a leaky integrate-and-fire model that was constrained with noise stimuli.

Our model of P-unit responses is calibrated to baseline activity and responses to step stimuli, but reproduces responses to sinusoidal and random AM as well as chirp stimuli with a high degree of accuracy (Fig. 4.8, Fig. 4.10 and Fig. 5.4). It therefore possesses quantitative predictive power and is suited to be used in "in silico" experiments as performed in Chapter 5. Simplified models will never embody a full representation of a real cell. They are built to answer a specific question and this should always be kept in mind when discussing outcomes (Herz et al., 2006). Nevertheless, the ability of a model to respond similarly to a real cell in a novel situation remains a fascinating property of models. The seldom occurrence of true quantitative predictions underpins how exceptional the match of our model predictions with the recorded data are. While the models of Pillow et al. (2005); Schaette et al. (2005) both included a phenomenological filter extracted from the responses, we show that a quantitative prediction of neuronal

cell responses is also possible with a mechanistic model.

7.4 Heterogeneity in P-units

The biophysical mechanisms that form the basis of our model also account for the heterogeneous response characteristics in different cells. When I calibrated the model parameter to different P-units, I could reproduce their responses with the same degree of accuracy (Fig. 4.3, Fig. 4.8, Fig. 4.10). By taking a distribution of values as the basis, I could build a heterogeneous population that matches the distribution of response characteristics of P-units (Fig. 5.4). I found two effects of the heterogeneity of P-units on signal encoding. First, single cells show resonances in their responses to beat frequencies that are multiples of their baseline firing rate (Fig. 4.8). Averaging over a population of cells cancels resonances which leads to a population tuning to sinusoidal stimuli that is smoother than the tuning of single cells (Fig. 4.9). Second, responses to chirps correlate with response characteristics of single cells. Distinct single cells optimally encode distinct chirp stimuli (Fig. 5.7).

How are the two effects related? In both effects, single cell responses exhibit greater inhomogeneities than the population response. Resonances make the tuning curves of single cells more irregular and chirp responses of a single cell exhibit more extremes than the average. I conceptually evaluate the variability of the single cell responses differently in the two cases. In the first case, I suppose that having a smooth population response is beneficial, as it erases ambiguity and nonlinearities in the coding of different frequencies and could aid the encoding of signals via sweeps on the cells' tuning curve (Chapter 3). In the second, I assume that the variability of the responses is exploited by downstream neurons to get clearer representations of different chirp stimuli. Both – a smooth population response and variable single cell responses – might be needed in different contexts. The smoothing of tuning curves could also be achieved in single cells by increasing the neuronal noise. However, such a high degree of noise might impair encoding in other contexts, e.g. chirp encoding.

Heterogeneity means that neurons that are different in physiology are used to encode the same stimulus. It is a form of degeneracy in which a system constitutes multiple structurally different elements performing the same task (Edelman and Gally, 2001). Degeneracy can make a system more robust to changes in the environment and it is ubiquitous in biological systems. In the genetic code, for example, many triplets code for the same amino acid. Different polypeptides can be folded such that they function similarly. The effect of heterogeneity on chirp encoding resembles a kind of degeneracy. To one single chirp stimulus, the benefit of having different cells is not apparent, as single cells respond better than average to such a stimulus. However, the diversity of AM stimuli elicited by chirps generates a pressure on populations to respond robustly to very different signals. Heterogeneous populations might be better suited for robust encoding in variable environments. The potential benefit of heterogeneity only become evident when using a range of different chirp stimuli. This underlines the importance

of using the range of possible naturally occurring contexts when characterising a biological system (Chapter 3 and 5).

Chapter 8

Outlook

In the following I will propose specific research questions that result from my findings. Future projects could evolve in two directions. First, the results on chirp encoding call for behavioural studies on the perception of big and small chirps at different background beats. Second, the possibility to create model populations that closely resemble natural heterogeneous populations allows for a thorough investigation of population responses. I will now elaborate on each of them in more detail.

P-unit receptor neurons respond with opposite tendencies to chirps of fixed characteristics depending on the underlying beat frequency. These opposite responses are believed to trigger responses in different target neurons. Plus, on some backgrounds they show an equivalent response to a small chirp as they have been described to exhibit in response to a big chirp (fast beats, Benda et al., 2006). This calls for an investigation of the behavioural responses small chirps elicit depending on the underlying beat and the distinction the fish make between big and small chirps on fast beats.

Fish preferentially chirp in a short time window after having perceived the chirp of another fish. Behavioural thresholds of chirp encoding have been investigated by testing this echo response (Salgado and Zupanc, 2011). Exploring the echo response on different background beats could give insights into whether or not the perception of small chirps is modified by the background. Does the echo response exhibit the same magnitude regardless of the background? How does its behaviour evolve over trial time? Are behaviour and stimulation frequency similarly related for small and big chirp stimuli? These aspects are well-known for pure chirp production in response to EOD stimuli of different frequencies (Bastian et al., 2001; Engler and Zupanc, 2001). However, the relation between echo response and stimulation frequency remains unknown.

In Chapter 3 we propose that the small chirp could be used to test the sign of the difference frequency of fast beats. It elicits a desynchronisation in cases in which the EODf of the communicating fish is higher than the EODf of the receiving fish. In contrast, it synchronises the cells if the communicator's EODf is above the receiver's EODf. The mechanism of how fish are thought to sense the sign of a beat's difference frequency (Bullock and Heiligenberg, 1986; Kawasaki et al., 1988) can very well be applied at low

frequencies. At higher frequencies, in which a beat consists of only few EOD cycles, it is more difficult to implement. The small chirp could fill that gap.

Such a fundamentally different function of the signal itself would likely show up as a deviation in chirping behaviour. If the small chirp is used on slow beats to mediate an encounter (Hupé et al., 2008) but as a means to test the sign of a frequency difference on fast beats, I would suspect to see a distinct temporal evolution of chirping behaviour. While fish would likely continuously chirp at high rates in the first case, a few chirps would suffice in the second case to get the necessary information. This fits to the observation that fish chirp preferentially on beats of low frequency (Bastian et al., 2001; Engler and Zupanc, 2001). A more detailed analysis of the temporal evolution and other aspects of the chirping behaviour could shed more light on the functions of chirps at different beat contexts.

In the electrosensory lateral line lobe, where information is read out of P-unit activity, pyramidal cells are estimated to pool over 1000 neurons (in the lateral segment involved in electrocommunication, Maler, 2009). To get a realistic estimate of the P-unit population response, the sample of recordings has to be on this order. However, such numbers are not feasible to obtain in electrophysiological recordings, in which a good experiment yields a handful of good data sets. With the model, on the other hand, large numbers of neurons can be simulated and multiple questions on population coding can be tackled.

Under baseline conditions, only few P-units fire during one EOD cycle, but this number is in- or decreased in the presence of a stimulus. Such changes in the number of synchronously firing neurons can easily be detected by downstream neurons and have been suggested to constitute the code employed by the early electrosensory system (Chapter 4 and 7). The relevant signal for this code on the single cell level is the correlation over trials. The fact that the model can faithfully reproduce this measure (Fig. 4.9) allows for a realistic examination of details on the encoding between P-units and ELL. For example, the threshold for detecting a stimulus could be predicted. This would require determining the minimal intensity that significantly changes the number of spikes in a population. The sensitivity is likely to depend on the number of neurons taken into account. It is therefore important to have access to a sample of neurons of realistic size to assess the sensory threshold.

Other questions require to test a large number of stimuli. One example is the discriminability of different chirp stimuli, a question that was touched upon in Chapter 3. Each fish produces slightly different small chirps and this might depend on their hormone levels (Dulka et al., 1995). The parameters of a chirp thus potentially carry important information for the receiving fish. However, Marsat and Maler (2010) argued, that the large variability of responses to one small chirp, especially caused by the beat phase at which the chirp occurs, makes the discriminability of different small chirps impossible. I have shown in Chapter 3 that the variability of chirp responses originating from cell heterogeneity is greater than that caused by the beat phase. To answer whether fish can distinguish different chirps and if so how large the difference in chirp parameters has to be, chirps of many different parameters would have to be tested in many different

cells. This is now possible with the model.

Detection thresholds and discriminability of different stimuli are essentially behavioural questions. A powerful approach would integrate behavioural experiments with model predictions. Electric fish are particularly well-suited for such an integrated approach as their behaviour is easily observable and stimuli can be quantified, analysed and simulated well. This thesis combined electrophysiological and modelling approaches with behavioural findings from earlier studies. The conclusions concern all the different disciplines demonstrating how an interdisciplinary approach in the end benefits every individual discipline involved.

Bibliography

Adrian E (1928) *The basis of sensation.* Christophers. [6]

Anderson WS, Kreiman G (2011) Neuroscience: what we cannot model, we do not understand. *Curr Biol* 21: R123–R125. [51]

Arieli A, Sterkin A, Grinvald A, Aertsen A (1996) Dynamics of ongoing activity: explanation of the large variability in evoked cortical responses. *Science* 273: 1868–1871. [7]

Averbeck BB, Latham PE, Pouget A (2006) Neural correlations, population coding and computation. *Nat Rev Neurosci* 7: 358–366. [120]

Babineau D, Lewis JE, Longtin A (2007) Spatial acuity and prey detection in weakly electric fish. *PLoS Comput Biol* 3: e38. [79]

Bailey W, Greenfield M, Shelly T (1993) Transmission and perception of acoustic signals in the desert clicker, *Ligurotettix coquilletti* (orthoptera: Acrididae). *Journal of Insect Behvior* 6: 141–154. [50]

Barlow H (1972) Single units and sensation: A neuron doctrine for perceptual psychology? *Perception* 1: 371–394. [10, 11]

Barlow HB, Levick WR, Yoon M (1971) Responses to single quanta of light in retinal ganglion cells of the cat. *Vision Res* Suppl 3: 87–101. [6, 7]

Barlow RB, Kaplan E (1971) Limulus lateral eye: properties of receptor units in the unexcised eye. *Science* 174: 1027–1029. [11]

Bastian J, Chacron MJ, Maler L (2004) Plastic and nonplastic pyramidal cells perform unique roles in a network capable of adaptive redundancy reduction. *Neuron* 41: 767–779. [19, 22, 23, 47]

Bastian J, Courtright J (1991) Morphological correlates of pyramidal cell adaptation rate in the electrosensory lateral line lobe of weakly electric fish. *J Comp Physiol A* 168: 393–407. [18]

Bastian J, Schniederjan S, Nguyenkim J (2001) Arginine vasotocin modulates a sexually dimorphic communication behavior in the weakly electric fish *Apteronotus leptorhynchus*. *J Exp Biol* 204: 1909–1923. [12, 14, 17, 27, 32, 48, 118, 125, 126]

Benda J, Herz AVM (2003) A universal model for spike-frequency adaptation. *Neural Comput* 15: 2523–2564. [50, 60, 73, 78]

Benda J, Longtin A, Maler L (2005) Spike-frequency adaptation separates transient communication signals from background oscillations. *J Neurosci* 25: 2312–2321. [8, 16, 21, 27, 30, 31, 35, 47, 48, 50, 52, 58, 68, 69, 77, 78]

Benda J, Longtin A, Maler L (2006) A synchronization-desynchronization code for natural communication signals. *Neuron* 52: 347–358. [8, 21, 22, 27, 29, 31, 35, 36, 46, 47, 48, 78, 79, 104, 118, 125]

Benda J, Maler L, Longtin A (2010) Linear versus nonlinear signal transmission in neuron models with adaptation currents or dynamic thresholds. *J Neurophysiol* 104: 2806–2820. [58, 68, 69, 73, 77, 78, 98]

Bennett MV, Sandri C, Akert K (1989) Fine structure of the tuberous electroreceptor of the high-frequency electric fish, *Sternarchus albifrons* (gymnotiformes). *J Neurocytol* 18: 265–283. [51]

Benzi R, Sutera A, Vulpiani A (1981) The mechanism of stochastic resonance. *J. Phys. A: Math. Gen.* 14: 453–457. [7]

Berman, Maler (1999) Neural architecture of the electrosensory lateral line lobe: adaptations for coincidence detection, a sensory searchlight and frequency-dependent adaptive filtering. *J Exp Biol* 202: 1243–1253. [119]

Berman NJ, Maler L (1998) Inhibition evoked from primary afferents in the electrosensory lateral line lobe of the weakly electric fish (*Apteronotus leptorhynchus*). *J Neurophysiol* 80: 3173–3196. [19, 30, 37, 47, 56, 87, 119]

Bialek W, Setayeshgar S (2005) Physical limits to biochemical signaling. *Proc Natl Acad Sci U S A* 102: 10040–10045. [7]

Blumhagen F, Zhu P, Shum J, Schärer YPZ, Yaksi E, Deisseroth K, Friedrich RW (2011) Neuronal filtering of multiplexed odour representations. *Nature* 479: 493–498. [8]

Bol K, Marsat G, Harvey-Girard E, Longtin A, Maler L (2011) Frequency-tuned cerebellar channels and burst-induced ltd lead to the cancellation of redundant sensory inputs. *J Neurosci* 31: 11028–11038. [19, 23]

Boucsein C, Tetzlaff T, Meier R, Aertsen A, Naundorf B (2009) Dynamical response properties of neocortical neuron ensembles: multiplicative versus additive noise. *J Neurosci* 29: 1006–1010. [49]

Brette R, Gerstner W (2005) Adaptive exponential integrate-and-fire model as an effective description of neuronal activity. *J Neurophysiol* 94: 3637–3642. [78, 121]

Bro-Jørgensen J (2010) Dynamics of multiple signalling systems: animal communication in a world in flux. *Trends Ecol Evol* 25: 292–300. [12]

Brunel N, Chance FS, Fourcaud N, Abbott LF (2001) Effects of synaptic noise and filtering on the frequency response of spiking neurons. *Phys Rev Lett* 86: 2186–2189. [70, 78]

Bullock TH (1969) Species differences in effect of electroreceptor input on electric organ pacemakers and other aspects of behavior in electric fish. *Brain Behav. Evol.* 2: 85–118. [18]

Bullock TH, Heiligenberg W, editors (1986) *Electroreception*. John Wiley & Sons. [16, 19, 49, 125]

Butera RJ, Rinzel J, Smith JC (1999) Models of respiratory rhythm generation in the pre-Bötzinger complex. ii. populations of coupled pacemaker neurons. *J Neurophysiol* 82: 398–415. [103]

Butts DA, Weng C, Jin J, Yeh CI, Lesica NA, Alonso JM, Stanley GB (2007) Temporal precision in the neural code and the timescales of natural vision. *Nature* 449: 92–95. [11, 49]

Cajal SR (1899) Textura del sistema nervioso del hombre y de los vertebrados. *Imprenta y Librería de Nicolás Moya* 1: 20. [5]

Camera GL, Rauch A, Lüscher HR, Senn W, Fusi S (2004) Minimal models of adapted neuronal response to *in vivo*-like input currents. *Neural Comput* 16: 2101–2124. [121]

Caputi AA, Budelli R (2006) Peripheral electrosensory imaging by weakly electric fish. *J Comp Physiol A Neuroethol Sens Neural Behav Physiol* 192: 587–600. [13]

Carr CE, Maler L, Sas E (1982) Peripheral organization and central projections of the electrosensory nerves in gymnotiform fish. *J Comp Neurol* 211: 139–153. [13, 18, 47, 81]

Chacron MJ, Doiron B, Maler L, Longtin A, Bastian J (2003) Non-classical receptive field mediates switch in a sensory neuron's frequency tuning. *Nature* 423: 77–81. [81]

Chacron MJ, Fortune ES (2010) Subthreshold membrane conductances enhance directional selectivity in vertebrate sensory neurons. *J Neurophysiol* 104: 449–462. [23]

Chacron MJ, Longtin A, Maler L (2001)a Negative interspike interval correlations increase the neuronal capacity for encoding time-dependent stimuli. *J Neurosci* 21: 5328–5343. [51, 58, 69]

Chacron MJ, Longtin A, Maler L (2001)b Simple models of bursting and non-bursting p-type electroreceptors. *Neurocomputing* 38-40: 129–139. [21]

Chacron MJ, Longtin A, Maler L (2005)a Delayed excitatory and inhibitory feedback shape neural information transmission. *Phys Rev E Stat Nonlin Soft Matter Phys* 72: 051917. [104]

Chacron MJ, Longtin A, Maler L (2011) Efficient computation via sparse coding in electrosensory neural networks. *Curr Opin Neurobiol* 21: 752–760. [13, 22, 23, 118]

Chacron MJ, Longtin A, St-Hilaire M, Maler L (2000) Suprathreshold stochastic firing dynamics with memory in P-type electroreceptors. *Phys Rev Lett* 85: 1576–1579. [52, 77]

Chacron MJ, Maler L, Bastian J (2005)b Electroreceptor neuron dynamics shape information transmission. *Nat Neurosci* 8: 673–678. [19, 21, 36, 47, 119]

Chacron MJ, Maler L, Bastian J (2005)c Feedback and feedforward control of frequency tuning to naturalistic stimuli. *J Neurosci* 25: 5521–5532. [119]

Chacron MJ, Toporikova N, Fortune ES (2009) Differences in the time course of short-term depression across receptive fields are correlated with directional selectivity in electrosensory neurons. *J Neurophysiol* 102: 3270–3279. [23]

Chang EF, Merzenich MM (2003) Environmental noise retards auditory cortical development. *Science* 300: 498–502. [11]

Chechik G, Anderson MJ, Bar-Yosef O, Young ED, Tishby N, Nelken I (2006) Reduction of information redundancy in the ascending auditory pathway. *Neuron* 51: 359–368. [11]

Chelaru MI, Dragoi V (2008) Efficient coding in heterogeneous neuronal populations. *Proc Natl Acad Sci U S A* 105: 16344–16349. [10, 81, 103, 104]

Chen F, Zhang YT (2007) An integrate-and-fire-based auditory nerve model and its response to high-rate pulse train. *Neurocomputing* 70: 1051–1055. [121]

Chen L, House JL, Krahe R, Nelson ME (2005) Modeling signal and background components of electrosensory scenes. *J Comp Physiol A Neuroethol Sens Neural Behav Physiol* 191: 331–345. [79]

Cherry EC (1953) Some experiments on the recognition of speech, with one and with two ears. *The Journal of the Acoustical Society of America* 25: 975–979. [27]

Clopath C, Jolivet R, Rauch A, Lüscher H, Gerstner W (2007) Predicting neuronal activity with simple models of the threshold type: Adaptive exponential integrate-and-fire model with two compartments. *Neurocomputing* 70: 1668 – 1673. [121]

Cuddy M, Aubin-Horth N, Krahe R (2012) Electrocommunication behaviour and non invasively-measured androgen changes following induced seasonal breeding in the weakly electric fish, *Apteronotus leptorhynchus*. *Horm Behav* 61: 4–11. [14, 17, 118]

Dan Y, Alonso JM, Usrey WM, Reid RC (1998) Coding of visual information by precisely correlated spikes in the lateral geniculate nucleus. *Nat Neurosci* 1: 501–507. [8]

Diesmann M, Gewaltig MO, Aertsen A (1999) Stable propagation of synchronous spiking in cortical neural networks. *Nature* 402: 529–533. [10, 79]

Douglass JK, Wilkens L, Pantazelou E, Moss F (1993) Noise enhancement of information transfer in crayfish mechanoreceptors by stochastic resonance. *Nature* 365: 337–340. [7]

Druckmann S, Berger TK, Schürmann F, Hill S, Markram H, Segev I (2011) Effective stimuli for constructing reliable neuron models. *PLoS Comput Biol* 7: e1002133. [78]

Dulka JG, Maler L, Ellis W (1995) Androgen-induced changes in electrocommunicatory behavior are correlated with changes in substance P-like immunoreactivity in the brain of the electric fish *Apteronotus leptorhynchus*. *J Neurosci* 15: 1879–1890. [17, 126]

Dunlap KD (2002) Hormonal and body size correlates of electrocommunication behavior during dyadic interactions in a weakly electric fish, *Apteronotus leptorhynchus*. *Horm Behav* 41: 187–194. [16, 48]

Dunlap KD, Larkins-Ford J (2003) Production of aggressive electrocommunication signals to progressively realistic social stimuli in male *Apteronotus leptorhynchus*. *Ethology* 109: 243–258. [17]

Dunlap KD, Thomas P, Zakon HH (1998) Diversity of sexual dimorphism in electrocommunication signals and its androgen regulation in a genus of electric fish, *Apteronotus*. *J Comp Physiol A* 183: 77–86. [17]

Edelman GM, Gally JA (2001) Degeneracy and complexity in biological systems. *Proc Natl Acad Sci U S A* 98: 13763–13768. [122]

Ellis LD, Mehaffey WH, Harvey-Girard E, Turner RW, Maler L, Dunn RJ (2007) SK channels provide a novel mechanism for the control of frequency tuning in electrosensory neurons. *J Neurosci* 27: 9491–9502. [22]

Engler G, Fogarty CM, Banks JR, Zupanc GK (2000) Spontaneous modulations of the electric organ discharge in the weakly electric fish, *Apteronotus leptorhynchus*: a biophysical and behavioral analysis. *J Comp Physiol A* 186: 645–660. [14, 32]

Engler G, Zupanc GK (2001) Differential production of chirping behavior evoked by electrical stimulation of the weakly electric fish, *Apteronotus leptorhynchus*. *J Comp Physiol A* 187: 747–756. [12, 14, 17, 27, 32, 48, 118, 125, 126]

Ermentrout B (1996) Type I membranes, phase resetting curves, and synchrony. *Neural Comput* 8: 979–1001. [78]

Faisal AA, Selen LPJ, Wolpert DM (2008) Noise in the nervous system. *Nat Rev Neurosci* 9: 292–303. [6]

Farkhooi F, Strube-Bloss MF, Nawrot MP (2009) Serial correlation in neural spike trains: experimental evidence, stochastic modeling, and single neuron variability. *Phys Rev E Stat Nonlin Soft Matter Phys* 79: 021905. [58]

Fitzpatrick DC, Batra R, Stanford TR, Kuwada S (1997) A neuronal population code for sound localization. *Nature* 388: 871–874. [7, 105]

Fortune ES (2006) The decoding of electrosensory systems. *Curr Opin Neurobiol* 16: 474–480. [13]

Fortune ES, Rose GJ (2000) Short-term synaptic plasticity contributes to the temporal filtering of electrosensory information. *J Neurosci* 20: 7122–7130. [23]

Fortune ES, Rose GJ (2001) Short-term synaptic plasticity as a temporal filter. *Trends Neurosci* 24: 381–385. [23]

Fourcaud-Trocmé N, Hansel D, van Vreeswijk C, Brunel N (2003) How spike generation mechanisms determine the neuronal response to fluctuating inputs. *J Neurosci* 23: 11628–11640. [70, 78]

Franco L, Rolls ET, Aggelopoulos NC, Jerez JM (2007) Neuronal selectivity, population sparseness, and ergodicity in the inferior temporal visual cortex. *Biol Cybern* 96: 547–560. [8]

Fugère V, Ortega H, Krahe R (2011) Electrical signalling of dominance in a wild population of electric fish. *Biol Lett* 7: 197–200. [16, 48]

Gabbiani F, Metzner W, Wessel R, Koch C (1996) From stimulus encoding to feature extraction in weakly electric fish. *Nature* 384: 564–567. [58]

Georgopoulos AP, Schwartz AB, Kettner RE (1986) Neuronal population coding of movement direction. *Science* 233: 1416–1419. [7, 105]

Gerstner W (2000) Population dynamics of spiking neurons: fast transients, asynchronous states, and locking. *Neural Comput* 12: 43–89. [120]

Gifford GW, MacLean KA, Hauser MD, Cohen YE (2005) The neurophysiology of functionally meaningful categories: macaque ventrolateral prefrontal cortex plays a critical role in spontaneous categorization of species-specific vocalizations. *J Cogn Neurosci* 17: 1471–1482. [117]

Goldman MS, Golowasch J, Marder E, Abbott LF (2001) Global structure, robustness, and modulation of neuronal models. *J Neurosci* 21: 5229–5238. [102]

Gollisch T, Meister M (2008) Rapid neural coding in the retina with relative spike latencies. *Science* 319: 1108–1111. [6, 8]

Golomb, Rinzel (1993) Dynamics of globally coupled inhibitory neurons with heterogeneity. *Phys Rev E Stat Phys Plasmas Fluids Relat Interdiscip Topics* 48: 4810–4814. [103]

Golowasch J, Goldman MS, Abbott LF, Marder E (2002) Failure of averaging in the construction of a conductance-based neuron model. *J Neurophysiol* 87: 1129–1131. [-]

Gussin D, Benda J, Maler L (2007) Limits of linear rate coding of dynamic stimuli by electroreceptor afferents. *J Neurophysiol* 97: 2917–2929. [10, 19, 50, 54, 58, 60, 78, 82, 89, 102]

Hagedorn M, Heiligenberg W (1985) Court and spark: electric signals in the courtship and mating of gymnotoid fish. *Animal Behavior* 33: 254–265. [14, 15, 16]

Hagiwara S, Morita H (1963) Coding mechanisms of electro-receptor fibers in some electric fish. *J Neurophysiol* 26: 551–567. [49]

Harvey-Girard E, Dunn RJ, Maler L (2007) Regulated expression of N-methyl-D-aspartate receptors and associated proteins in teleost electrosensory system and telencephalon. *J Comp Neurol* 505: 644–668. [18]

Heiligenberg W, Dye J (1982) Labelling of electroreceptive afferents in a gymnotoid fish by intracellular injection of HRP: The mystery of multiple maps. *Journal of Comparative Physiology A: Neuroethology, Sensory, Neural, and Behavioral Physiology* 148: 287–296. [18, 47, 69]

Herz AVM, Gollisch T, Machens CK, Jaeger D (2006) Modeling single-neuron dynamics and computations: a balance of detail and abstraction. *Science* 314: 80–85. [120, 121]

Hill PSM (2009) How do animals use substrate-borne vibrations as an information source? *Naturwissenschaften* 96: 1355–1371. [12]

Holt LL, Lotto AJ (2010) Speech perception as categorization. *Atten Percept Psychophys* 72: 1218–1227. [117]

Hopkins CD (1974) Electric communication: Functions in the social behavior of *Eigenmannia virescens*. *Behaviour* 50: 270–305. [22]

Hospedales TM, van Rossum MCW, Graham BP, Dutia MB (2008) Implications of noise and neural heterogeneity for vestibulo-ocular reflex fidelity. *Neural Comput* 20: 756–778. [10, 81, 103, 104]

Hubel DH, Wiesel TN (1959) Receptive fields of single neurones in the cat's striate cortex. *J Physiol* 148: 574–591. [6]

Humayun M, de Juan E, , Weiland J, Dagnelie G, Katona S, Greenberg R, Suzuki S (1999) Pattern electrical stimulation of the human retina. *Vision Research* 39: 2569–2576. [121]

Hupé GJ, Lewis JE (2008) Electrocommunication signals in free swimming brown ghost knifefish, *Apteronotus leptorhynchus*. *J Exp Biol* 211: 1657–1667. [14, 17, 48]

Hupé GJ, Lewis JE, Benda J (2008) The effect of difference frequency on electrocommunication: chirp production and encoding in a species of weakly electric fish, *Apteronotus leptorhynchus*. *J Physiol Paris* 102: 164–172. [18, 23, 27, 48, 49, 104, 113, 118, 126]

Izhikevich EM (2004) Which model to use for cortical spiking neurons? *IEEE Trans Neural Netw* 15: 1063–1070. [76]

Jaeger D, Schutter ED, Bower JM (1997) The role of synaptic and voltage-gated currents in the control of Purkinje cell spiking: a modeling study. *J Neurosci* 17: 91–106. [77]

Johansson BG, Jones TM (2007) The role of chemical communication in mate choice. *Biol Rev Camb Philos Soc* 82: 265–289. [12]

Jolivet R, Gerstner W (2004) Predicting spike times of a detailed conductance-based neuron model driven by stochastic spike arrival. *J Physiol Paris* 98: 442–451. [121]

Jolivet R, Kobayashi R, Rauch A, Naud R, Shinomoto S, Gerstner W (2008) A benchmark test for a quantitative assessment of simple neuron models. *J Neurosci Methods* 169: 417–424. [121]

Jolivet R, Rauch A, Lüscher HR, Gerstner W (2006) Predicting spike timing of neocortical pyramidal neurons by simple threshold models. *J Comput Neurosci* 21: 35–49. [121]

Jones PW, Gabbiani F (2010) Synchronized neural input shapes stimulus selectivity in a collision-detecting neuron. *Curr Biol* 20: 2052–2057. [8]

Kara P, Reinagel P, Reid RC (2000) Low response variability in simultaneously recorded retinal, thalamic, and cortical neurons. *Neuron* 27: 635–646. [48]

Kashimori Y, Goto M, Kambara T (1996) Model of P- and T-electroreceptors of weakly electric fish. *Biophys J* 70: 2513–2526. [52, 76]

Kawasaki M, Rose G, Heiligenberg W (1988) Temporal hyperacuity in single neurons of electric fish. *Nature* 336: 173–176. [49, 125]

Keat J, Reinagel P, Reid RC, Meister M (2001) Predicting every spike: a model for the responses of visual neurons. *Neuron* 30: 803–817. [121]

Kelley DB, Bass AH (2010) Neurobiology of vocal communication: mechanisms for sensorimotor integration and vocal patterning. *Curr Opin Neurobiol* 20: 748–753. [12]

Kelly M, Babineau D, Longtin A, Lewis JE (2008) Electric field interactions in pairs of electric fish: modeling and mimicking naturalistic inputs. *Biol Cybern* 98: 479–490. [13, 16, 19, 79]

Kilgard MP, Merzenich MM (1999) Distributed representation of spectral and temporal information in rat primary auditory cortex. *Hear Res* 134: 16–28. [7, 105]

Knight BW (1972)a Dynamics of encoding in a population of neurons. *J. Gen. Physiol* 59: 734–766. [8, 50]

Knight BW (1972)b The relationship between the firing rate of a single neuron and the level of activity in a population of neurons. experimental evidence for resonant enhancement in the population response. *J Gen Physiol* 59: 767–778. [70, 78]

Koch C, Segev I (2000) The role of single neurons in information processing. *Nat Neurosci* 3 Suppl: 1171–1177. [120]

Kohn A, Smith MA (2005) Stimulus dependence of neuronal correlation in primary visual cortex of the macaque. *J Neurosci* 25: 3661–3673. [8, 104]

Kolodziejski JA, Sanford SE, Smith GT (2007) Stimulus frequency differentially affects chirping in two species of weakly electric fish: implications for the evolution of signal structure and function. *J Exp Biol* 210: 2501–2509. [14, 32, 108]

Krahe R, Bastian J, Chacron MJ (2008) Temporal processing across multiple topographic maps in the electrosensory system. *J Neurophysiol* 100: 852–867. [22, 23, 47, 81, 119]

Krahe R, Gabbiani F (2004) Burst firing in sensory systems. *Nat Rev Neurosci* 5: 13–23. [23]

Kreiman G, Krahe R, Metzner W, Koch C, Gabbiani F (2000) Robustness and variability of neuronal coding by amplitude-sensitive afferents in the weakly electric fish eigenmannia. *J Neurophysiol* 84: 189–204. [52]

Kumar A, Rotter S, Aertsen A (2010) Spiking activity propagation in neuronal networks: reconciling different perspectives on neural coding. *Nat Rev Neurosci* 11: 615–627. [10]

Lapicque L (1907) Recherches quantitatives sur l'excitation électrique des nerfs traitée comme une polarization. *J. Physiol. Pathol. Gen.* 9: 620–635. [60, 120]

Larimer JL, MacDonald JA (1968) Sensory feedback from electroreceptors to electromotor pacemaker centers in gymnotids. *Am J Physiol* 214: 1253–1261. [14]

Laughlin SB (2001) Energy as a constraint on the coding and processing of sensory information. *Curr Opin Neurobiol* 11: 475–480. [11]

Laurent G (1996) Dynamical representation of odors by oscillating and evolving neural assemblies. *Trends Neurosci* 19: 489–496. [8]

Lewis JE, Lindner B, Laliberté B, Groothuis S (2007) Control of neuronal firing by dynamic parallel fiber feedback: implications for electrosensory reafference suppression. *J Exp Biol* 210: 4437–4447. [19]

Lindner B, Longtin A, Bulsara A (2003) Analytic expressions for rate and CV of a type I neuron driven by white gaussian noise. *Neural Comput* 15: 1760–1787. [78]

Liu YH, Wang XJ (2001) Spike-frequency adaptation of a generalized leaky integrate-and-fire model neuron. *Journal of Computational Neuroscience* 10: 25–45. [68, 69]

Longtin, Bulsara, Moss (1991) Time-interval sequences in bistable systems and the noise-induced transmission of information by sensory neurons. *Phys Rev Lett* 67: 656–659. [7]

Machens CK, Stemmler MB, Prinz P, Krahe R, Ronacher B, Herz AV (2001) Representation of acoustic communication signals by insect auditory receptor neurons. *J Neurosci* 21: 3215–3227. [11]

MacIver MA, Sharabash NM, Nelson ME (2001) Prey-capture behavior in gymnotid electric fish: motion analysis and effects of water conductivity. *J Exp Biol* 204: 543–557. [13]

Mainen ZF, Sejnowski TJ (1995) Reliability of spike timing in neocortical neurons. *Science* 268: 1503–1506. [6, 11]

Maler L (1979) The posterior lateral line lobe of certain gymnotoid fish: quantitative light microscopy. *J Comp Neurol* 183: 323–363. [18]

Maler L (2009) Receptive field organization across multiple electrosensory maps. I. columnar organization and estimation of receptive field size. *J Comp Neurol* 516: 376–393. [22, 47, 81, 126]

Maler L, Sas E, Carr CE, Matsubara J (1982) Efferent projections of the posterior lateral line lobe in gymnotiform fish. *J Comp Neurol* 211: 154–164. [19]

Maler L, Sas E, Johnston S, Ellis W (1991) An atlas of the brain of the electric fish *Apteronotus leptorhynchus*. *J Chem Neuroanat* 4: 1–38. [19]

Marder E, Goaillard JM (2006) Variability, compensation and homeostasis in neuron and network function. *Nat Rev Neurosci* 7: 563–574. [105]

Marder E, Taylor AL (2011) Multiple models to capture the variability in biological neurons and networks. *Nat Neurosci* 14: 133–138. [81]

Marsat G, Maler L (2010) Neural heterogeneity and efficient population codes for communication signals. *J Neurophysiol* 104: 2543–2555. [8, 21, 43, 48, 118, 126]

Marsat G, Maler L (2012) Preparing for the unpredictable: Adaptive feedback enhances the response to unexpected communication signals. *J Neurophysiol* 107: 1241–1246. [8, 13, 22, 23, 47]

Marsat G, Proville R, Maler L (2009) Transient signals trigger synchronous bursts in an identified population of neurons. *J Neurophysiol* 102: 714–723. [8, 22, 23, 47, 48, 119]

May B, Moody DB, Stebbins WC (1989) Categorical perception of conspecific communication sounds by japanese macaques, *Macaca fuscata*. *J Acoust Soc Am* 85: 837–847. [117]

McGillivray P, Vonderschen K, Fortune ES, Chacron MJ (2012) Parallel coding of first- and second-order stimulus attributes by midbrain electrosensory neurons. *J Neurosci* 32: 5510–5524. [77]

McKibben JR, Bass AH (1998) Behavioral assessment of acoustic parameters relevant to signal recognition and preference in a vocal fish. *J Acoust Soc Am* 104: 3520–3533. [27]

Mehaffey WH, Maler L, Turner RW (2008) Intrinsic frequency tuning in ELL pyramidal cells varies across electrosensory maps. *J Neurophysiol* 99: 2641–2655. [22]

Mejias JF, Longtin A (2012) Optimal heterogeneity for coding in spiking neural networks. *Phys Rev Lett* 108: 228102. [103]

Metzner W, Heiligenberg W (1991) The coding of signals in the electric communication of the gymnotiform fish *Eigenmannia*: from electroreceptors to neurons in the torus semicircularis of the midbrain. *J Comp Physiol A* 169: 135–150. [19, 22]

Metzner W, Juranek J (1997) A sensory brain map for each behavior? *Proc Natl Acad Sci U S A* 94: 14798–14803. [22, 47, 119]

Meyer JH, Leong M, Keller CH (1987) Hormone-induced and maturational changes in electric organ discharges and electroreceptor tuning in the weakly electric fish *Apteronotus*. *J Comp Physiol A* 160: 385–394. [14, 48]

Middleton JW, Longtin A, Benda J, Maler L (2009) Postsynaptic receptive field size and spike threshold determine encoding of high-frequency information via sensitivity to synchronous presynaptic activity. *J Neurophysiol* 101: 1160–1170. [47, 79, 119]

Miura K, Mainen ZF, Uchida N (2012) Odor representations in olfactory cortex: distributed rate coding and decorrelated population activity. *Neuron* 74: 1087–1098. [8]

Moortgat KT, Keller CH, Bullock TH, Sejnowski TJ (1998) Submicrosecond pacemaker precision is behaviorally modulated: the gymnotiform electromotor pathway. *Proc Natl Acad Sci U S A* 95: 4684–4689. [14]

Narayan SS, Temchin AN, Recio A, Ruggero MA (1998) Frequency tuning of basilar membrane and auditory nerve fibers in the same cochleae. *Science* 282: 1882–1884. [49, 50]

Naruse M, Kawasaki M (1998) Possible involvement of the ampullary electroreceptor system in detection of frequency-modulated electrocommunication signals in *Eigenmannia*. *J Comp Physiol A* 183: 543–552. [22]

Nassi JJ, Callaway EM (2009) Parallel processing strategies of the primate visual system. *Nat Rev Neurosci* 10: 360–372. [10, 118]

Neklen I, Rotman Y, Yosef OB (1999) Responses of auditory-cortex neurons to structural features of natural sounds. *Nature* 397: 154–157. [49]

Nelder JA, Mead R (1965) A simplex method for function minimization. *Computer Journal* 7: 308–313. [54]

Nelson DA, Marler P (1989) Categorical perception of a natural stimulus continuum: birdsong. *Science* 244: 976–978. [117]

Nelson ME, Xu Z, Payne JR (1997) Characterization and modeling of P-type electrosensory afferent responses to amplitude modulations in a wave-type electric fish. *J Comp Physiol A* 181: 532–544. [18, 21, 49, 52, 60, 69, 77, 119]

Niven JE, Laughlin SB (2008) Energy limitation as a selective pressure on the evolution of sensory systems. *J Exp Biol* 211: 1792–1804. [11]

Olshausen BA, Field DJ (2004) Sparse coding of sensory inputs. *Curr Opin Neurobiol* 14: 481–487. [8]

Olypher AV, Calabrese RL (2007) Using constraints on neuronal activity to reveal compensatory changes in neuronal parameters. *J Neurophysiol* 98: 3749–3758. [102]

Osorio D, Vorobyev M (2008) A review of the evolution of animal colour vision and visual communication signals. *Vision Res* 48: 2042–2051. [12]

Padmanabhan K, Urban NN (2010) Intrinsic biophysical diversity decorrelates neuronal firing while increasing information content. *Nat Neurosci* 13: 1276–1282. [10, 81, 104]

Panzeri S, Brunel N, Logothetis NK, Kayser C (2010) Sensory neural codes using multiplexed temporal scales. *Trends Neurosci* 33: 111–120. [5]

Pennartz CMA, van Wingerden M, Vinck M (2011) Population coding and neural rhythmicity in the orbitofrontal cortex. *Ann N Y Acad Sci* 1239: 149–161. [8]

Perkel D, Bullock T (1968) Neural coding: a report based on an NRP work session. *Neurosci. Res. Program Bull.* 6: 219–349. [10]

Pillow JW, Paninski L, Uzzell VJ, Simoncelli EP, Chichilnisky EJ (2005) Prediction and decoding of retinal ganglion cell responses with a probabilistic spiking model. *J Neurosci* 25: 11003–11013. [121]

Pouget A, Dayan P, Zemel R (2000) Information processing with population codes. *Nat Rev Neurosci* 1: 125–132. [7, 8, 81]

Prather JF, Nowicki S, Anderson RC, Peters S, Mooney R (2009) Neural correlates of categorical perception in learned vocal communication. *Nat Neurosci* 12: 221–228. [117]

Pressley J, Troyer TW (2011) The dynamics of integrate-and-fire: Mean versus variance modulations and dependence on baseline parameters. *Neural Computation* 23: 1234–1247. [50]

Prinz AA, Bucher D, Marder E (2004) Similar network activity from disparate circuit parameters. *Nat Neurosci* 7: 1345–1352. [102, 103]

Ratnam R, Nelson ME (2000) Nonrenewal statistics of electrosensory afferent spike trains: implications for the detection of weak sensory signals. *J Neurosci* 20: 6672–6683. [51, 58]

Rauch A, Camera GL, Luscher HR, Senn W, Fusi S (2003) Neocortical pyramidal cells respond as integrate-and-fire neurons to *in vivo*-like input currents. *J Neurophysiol* 90: 1598–1612. [121]

Requarth T, Sawtell NB (2011) Neural mechanisms for filtering self-generated sensory signals in cerebellum-like circuits. *Curr Opin Neurobiol* 21: 602–608. [19]

Ringach DL, Shapley RM, Hawken MJ (2002) Orientation selectivity in macaque V1: diversity and laminar dependence. *J Neurosci* 22: 5639–5651. [10, 81]

Roddey JC, Girish B, Miller JP (2000) Assessing the performance of neural encoding models in the presence of noise. *J Comput Neurosci* 8: 95–112. [57]

Rolls ET, Treves A (2011) The neuronal encoding of information in the brain. *Prog Neurobiol* 95: 448–490. [5, 6]

Rose GJ (2004) Insights into neural mechanisms and evolution of behaviour from electric fish. *Nat Rev Neurosci* 5: 943–951. [19]

Roth A, Häusser M (2001) Compartmental models of rat cerebellar Purkinje cells based on simultaneous somatic and dendritic patch-clamp recordings. *J Physiol* 535: 445–472. [77]

Salgado JAG, Zupanc GKH (2011) Echo response to chirping in the weakly electric brown ghost knifefish (*Apteronotus leptorhynchus*): role of frequency and amplitude modulations. *Can. J. Zool.* 89: 498–508. [17, 27, 118, 125]

Saul AB, Humphrey AL (1990) Spatial and temporal response properties of lagged and nonlagged cells in cat lateral geniculate nucleus. *J. Neurophysiol.* 64: 206–224. [49]

Savard M, Krahe R, Chacron MJ (2011) Neural heterogeneities influence envelope and temporal coding at the sensory periphery. *Neuroscience* 172: 270–284. [21, 77, 78, 103, 104]

Schaette R, Gollisch T, Herz AVM (2005) Spike-train variability of auditory neurons in vivo: dynamic responses follow predictions from constant stimuli. *J Neurophysiol* 93: 3270–3281. [121]

Scheich H, Bullock TH, Hamstra RH (1973) Coding properties of two classes of afferent nerve fibers: high-frequency electroreceptors in the electric fish, *Eigenmannia*. *J Neurophysiol* 36: 39–60. [18, 51, 58]

Schmidt AKD, Riede K, Römer H (2011) High background noise shapes selective auditory filters in a tropical cricket. *J Exp Biol* 214: 1754–1762. [12]

Schwalger T, Lindner B (2013) Patterns of interval correlations in neural oscillators with adaptation. in preparation. [68, 69]

Shamir M, Sompolinsky H (2006) Implications of neuronal diversity on population coding. *Neural Comput* 18: 1951–1986. [10, 81, 104]

Shumway CA, Maler L (1989) GABAergic inhibition shapes temporal and spatial response properties of pyramidal cells in the electrosensory lateral line lobe of gymnotiform fish. *J Comp Physiol A* 164: 391–407. [18, 118]

Silberberg G, Bethge M, Markram H, Pawelzik K, Tsodyks M (2004) Dynamics of population rate codes in ensembles of neocortical neurons. *J Neurophysiol* 91: 704–709. [49]

Simes RJ (1986) An improved Bonferroni procedure for multiple tests of significance. *Biometrika* 73: 751–754. [39]

Singer W, Gray CM (1995) Visual feature integration and the temporal correlation hypothesis. *Annu Rev Neurosci* 18: 555–586. [6]

Smith GT (2006) Pharmacological characterization of ionic currents that regulate high-frequency spontaneous activity of electromotor neurons in the weakly electric fish, *Apteronotus leptorhynchus*. *J Neurobiol* 66: 1–18. [19]

Smith GT, Zakon HH (2000) Pharmacological characterization of ionic currents that regulate the pacemaker rhythm in a weakly electric fish. *J Neurobiol* 42: 270–286. [19]

Softky WR, Koch C (1993) The highly irregular firing of cortical cells is inconsistent with temporal integration of random EPSPs. *J Neurosci* 13: 334–350. [79]

Stacey N, Chojnacki A, Narayanan A, Cole T, Murphy C (2003) Hormonally derived sex pheromones in fish: exogenous cues and signals from gonad to brain. *Can J Physiol Pharmacol* 81: 329–341. [12]

Stamper S, Carrera-G E, Tan E, Fugère V, Krahe R, Fortune E (2010) Species differences in group size and electrosensory interference in weakly electric fishes: implications for electrosensory processing. *Behav Brain Res* 207: 368–376. [47, 48, 78]

Stocks (2000) Suprathreshold stochastic resonance in multilevel threshold systems. *Phys Rev Lett* 84: 2310–2313. [8, 10]

Straka H, Vibert N, Vidal PP, Moore LE, Dutia MB (2005) Intrinsic membrane properties of vertebrate vestibular neurons: function, development and plasticity. *Prog Neurobiol* 76: 349–392. [49]

Tallarovic SK, Zakon HH (2002) Electrocommunication signals in female brown ghost electric knifefish, *Apteronotus leptorhynchus*. *J Comp Physiol A Neuroethol Sens Neural Behav Physiol* 188: 649–657. [14]

Taylor AL, Goaillard JM, Marder E (2009) How multiple conductances determine electrophysiological properties in a multicompartment model. *J Neurosci* 29: 5573–5586. [103]

Tchumatchenko T, Malyshev A, Wolf F, Volgushev M (2011) Ultrafast population encoding by cortical neurons. *J Neurosci* 31: 12171–12179. [49]

Theunissen F, Miller JP (1995) Temporal encoding in nervous systems: a rigorous definition. *J Comput Neurosci* 2: 149–162. [6]

Theunissen FE, Sen K, Doupe AJ (2000) Spectral-temporal receptive fields of nonlinear auditory neurons obtained using natural sounds. *The Journal of Neuroscience* 20(6): 2315–2331. [49]

Thorpe S, Fize D, Marlot C (1996) Speed of processing in the human visual system. *Nature* 381: 520–522. [11]

Todd BS, Andrews DC (1999) The identification of peaks in physiological signals. *Comput Biomed Res* 32: 322–335. [28]

Tolhurst DJ, Movshon JA, Dean AF (1983) The statistical reliability of signals in single neurons in cat and monkey visual cortex. *Vision Res* 23: 775–785. [6]

Tomko GJ, Crapper DR (1974) Neuronal variability: non-stationary responses to identical visual stimuli. *Brain Res* 79: 405–418. [6]

Tovée MJ, Rolls ET, Treves A, Bellis RP (1993) Information encoding and the responses of single neurons in the primate temporal visual cortex. *J Neurophysiol* 70: 640–654. [6]

Triefenbach F, Zakon H (2008) Changes in signalling during agonistic interactions between male weakly electric knifefish, *Apteronotus leptorhynchus*. *Animal Behavior* 75: 1263–1272. [14, 16, 48]

Turner RW, Lemon N, Doiron B, Rashid AJ, Morales E, Longtin A, Maler L, Dunn RJ (2002) Oscillatory burst discharge generated through conditional backpropagation of dendritic spikes. *J Physiol Paris* 96: 517–530. [22]

Uchida N, Mainen ZF (2003) Speed and accuracy of olfactory discrimination in the rat. *Nat Neurosci* 6: 1224–1229. [11]

van Hateren JH, Kern R, Schwerdtfeger G, Egelhaaf M (2005) Function and coding in the blowfly H1 neuron during naturalistic optic flow. *J Neurosci* 25: 4343–4352. [49]

van Rossum MC (2001) A novel spike distance. *Neural Comput* 13: 751–763. [31, 43]

van Rossum MCW, O'Brien BJ, Smith RG (2003) Effects of noise on the spike timing precision of retinal ganglion cells. *J Neurophysiol* 89: 2406–2419. [7]

van Rossum MCW, Turrigiano GG, Nelson SB (2002) Fast propagation of firing rates through layered networks of noisy neurons. *J Neurosci* 22: 1956–1966. [10]

Vernaleo BA, Dooling RJ (2011) Relative salience of envelope and fine structure cues in zebra finch song. *J Acoust Soc Am* 129: 3373–3383. [27]

Vinje WE, Gallant JL (2000) Sparse coding and decorrelation in primary visual cortex during natural vision. *Science* 287: 1273–1276. [11, 49]

Vogel A, Hennig RM, Ronacher B (2005) Increase of neuronal response variability at higher processing levels as revealed by simultaneous recordings. *J. Neurophysiol.* 93: 3548–3559. [48]

Vonderschen K, Chacron MJ (2011) Sparse and dense coding of natural stimuli by distinct midbrain neuron subpopulations in weakly electric fish. *J Neurophysiol* 106: 3102–3118. [11, 23, 31, 39, 43, 48, 87]

Walz H, Hupé GJ, Benda J, Lewis JE (2012) The neuroethology of electrocommunication: How signal background influences sensory encoding and behaviour in *Apteronotus leptorhynchus*. *J Physiol Paris* 107: 13–25. [17, 27, 43, 104, 118]

Wang X, Merzenich MM, Beitel R, Schreiner CE (1995) Representation of a species-specific vocalization in the primary auditory cortex of the common marmoset: temporal and spectral characteristics. *J Neurophysiol* 74: 2685–2706. [50]

Waser P, Brown C (1986) Habitat acoustics and primate communication. *American Journal of Primatology* 10: 135–154. [12]

Werner G, Mountcastle VB (1963) The variability of central neural activity in a sensory system, and its implications for the central reflection of sensory events. *J Neurophysiol* 26: 958–977. [6]

Wessel R, Koch C, Gabbiani F (1996) Coding of time-varying electric field amplitude modulations in a wave-type electric fish. *J Neurophysiol* 75: 2280–2293. [21, 51, 58, 69, 82, 104]

Wilson MA, McNaughton BL (1993) Dynamics of the hippocampal ensemble code for space. *Science* 261: 1055–1058. [7, 105]

Xu Z, Payne JR, Nelson ME (1996) Logarithmic time course of sensory adaptation in electrosensory afferent nerve fibers in a weakly electric fish. *J Neurophysiol* 76: 2020–2032. [21, 58]

Yang S, Yang S, Cox CL, Llano DA, Feng AS (2012) Cell's intrinsic biophysical properties play a role in the systematic decrease in time-locking ability of central auditory neurons. *Neuroscience* 208: 49–57. [11]

Yu N, Hupé G, Garfinkle C, Lewis JE, Longtin A (2012) Coding conspecific identity and motion in the electric sense. *PLoS Comput Biol* 8: e1002564. [12, 78, 79]

Zakon H, Oestreich J, Tallarovic S, Triefenbach F (2002) Eod modulations of brown ghost electric fish: JARs, chirps, rises, and dips. *J Physiol Paris* 96: 451–458. [14, 48, 78]

Zakon HH (1986) *Electroreception Wiley, New York* 0: 103–105. [18, 58]

Zakon HH, Dunlap KD (1999) Sex steroids and communication signals in electric fish: a tale of two species. *Brain Behav Evol* 54: 61–69. [48]

Zeki S (2001) Localization and globalization in conscious vision. *Annu Rev Neurosci* 24: 57–86. [117]

Zhang LI, Tan AYY, Schreiner CE, Merzenich MM (2003) Topography and synaptic shaping of direction selectivity in primary auditory cortex. *Nature* 424: 201–205. [50]

Zohary E, Shadlen MN, Newsome WT (1994) Correlated neuronal discharge rate and its implications for psychophysical performance. *Nature* 370: 140–143. [8, 104]

Zupanc G, Maler L (1993) Evoked chirping in the weakly electric fish, *Apteronotus leptorhynchus*: a biophysical and behavioral analysis. *Can. J. Zool.* 71: 2301–2310. [12, 14, 16, 17, 27, 43, 104]

Zupanc GKH (2002) From oscillators to modulators: behavioral and neural control of modulations of the electric organ discharge in the gymnotiform fish, *Apteronotus leptorhynchus*. *J Physiol Paris* 96: 459–472. [14, 47]

Zupanc GKH, Sîrbulescu RF, Nichols A, Ilies I (2006) Electric interactions through chirping behavior in the weakly electric fish, *Apteronotus leptorhynchus*. *J Comp Physiol A Neuroethol Sens Neural Behav Physiol* 192: 159–173. [14, 17, 118]

Zupanc M, Engler G, Midson A, Oxberry H, Hurst L, Symon M, Zupanc G (2001) Lightdark changes in spontaneous modulations of the electric organ discharge in the weakly electric fish, *Apteronotus leptorhynchus*. *Animal Behavior* 62: 1119–1128. [13]

Appendix

List of Abbreviations

AM amplitude modulation

CMS centromedial segment

CLS centrolateral segment

CSI chirp selectivity index

CV coefficient of variation

DAP depolarising after potential

EGp eminentia granularis pars posterior

ELL electrosensory lateral line

EOD electric organ discharge

EODf EOD frequency

ISI interspike interval

JAR jamming avoidance response

LIF leaky integrate-and-fire

LIFAC leaky integrate-and-fire with adaptation current

LIFDC leaky integrate-and-fire with dynamic threshold

LS lateral segment

MS medial segment

nP nucleus praeeminentialis

PSTH peri-stimulus time histogram

RAM random amplitude modulation

SAM sinusoidal amplitude modulation

SC serial correlation

TS torus semicircularis

VS vector strength

Journal of Physiology - Paris 107 (2013) 13–25

Contents lists available at SciVerse ScienceDirect

Journal of Physiology - Paris

journal homepage: www.elsevier.com/locate/jphysparis

Review Article

The neuroethology of electrocommunication: How signal background influences sensory encoding and behaviour in Apteronotus leptorhynchus

Henriette Walz [a], Ginette J. Hupé [b], Jan Benda [c,*], John E. Lewis [b]

[a] Bernstein Center for Computational Neuroscience Munich, 82152 Martinsried, Germany
[b] Department of Biology and Centre for Neural Dynamics, University of Ottawa, Ottawa, ON, Canada K1N 6N5
[c] Institute of Neurobiology, University of Tübingen, 72076 Tübingen, Germany

ARTICLE INFO

Article history:
Available online 5 September 2012

Keywords:
Sensory coding
Natural behaviour
Animal communication
Weakly electric fish

ABSTRACT

Weakly-electric fish are a well-established model system for neuroethological studies on communication and aggression. Sensory encoding of their electric communication signals, as well as behavioural responses to these signals, have been investigated in great detail under laboratory conditions. In the wave-type brown ghost knifefish, *Apteronotus leptorhynchus*, transient increases in the frequency of the generated electric field, called chirps, are particularly well-studied, since they can be readily evoked by stimulating a fish with artificial signals mimicking conspecifics. When two fish interact, both their quasi-sinusoidal electric fields (called electric organ discharge, EOD) superimpose, resulting in a beat, an amplitude modulation at the frequency difference between the two EODs. Although chirps themselves are highly stereotyped signals, the shape of the amplitude modulation resulting from a chirp superimposed on a beat background depends on a number of parameters, such as the beat frequency, modulation depth, and beat phase at which the chirp is emitted. Here we review the influence of these beat parameters on chirp encoding in the three primary stages of the electrosensory pathway: electroreceptor afferents, the hindbrain electrosensory lateral line lobe, and midbrain torus semicircularis. We then examine the role of these parameters, which represent specific features of various social contexts, on the behavioural responses of *A. leptorhynchus*. Some aspects of the behaviour may be explained by the coding properties of early sensory neurons to chirp stimuli. However, the complexity and diversity of behavioural responses to chirps in the context of different background parameters cannot be explained solely on the basis of the sensory responses and thus suggest that critical roles are played by higher processing stages.

Contents

* Corresponding author.
E-mail address: jan.benda@uni-tuebingen.de (J. Benda).

0928-4257/$ - see front matter © 2012 Elsevier Ltd. All rights reserved.
http://dx.doi.org/10.1016/j.jphysparis.2012.07.001

1. Introduction

During social encounters, many animals use communication signals to transmit a variety of information, such as individual identity and motivational state, that is used to dynamically modulate behavioural strategies. Across taxa, signals involving mechanical (including acoustic and vibrational stimuli; Hill, 2009; Kelley and Bass, 2010), visual (Osorio and Vorobyev, 2008), chemical (Stacey et al., 2003; Johansson and Jones, 2007) and electric modalities as well as a mixture of them (Bro-Joergensen, 2010) have been characterized. Responding to these signals appropriately can be crucial for reproductive success, as well as the survival of an individual (Kelley and Bass, 2010). Accordingly, understanding why and how signals are produced has been a central goal in animal ethology.

The accurate detection of communication signals depends crucially on signal encoding by the nervous system which can be limited by internal and external noise (Waser and Brown, 1986; Schmidt et al., 2011). In the auditory and electrosensory systems, communication signals can be produced in the presence of an ongoing background signal that is a consequence of the interaction itself (Zupanc and Maler, 1993; Kelley and Bass, 2010). Different aspects of this background signal, including its frequency and contrast also provide behaviourally relevant information about social context, i.e. the identity and proximity of interacting individuals (Engler and Zupanc, 2001; Bastian et al., 2001; Yu et al., 2012).

To explore both the meaning of communication signals, and the mechanisms by which they are encoded, it is necessary to consider an integrated description of how sensory stimuli, neural responses, and behaviour change during the social interactions. The study of communication also offers a framework for studying the encoding of sensory stimuli, in that encoding principles and stimulus sensitivities can be inferred directly from behavioural experiments. Behavioural adjustments produced in response to conspecific or simulated communication signals provide evidence that the receiving individual has detected the sensory stimuli. A combined analysis of neuronal encoding and behaviour is therefore profitable for both neurophysiology and ethology.

In this review, our goal is to exemplify this neuroethological approach in the context of electrocommunication among the Gymnotiform weakly electric fish *Apteronotus leptorhynchus*. Environmental conditions involving low-light and low electrosensory signal-to-noise ratio set a premium on efficient detection and processing of electrocommunication signals. For decades, studies examining the neurophysiological systems of weakly electric fish have provided insights into how natural behaviours are generated using relatively simple sensorimotor circuits (for recent reviews see: Chacron et al., 2011; Fortune and Chacron, 2011; Marsat et al., 2012). Further, electrocommunication signals are relatively easy to describe, classify and simulate, facilitating quantification and experimental manipulation. Weakly electric fish are therefore an ideal system for examining how communication signals influence sensory scenes, drive sensory system responses, and consequently exert effects on conspecific behaviour.

Electric communication signals can be analyzed by measuring properties of the complex electric field that results from the interaction of nearby fish. In *A. leptorhynchus*, the dipole-like electric field (electric organ discharge, EOD) oscillates in a quasi-sinusoidal fashion at frequencies from 700 to 1100 Hz (Zakon et al., 2002) with males emitting at higher frequencies than females (Meyer et al., 1987). When two fish with different EOD frequencies interact, the combination of their signals results in an amplitude modulation called a "beat"; the beat signal oscillates at the frequency difference between the fish. Beat signals are a direct consequence of social interactions and thus set the background of the electrosensory scene. In addition, through the individual EOD frequencies, information about sex, relative size and individual identities are represented in the beat signal. Physical movements result in slow amplitude modulations of the beat that can encode, among other things, aggressive approach and retreat behaviours (Yu et al., 2012). Electrocommunication signals are produced in these social contexts and thus must be detected amidst the resulting complex background.

One type of electrocommunication signal, the chirp, involves brief amplitude and frequency modulations of the EOD and thus induces transient perturbations of the ongoing beat signal (Zupanc and Maler, 1993). Chirp production in this species is sexually dimorphic: males emit chirps at high rates during agonistic encounters, while females do not. Chirp production is strongly influenced by steroid hormones (e.g. testosterone; Dulka and Maler, 1994; Dunlap, 2002) and neuromodulators (e.g. serotonin; Maler and Ellis, 1987; Smith and Combs, 2008). Recent physiological results suggest that encoding is influenced by serotonin as well (Deemyad et al., 2011).

Behavioural studies have focused on chirping behaviours under diverse conditions: from stimulating a restrained fish with signals mimicking a conspecific (Zupanc and Maler, 1993; Bastian et al., 2001; Engler and Zupanc, 2001) to observing freely-moving fish during social interactions (Dunlap and Larkins-Ford, 2003; Hupé and Lewis, 2008; Triefenbach and Zakon, 2008). The neural encoding of chirps has also been studied at successive stages from electroreceptor afferents (Benda et al., 2005, 2006), through the hindbrain (Marsat et al., 2009; Marsat and Maler, 2010, 2011), and up to the midbrain (Vonderschen and Chacron, 2011), albeit in limited and simplified background contexts. Furthermore, the neural circuitry that controls the production of these signals is well known (Zupanc, 2002).

We here focus on how context-dependent properties of the beat signal influence the neural encoding of chirps and correlate with chirp production and aggression responses to chirp stimuli. We begin with a description of the different beat perturbations that are generated by the interplay of chirps with the different background

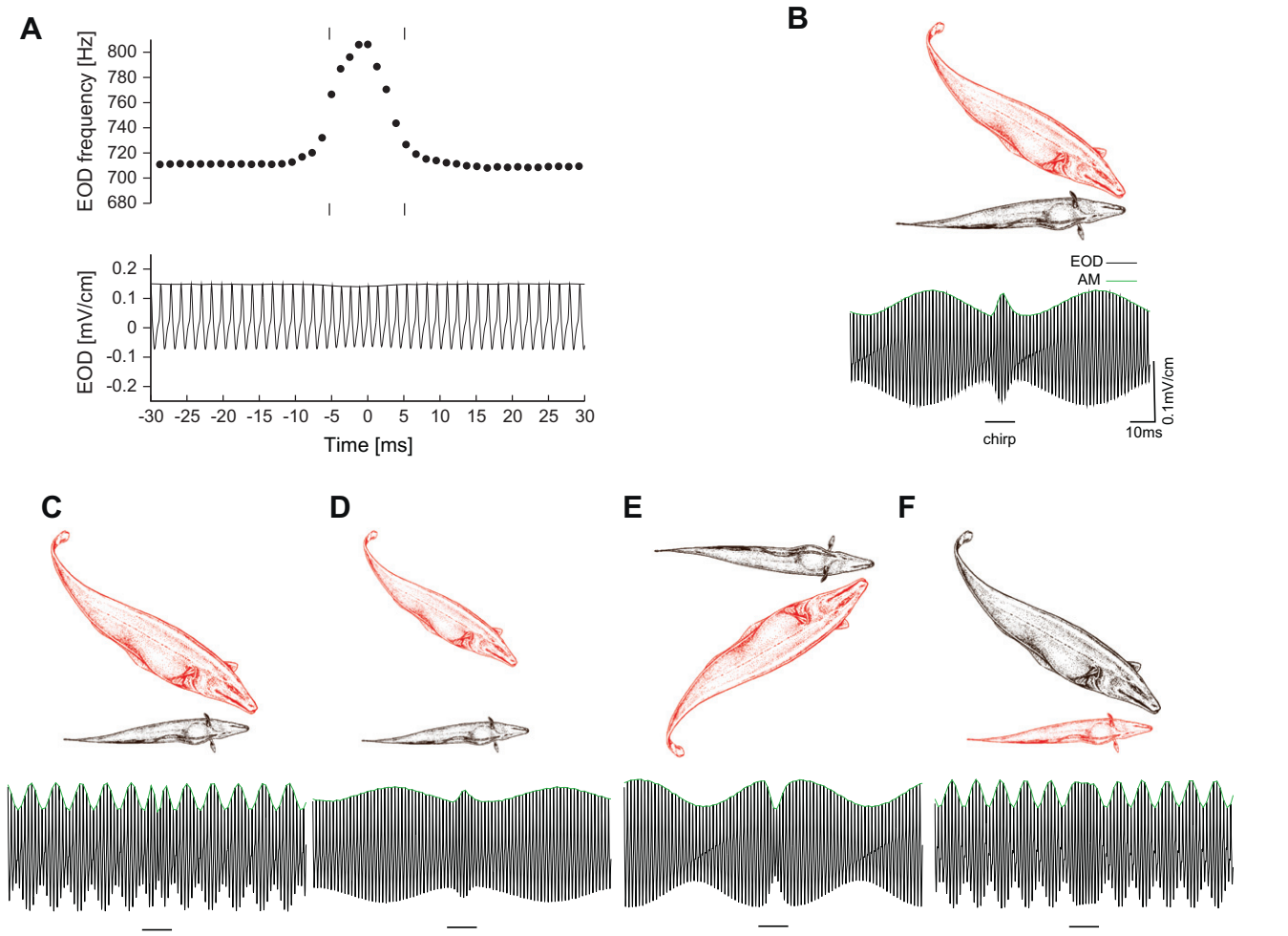

Fig. 1. Beat modulations induced by chirps during representative encounters between different pairs of fish. (A) shows one example of a small chirp as measured in a chirp chamber (for method descriptions see Fig. 3). When the instantaneous EOD frequency is plotted over time (upper panel), an increase from around 710 Hz to 810 Hz is seen. The amplitude is almost unchanged during the chirp, as seen when the EOD waveform is plotted over time (lower panel). (B–F) In each scenario, one fish emits the chirp shown in Fig. 1A, but under different simulated background conditions. The sketches of the fish demonstrate the encounter, with the chirping fish shown in red and the size of each fish reflecting its EODf (a higher EODf is indicated by a bigger size). (B) shows the encounter with a beat frequency of 20 Hz and a contrast of about 40%; (C) with a beat frequency of 100 Hz and 40% contrast; (D) shows the same encounter as in B but with a contrast of 20%; (E) shows an encounter similar to B but at a beat phase shifted 180°; (F) as in C, but the fish with the smaller EODf emits a chirp (the fish sketches are modified from Hagedorn and Heiligenberg 1985).

beat parameters encountered during interactions. Following this, we review how chirps are encoded at successive stages of the electrosensory pathway in different background conditions. We then integrate findings from behavioural studies to reveal how chirp production varies under different social contexts. In the final section, we incorporate principles from both neurophysiological and behavioural studies, to explore relationships between communication signal encoding and behaviour.

2. Signals and backgrounds in electrocommunication

Weakly electric fish use active electroreception to navigate and communicate under low light conditions (Zupanc et al., 2001). In active electroreception, animals produce an electric field using an electric organ (and this electric field is therefore called the electric organ discharge, EOD) and infer, from changes of the EOD, information about the location and identification of objects and conspecifics in their vicinity (e.g. MacIver et al., 2001; Kelly et al., 2008). However, perturbations result not only from objects and other fish, but also from self-motion and other factors. All of these together make up the electrosensory scene. The perturbed version of the fish's own field on its skin is called the electric image (Caputi and Budelli, 2006) which is sensed via specialized receptors distributed over the body surface (Carr et al., 1982). In the following, we will describe the modulations caused by the superposition of the electric fields of two interacting fish and by the production of specific communication signals.

2.1. Chirps involve transient increases in EOD frequency

Some weakly electric fish, the pulse-type fish, emit EODs in discrete pulses, while wave-type electric fish produce an EOD continuously, with a potential that oscillates with a specific frequency (the EOD frequency, EODf) that remains stable in time (exhibiting a coefficient of variation as low as 2×10^{-4}; Moortgat et al., 1998). During social encounters, wave-type fish often modulate the frequency as well as the amplitude of their field to communicate (Hagedorn and Heiligenberg, 1985). Several different types of electrocommunication signals have been identified, varying in the type and pattern of frequency and amplitude modulations of the EOD (Zakon et al., 2002; Zupanc, 2002). Communication signals in *A. leptorhynchus* have been classified into two classes: chirps are transient and stereotyped EODf excursions over tens of milliseconds (Zupanc et al., 2006), while rises are longer duration and more variable modulations of EODf, typically lasting for hundreds of milliseconds to seconds (Hagedorn and Heiligenberg, 1985; Tallarovic

and Zakon, 2002). Here, we focus on chirps because chirp encoding in the nervous system, in contrast to that of rises, has been the subject of a number of physiological studies and the behaviour is more stereotyped and is easier to quantify.

Several types of chirps have been distinguished (Zupanc et al., 2006, Types 1–6). Under most experimental conditions, the most commonly produced type is the "small chirp" (Type 2 chirp), with males producing these signals at high rates during agonistic interactions (e.g. Larimer and MacDonald, 1968; Hagedorn and Heiligenberg, 1985; Hupé et al., 2008; Triefenbach and Zakon, 2008). A small chirp is traditionally defined as a short duration (10–20 ms) increase in EODf of about 60–150 Hz (Fig. 1A; Zupanc and Maler, 1993; Engler and Zupanc, 2001). The only other chirp type observed across a number of experimental contexts and also studied electrophysiologically, is the big chirp (Type 1 chirp), so called because of the much larger increase in EODf (>350 Hz, Zupanc and Maler, 1993; Engler et al., 2000; Cuddy et al., 2012). The big chirp is accompanied by a marked decrease in EOD amplitude that is not seen in small chirps. Although the behavioural relevance of chirps remains unclear, researchers are beginning to gain insights about the relationship between chirping behaviours and aggression using a diversity of experimental approaches (see below).

2.2. The beat background and its social context

During the interaction of two wave-type fish, their electric fields superimpose and summate at every point in space. Measured across the skin of each fish, the combined signal consists of a carrier determined by its own EOD with a periodic amplitude modulation (AM) at a frequency equal to the difference of the two individual EODfs, the beat frequency (Fig. 1C and D). The beat frequency has been suggested to reflect different aspects of the social encounter (Bastian et al., 2001; Kolodziejski et al., 2007). Crucial to this idea is that EODf correlates with identifying characteristics of the emitting fish including sex and dominance status. Given that EODfs are sexually dimorphic in *A. leptorhynchus*, slower beat frequencies are more common in same-sex interactions. In addition, EODf has been found to be correlated with size and dominance (Hagedorn and Heiligenberg, 1985; Dunlap and Oliveri, 2002; Triefenbach and Zakon, 2008; Fugère et al., 2011), suggesting that the beat frequency also provides information about relative size and dominance status.

The depth of an AM signal (its peak to trough distance) is referred to as its contrast. The contrast of the beat, as well as its phase, are determined by the position and orientation of the two fish with respect to each other (Kelly et al., 2008), with contrast decreasing as the distance separating two fish increases (see Fig. 1B and D). During social interactions, fish experience increases and decreases in beat contrast due to their own movements and those of interacting conspecifics. More aggressive interactions involve more frequent and longer-lasting approach behaviours that are associated with similar changes in contrast. The contrast also depends on the amplitude of the EODs of both fish. At a given distance, fish with larger EOD amplitudes produce larger contrasts than do fish with lower amplitude EODs. The beat phase varies spatially along the fish's body in a manner that depends on their orientation (i.e. whether fish are positioned parallel or perpendicular to one another; Kelly et al., 2008; Heiligenberg, 1986).

2.3. Chirps modulate the beat background

Chirps involve brief changes in EOD frequency and thus directly influence the amplitude, frequency and the phase of the underlying beat (Benda et al., 2005; Zupanc and Maler, 1993). Even chirps of the same duration having identical frequency and amplitude modulations can induce very different effects on the composite signal received by the other fish depending on the specific beat parameters (Fig. 1). Classically, a small chirp has been described in the context of a slow beat and generated by the higher frequency fish (Fig. 1B, for a beat frequency of 20 Hz), and in the example shown it causes a fast amplitude upstroke. However, the amplitude modulation looks different if the underlying beat is fast. The chirp still accelerates the beat, but now does so over multiple beat cycles (Fig. 1C, frequency difference of 100 Hz). Because the distance between the two fish influences the contrast, the AM caused by the chirp is smaller when fish are farther apart (compare Fig. 1B and D). However, the position of the chirping fish relative to the other fish also plays a critical role: the beat phase is 180° out of phase between the right and left sides of the receiving fish, so the same chirp will occur at two different phases on each side of the body (Fig. 1B and E). In all these cases, the chirp is produced by the fish with the higher EODf. A different picture emerges if the chirping fish emits the lower EODf because under these conditions, a chirp transiently decreases the beat frequency and decelerates the beat (Fig. 1F). In summary, the beat signal is not simply a static background noise source over which a chirp must be detected, but rather, it dynamically interacts with the chirp signal in a way that depends on social context. Thus, reliably detecting and encoding chirps presents a significant challenge for the electrosensory system.

3. Electrosensory pathways and principles of chirp encoding

Central to the detection and discrimination of a chirp is its representation in the nervous system. Chirp encoding has been studied in electroreceptor afferents called P-units (Benda et al., 2005, 2006; Hupé et al., 2008), and in primary electrosensory nuclei called the electrosensory lateral line lobe, ELL (Marsat et al., 2009; Marsat and Maler, 2010, 2012) and torus semicircularis, TS (Vonderschen and Chacron, 2011). In this section, we summarize how beat frequency, contrast and phase influence the processing of chirps at these different stages.

3.1. Electrosensory pathways

As all Gymnotiform fish, *A. leptorhynchus* possesses two kinds of electroreceptors on its skin that are activated by electric signals with different properties. Ampullary receptors are tuned to the low frequencies and DC signals associated with the passive electric sense, while tuberous receptors are tuned to the EOD frequency and comprise the active electric sense. In contrast to those in other species (*Eigenmannia*, see Hopkins, 1974; Metzner and Heiligenberg, 1991; Naruse and Kawasaki, 1998), *A. leptorhynchus* chirps do not contain DC components and are thus thought to be encoded by tuberous receptors.

Each electroreceptor organ is made up of several electroreceptor cells and innervated by afferents that make up the octavolateralis nerve (Zakon, 1986) projecting to the brain. Among the tuberous receptor afferents, two subpopulations can be discriminated (Scheich et al., 1973): *P*-type electroreceptor afferents called P-units respond by phase-locking to the EOD, firing an action potential with a probability that depends on the amplitude of the EOD received at the skin surface (Bullock, 1969; Nelson et al., 1997), while *T*-type electroreceptor afferents fire in response to every EOD cycle at a particular phase in the cycle. Electroreceptor afferents project to the ELL of the hindbrain, the first stage in which electrosensory information is processed in the central nervous system (see Fig. 2A). Here, the axons of P-unit afferents trifurcate to connect to pyramidal neurons in three different maps of the electroreceptive body surface (Heiligenberg and Dye, 1982; Carr et al., 1982), represented in regions called the centromedial

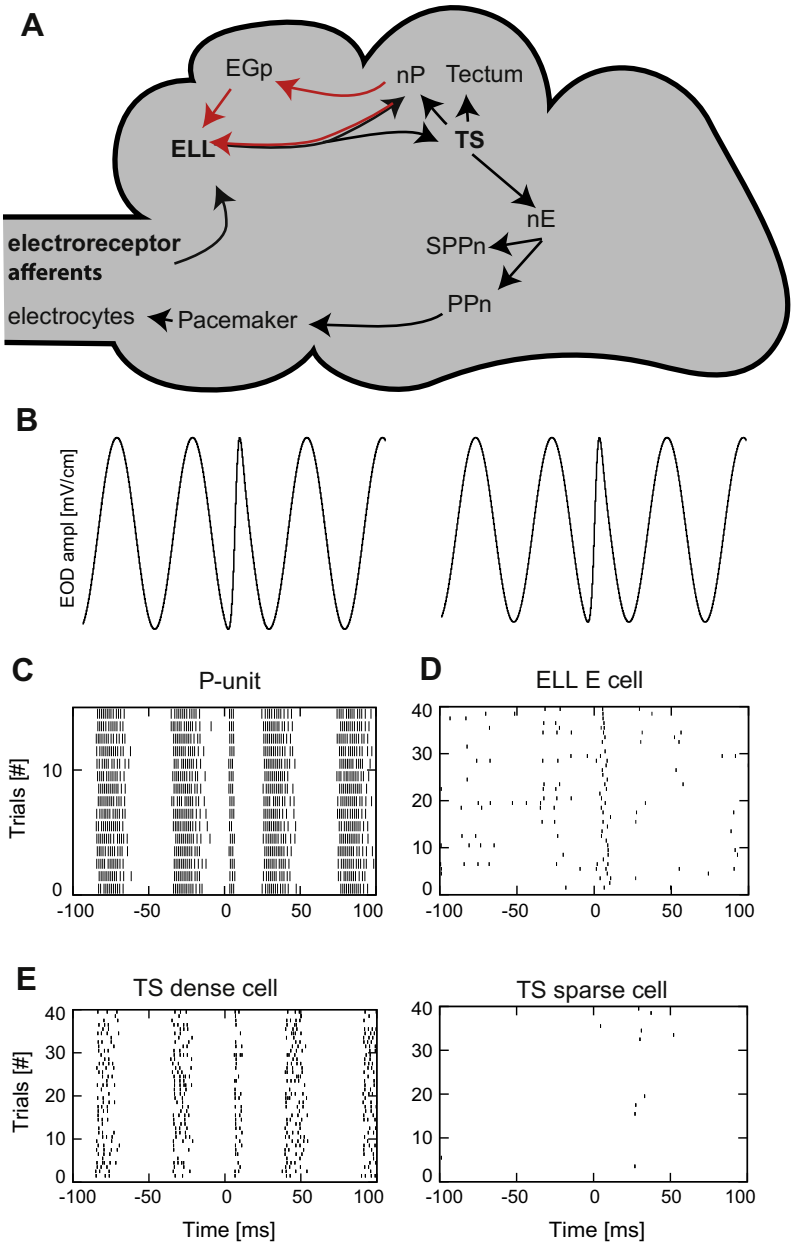

Fig. 2. The electrosensory processing stages and their response to a chirp. (A) Connectivity between the different brain nuclei involved is indicated by arrows, with black arrows depicting ascending projections and red arrows feedback. ELL, electrosensory lateral line lobe; EGp, eminentia granularis pars posterior; nP, nucleus praeeminentialis; TS, torus semicircularis; nE, nucleus electrosensorius; SPPn, sublemniscal prepacemaker nucleus; Ppn, prepacemaker nucleus. (B) The same chirp stimulus was used to stimulate cells of the different processing stages. It consisted of a chirp with a frequency excursion of 60 Hz and a beat frequency of 20 Hz. The responses of P-unit electroreceptor afferents (C), pyramidal cells of the hindbrain electrosensory lateral line lobe (ELL; D) and of two types of neurons in the midbrain torus semicircularis (TS; the dense and sparse coding cells in the left and right column, respectively) to this chirp stimulus are shown as raster plots. The data from p-units was recorded by H. Walz following the methods described in Benda et al. (2005); data from ELL and TS were kindly provided by M. Chacron (for methods see Vonderschen and Chacron, 2011).

segment (CMS), centrolateral segment (CLS) and lateral segment (LS), respectively. A fourth segment, the medial segment (MS) processes information carried by ampullary receptors and will not be described in detail here. ELL pyramidal neurons can be further categorized as superficial, intermediate and deep cells based on their morphology and physiology (Bastian and Courtright, 1991; Harvey-Girard et al., 2007).

Pyramidal ELL neurons then project to higher processing areas including the nucleus praeeminentialis (nP) and torus semicircularis (TS, an inferior colliculus homologue, Fig. 2A; Metzner and Heiligenberg, 1991; Maler et al., 1991; Rose, 2004). nP provides direct and indirect (via the eminentia granularis pars posterior, EGp) feedback that is involved in reafference suppression and enhanced feature detection (Berman and Maler, 1998; Bastian et al., 2004; Lewis et al., 2007; Bol et al., 2011; Requarth and Sawtell, 2011). In the TS, the pyramidal cells of the lateral segment converge together with cells of other types and all four ELL maps (Maler et al., 1982).

The TS projects to the tectum, to the diencephalic nucleus electrosensorius (nE), as well as back to nP (Maler et al., 1991; Rose, 2004). The sensorimotor nE integrates convergent electrosensory information and sends projections to two prepacemaker nuclei: the sublemniscal prepacemaker nucleus (sPPn) and the diencephalic prepacemaker nucleus (PPn) that are responsible for controlling the frequency of the EOD set by the medullary

pacemaker nucleus (Pn). Spatially specific stimulation of the nE by glutamate iontophoresis results in EODf modulations (rises and chirps) via distinct inputs to the PPn (Rose, 2004). The sPPn and PPn project to the medullary pacemaker nucleus (Pn). The Pn contains electrotonically-coupled pacemaker neurons, whose endogenously oscillating membrane potential sets the EODf, and relay cells which propagate these signals to the electric organ (Smith and Zakon, 2000; Smith, 2006).

The most direct route that information can flow from sensory input to motor output is from electroreceptors to ELL, TS, nE, prepacemaker nuclei and then to the pacemaker nucleus. This direct route is indeed thought to form the basis of the jamming avoidance response (Heiligenberg, 1986; Rose, 2004), a behaviour that involves the fish changing their EOD frequency when stimulated with an EOD of similar frequency.

3.2. Chirps are encoded by electroreceptor afferents

To date, the afferent encoding of chirps has exclusively been studied in the tuberous P-unit receptors. In response to a step increase in EOD amplitude, P-units exhibit pronounced spike frequency adaptation (Xu et al., 1996; Nelson et al., 1997; Chacron et al., 2001; Benda et al., 2005). Spike-frequency adaptation involves a strong peak in firing response to the onset of a constant stimulus, followed by a decrease to a lower steady state response. Thus, adaptation acts as a high-pass filter, reducing the response to low stimulus frequencies, such as beat frequencies lower than about 25 Hz (Xu et al., 1996; Nelson et al., 1997; Benda et al., 2005). When produced by the higher frequency fish, chirps transiently increase the frequency content of the beat signal such that adaptation is transiently overcome. The result is a strong response similar to those evoked by the onset of a constant stimulus – provided the chirp is emitted during a sufficiently slow beat background (see Fig. 2C). The increase in firing rate is accompanied by an increase in P-unit population synchrony (Benda et al., 2006). The degree of synchrony between P-units is maximal for an intermediate range of beat frequencies (30–80 Hz) and decays for higher beat frequencies. Small chirps at beats faster than 30 Hz accelerate the beat frequency into a regime in which the synchrony between P-units decreases relative to their response to the beat. Hence, while P-units are synchronized by chirps occurring at beats slower than approx. 30 Hz, they are desynchronized by the same chirps presented in conjunction with faster beats (Hupé et al., 2008; Walz et al., 2010).

The increase of the EOD frequency associated with big chirps is so large that they decrease the rate as well as the synchrony of P-units regardless of the underlying beat frequency (although there seems to be an increase in single unit reliability at beats <10 Hz, Benda et al., 2006); this effect is enhanced by the concomitant decrease in EOD amplitude typical of big chirps. The enhanced response to small chirps at slow beats, as well as the decrease in response to small and big chirps at fast beats, are seen in measures of the firing rate as well as in measures of synchronization (Benda et al., 2006).

3.3. Chirp encoding in the electrosensory lateral line lobe

The next processing stage is the electrosensory lateral line lobe (ELL). There are two main classes of pyramidal neurons in each segment of the ELL. E-cells receive direct input from P-units and are excited when P-units increase their rate (i.e. during EOD amplitude increases), while I-cells receive the P-unit input via disynaptic connections from interneurons and are inhibited by an increase in afferent rate (Maler, 1979; Shumway and Maler, 1989).

As a consequence of differential ion channel distributions (Ellis et al., 2007; Mehaffey et al., 2008) as well as different connectivity to the afferent neurons (Maler, 2009), E-cells of all three segments exhibit very different response properties to P-unit inputs. From the CMS to the LS, neurons are increasingly responsive to higher frequency AMs (Krahe et al., 2008) and have larger receptive fields. Both characteristics, high-pass frequency tuning and large receptive fields, make neurons of the LS most responsive to communication signals (Marsat et al., 2009); compared to signals encountered during navigation and hunting, communication signals are much higher in frequency and more spatially broad. Not surprisingly, the LS has been shown to be crucial for communication behaviour (Metzner and Juranek, 1997).

Feedback to ELL from nP and EGp plays an important role in chirp encoding. Superficial E-cells of the LS respond with a highly reliable and synchronous burst of spikes to small chirps emitted at slow beats (Fig. 2D; Marsat et al., 2009). The second spike of the burst is not phase-locked to the EOD, indicating that it is not caused by input from P-units. The bursting mechanism relies on a depolarizing after potential (DAP) that stems from backpropagating action potentials from the dendrites (Turner et al., 2002; Marsat and Maler, 2012). In these cells, the indirect feedback from EGp provides a negative image of a low frequency beat (Bastian et al., 2004). During an ongoing beat, feedback and input are antiphase, but the chirp shifts the phase of the beat stimulus. When this occurs, the feedback coincides with the DAP and a spike in response to a chirp is more likely to be followed by a second one (Marsat and Maler, 2012). Such bursts may facilitate chirp detection, similar to many systems where bursts enhance signal detection by increasing the signal-to-noise ratio (for a review, see Krahe and Gabbiani, 2004). The feedback, however, is only present in response to beats of frequencies up to 20 Hz (Bol et al., 2011; Bastian et al., 2004). The enhancement of the ELL response by feedback to small chirps is therefore likely to be even more confined to low beat frequencies than the P-unit response.

Big chirps are encoded by a strong increase in firing rate in I-cells of all maps and types (superficial, intermediate and deep, Marsat et al., 2009). This is expected since they cause a decrease in the response of P-units and because, in contrast to E-cells, I-cells of different maps and morphology do not show strong differences in frequency tuning (Krahe et al., 2008).

3.4. Higher level processing of chirps

The main target area of the ELL for further information processing is the TS. TS cells can be grouped into two categories according to their baseline firing rate and selectivity to different chirp stimuli (Vonderschen and Chacron, 2011; Chacron et al., 2011). One category, the densely coding neurons, produce responses that resemble those of ELL pyramidal cells (Fig. 2E, left), while cells in the other category respond much more sparsely, i.e. with a higher selectivity (Fig. 2E, right). Compared to the densely coding TS cells and ELL pyramidal cells, sparsely coding TS cells do not respond during the beat and respond similarly to chirps with certain attributes, but not at all to those with others (see also Fig. 2 in Vonderschen and Chacron, 2011). This population of TS cells can thus, in principle, detect the presence of certain categories of chirps and differentiates between them. How this selectivity arises is currently unknown. The synapses between ELL pyramidal cells and TS neurons show pronounced short-term synaptic plasticity that can act as a temporal filter passing low or high frequencies (Fortune and Rose, 2000, 2001, shown for *Eigenmannia*). This synaptic plasticity has been shown to create direction selectivity to moving electrosensory images in TS neurons (Chacron et al., 2009; Chacron and Fortune, 2010). Whether synaptic plasticity sharpens responses to chirps is unknown. Cells that respond selectively to chirps are not direction selective and vice versa (Vonderschen and Chacron, 2011).

3.5. Large contrasts enhance the encoding of beats and chirps

So far, we have primarily considered the effect of beat frequency on chirp encoding. We will now turn to the influence of beat phase and contrast. The encoding of beats and chirps at different contrasts has been studied only in P-units. P-units respond linearly to increasing contrasts within a certain range (Gussin et al., 2007). The responses of P-units to chirps and beats are greater for larger contrasts, however, the relative response to chirps is qualitatively independent of the contrast (Benda et al., 2006). At higher contrasts, the responses of P-units become nonlinear (due to rectification) suggesting that responses to chirps will change (Savard et al., 2011). For example, at beat frequencies in which the chirp elicits a stronger response than the underlying beat, the response is cut off and both chirp and beat elicit responses that are equally strong.

Heterogeneity in the characteristics of P-units (Gussin et al., 2007) as well as in spatial properties of the signal (Kelly et al., 2008), however, result in saturation of their responses at different levels of beat contrast. Using whole-nerve recordings, Benda et al. (2006) showed that the population response begins saturating at contrasts around 20%. Whether or not saturation effects make the detection of chirps more difficult for interacting *A. leptorhynchus* remains to be tested with behavioural experiments.

3.6. The phase of the beat influences chirp encoding at low frequencies

The timing within the beat cycle at which a chirp is produced strongly affects the shape of the AM at beat frequencies lower than 30 Hz (Fig. 1), causing either transient upstrokes or downstrokes. In response to a chirp that causes an upstroke, a strong increase in firing rate is seen in P-units, whereas in response to a chirp that results in a downstroke, P-units cease firing. However, when chirps occur at times between a trough and a peak, the resulting AM contains parts of an upstroke as well as a downstroke and the response is similar to the case of a pure upstroke (Benda et al., 2005).

One way to characterize whether a certain attribute of a chirp significantly influences its encoding, is to analyze whether a response is sufficient to differentiate between chirps of different values of this attribute. This is traditionally done in a discrimination analysis (Green and Swets, 1974) and such an analysis has been conducted using responses in the ELL and TS (Marsat and Maler, 2010; Vonderschen and Chacron, 2011). At both processing stages, responses to the same chirp presented at different phases of the beat are significantly different. The beat phase selectivity of ELL and TS neurons to chirp stimuli suggests that there may be a behavioural relevance of chirps produced at different times in the beat phase cycle and that fish could therefore control chirp production to influence perception by the other fish. If this were the case, one would expect a nonuniform distribution of chirps over the beat cycle (see behavioural section for further discussion).

As discussed earlier, the amplitude modulation of a chirp depends on whether the emitting fish carries the higher or lower EODf (the sign of the frequency difference, see Fig. 1E). The results from electrophysiological studies about the encoding mechanisms suggest that the responses of P-units, ELL and TS to chirps will also depend on whether the chirping fish has the lower or higher EODf. However, this remains to be shown as all electrophysiological studies thus far have been conducted using positive difference frequencies.

4. Behavioural responses to chirp stimuli

In the previous section we reviewed how electrophysiological responses to chirps in electrosensory afferents and primary integration centers are influenced by parameters of the background signal, including beat frequency, contrast, and beat phase. In this section, we will review evidence from the literature that describes how behavioural responses to chirps are influenced by these same parameters. We will begin with a brief discussion of *A. leptorhynchus* responses to different chirp stimuli characterized using a simplified experimental design, addressing how chirp delivery influences chirp production rates depending on stimulus parameters (the beat frequency and contrast, and the rates and pattern of chirps delivered). Following this, we will examine how chirping and aggressive responses to conspecific chirps are influenced by beat parameters under more natural contexts. We focus primarily on small chirps, with some discussion of big chirps at the end of the section. Throughout, we consider whether what is known about sensory encoding is sufficient for explaining the relationships between behavioural responses to chirps and the background beat parameters.

4.1. Chirping in chirp chambers

Stimulus specific behavioural responses have been characterized using "chirp chamber" experiments, wherein the EOD modulations produced by individual fish restrained in tubes are recorded in response to electrical stimuli (sinusoidal or EOD mimics) of

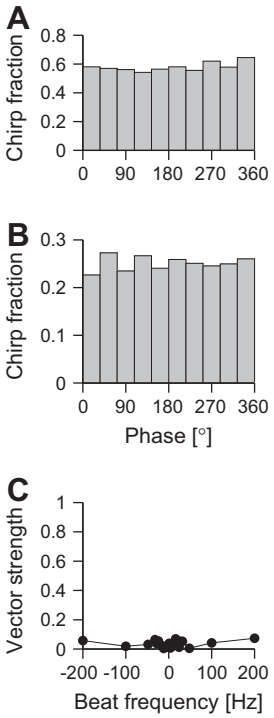

Fig. 3. Beat phase and chirp production. (A) Shows a histogram of all chirps over beat phase recorded in 66 chirp chamber experiments with a stimulation of 4 Hz above the fish's own EODf. Fish were placed in a tube and stimulated with mimics of conspecifics using two carbon electrodes, one on either side of its body. The fish's field was measured with silver chloride electrodes placed near the head and the tail of the fish and chirps were detected as frequency increases of more than 10 Hz of the EODf using custom made software. To exclude effects of an overall higher chirp rate of individual fish, we normalized the histograms with the overall chirp rate for each fish. Shown are the number of chirps in each phase bin (of 36°) divided by the number of all emitted chirps of this fish, then summed over all experimental conditions. For a more detailed description of chirp chamber experiments see Bastian et al., 2001. (B) Shows the results from the same experiments under a stimulation with 48 Hz above the fish EODf. (C) For each stimulation frequency we calculated the vector strength of the histogram. The vector strength is a measure for phase locking and ranges from 0 to 1. As we find values of 0.1 for all stimulation frequencies, this shows that chirp production rates do not depend on beat phase.

varying frequency and amplitude (Dulka et al., 1995; Zupanc and Maler, 1993; Engler and Zupanc, 2001). In these conditions, chirp production rates of males decrease with increasing beat frequency (Engler and Zupanc, 2001; Bastian et al., 2001) regardless of the sign of the frequency difference. This selective behavioural response corresponds well with the range of beat frequencies over which chirps lead to the greatest increases in P-unit synchrony and enhancement of chirp encoding in the ELL by feedback mechanisms. Beat contrast also influences the chirp production rates of fish in chirp chambers. These experiments have suggested stimulus intensities greater than 50 μV/cm are required to elicit chirp responses in *A. leptorhynchus* (Dunlap et al., 1998; Engler and Zupanc, 2001; Zupanc et al., 2006). Further, chirp production rates of males increase with increasing stimulus intensity i.e. increasing contrast (Zupanc and Maler, 1993; Engler and Zupanc, 2001).

Chirp chambers have also been used to characterize the occurrence of chirps relative to the phase of the beat. In chirp chamber experiments using slow beat stimuli, chirps were produced at all beat phases (Zupanc and Maler, 1993). To investigate whether there might be effects of beat phase on chirp production at other beat frequencies, we performed chirp chamber experiments using various stimulation frequencies (Fig. 3). The data shows that chirps were produced at equal rates across all beat phases (Fig. 3C). Thus, fish will likely be exposed to chirps at all different beat phases. Marsat and Maler (2010) suggested that the high variability in the response of pyramidal cells, resulting from chirps at different beat phases, hinders the fish's ability to distinguish between chirps of different parameters. However, fish often emit chirps in bursts and the electric image evoked by the chirp is heterogeneous along the body (Kelly et al., 2008). This means that receiver fish likely have access to information about a chirp at multiple beat phases. The absence of a pronounced relationship between chirp production times and beat phase does not necessarily imply that beat phase is not behaviourally relevant. Even if the fish might not control the production at certain beat phases, chirps emitted at certain beat phases could still be represented better in the nervous system and evoke stronger behavioural responses. In free-swimming conditions, the exact phase of the beat at the skin of a fish is hard to infer and no such analysis has been done so far. However, such experiments could give important information in this direction.

Chirp chamber experiments have also been performed using playback stimuli containing chirps. In these experiments, chirping also decreases with increasing beat frequency similar to the response to stimulus EODs that do not contain chirps (Engler and Zupanc, 2001; Triefenbach, 2005). Interestingly though, overall chirping rates are lower when playbacks contain chirps, suggesting that in these conditions, chirp reception inhibits the chirp production rates of receiving fish (Dunlap and Larkins-Ford, 2003; Triefenbach, 2005). Chirp production rates in response to playbacks with chirps approximately 3 cm and 10 cm from the receiving fish (resulting in field intensities of 0.5 mV/cm and 0.075 mV/cm, respectively, near the receiving fish) also increase with higher intensity stimuli (Dunlap and Larkins-Ford, 2003). However, as will be discussed in the following section, these relationships are more complicated during natural interactions.

4.2. Behavioural responses to chirps under more natural experimental conditions

The stimuli presented and experimental conditions used in chirp chamber experiments are similar to those used in electrophysiological experiments, but both lack many features common to natural interactions. While many of the observations found in chirp chambers carry over to more natural experimental conditions involving staged social interactions (Dunlap and Larkins-Ford, 2003; Zupanc et al., 2006; Triefenbach and Zakon, 2008; Hupé et al., 2008), there are also important differences, suggesting that the complexity of chirping behaviours produced under increasingly naturalistic conditions involves the integration of multiple features of a social interaction. As described earlier, the beat background during conspecific interactions can be quite complex because fish constantly change position relative to one another and produce rapid frequency and amplitude modulations in varying temporal patterns.

4.2.1. Chirp response rates and patterns are influenced by the experimental setting and behaviour of interacting conspecifics

When two fish confined to separate tubes interact electrically (but not physically), the chirp production pattern of one fish is correlated with that of the other fish (Zupanc et al., 2006). Correlation analyses of the instantaneous chirp rates of fish responding to chirps suggest that following chirp reception there is a short-term inhibition of chirping (~100–200 ms) which precedes a subsequent period of chirp rate enhancement (Zupanc et al., 2006; Hupé and Lewis, 2008; Gama Salgado and Zupanc, 2011).

From a sensory coding perspective, this so-called "echo response" implies that conspecific (or artificial) chirps are discriminated by the sensory system of a receiving individual amongst various background beat modulations. It is thus a convenient measure of sensory detection at the behavioural level. Using EOD playbacks, Gama Salgado and Zupanc (2011) found that 20 ms-long chirp mimics with a frequency increase of just 1.2%, delivered with an interchirp interval of 0.6 s, were sufficient to induce a robust echo response. This indicates that the typical frequency excursion associated with small chirps (~50–100 Hz) is at least five times greater than the behavioural threshold for chirp detection. These results were characterized with beat background conditions optimal for chirp encoding: in response to a signal delivered at a high stimulus intensity (mimicking an inter-individual distance of approximately 1–2 cm) with an EODf similar to that of the stimulated fish (±10 Hz) (Gama Salgado and Zupanc, 2011).

The pattern of chirp stimuli also influences both the chirping and aggressive responses of free-swimming fish. With EOD playbacks containing chirps delivered in a random sequence, the chirp and aggressive responses of male *A. leptorhynchus* decrease with the number of chirps delivered (Hupé, 2012). In addition, fish echo more often in response to higher randomly patterned stimulus chirp rates, produce fewer chirps and are less aggressive towards stimulus mimics (Hupé, 2012). This inhibition of chirping was not observed in fish responding to playbacks during which chirps are delivered interactively (stimulus chirps echo those produced by the real fish with a latency of 200 ms). These observations suggest that both the rate and pattern of chirps delivered differentially influence behaviour and provide evidence that chirps received are temporally integrated in electrosensory systems.

4.2.2. The influence of beat frequency

The relationship between chirp rate and beat frequency characterized in chirp chamber studies persists across a number of behavioural scenarios (Dunlap and Larkins-Ford, 2003; Zupanc et al., 2006; Hupé et al., 2008). These results imply that chirps are produced at high rates during stimulus conditions that represent more aggressive same-sex contexts. Given that EODf is related to indicators of dominance among males, increased chirping and physical escalation are expected between more closely matched individuals (see Section 2, Fugère et al., 2011).

Along these lines, it follows that chirp rates should be asymmetrical with respect to the sign of the frequency difference. Contrary to this prediction, results from chirp chamber studies reveal no significant dependence of chirp rates on the sign of the frequency difference (Engler and Zupanc, 2001; Bastian et al., 2001). However, contrary to the results from chirp chambers, there is growing evi-

dence that under more natural experimental conditions, fish respond in a way that depends on the sign of the frequency difference. During experiments in which one fish is restrained in the center of a tank in an electrically transparent hammock, and another fish swims freely around it, the chirp rates of the free-swimming fish correlate significantly with the magnitude and the sign of the frequency difference (Hupé, 2012), Additionally, playbacks of lower frequency EODs without chirps elicit more approach behaviours from fish than do playbacks of an EOD of the same frequency with chirps, or playbacks of higher frequency EODs regardless of whether they contain chirps or not (Triefenbach, 2005).

Although small chirps are produced infrequently in response to large beat frequencies, analysis of the chirp echo response has demonstrated that free-swimming fish reciprocate chirps at rates significantly greater than chance even during social pairings that result in high beat frequencies (Hupé et al., 2008), evidence that small chirps can be encoded across the range of all beat frequencies encountered.

4.2.3. The effect of beat contrast

Chirp rates of pairs of males, each confined to a separate tube, change significantly only when the tubes are positioned within 10 cm of one another, suggesting that the dependence of chirp production on contrast characterized in chirp chambers extends to dyadic interactions (Zupanc et al., 2006). When one or both of two interacting fish are unrestrained, contrasts change dynamically throughout the interaction and can provide fish with information about conspecific motion and proximity (Yu et al., 2012). During such free swimming interactions, there are significant correlations between measures of aggression (associated with large increases in contrast) and average chirping rates (Triefenbach and Zakon, 2008; Hupé and Lewis, 2008).

To further characterize the temporal relationship between chirping and contrast, we quantified, over time, the relationship between chirp production and the distance separating a chirping fish and the playback mimic to which it is responding (methods described in Hupé, 2012). Fig. 4 shows the mean distances centered at the time of chirp production (Fig. 4A), and centered at the time of delivered chirps (Fig. 4B), in one free-swimming fish responding to a low beat frequency EOD playback with chirps delivered to echo those of the real fish, calculated for every minute of a 10 min trial (Hupé, 2012). At the onset of the trial (within the first couple of minutes), the fish remains at a distance from the mimic, and during this time chirps are produced when the distance separating the fish and mimic is largest (when contrasts are small). Further into the trial (from 3 to 4 min onward), the fish spends more time in close proximity to the mimic and produces its chirps during, or slightly following, times when mean distances are the smallest (corresponding to large contrasts that occur during approach behaviours). This suggests that the timing of chirps produced does not depend only on the absolute contrast or on specific types of contrast changes. Further, it is expected that the distance relationships in Fig. 4A and B should be similar, because chirps delivered echo those produced by the fish. However, the relationship between chirp time and distance is more pronounced for chirps produced than for chirps delivered, suggesting that chirp production may be influenced more strongly by contrast than by conspecific chirps. The strength of these relationships may also depend on the experimental and social conditions under which the behaviours are examined. Future studies should address how aggressive behaviours are differentially patterned with chirping under conditions that more closely represent natural interactions.

4.3. Big and small chirps: differential chirp production and associated behaviours

Up to now we have exclusively considered the behavioural responses to stimulation with EODs containing small chirps. However, behavioural results from playback experiments suggest that the chirp types are differentially encoded. Playbacks with big chirps increase the production of big chirps relative to small chirps, and evoke approach behaviours in both male and female fish (Triefenbach, 2005). This is consistent with the idea that big chirps are an attractive signal, as predicted from observations of interacting fish during reproductive contexts (Hagedorn and Heiligenberg, 1985), chirp chamber studies (Bastian et al., 2001; Engler and Zupanc, 2001), and freely interacting *A. leptorhynchus* (Hupé, 2012).

The relative production rates of small chirps and big chirps are also influenced by the frequency and contrast of the beat background, chirp stimulus parameters, as well as experimental setting (Triefenbach, 2005; Hupé and Lewis, 2008). Under a variety of conditions, males preferentially produce big chirps in response to stimulation with high beat frequencies (Engler and Zupanc, 2001; Bastian et al., 2001). High beat frequencies occur during opposite sex-interactions and during interactions between same sex individuals with large differences in EODf, providing additional evidence that big chirps function in attraction, reproduction (Engler and Zupanc, 2001; Zakon et al., 2002) and/or to signal sub-

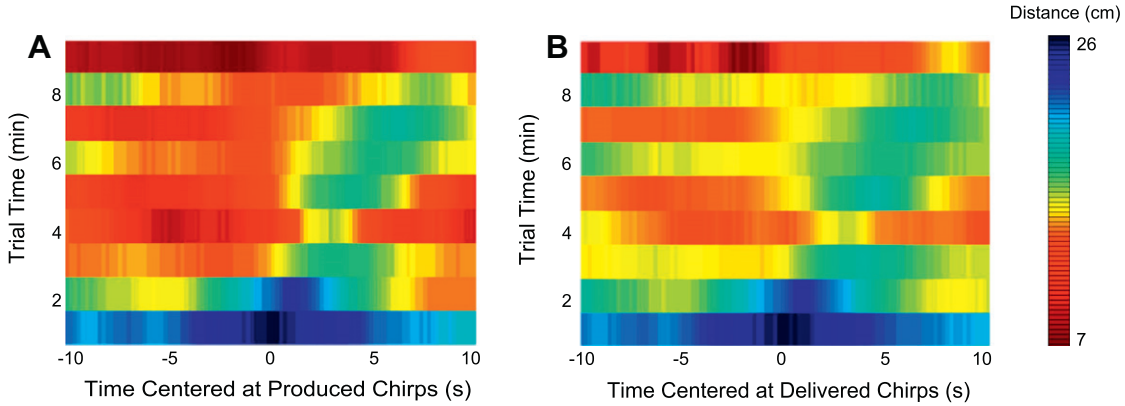

Fig. 4. Chirp patterning over time. Chirps are patterned with contrast changes that result from physical movements in a manner that changes over time. The mean distance separating a free-swimming fish and a playback mimic calculated over 20 s centered at the time of (A) chirp production and (B) chirp delivery. Distances are depicted in the colour of each 100 ms bin centered at the time of chirp production or delivery, averaged over 1 min bins for every minute of a 10 min interactive chirp playback trial. The colour bar denotes the linearly distributed representation of distances. Playback stimuli EODs were delivered through a mimic at a frequency slightly higher (+10 Hz) than that of the real fish, with an amplitude matching that of the real fish, and chirps were delivered to echo those produced by the real fish with a latency of 200 ms (methods described in Hupé, 2012).

ordinance (Cuddy et al., 2012). This proposed function is further supported by results from dyadic experiments in which less aggressive males produce significantly more big chirps than do more aggressive males (Hupé, 2012).

If two communication signals convey different meaning, they must be discriminated in sensory systems. Signals that convey opposite behavioural states (i.e. aggression and submission) often comprise opposite extremes of some variable in signal space (i.e. frequency, duration) presumably to reduce receiver error (Morton, 1977; Hurd et al., 1995; Triefenbach and Zakon, 2003). As described in the previous sections, responses to big and small chirps can be discriminated at all stages in the early electrosensory pathway when they are emitted on a slow beat background. During fast beats, both small and big chirps desynchronize P-unit electroreceptors, so how these two signals are distinguished in subsequent processing stages is not clear.

4.4. Behavioural responses to chirps depend on the interplay of individual propensities and stimulus condition

Pronounced individual differences in chirp responses have been observed in multiple contexts (Dunlap and Larkins-Ford, 2003; Gama Salgado and Zupanc, 2011); and interestingly, the chirp rates of fish to EOD playbacks with and without chirps are correlated (Dunlap and Larkins-Ford, 2003). Some variation is explained by body size, as larger males chirp more overall, maintain higher chirp rates, and are less likely to decrease chirp rate in response to chirp containing EOD playbacks compared to smaller males (Triefenbach, 2005). This is consistent with the idea that the chirping by more dominant males is less affected by threatening stimuli than that of less dominant (smaller, low EODf) males (Triefenbach and Zakon, 2008; Hupé, 2012). These selective responses to different chirp stimuli suggest that responses to chirps can be influenced by the threat potential and the condition of the receiver (Triefenbach, 2005). Individual differences could at least in part be a consequence of differential chirp encoding and processing by electrosensory pathways.

A complex behavioural repertoire is revealed through a comparison of behavioural responses to chirp stimuli presented under different experimental conditions. The information contained in the beat frequency and beat contrast influence both chirp encoding and chirp production behaviours. While differences in chirp encoding under specific beat background conditions may account for some of this variation in behavioural response, it appears that higher processing of conspecific chirps may be categorical (small versus big chirp) and subject to modification by a number of influences.

5. Integration of encoding and behaviour

Characterizations of chirping behaviours in male and female *A. leptorhynchus* have revealed that chirp production patterns can be very complex, influenced by a variety of internal and external factors. As demonstrated, some of the complexity of chirping behaviour may be explained by features of chirp encoding in early sensory pathways. Many aspects of chirping behaviour, however, might only be reflected in higher processing stages, downstream from the primary integration centers that have been studied so far.

5.1. What encoding can tell us about behaviour

Describing the physical properties of the sensory environment of an animal provides information about the nature of the stimuli that activate the receptor cells of a certain modality. However, the internal representation of these stimuli is ultimately responsible for the information an animal has access to about the outside world. Here we have examined how conspecific signals are encoded when presented in conjunction with different background parameters and discuss which aspects of encoding may influence behavioural responses. Small chirps are particularly well-encoded when they are emitted at slow beats (Benda et al., 2005; Marsat et al., 2009; Marsat and Maler, 2010). Behavioural investigations show, however, that they are detected by the fish even when occurring on faster beats, during which chirps have an opposite effect on the response of receptor cells (Hupé et al., 2008). Although the ELL responses have only been studied in a limited context, i.e. a chirp on a 5 Hz beat (Marsat and Maler, 2010), and the question of how chirps are encoded in conjunction with different beat frequencies has not been analyzed in detail in the TS, the distinct responses to a chirp at a slow and a fast beat suggest that chirp encoding at low and high beat frequencies is routed through different streams. In the ELL, for example, we would expect E cells to respond to small chirps occurring at low beat frequencies (as shown by Marsat and Maler, 2010) and I cells to be responsive to small chirps occurring at high beat frequencies. Furthermore, the way small chirps are encoded by P-units at high beat frequencies seems to be similar to the encoding of big chirps at these frequencies.

Chirp encoding in the early electrosensory pathway suggests two aspects that future behavioural investigations should consider. First, since the effect or relevance of a chirp might depend on whether they are emitted at low or high beat frequencies, a more careful analysis of behavioural responses at different beat frequencies is warranted. Second, the categorical distinction between small and big chirps might depend on beat frequency and should be examined further. If behavioural studies confirm a clear distinction between big and small chirps at high beat frequencies, the encoding of big and small chirps at these frequencies might rely on mechanisms and effects that have not been examined in physiological studies so far.

The encoding principles investigated so far in the early electrosensory pathway can only provide hints to the overall representation of the stimulus. Processing at the neural population level could lead to enhanced detection or discrimination in successive stages. Even at the initial stage from P units to the ELL, there is a high degree of convergence (by a factor of 1:1000 in LS; Maler, 2009); this is also most likely occurring between ELL and TS. Additionally, in the TS, the information encoded by P-units converges with information about low frequencies and phase differences in the EOD signal that is encoded by ampullary receptors and in T-units, respectively (Metzner and Heiligenberg, 1991; Kawasaki et al., 1988). Beats as well as the amplitude modulations caused by chirps generate no low-frequency signals that might be detected by the ampullary system. However, Dunlap et al. (2010) demonstrated that *A. leptorhynchus* also chirps in response to the low frequency signals preferred by ampullary receptors. This behaviour suggests that information from the ampullary system could be used to trigger chirp production. Chirp encoding in T-units has not been studied to date, but could provide a complementary stream of information.

5.2. What behaviour can tell us about encoding

Studies of the encoding of sensory stimuli shed light onto the mechanisms by which sensory information may be represented in a nervous system. However, only behavioural studies can ultimately show whether a signal is detected and differentiated by the animal.

The complex temporal patterning observed between chirp production and physical aggression, occurs over subsecond timescales (Triefenbach and Zakon, 2008; Hupé et al., 2008; Gama Salgado and Zupanc, 2011). This provides evidence that the electrosensory

system is able to encode and respond to chirps occurring at rates as high as 3–5 chirps per second (Hupé and Lewis, 2008; Gama Salgado and Zupanc, 2011). In many systems, antiphonal exchanges such as the chirping echo response, mediate mutual assessment of individual status. Coordinated signalling behaviours are often exchanged during confrontations as a means to prevent the costs associated with escalation (Triefenbach and Zakon, 2008) and necessitate that signal timing and quality are rapidly and faithfully represented in sensory pathways.

An even faster control of chirp production time than observed in behavioural experiments seems, however, not possible or necessary. Although at early electrosensory stages the phase in the beat at which a chirp occurs strongly influences chirp encoding, chirps do not appear to be produced with any phase preference. This does not necessarily imply that beat phase is irrelevant. Chirps emitted at certain beat phases could still be represented better in the nervous system and therefore potentially evoke stronger behavioural responses. In free-swimming conditions, the exact phase of the beat at the skin of a fish is hard to infer and no such analysis has been done so far. However, experiments investigating the influence of beat phase on the echo response, for example, could give important information in this direction.

Under various experimental conditions, fish tend to produce chirps in bursts (Zupanc et al., 2006; Hupé and Lewis, 2008). Bursts of chirps might allow for neural responses to integrate over successive chirps in higher processing stages, leading to a larger signal-to-noise ratio. Up to the level of the TS, this is clearly not the case. All time scales of the responses are still fast and chirps separated by 400 ms will be processed as separate signals. Alternatively, emitting chirps in bursts might simply increase the chance of some chirps occurring at beat phases at which they are perceived best.

The difference between chirping responses to playback chirps and to those produced by two physically interacting fish suggests that spatiotemporal electric field complexities resulting from relative motion significantly influence chirping and aggressive responses to chirps (Dunlap and Larkins-Ford, 2003). Furthermore, during dyadic interactions, chirps are produced preferentially when fish are positioned in a head-to-tail orientation compared to when oriented head-to-head (Triefenbach and Zakon, 2008). Future studies should characterize the electric image modulations produced during chirping in each of these orientations, and electrosensory responses to these different stimuli.

In other systems, signal attributes such as maximal frequency excursion and duration provide information about the identity and attractiveness of conspecifics: individual identity in damselfish (Myrberg and Riggio, 1985) and attractiveness in crickets (Hennig, 2003). This could also be the case for chirping in *A. leptorhynchus* (Dulka et al., 1995). However, the great variability involved in encoding one chirp at different beat phases at the level of the ELL has led to the suggestion that the differentiation between chirps of different attributes is impossible for the fish (Marsat and Maler, 2010). To ultimately evaluate this possibility, the whole parameter space of chirp patterning and beat backgrounds must be taken into account. Also, other parameters such as EODf, beat frequency and chirp production rates already convey redundant information about identity and dominance status, suggesting that specific chirp attributes may be less important. Evidence from choice experiments in which females prefer males with higher EODf (Bargeletti, Gogarten and Krahe, personal communication) show that this information seems to be relevant in reproductive contexts as does the observation that fish increase their EODf in breeding conditions (Cuddy et al., 2012).

However, negative results from behavioural experiments do not necessarily mean that a chirp has not been detected by a receiving fish. Chirping is not a reflexive behaviour and whether or not a fish chirps in response to a stimulus chirp or EOD does not only depend on signal detectability but also on the receiver's motivation and behavioural strategy, as well as the experimental context and various other factors. Carefully designed experiments are required to tease out the relative effects of these different factors on behavioural thresholds.

5.3. The complexity of chirp encoding and behaviour: future directions

The diversity and context specificity of behavioural responses to chirps under more realistic experimental conditions demonstrate that many factors are integrated to influence these responses. Despite the extensive description of chirp encoding in the first three stages of electrosensory processing and the growing body of behavioural characterizations, many open questions about chirp encoding remain. There is a need for a description of electrosensory responses to chirping in higher brain areas as well as behavioural and physiological experiments performed under increasingly natural conditions.

Male and female *A. leptorhynchus* behave very differently to chirp stimuli, with only males producing chirps (Dulka and Maler, 1994; Dulka et al., 1995). These behavioural differences are likely a consequence of hormonal modulation of chirp production pathways (Telgkamp et al., 2007; Smith and Combs, 2008). Recent evidence suggests that encoding pathways are sensitive to neuromodulation by circulating hormone levels (Deemyad et al., 2011). This *in vitro* study showed that serotonin increases the excitability and the burst firing of the ELL E-cells that are responsible for encoding chirps. The effects of neuromodulation on chirp encoding is an exciting finding that should be investigated *in vivo* and in more detail in future studies.

So far, physiological experiments have characterized responses to stimuli containing chirps on a beat with a constant contrast, presented in conditions similar to those used in chirp chamber behavioural experiments. Certain aspects of movement that are reflected in contrast changes of the beat are correlated with chirping (Hupé, 2012). Whether or not contrast changes will influence chirp encoding is another important question for future physiological or modeling studies (see Yu et al., 2012), in particular at higher processing stages. Future studies should also examine electrophysiological responses to stimulus chirps that incorporate elements of the spatiotemporal electric field complexities generated during conspecific interactions, and compare these to the responses to self-generated chirps. Clearly, behavioural responses to chirps are influenced by the context under which they are characterized, and stimulus paradigms that represent more natural electric scenes should be a priority.

Acknowledgements

We are grateful to Franziska Kümpfbeck for performing chirp chamber experiments and to Jörg Henninger for helping with the analysis. H.W. and J.B. were supported by The German Federal Ministry of Education and Research Bernstein Award 01GQ0802, J.L. received funding from the NSERC (Natural Sciences and Engineering Research Council of Canada) Discovery program and G.J.H. was funded by a NSERC PGS (postgraduate scholarship).

References

Bastian, J., Chacron, M.J., Maler, L., 2004. Plastic and nonplastic pyramidal cells perform unique roles in a network capable of adaptive redundancy reduction. Neuron 41, 767–779.

Bastian, J., Courtright, J., 1991. Morphological correlates of pyramidal cell adaptation rate in the electrosensory lateral line lobe of weakly electric fish. J. Comp. Physiol. A 168, 393–407.

Bastian, J., Schniederjan, S., Nguyenkim, J., 2001. Arginine vasotocin modulates a sexually dimorphic communication behavior in the weakly electric fish *Apteronotus leptorhynchus*. J. Exp. Biol. 204, 1909–1923.

Benda, J., Longtin, A., Maler, L., 2005. Spike-frequency adaptation separates transient communication signals from background oscillations. J. Neurosci. 25, 2312–2321.

Benda, J., Longtin, A., Maler, L., 2006. A synchronization–desynchronization code for natural communication signals. Neuron 52, 347–358.

Berman, N.J., Maler, L., 1998. Inhibition evoked from primary afferents in the electrosensory lateral line lobe of the weakly electric fish (*Apteronotus leptorhynchus*). J. Neurophysiol. 80, 3173–3196.

Bol, K., Marsat, G., Harvey-Girard, E., Longtin, A., Maler, L., 2011. Frequency-tuned cerebellar channels and burst-induced LTD lead to the cancellation of redundant sensory inputs. J. Neurosci. 31, 11028–11038.

Bro-Joergensen, J., 2010. Dynamics of multiple signalling systems: animal communication in a world in flux. Trends Ecol. Evol. 25, 292–300.

Bullock, T.H., 1969. Species differences in effect of electroreceptor input on electric organ pacemakers and other aspects of behavior in electric fish. Brain Behav. Evol. 2, 85–118.

Caputi, A.A., Budelli, R., 2006. Peripheral electrosensory imaging by weakly electric fish. J. Comp. Physiol. A Neuroethol. Sens. Neural. Behav. Physiol. 192, 587–600.

Carr, C.E., Maler, L., Sas, E., 1982. Peripheral organization and central projections of the electrosensory nerves in gymnotiform fish. J. Comp. Neurol. 211, 139–153.

Chacron, M.J., Fortune, E.S., 2010. Subthreshold membrane conductances enhance directional selectivity in vertebrate sensory neurons. J. Neurophysiol. 104, 449–462.

Chacron, M.J., Longtin, A., Maler, L., 2001. Negative interspike interval correlations increase the neuronal capacity for encoding time-dependent stimuli. J. Neurosci. 21, 5328–5343.

Chacron, M.J., Longtin, A., Maler, L., 2011. Efficient computation via sparse coding in electrosensory neural networks. Curr. Opin. Neurobiol. 21, 752–760.

Chacron, M.J., Toporikova, N., Fortune, E.S., 2009. Differences in the time course of short-term depression across receptive fields are correlated with directional selectivity in electrosensory neurons. J. Neurophysiol. 102, 3270–3279.

Cuddy, M., Aubin-Horth, N., Krahe, R., 2012. Electrocommunication behaviour and non-invasively *Apteronotus leptorhynchus*. Horm. Behav. 61, 4–11.

Deemyad, T., Maler, L., Chacron, M.J., 2011. Inhibition of SK and M channel-mediated currents by 5-HT enables parallel processing by burtsts and isolated spikes. J. Neurophysiol. 105, 1276–1294.

Dunlap, K.D., 2002. Hormonal and body size correlates of electrocommunication behavior during dyadic interactions in a weakly electric fish, *Apteronotus leptorhynchus*. Horm. Behav. 41, 187–194.

Dunlap, K.D., Larkins-Ford, J., 2003. Production of aggressive electrocommunication signals to progressively realistic social stimuli in male *Apteronotus leptorhynchus*. Ethology 109, 243–258.

Dunlap, K.D., Oliveri, L.M., 2002. Retreat site selection and social organization in captive electric fish, *Apteronotus leptorhynchus*. J. Comp. Physiol. A 188, 469–477.

Dunlap, K.D., Thomas, P., Zakon, H.H., 1998. Diversity of sexual dimorphism in electrocommunication signals and its androgen regulation in a genus of electric fish, *Apteronotus*. J. Comp. Physiol. A 183, 77–86.

Dunlap, K.D., DiBenedictis, B.T., Banever, S.R., 2010. Chirping response of weakly electric knife fish (*Apteronotus leptorhynchus*) to low-frequency electric signals and to heterospecific electric fish. J. Exp. Biol. 213, 2234–2242.

Dulka, J.G., Maler, L., 1994. Testosterone modulates female chirping behavior in the weakly electric fish *Apteronotus leptorhynchus*. J. Comp. Physiol. A 174 (3), 331–343.

Dulka, J.G., Maler, L., Ellis, W., 1995. Androgen-induced changes in electrocommunicatory behavior are correlated with changes in substance P-like immunoreactivity in the brain of the electric fish *Apteronotus leptorhynchus*. J. Neurosci. 15 (3), 1879–1890.

Ellis, L.D., Mehaffey, W.H., Harvey-Girard, E., Turner, R.W., Maler, L., Dunn, R.J., 2007. Sk channels provide a novel mechanism for the control of frequency tuning in electrosensory neurons. J. Neurosci. 27, 9491–9502.

Engler, G., Fogarty, C.M., Banks, J.R., Zupanc, G.K., 2000. Spontaneous modulations of the electric organ discharge in the weakly electric fish, *Apteronotus leptorhynchus*: a biophysical and behavioral analysis. J. Comp. Physiol. A 186, 645–660.

Engler, G., Zupanc, G.K., 2001. Differential production of chirping behavior evoked by electrical stimulation of the weakly electric fish, *Apteronotus leptorhynchus*. J. Comp. Physiol. A 187, 747–756.

Fortune, E.S., Chacron, M.J., 2011. Physiology of tuberous electrosensory systems. In: Farrell, A.P. (Ed.), Encyclopedia of Fish Physiology: From Genome to Environment. vol. 1, pp. 366–374.

Fortune, E.S., Rose, G.J., 2000. Short-term synaptic plasticity contributes to the temporal filtering of electrosensory information. J. Neurosci. 20, 7122–7130.

Fortune, E.S., Rose, G.J., 2001. Short-term synaptic plasticity as a temporal filter. Trends Neurosci. 24, 381–385.

Fugère, V., Ortega, H., Krahe, R., 2011. Electrical signalling of dominance in a wild population of electric fish. Biol. Lett. 7, 197–200.

Gama Salgado, J.A., Zupanc, G.K.H., 2011. Echo response to chirping in the weakly electric brown ghost knifefish (*Apteronotus leptorhynchus*): role of frequency and amplitude modulations. Can. J. Zool. 89 (6), 498–508.

Green, D.M., Swets, J.A., 1974. Signal Detection Theory and Psychophysics. Robert Krieger Publ. Comp.

Gussin, D., Benda, J., Maler, L., 2007. Limits of linear rate coding of dynamic stimuli by electroreceptor afferents. J. Neurophysiol. 97, 2917–2929.

Hagedorn, M., Heiligenberg, W., 1985. Court and spark: electric signals in the courtship and mating of gymnotoid fish. Animal Behav. 33, 254–265.

Harvey-Girard, E., Dunn, R.J., Maler, L., 2007. Regulated expression of N-methyl-D-aspartate receptors and associated proteins in teleost electrosensory system and telencephalon. J. Comp. Neurol. 505, 644–668.

Heiligenberg, W., 1986. Electroreception. John Wiley & Sons.

Heiligenberg, W., Dye, J., 1982. Labelling of electroreceptive afferents in a gymnotoid fish by intracellular injection of HRP: the mystery of multiple maps. J. Comp. Physiol. A 148, 287–296.

Hennig, R.M., 2003. Acoustic feature extraction by cross-correlation in crickets? J. Comp. Physiol. A 189, 589–598.

Hill, P.S.M., 2009. How do animals use substrate-borne vibrations as an information source? Naturwissenschaften 96, 1355–1371.

Hopkins, C.D., 1974. Electric communication: functions in the social behavior of eigenmannia virescens. Behaviour 50, 270–305.

Hupé, G.J., 2012. Electrocommunication in a Species of Weakly Electric FISH, *Apteronotus leptorhynchus*: Signal patterning and Behaviour. PhD Thesis, University of Ottawa, Ottawa, ON.

Hupé, G.J., Lewis, J.E., 2008. Electrocommunication signals in free swimming brown ghost knifefish, *Apteronotus leptorhynchus*. J. Exp. Biol. 211, 1657–1667.

Hupé, G.J., Lewis, J.E., Benda, J., 2008. The effect of difference frequency on electrocommunication: chirp production and encoding in a species of weakly electric fish, *Apteronotus leptorhynchus*. J. Physiol. Paris 102, 164–172.

Hurd, P.L., Wachtmeister, C.A., Enquist, M., 1995. Darwin's principle of antithesis revisited: a role for perceptual biases in the evolution of intraspecific signals. Proc. R. Soc. Lond. 259 (1355), 201–205.

Johansson, B.G., Jones, T.M., 2007. The role of chemical communication in mate choice. Biol. Rev. Camb. Philos. Soc. 82, 265–289.

Kawasaki, M., Rose, G., Heiligenberg, W., 1988. Temporal hyperacuity in single neurons of electric fish. Nature 336, 173–176.

Kelley, D.B., Bass, A.H., 2010. Neurobiology of vocal communication: mechanisms for sensorimotor integration and vocal patterning. Curr. Opin. Neurobiol. 20, 748–753.

Kelly, M., Babineau, D., Longtin, A., Lewis, J.E., 2008. Electric field interactions in pairs of electric fish: modeling and mimicking naturalistic input. Biol. Cybern. 98, 479–490.

Kolodziejski, J.A., Sanford, S.E., Smith, G.T., 2007. Stimulus frequency differentially affects chirping in two species of weakly electric fish: implications for the evolution of signal structure and function. J. Exp. Biol. 210, 2501–2509.

Krahe, R., Bastian, J., Chacron, M.J., 2008. Temporal processing across multiple topographic maps in the electrosensory system. J. Neurophysiol. 100, 852–867.

Krahe, R., Gabbiani, F., 2004. Burst firing in sensory systems. Nat. Rev. Neurosci. 5, 13–23.

Larimer, J.L., MacDonald, J.A., 1968. Sensory feedback from electroreceptors to electromotor pacemaker centers in gymnotids. Am. J. Physiol. 214, 1253–1261.

Lewis, J.E., Lindner, B., Laliberté, B., Groothuis, S., 2007. Control of neuronal firing by dynamic parallel fiber feedback: implications for electrosensory reafference suppression. J. Exp. Biol. 210, 4437–4447.

MacIver, M.A., Sharabash, N.M., Nelson, M.E., 2001. Prey-capture behavior in gymnotid electric fish: motion analysis and effects of water conductivity. J. Exp. Biol. 204, 543–557.

Maler, L., 1979. The posterior lateral line lobe of certain gymnotoid fish: quantitative light microscopy. J. Comp. Neurol. 183, 323–363.

Maler, L., 2009. Receptive field organization across multiple electrosensory maps. i. Columnar organization and estimation of receptive field size. J. Comp. Neurol. 516, 376–393.

Maler, L., Ellis, W.G., 1987. Inter-male aggressive signals in weakly electric fish are modulated by monoamines. Behav. Brain Res. 25, 75–81.

Maler, L., Sas, E., Carr, C.E., Matsubara, J., 1982. Efferent projections of the posterior lateral line lobe in gymnotiform fish. J. Comp. Neurol. 211, 154–164.

Maler, L., Sas, E., Johnston, S., Ellis, W., 1991. An atlas of the brain of the electric fish *Apteronotus leptorhynchus*. J. Chem. Neuroanat. 4, 1–38.

Marsat, G., Longtin, A., Maler, L., 2012. Cellular and circuit properties supporting different sensory coding strategies in electric fish and other systems. Curr. Opin. Neurobiol. 22, 1–7.

Marsat, G., Maler, L., 2010. Neural heterogeneity and efficient population codes for communication signals. J. Neurophysiol. 104, 2543–2555.

Marsat, G., Maler, L., 2012. Preparing for the unpredictable: adaptive feedback enhances the response to unexpected communication signals. J. Neurophysiol. 107, 1241–1246.

Marsat, G., Proville, R., Maler, L., 2009. Transient signals trigger synchronous bursts in an identified population of neurons. J. Neurophysiol. 102, 714–723.

Mehaffey, W.H., Maler, L., Turner, R.W., 2008. Intrinsic frequency tuning in ell pyramidal cells varies across electrosensory maps. J. Neurophysiol. 99, 2641–2655.

Metzner, W., Heiligenberg, W., 1991. The coding of signals in the electric communication of the gymnotiform fish eigenmannia: from electroreceptors to neurons in the torus semicircularis of the midbrain. J. Comp. Physiol. A 169, 135–150.

Metzner, W., Juranek, J., 1997. A sensory brain map for each behavior? Proc. Natl. Acad. Sci. USA 94, 14798–14803.

Meyer, J.H., Leong, M., Keller, C.H., 1987. Hormone-induced and ontogenetic changes in electric organ discharge and electroreceptor tuning in the weakly electric fish *Apteronotus*. J. Comp. Physiol. A 160, 385–394.
Moortgat, K.T., Keller, C.H., Bullock, T.H., Sejnowski, T.J., 1998. Submicrosecond pacemaker precision is behaviorally modulated: the gymnotiform electromotor pathway. Proc. Natl. Acad. Sci. USA 95, 4684–4689.
Morton, E.S., 1977. On the occurrence and significance of motivation-structural rules in some bird and mammal sounds. Amer. Nat. 111 (981), 855–869.
Myrberg, A.A., Riggio, J.R., 1985. Acoustically mediated individual recognition by a coral reef fish (*Pomacentrus partitus*). Anim. Behav. 33, 411–416.
Naruse, M., Kawasaki, M., 1998. Possible involvement of the ampullary electroreceptor system in detection of frequency-modulated electrocommunication signals in eigenmannia. J. Comp. Physiol. A 183, 543–552.
Nelson, M.E., Xu, Z., Payne, J.R., 1997. Characterization and modeling of *P*-type electrosensory afferent responses to amplitude modulations in a wave-type electric fish. J. Comp. Physiol. A 181, 532–544.
Osorio, D., Vorobyev, M., 2008. A review of the evolution of animal colour vision and visual communication signals. Vision Res. 48, 2042–2051.
Requarth, T., Sawtell, N.B., 2011. Neural mechanisms for filtering self-generated sensory signals in cerebellum-like circuits. Curr. Opin. Neurobiol. 21, 602–608.
Rose, G.J., 2004. Insights into neural mechanisms and evolution of behaviour from electric fish. Nat. Rev. Neurosci. 5, 943–951.
Savard, M., Krahe, R., Chacron, M.J., 2011. Neural heterogeneities influence envelope and temporal coding at the sensory periphery. Neuroscience 172, 270–284.
Scheich, H., Bullock, T.H., Hamstra, R.H., 1973. Coding properties of two classes of afferent nerve fibers: high-frequency electroreceptors in the electric fish, eigenmannia. J. Neurophysiol. 36, 39–60.
Schmidt, A.K.D., Riede, K., Römer, H., 2011. High background noise shapes selective auditory filters in a tropical cricket. J. Exp. Biol. 214, 1754–1762.
Shumway, C.A., Maler, L., 1989. GABAergic inhibition shapes temporal and spatial response properties of pyramidal cells in the elctrosensory lateral line lobe of gymnotiform fish. J. Comp. Physiol. A 164, 391–407.
Smith, G.T., 2006. Pharmacological characterization of ionic currents that regulate high-frequency spontaneous activity of electromotor neurons in the weakly electric fish, *Apteronotus leptorhynchus*. J. Neurobiol. 66, 1–18.
Smith, G.T., Combs, N., 2008. Serotonergic activation of 5HT1A and 5HT2 receptors modulates sexually dimorphic communication signals in the weakly electric fish *Apteronotus leptorhynchus*. Horm. Behav. 54, 69–82.
Smith, G.T., Zakon, H.H., 2000. Pharmacological characterization of ionic currents that regulate the pacemaker rhythm in a weakly electric fish. J. Neurobiol. 42, 270–286.
Stacey, N., Chojnacki, A., Narayanan, A., Cole, T., Murphy, C., 2003. Hormonally derived sex pheromones in fish: exogenous cues and signals from gonad to brain. Can. J. Physiol. Pharmacol. 81, 329–341.
Tallarovic, S.K., Zakon, H.H., 2002. Electrocommunication signals in female brown ghost electric knifefish, *Apteronotus leptorhynchus*. J. Comp. Physiol. A Neuroethol. Sens Neural. Behav. Physiol. 188, 649–657.
Telgkamp, P., Combs, N., Smith, G.T., 2007. Serotonin in a diencephalic nucleus controlling communication in an electric fish: sexual dimorphism and relationship to indicators of dominance. Dev. Neurobiol. 67, 339–354.
Triefenbach, F.A., 2005. Communication in the weakly electric brown ghost knifefish, *Apteronotus leptorhynchus*. PhD Thesis, University of Texas at Austin, Austin, TX.
Triefenbach, F., Zakon, H., 2003. Effects of sex, sensitivity and status on cue recognition in the weakly electric fish *Apteronotus leptorhynchus*. Animal Behav. 65, 19–28.
Triefenbach, F., Zakon, H., 2008. Changes in signalling during agonistic interactions between male weakly electric knifefish, *Apteronotus leptorhynchus*. Animal Behav. 75, 1263–1272.
Turner, R.W., Lemon, N., Doiron, B., Rashid, A.J., Morales, E., Longtin, A., Maler, L., Dunn, R.J., 2002. Oscillatory burst discharge generated through conditional backpropagation of dendritic spikes. J. Physiol. Paris 96, 517–530.
Vonderschen, K., Chacron, M.J., 2011. Sparse and dense coding of natural stimuli by distinct midbrain neuron subpopulations in weakly electric fish. J. Neurophysiol. 106, 3102–3118.
Walz, H., Grewe, J., Benda, J., 2010. Communication signals in a wave-type electric fish are encoded by synchronization and desynchronization depending on the social context. In: Front. Comput. Neurosci. Conference Abstract: Bernstein Conference on Computational Neuroscience.
Waser, P., Brown, C., 1986. Habitat acoustics and primate communication. Amer. J. Primatol. 10, 135–154.
Xu, Z., Payne, J.R., Nelson, M.E., 1996. Logarithmic time course of sensory adaptation in electrosensory afferent nerve fibers in a weakly electric fish. J. Neurophysiol. 76, 2020–2032.
Yu, N., Hupé, G., Garfinkle, C., Lewis, J.E., Longtin, A., 2012. Coding conspecific identity and motion in the electric sense. PLoS Comput. Biol. 8 (7), e1002564.
Zakon, H., Oestreich, J., Tallarovic, S., Triefenbach, F., 2002. Eod modulations of brown ghost electric fish: JARs, chirps, rises, and dips. J. Physiol. Paris 96, 451–458.
Zakon, H.H., 1986. The emergence of tuning in newly generated tuberous electroreceptors. J. Neurosci. 6, 3297–3308.
Zupanc, G., Maler, L., 1993. Evoked chirping in the weakly electric fish, *Apteronotus leptorhynchus*: a biophysical and behavioral analysis. Can. J. Zool. 71, 2301–2310.
Zupanc, M.M., Engler, G., Midson, A., Oxberry, H., Hurst, L.A., Symon, M.R., Zupanc, G.K.H., 2001. Lightdark changes in spontaneous modulations of the electric organ discharge in the weakly electric fish, *Apteronotus leptorhynchus*. Animal Behav. 62, 1119–1128.
Zupanc, G.K.H., 2002. From oscillators to modulators: behavioral and neural control of modulations of the electric organ discharge in the gymnotiform fish, apteronotus leptorhynchus. J. Physiol. Paris 96, 459–472.
Zupanc, G.K.H., Sîrbulescu, R.F., Nichols, A., Ilies, I., 2006. Electric interactions through chirping behavior in the weakly electric fish, *Apteronotus leptorhynchus*. J. Comp. Physiol. A Neuroethol. Sens Neural Behav. Physiol. 192, 159–173.

Danksagung/Acknowledgements

Ich möchte mich ganz herzlich bei Jan Benda, dem Betreuer dieser Arbeit, bedanken, der mich an die elektrischen Fische herangeführt hat und mir die Möglichkeit gegeben hat, dieses interdisziplinäre Projekt zu bearbeiten. Seine Begeisterung für die Fische, aber auch über jeden noch so kleinen Fortschritt in der Arbeit hat mir über so manche Frustration hinweg geholfen. Ebenfalls immer wieder geholfen hat seine Unterstützung in der Datenauswertung. Ich hoffe, dass ich vieles von dem, was ich darüeber in den letzten Jahren gelernt habe, werde mitnehmen können. Ich möchte ihm auch für seine Unterstützung danken, sowohl inhaltlich als auch organisatorisch eigene Wege zu gehen. Das hat es mir u.a. ermöglicht, in der Zeit so vielfältige Dinge wie Exkursionen und Filmprojekte zu verfolgen. Außerdem möchte ich mich besonders bei Jan Grewe für die tagtägliche Unterstützung in der professionellen und persönlichen Welt bedanken. Ohne ihn wäre ich wahrscheinlich über den Herausforderungen der Experimente verzweifelt. Ich danke Karin, Florian und Franziska, dass sie wunderbare Labornachbarn waren. Fürs intensive Fehlerlesen bedanke ich mich bei Jan B, Jan G, Valérie, Karin und Ines.

I feel very lucky to have been part of the electric fish community and to have had the chance to work with so many amazing people and scientists. I thank Leonard Maler for providing me with the opportunity to stay in his lab for two months and for support in various forms since then. I thank André Longtin for many fruitful discussions and John Lewis for a very pleasant collaboration. I thank Ginette Hupé for never ending personal and professional inspiration. Rüdiger Krahe and Jörg Henninger I thank tremendously for letting me be part of the Panama excursion.

Die letzten Jahre waren vor allem eine bereichernde und schöne Zeit. Nicht unerheblichen Anteil daran hatten viele tolle Menschen in meiner Familie und meinem Freundeskreis. Ihnen allen sei hiermit herzlichst gedankt. Es ist schön, dass es Euch gibt!